Changing dominance of high-latitude intermediate waters and its impact on the equatorial nutrient-budget

– Implications from foraminiferal geochemistry

Dissertation

zur Erlangung des akademischen Grades
eines Doktors der Naturwissenschaften

– Dr. rer. nat. –

am Fachbereich Geowissenschaften
der Universität Bremen

vorgelegt von

Nadine Rippert

Bremen, 2016

Wissenschaftliche Betreuung und Begutachtung:

Prof. Dr. Ralf Tiedemann

Alfred-Wegener-Institut
Helmholtz-Zentrum für Polar- und Meeresforschung
Am Alten Hafen 26
27568 Bremerhaven
Deutschland

Prof. Dr. Gerhard Bohrmann

Universität Bremen
Fachbereich Geowissenschaften
Klagenfurter Straße
28359 Bremen
Deutschland

Eidesstattliche Erklärung

Hiermit versichere ich an Eides statt, dass ich die vorliegende Arbeit ohne unerlaubte fremde Hilfe Dritter und unter Verwendung keiner anderen als die von mir angegebenen Quellen und Hilfsmittel angefertigt habe.

Die aus fremden Quellen wörtlich oder inhaltlich übernommenen Informationen sind als solche kenntlich gemacht.

Bremen, 12.10.2016

Nadine Rippert

Ich sage nicht, dass es leicht wird, aber es wird sich lohnen.

(*Art Williams*)

Abstract

The equatorial Pacific holds the potential to investigate the climate variability of the Earth as it connects both hemispheres via the atmospheric and oceanic circulation. The modern Equatorial Pacific Intermediate Water (EqPIW) is fed by three end-member components: Southern Ocean Intermediate Water (SOIW), Pacific Deep Water (PDW) and, by a smaller proportion, North Pacific Intermediate Water (NPIW). This modern configuration of end-members in the EqPIW results in low productivity of siliceous phytoplankton in the Eastern Equatorial Pacific (EEP) today as SOIW is depleted in silicic acid compared to other nutrients. An increased primary production during glacials has often been attributed to an enhanced contribution of SOIW to equatorial sub-surface waters. However, there is growing debate over whether SOIW was capable of stimulating glacial equatorial productivity. This is in light of the fact that nutrients appear to have been trapped in glacial Southern Ocean waters. Furthermore, recent studies point towards a change in the lateral and vertical extent of both SOIW and NPIW during glacials, impacting the supply of nutrients to the EEP. Ultimately, the effect of these intermediate water mass changes on equatorial waters remains elusive.

Most upper ocean water mass reconstructions are based on planktonic foraminifera tests. Different foraminiferal species preferentially dwell in distinct water depths and thus, the calcitic tests of these species can be used to infer past climate conditions. However, it has been shown that the Apparent Calcification Depths (ACDs) of foraminiferal species are spatially non-uniform. To-date, there are no ACD reconstructions from the equatorial Pacific based on multinet data. This thesis assesses equatorial foraminiferal ACDs to identify a species suitable to trace nutrient-inflow of extra-tropical intermediate water masses. Using this determined species, this thesis then reconstructs the effect of variable nutrient injections from extra-tropical water masses on the equatorial Pacific upwelling waters using benthic and planktonic foraminiferal carbon isotopes ($\delta^{13}C$). In combination with published records of neodymium isotopes (ε_{Nd}) and foraminiferal $\delta^{13}C$ values from the subarctic Pacific, the eastern North Pacific, the eastern tropical North Pacific as well as the southeast and southwest Pacific, this thesis aims to improve our knowledge of end-member contributions on EqPIW during the last two glacial-interglacial cycles, focusing in at higher resolution during Marine Isotope Stage (MIS) 2.

The results of this thesis are presented in three manuscripts. The first manuscript examines foraminiferal calcification depths in the western equatorial Pacific using living planktonic foraminifera in combination with foraminiferal abundances. Despite the relatively deep thermocline in the Western Pacific Warm Pool (WPWP), the relative order of the five investigated species was

comparable to other ocean basins. However, absolute ACDs differed due to the local hydrography in the WPWP. Surface mixed layer dwellers *Globigerinoides ruber* and *Globigerinoides sacculifer* were apparent at ~95 m and ~115 m water depth, and were found in low abundances during the sampling time. The comparatively deep thermocline between 130 – 230 m below sea level subsequently led to relatively deep calcification depths of *Neogloboquadrina dutertrei* and *Pulleniatina obliquiloculata*. Hence, both species occupy a depth habitat towards the top, and within, the thermocline. One of our major findings was that the planktonic species *Globorotaloides hexagonus* was found to occupy a deep habitat (~450 m water depth) within the Pacific. This sub-thermocline species seems to favour cool, nutrient-rich water masses and was shown to be a suitable archive for tracing nutrient-inflow of high latitude intermediate water masses on equatorial Pacific sub-thermocline.

The second and third manuscripts deal with the ventilation of Glacial North Pacific Intermediate Water (GNPIW) and its influence on the EqPIW during the past 60 ka (*Manuscript 2*) and during the last two glacial-interglacial cycles (*Manuscript 3*). It was shown that $\delta^{13}C$ records from the Bering Sea (as an indicator for GNPIW), the eastern tropical North Pacific and the EqPIW (measured on *G. hexagonus*) exhibit a similar temporal evolution during MIS 2. In addition, the absolute ε_{Nd} signatures from the Bering Sea and the eastern North Pacific are similar during this time period. The $\delta^{13}C$ difference between the equatorial record and northern and southern signatures, respectively, was calculated to infer the relative change of high latitude intermediate water contribution on equatorial sub-thermocline nutrient concentrations. Most interestingly, in times when the $\delta^{13}C$ differences between the EqPIW record and two Southern Ocean cores are greatest (late MIS 2 and MIS 6), the difference in $\delta^{13}C$ between the North Pacific and EEP is smallest. These results indicate increased GNPIW ventilation during glacials that spreads southward towards the eastern tropical North Pacific. During peak glacials the southward expansion of GNPIW was at a maximum and extended into the equatorial Pacific. Together with newly published evidence for a shallower penetration of relatively nutrient-depleted SOIW during glacials, these results point towards repeated episodes of reduced southern-sourced nutrient-injections into EqPIW during peak glacials. In contrast, the enhanced ventilation of nutrient-elevated GNPIW resulted in a comparatively increased nutrient contribution to the EqPIW. This intensified GNPIW nutrient-inflow possibly relaxed the nutrient limitation in the EEP, stimulating primary productivity in the EEP during peak MIS 2. As a consequence, the invigorated glacial biological pump would have sequestered more carbon dioxide (CO_2) from the atmosphere into the ocean. And thus, in summary, this thesis has contributed important new insights into the role of the dynamics of the EEP in driving the glacial reduction in atmospheric CO_2 concentrations.

Kurzfassung

Der äquatoriale Pazifik verbindet die Nord- und Südhemisphäre mittel atmosphärischer und ozeanischer Zirkulation und ermöglicht somit die Erforschung der Klimaschwankungen der Erde. Das heutige äquatoriale Pazifische Zwischenwasser (EqPIW) wird gespeist aus drei Ursprungswassermassen: aus dem Südozeanischen Zwischenwasser (SOIW), dem Pazifischen Tiefenwasser (PDW) und zu sehr geringen Anteilen aus dem Nordpazifischen Zwischenwasser (NPIW). Der geringe Anteil an Kieselsäure im SOIW, im Vergleich zu anderen Nährstoffen, ist maßgeblich für die heutige geringe Primärproduktivität von kieseligem Phytoplankton im östlichen äquatorialen Pazifik (EEP) verantwortlich. Eine erhöhte Primärproduktion im letzten Glazial wird häufig mit einer erhöhten Zufuhr von SOIW in das äquatoriale Strömungssystem erklärt. Allerdings wird in der Literatur intensiv diskutiert, ob SOIW überhaupt in der Lage war die glaziale Produktivität am Äquator zu stimulieren, da Nährstoffe während des Glazials eher im Südozean gebunden waren. Darüber hinaus weisen neue Studien darauf hin, dass sich die laterale und vertikale Ausdehnung von SOIW als auch von NPIW während der Glaziale verändert hat. Die Auswirkung dieser veränderten Zwischenwassermassen auf das äquatoriale Strömungssystem ist bis heute jedoch unklar.

Rekonstruktionen der oberen Wassersäule basieren oftmals auf Analysen an planktischen Foraminiferengehäusen. Unterschiedliche Arten leben und kalzifizieren in bestimmten Wassertiefen und eignen sich daher ideal zur Bestimmung vergangener Klimabedingungen. Es hat sich jedoch herausgestellt, dass sich die scheinbaren Kalzifizierungstiefen (ACDs) der Foraminiferenarten regional unterscheiden können. Es existiert jedoch bis heute keine ACD Bestimmungen aus Multinetzdaten aus dem äquatorialen Pazifik. Diese Dissertation bestimmt die ACDs verschiedener Foraminiferenarten, um eine Art zu ermitteln, die den Nährstoffeintrag aus den Zwischenwassermassen der hohen Breiten aufzeigen kann. Diese Art wurde anschließend verwendet, um den Effekt variabler Nährstoffzufuhr aus unterschiedlichen Ursprungswassermassen auf den äquatorialen Pazifik mittels benthischer und planktischer Kohlenstoffisotope ($\delta^{13}C$) zu rekonstruieren. Die gemessenen $\delta^{13}C$ Werte werden mit bereits publizierten $\delta^{13}C$ Werten und Neodym-Isotopendaten (ε_{Nd}), welche an Foraminiferen aus Sedimentkernen vom subarktischen Pazifik, dem östlichen Nordpazifik, dem östlichen tropischen Nordpazifik sowie dem südöstlichen und südwestlichen Pazifik gemessen wurden, kombiniert. Letztendlich zielt diese Dissertation darauf ab, das Wissen über die Quellen und Steuerungsmechanismen der Nährstoffzufuhr im EqPIW während der letzten zwei Glazial-Interglazialzyklen und in höherer Auflösung während des Marinen Isotopenstadiums (MIS) 2 zu verbessern.

Die Ergebnisse dieser Arbeit werden in drei Manuskripten vorgestellt. Das erste Manuskript befasst sich mit der Proxygenerierung und der daraus abgeleiteten ACDs planktischer Foraminiferen im westlichen äquatorialen Pazifik anhand fünf lebender planktischer Foraminiferenarten in Kombination mit Häufigkeitsverteilungen von Foraminiferenarten. Trotz der relativ tiefen Thermokline im Westpazifischen Warmwasserpools (WPWP) glich die relative Abfolge der fünf Arten derer aus anderen Ozeanen. Die absoluten ACDs unterschieden sich jedoch auf Grund der lokalen Hydrographie im WPWP. Dabei zeigen die oberflächennahen Arten *Globigerinoides ruber* und *Globigerinoides sacculifer* ACDs um jeweils ~95 m und ~115 m an, waren aber in nur geringen Häufigkeiten während der Probennahme vorhanden. Die verhältnismäßig tiefe Thermokline zwischen 130 – 230 m führte zu entsprechend tiefen ACDs von *Neogloboquadrina dutertrei* und *Pulleniatina obliquiloculata* am oberen Rand und innerhalb der Thermokline. Bedeutend war der Fund der im Pazifik tieflebenden (~450 m) planktischen Art *Globorotaloides hexagonus*. Diese sub-thermokline Art kalzifiziert augenscheinlich in kühlen, nährstoff-reichem Wassermassen und stellte sich damit als ein verlässlicher Proxy zur Rekonstruktion von Nährstoffkonzentrationen im sub-thermoklinen Bereich heraus.

Das zweite und dritte Manuskript beschäftigen sich mit der Ventilation des Glazialen Nordpazifischen Zwischenwassers (GNPIW) und dessen Einfluss auf das EqPIW während der letzten 60 ka (*Manuskript 2*) und der letzten zwei Glazial-Interglazialzyklen (*Manuskript 3*). Es konnte gezeigt werden, dass $\delta^{13}C$ Datensätze aus der Bering See (als ein Anzeiger für GNPIW), dem östlichen tropischen Nordpazifik und dem EqPIW (gemessen an *G. hexagonus*) während MIS 2 einen ähnlichen zeitlichen Verlauf nehmen. Weiterhin wurde hervorgehoben, dass sich die absoluten ε_{Nd} Signaturen aus der Bering See und dem östlichen Nordpazifik in der gleichen Zeit kaum unterscheiden. Die $\delta^{13}C$ Differenz zwischen dem EqPIW und dem Südozean sowie Nordpazifik wurde berechnet um Rückschlüsse über die relativen Änderungen in den Steuerungsmechanismen zu schließen. Auffallend war, dass zu Zeiten in denen der $\delta^{13}C$ Unterschied zwischen der äquatoriale sub-Thermokline und dem Südozean am ausgeprägtesten war (spätes MIS 2 und MIS 6), die $\delta^{13}C$ Differenz zwischen dem Nordpazifik und dem EEP am geringsten war. Diese Ergebnisse zeigen somit, dass es während der Glaziale zu einer verstärkten Ventilation des GNPIW gekommen ist, die sich bis in den östlichen tropischen Nordpazifik erstreckte. Sie erreichte ihren Höhepunkt mit dem Erreichen des Äquators während der Hochglaziale. Im Zusammenhang mit neuen Studien, die auf eine Verflachung des relativ nährstoff-abgereicherten SOIW während der Glaziale hinweisen, zeigen die Ergebnisse dieser Dissertation eine wiederholt abnehmende Nährstoffzufuhr von südlichen Wassermassen während der Hochglaziale. Dahingegend schien die erhöhte Ventilation von GNPIW zu einer vergleichsweise gesteigerten Nährstoffzufuhr in das EqPIW zu führen. Dies wiederum hob vermutlich die Nährstofflimitierung im EEP auf und könnte die erhöhte Produktivität im EEP während des späten MIS 2 mit erklären. Als Konsequenz darauf, würde die gestärkte biologische Pumpe mehr Kohlenstoffdioxid (CO_2) aus der Atmosphäre in den Ozean sequestrieren. Letztendlich tragen die Ergebnisse dieser Dissertation somit zu den laufenden Diskussionen der abnehmenden glazialen CO_2 Konzentrationen bei.

Table of Contents

Eidesstattliche Erklärung ..... **I**

Abstract ..... **II**

Kurzfassung ..... **IV**

Table of Contents ..... **VI**

List of Figures ..... **IX**

List of Tables ..... **XI**

1. Introduction **1**

1.1 General introduction 1

1.2 Modern oceanographic setting 3

1.2.1 Western Pacific Warm Pool versus Pacific Equatorial Divergence 5

1.3 Relevant (paleoceanographic) research related to this thesis 7

1.4 Planktonic foraminifera as paleo-proxies 9

1.4.1 Brief overview of planktonic foraminiferal ecology 9

1.4.2 General influence on foraminiferal shells 10

1.4.2.1 Stable isotopes 10

1.4.2.2 Mg/Ca paleothermometry 13

1.5 Aims of the thesis 14

1.6 Author's contribution 15

2. Material and Methods **17**

2.1 Study material 17

2.1.1 Western equatorial Pacific 17

2.1.2 Eastern Equatorial Pacific (EEP) 19

2.2. Applied methods 19

2.2.1 Foraminiferal counting 19

2.2.2 Stable isotope analyses 21

2.2.3 Determination of trace element ratios 21

2.2.3.1 Mg/Ca paleothermometry 22

2.3 Assessment of apparent calcification depth 23

2.4 Stratigraphy of ODP Site 1240 23

3. Manuscript I – Constraining foraminiferal calcification depths in the Western Pacific Warm Pool **25**

published in Marine Micropaleontology 128, 14-27

3.1 Introduction 26

3.1.1 Foraminiferal ecological preferences and hydrographic setting 28

3.2 Material and Methods 30
3.2.1 Sample material 30
3.2.2 Handling foraminiferal assemblage counts 30
3.2.3 Determination of Mg/Ca ratios and calculation of water temperatures 31
3.2.4 Stable isotope analyses 34
3.2.5 Estimation of the apparent calcification depth 34
3.3 Results and Discussion 37
3.3.1 Hydrological conditions in the upper ocean water column 37
3.3.2 Vertical distribution of planktonic foraminifers in the water column 39
3.3.3 Foraminiferal apparent calcification depth 41
3.3.3.1 Apparent calcification depths of *G. ruber* and *G. sacculifer* 43
3.3.3.2 Apparent calcification depths of *N. dutertrei* and *P. obliquiloculata* 44
3.3.3.3 Apparent calcification depths of *G. hexagonus* 45
3.3.4 Foraminiferal carbon isotope disequilibrium 47
3.4 Conclusions 49
3.5 Supplementary data 52

4. Manuscript II – Evidence for enhanced convection of North Pacific Intermediate Water to the low-latitude Pacific under glacial conditions 63
Paleoceanography (under review)

4.1 Introduction 64
4.2 Materials and Methods 68
4.2.1 Stable carbon ($\delta^{13}C$) and oxygen ($\delta^{18}O$) isotope measurements from benthic and deep-dwelling planktonic foraminifera 68
4.2.2 Stable oxygen isotope composition ($\delta^{18}O$) and apparent calcification depth of deep-dwelling planktonic foraminifera *G. hexagonus* 69
4.2.3 Stratigraphic approach and age models 71
4.3 Results 71
4.4 Discussion 74
4.4.1 Glacial contribution of northern- *versus* southern-sourced intermediate waters in the Eastern Tropical North Pacific (~8°N) 74
4.4.2 Evidence for increased GNPIW influence in the Eastern Equatorial Pacific since MIS 2? 78
4.4.3 “North Pacific Nutrient Leakage” 79
4.5 Conclusions 82
4.6 Supplementary data 83

5. Manuscript III – Alternating influence of northern versus southern-sourced water masses on the equatorial Pacific sub-thermocline duing the past 240 ka 87
to be submitted to Paleoceanography

5.1 Introduction 88
5.1.1 Modern oceanography and hydrography 90
5.2 Materials and Methods 92
5.2.1 Material and stable isotope analyses 92
5.2.2 Stratigraphic approach 93
5.3 Carbon isotopes as proxy for nutrient concentrations 94

5.4 Results 96
5.5 Discussion 97
5.5.1 Reduced SOIW-nutrient contribution on equatorial sub-thermocline during peak glacials 97
5.5.2 Northern-sourced nutrient influence on EqPIW during peak glacials 100
5.5.3 Deglacial and interglacial change in EEP nutrient-concentrations 104
5.6 Conclusions 105
5.7 Supplementary data 106

6. Conclusion and Outlook 109
6.1 Conclusion 109
6.2 Outlook 110

Acknowledgement XII

Data Handling XIII

References XIV

Appendix XXXV
A.I. Co-authored ISI peer-reviewed publication
A.II. First author ISI peer-reviewed publication
A.III. List of Abbreviations

List of Figures

Figure 1.1. Modern global ocean overturning circulation schema from a Southern Ocean perspective. 2

Figure 1.2. Map of the Pacific Ocean with major currents and water masses..... 4

Figure 1.3. Annual temperatures and nitrate concentrations in the equatorial Pacific. 6

Figure 1.4. Summary of the influencing factors on the stable oxygen ($\delta^{18}O$) and carbon ($\delta^{13}C$) isotope composition as well as on the Magnesium/Calcium (Mg/Ca) ratio of planktonic foraminiferal tests. 11

Figure 1.5. Temperature versus $\delta^{18}O_{calcite\ minus\ seawater\ [c\text{-}w]}$ with various published paleo-temperature equations. 12

Figure 1.6. Mg/Ca ratios of various planktonic foraminifera species versus water temperature. . 14

Figure 2.1. Map of the equatorial Pacific with CTD station SO225-21-1, multinet station SO225-21-3 as well as the location of sediment core ODP Site 1240. 17

Figure 2.2. Water column temperature record of the uppermost 500 m measured at station SO225-21 together with the five chosen multinet-intervals. 18

Figure 2.3. Multinet sample from 0 – 50 m water depth show the various size fractions of the recovered material. 20

Figure 2.4. The different morphotypes of *Globigerinoides ruber*. 20

Figure 2.5. Foraminiferal species analysed for Mg/Ca. 22

Figure 3.1. Upper ocean conditions of the equatorial Pacific. 27

Figure 3.2. Water column characteristics of the uppermost 500 m at multinet station SO225-21-03 along the towed net intervals. 37

Figure 3.3. Planktonic foraminiferal abundances for five paleoceano-graphically important species plotted with *in-situ* data of temperature and chlorophyll-a. 39

Figure 3.4. Assessment of Apparent Calcification Depths for selected color-coded planktonic foraminiferal species from multinet station SO225-21. 42

Figure 3.5. Measured $\delta^{13}C_{calcite}$ of selected living planktonic foraminifera in comparison to the *in-situ* measured $\delta^{13}C_{DIC}$ measured at multinet station SO225-21-3. 47

Figure S3.5.3. Foraminiferal Mg/Ca derived temperatures for mean Mg/Ca values determined over a whole test using various calibration equations. 58

Figure S3.5.5. Calculated $\delta^{18}O_{water}$ of the five respective species in comparison to measured $\delta^{18}O_{seawater}$. 62

Figure 4.1. Bathymetric chart and latitudinal profile of present-day silicic acid concentrations of the Pacific Ocean. 65

Figure 4.2. Apparent Calcification Depth of planktonic foraminifera *G. hexagonus* in the Eastern Equatorial Pacific. 70

Figure 4.3. Stratigraphic framework for both sediment cores considered (*Manuscript II*). 72

Figure 4.4. Detailed comparison of mid-depth benthic $\delta^{13}C$ record from the subarctic Pacific with $\delta^{13}C$ record from the Eastern Equatorial Pacific during the past 60 kyr. 73

Figure 4.5. Benthic $\delta^{13}C$ records and ε_{Nd} signatures from intermediate waters of the North Pacific (GNPIW), off Baja California, the Eastern Tropical North Pacific (EqPIW) and the Southern Ocean (AAIW) compared to benthic $\delta^{13}C$ deep-water (PDW) variability for the last 60 kyr. 75

Figure 4.6. Reconstructed $\delta^{13}C$ variability of GNPIW versus AAIW compared to glacial changes in $\delta^{13}C$ of sub-thermocline waters, biological productivity and nutrient utilization in the Eastern Equatorial Pacific and Southern Ocean. 80

Figure 5.1. Overview of Pacific Ocean current system and hydrography. 90

Figure 5.2. Stratigraphic correlation of published and newly generated $\delta^{18}O$ records with respect to the benthic $\delta^{18}O$ reference stack. 94

Figure 5.3. Compilation of Pacific carbon isotope records from the Pacific. 96

Figure 5.4. Comparison of different $\delta^{13}C$ records from the Pacific. 98

Figure 5.5. Schematic illustration of changing end-member contributions on EEP upwelling waters during interstadials and glacial maxima. 101

List of Tables

Table 3.1. Overview of net collections of five paleoceanographically important foraminiferal species. 32

Table 3.2. Equations used to convert foraminiferal Mg/Ca into temperatures and to calculate equilibrium $\delta^{18}O_{equilibrium}$. 33

Table 3.3. Specification of Apparent Calcification Depth of foraminiferal species at Manihiki Plateau. 35

Table 3.4. Foraminiferal $\delta^{13}C_{calcite}$ values with the determined $\delta^{13}C$-disequilibrium and $\delta^{13}C$-disequilibrium values using vital-corrected ACDs. 48

Table S3.5.1. Foraminiferal assemblage counting at station SO225-21 in December 2012. 53

Table S3.5.2. Mg/Ca values of single measurements. 54

Table S3.5.3. Calibration equations tested to convert measured Mg/Ca values into temperatures. 59

Table S3.5.4. Apparent Calcification Depths of selected planktonic foraminiferal species used in this study (*Manuscript I*). 60

Table S3.5.5. Equations used to calculate $\delta^{18}O_{water}$ of the respective foraminiferal species using mean Mg/Ca temperatures and mean $\delta^{18}O_{calcite}$ values. 62

Table S4.4.1. Stable isotope data ($\delta^{13}C$) of epibenthic foraminifera *Cibicides lobatulus* from sediment core SO201-2-101KL. 84

Table S4.4.2. Stable isotope data ($\delta^{13}C$) of deep-dwelling planktic foraminifera *Globorotaloides hexagonus* from ODP Site 1240. 85

Table 5.1. Modern geochemical characteristics for different intermediate and deep water-masses at their origin. 92

Table S5.7.1. Age control points for analysed sediment cores. 107

1. Introduction

1.1 General introduction

The Earth's climate system is strongly mediated by the complex interaction of ocean, atmosphere and biosphere. Understanding the climate forcing processes, the feedback mechanisms and the teleconnections of natural climate variability are one of the main motives of (paleo)climate research. Since the discovery of glacial-interglacial variations in atmospheric carbon dioxide (CO_2) concentrations, detected in Antarctic ice cores bubbles [*Petit et al*., 1999; *Lüthi et al*., 2008], scientists have tried to disentangle the causes of these reoccurring fluctuations. It has been suggested that the 80 – 100 ppm range of atmospheric CO_2 concentrations between glacial and interglacial periods is attributed to a combination of physical and biogeochemical processes that among others regulate the (deep) ocean carbon reservoir [*Sarmiento and Toggweiler*, 1984; *Siegenthaler and Wenk*, 1984; *Abelmann et al*., 2006; *Toggweiler et al.*, 2006; *Ronge et al*., 2016]. The deep ocean contains about 60 times more carbon than the atmosphere [*Falkowski et al*., 2000]. Thus, changes in carbon storage in the ocean interior are likely the main driver for atmospheric CO_2 fluctuations [*Sigman and Boyle*, 2000; *Toggweiler et al*., 2006; *Sigman et al.*, 2010; *Hendry* and *Brzezinski,* 2014].

The Southern Ocean acts as an important exchange area of water masses as it connects the world's major ocean basins [*Talley*, 2013]. In this area, upwelling water masses from the ocean interior containing older CO_2 mix with other water masses and transform into newly formed intermediate, deep and abyssal waters that are exported to the rest of the global ocean (Figure 1.1) [*Orsi et al.*, 1999; *Sarmiento et al*., 2004]. The Southern Ocean Intermediate Water (SOIW) [after *Pena et al*., 2013], the largest global intermediate water mass, is subducted ('thermocline ventilation') and transported equatorward into tropical regions where they eventually upwell [*Liu and Yang*, 2003]. Thereby, changes in the SOIW composition influence both the physical (e.g. by temperature changes) and the chemical (e.g. nutrient composition) properties of the tropical thermocline and intermediate waters [*Kessler*, 2006].

Over the last decades, the role of the tropics within the climate system has been increasingly explored and seems to be more important than previously expected [*Duplessy et al.*, 1988; *Herguera et al.*, 1992; *Spero and Lea*, 2002; *Pena et al*., 2008; *Pichevin et al*., 2009; *Martínez-Botí et al*., 2015]. The Western Pacific Warm Pool (WPWP) with its deep thermocline (~150 – 250 m in the centre [*Locarnini et al.*, 2013]) is one of the major sources of heat and moisture transfer from low to high latitudes. Changes in surface and sub-surface temperatures connected to variations

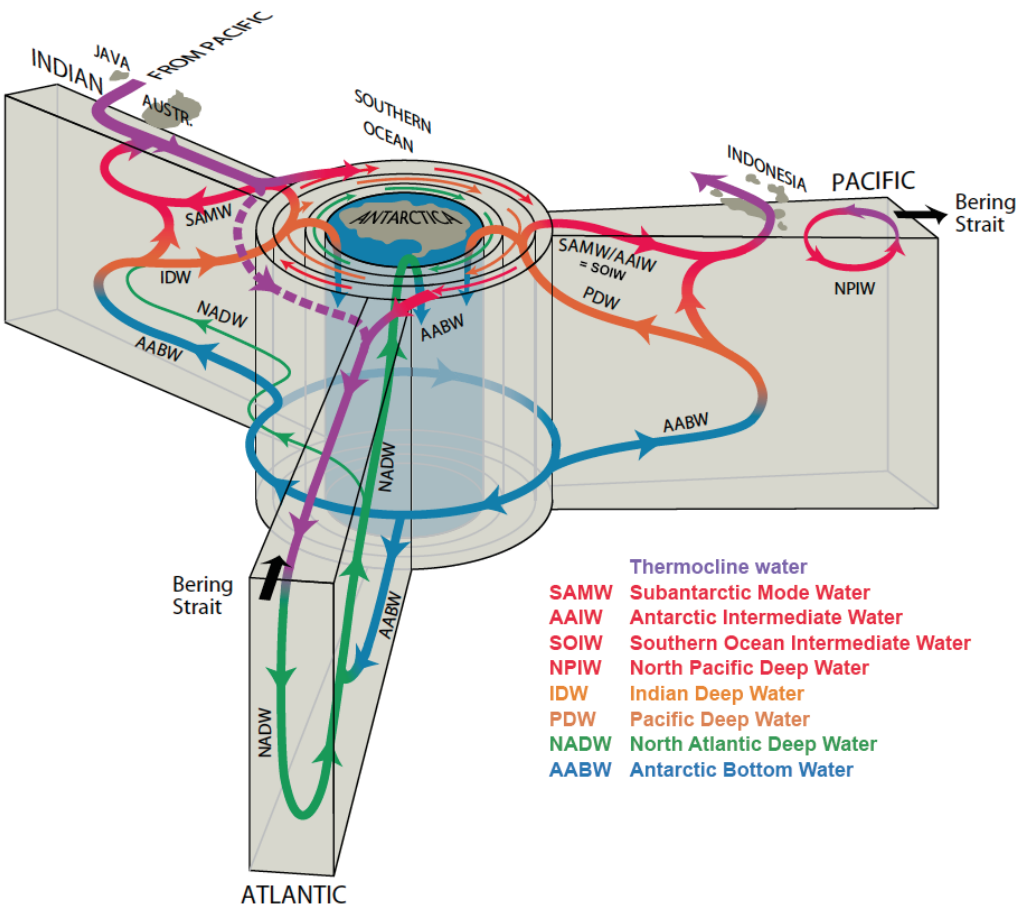

Figure 1.1. Modern global ocean overturning circulation schema from a Southern Ocean perspective [figure taken from *Talley*, 2013].

in the depth of the thermocline along the equator and a simultaneous shift of the wind systems (the combined effect was termed El Niño Southern Oscillation, ENSO) does not only affect regional fauna and precipitation, but also global climate through strong inter-hemispheric, extra-tropical and cross-basin connections [*Collins et al*., 2010; *NOAA* 2016]. Over longer timescales, changes in the strength and variability of the WPWP affect the east-west temperature gradient and is thus responsible for past ENSO variability [*Ford et al*., 2015]. In addition, variations in nutrient utilization revealed by silicon and nitrogen isotopes [*Pichevin et al*., 2009; *Dubois and Kienast*, 2011] as well as fluctuations in thorium-normalized organic carbon fluxes [*Kienast et al.*, 2007] indicate that equatorial productivity varied over glacial-interglacial timescales. The proposed invigorated biological pump in the Eastern Equatorial Pacific (EEP) during glacial boundary conditions [*Pichevin et al*., 2009] was attributed to a shift in the nutrient composition of equatorial upper-ocean waters due to variations in the nutrient injection of its end-member sources [*Loubere et al.,* 2003; *Robinson et al*., 2009; *Dubois et al.*, 2011; *Hendry and Brzezinski*, 2014]. As the EEP acts as one of the largest CO_2 sources on Earth today [*Takahashi et al*., 2009], a change in the nutrient concentration and an associated shift in productivity would have large repercussions for the atmospheric CO_2 budget. Hence, the equatorial Pacific is an important region for studying long-term environmental changes on both regional and global scales.

1.2 Modern oceanographic setting

The equatorial Pacific is characterized by a complex and highly dynamic current system. The westward flowing North Equatorial Current (NEC) and the South Equatorial Current (SEC) are both wind-driven surface currents, which respond quickly to variations in the wind field. The inter-hemispheric differences in the distribution of landmass and ocean area lead to stronger southern hemispheric wind field component and as a result, the SEC extends from 5°N to 25°S, whereas the NEC is strongest at ~15°N (Figure 1.2a) [*Tomczak and Godfrey*, 2005; *Kessler*, 2006]. Around the Philippines, the NEC divides into a northern branch (Kuroshio Current, KC) and a southern branch, which, in turn, feeds the eastward flowing North Equatorial Counter Current (NECC). The NECC, centred at 5°N, is also partly fed by the northern extension of the SEC during the southwest monsoon [*Tomczak and Godfrey*, 2005].

Despite the intensive surface currents, the most prominent current in the equatorial Pacific is the eastward-directed Equatorial Under Current (EUC) and the northern and southern subsurface countercurrents (NSCC and SSCC, respectively; also termed Tsuchiya Jets after *Tsuchiya*, [1972]) [*Johnson and Moore*, 1997; *Rowe et al*., 2000]. The EUC with a maximum width of 500 km extends from 40 to 280 m water depth with its peak velocity at ~200 m [*Wyrtki and Kilonski*, 1984; *Johnson et al*., 2002; *Tomczak and Godfrey*, 2005; *Grenier et al*., 2011]. As the EUC flows eastward across the equatorial Pacific its upper branch shoals parallel with the thermocline providing nutrients to the euphotic zone, stimulating primary productivity [*Dugdale et al*., 2002; *Ryan et al*., 2006]. The lower branch of the EUC does not upwell along the equator, but as it travels across the equator it receives nutrients from the Equatorial Pacific Intermediate Water (EqPIW) and provides nutrients to the upper EUC by diapycnal mixing [*Dugdale et al*., 2002; *Qu et al.*, 2009; *Bostock et al*., 2010; *Rafter and Sigman*, 2015]. Nutrients within the EUC and the underlying EqPIW primarily originate in the extra-tropical high-nutrient low-chlorophyll (HNLC) regions [*Johnson et al*., 2002; *Goodman et al*., 2005; *Qu et al*., 2009; *Grenier et al*., 2011]. To date, the EUC and EqPIW are mainly fed by nutrient-rich Pacific Deep Water (PDW) and SOIW and only a minor proportion can be attributed to North Pacific Intermediate Water (NPIW) (Figure 1.2b) [*Goodman et al*., 2005; *Tomczak and Godfrey*, 2005; *Bostock et al.*, 2010].

PDW is formed via the return flow of Circumpolar Deep Water (CDW) and Antarctic Bottom Water (AABW). CDW and AABW are formed primarily within the Antarctic Circumpolar Current and move slowly from the Southern Ocean towards the North Pacific. On its way, remineralisation of organic material and continuous biological export production from above leads to decreasing oxygen concentrations and nutrient accumulation. As a result, PDW is the oldest, most nutrient- and CO_2-enriched water mass in global ocean that occupies a depth range of 1500 – 3300 m [*Tomczak and Godfrey*, 2005; *Talley*, 2008].

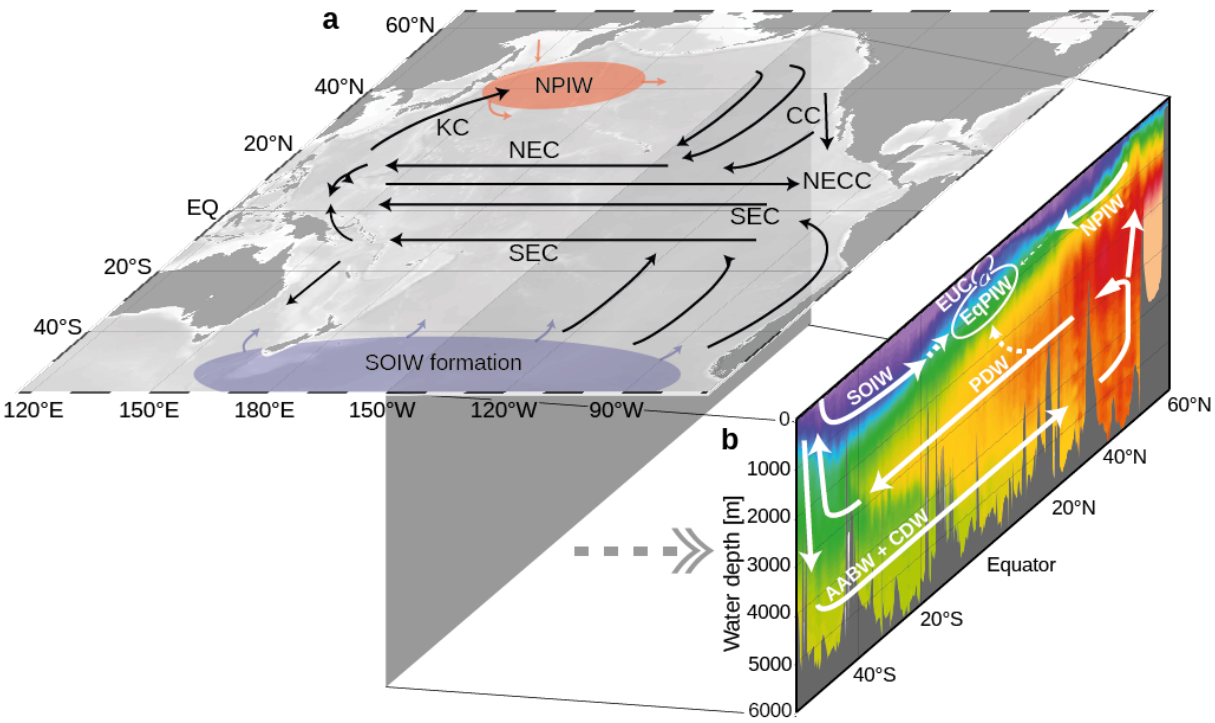

Figure 1.2. Map of the Pacific Ocean with major currents and water masses [after *Tchernia*, 1980; *Tomczak and Godfrey*, 2005; *Kessler*, 2006; *Bostock et al.*, 2010]. a: Surface water currents with formation region of Southern Ocean Intermediate Water (SOIW) and North Pacific Intermediate Water (NPIW). CC = California Current; KC = Kuroshio Current; NEC = North Equatorial Current; NECC = North Equatorial Counter Current; SEC = South Equatorial Current. b: Meridional depth transect of silicic acid concentration with major intermediate and deep currents overlain: EUC = Equatorial Undercurrent, EqPIW = Equatorial Pacific Intermediate Water, NPIW, SOIW, PDW = Pacific Deep Water, AABW = Antarctic Bottom Water, CDW = Circumpolar Deep Water. Colour shading shows silicic acid concentration with red indicating high concentrations and blue colours low silicic acid concentrations. Map and transect were generated using Ocean Data View [*Schlitzer*, 2015] with GLODAP Bottle Data [*Key et al.*, 2004].

SOIW comprises Subantarctic Mode Water (SAMW) and Antarctic Intermediate Water (AAIW) [after *Pena et al.*, 2013]. As SAMW travels within the Antarctic Circumpolar Current around the Antarctic continent it cools and freshens through deep winter mixing and isopycnal exchange along and across the Subantarctic Front [*McCartney*, 1977; *Bostock et al.*, 2013]. The densest SAMW near the Polar Front forms AAIW, which is characterized by a prominent salinity minimum (34.4 – 34.5) and an average potential density of 27.1 σ_θ [*McCartney*, 1977; *Bostock et al.*, 2010; 2013]. Different formation areas of AAIW exist but the majority is formed in the southeast Pacific Ocean, off southern Chile [*Sallée et al*, 2010; *Bostock et al.*, 2013]. Diatom blooms in the formation regions of SOIW remove silicic acid ($Si(OH)_4$) out of the surface waters and as a result, SOIW contains depleted silicon to nitrogen ratios [*Sarmiento et al.*, 2004; *Hendry and Brzezinski*, 2014]. The relatively low-silicon SOIW is then subducted along an isopycnal surface between 300 and 1300 m [*Sloyan and Rintoul*, 2001; *Bostock et al.*, 2013] and seems to follow the wind-driven

subtropical gyre water circulation equatorwards before feeding into the low-latitude equatorial thermocline and intermediate waters [*Tomczak and Godfrey*, 2005]. This has the effect that, although approximately two-thirds of EUC waters are supplied by SOIW today [*Goodman et al*., 2005; *Qu et al*., 2009], SOIW contributes about half of the nitrate supply and only roughly 30 % of the total modern equatorial $Si(OH)_4$ supply [*Dugdale et al*., 2002; *Sarmiento et al.*, 2004].

Today, NPIW only contributes insignificantly to EqPIW (Figure 1.2b). In contrast to SOIW, nutrient depletion by biological productivity is relatively limited in NPIW as it is never exposed to the surface and consequently, nutrient levels remain high [*Talley*, 1991; *Sarmiento et al.*, 2004]. A mixing of different water masses in the northwest Pacific with the major contribution of Okhotsk Sea Intermediate Water (OSIW) forms NPIW. OSIW, in turn, is formed in coastal polynyas during wintertime sea-ice formation within the Sea of Okhotsk [*Talley*, 1993; *Shcherbina et al*., 2003]. NPIW spreads out at 300 – 800 m water depth and is characterized by a salinity minimum (33.9 – 34.1) with low oxygen concentrations (0 – 150 µmol/kg) and an average potential density of 26.8 σ_θ [*Dickson et al*., 2000; *Bostock et al*., 2010]. Although, the lateral extent of NPIW is restricted to 15 – 20°N today, the influence NPIW extends to the equatorial Pacific through the Celebes Sea, where it accounts for ~70 % of the modern $Si(OH)_4$ supply [*Sarmiento et al*., 2004; *Bostock et al.*, 2010].

1.2.1 Western Pacific Warm Pool versus Pacific Equatorial Divergence

The equatorial Pacific is divided into two distinct biogeochemical provinces: the WPWP and the contrasting EEP with offshore equatorial upwelling (also termed Pacific Equatorial Divergence, PEqD) (Figure 1.3a). The WPWP is the largest warm water body on Earth. The surface layer is characterised by temperatures consistently higher than 28°C, low salinities (<35) and relatively low nutrient concentrations (<0.1 µM NO_3^- ; <0.2 µM PO_4^{3-}) [*Yan et al.*, 1992; *Blanchot et al*., 2001; *Rafter and Sigman,* 2015]. The pycnocline, which is associated with the deep thermocline, separates oligotrophic surface waters from nutrient-enriched sub-surface water masses [*Herbland and Voituriez*, 1979; *Mackey et al.*, 1995; *Radenac and Rodier*, 1996]. The equatorial thermocline shoals from the west to the east Pacific, reaching depths as shallow as 30 m in the EEP (Figure 1.3b) [*Locarnini et al.,* 2013]. The shoaled thermocline in the eastern Pacific results in the PEqD being characterized by lower temperatures (<28°C), higher salinities (>35) and elevated macronutrients levels (3 – 4 µM NO_3^- ; 0.4 – 0.5 µM PO_4^{3-}) [*Blanchot et al.*, 2001; *Le Borgne et al*., 2002]. Although chlorophyll-a concentrations are higher in the PEqD compared to the WPWP, primary productivity by siliceous phytoplankton is hindered in the PEqD due to the limitation of $Si(OH)_4$ and iron [*Broecker and Peng*, 1982; *Dugdale et al.*, 2002; *Sarmiento et al*., 2004; *Ryan et al*., 2006]. This makes the PEqD (in particular the EEP) one of the largest HNLC regions of the world [*Minas et al*., 1986]. As a consequence of the low productivity, the EEP acts as the main global marine source for atmospheric CO_2 today [*Takahashi et al*., 2009].

Another important feature of the equatorial Pacific is the interannual instability in the coupled ocean-atmosphere system known as ENSO. On timescales between two to seven years the EEP experiences anomalously warm (El Niño) and cold (La Niña) conditions, and the opposite in the WPWP. These swings in temperature are associated with changes in the depth of the thermocline and consequently with variations in the availability of nutrients in the photic zone [*Le Borgne et al*., 2002]. Through changes in primary productivity, ENSO is expected to have large repercussions for global atmospheric CO_2 concentrations and the global carbon budget [*Feely et al*., 2002]. Additionally, during ENSO, the strength of the trade winds and the position of the atmospheric convection influence the hydrography of the equatorial Pacific [*Collins et al*., 2010]. Changes in the atmospheric convection affects the upwelling of water masses along the equator and thereby, the zonal extension of the WPWP and PEqD [*Le Borgne et al*., 2002].

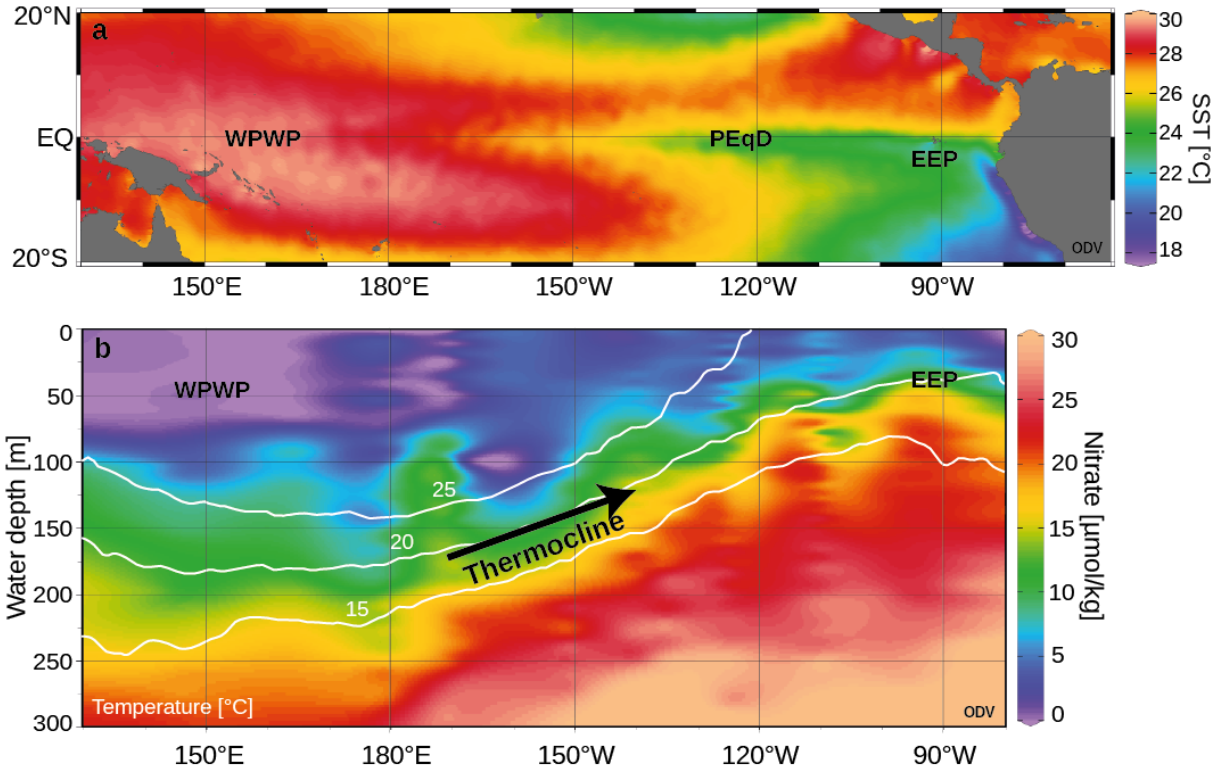

Figure 1.3. Annual temperatures and nitrate concentrations in the equatorial Pacific. a: annual Sea-Surface Temperature (SST) map with the Western Pacific Warm Pool (WPWP), the Pacific Equatorial Divergence (PEqD) and the Eastern Equatorial Pacific (EEP). b: zonal annual nitrate concentrations overlaid by annual temperature contours (white) along the equator showing the higher nitrate concentration in subsurface waters of the EEP compared to the WPWP concurrent with the shoaling of the thermocline. Surface map and transect were generated using Ocean Data View [*Schlitzer*, 2015] with data of the World Ocean Atlas 2013 [a, *Locarnini et al*., 2013] and GLODAP Bottle Data [b, *Key et al*., 2004].

1.3 Relevant (paleoceanographic) research related to this thesis

Information regarding past ocean and climate changes can be decrypted using paleoceanographic proxies. A commonly used archive to measure the of desired but unobservable variables such as temperature, salinity and surface water CO_2 concentrations, are carbonate shells of planktonic foraminifera, a group of cosmopolitan free-floating marine protozoa. Foraminifera live vertically dispersed in the upper ocean water column, with different species dwelling in distinct water masses. It should be noted that for precise interpretation of paleo-data from foraminifera, it is crucial to know the calcification depth of the analysed foraminiferal species as precisely as possible. Planktonic foraminifera are known to migrate within the water column during their ontogeny [*Hemleben and Bijma*, 1994]. Consequently, the reconstructed habitat depth using geochemical signals will always represent an integrated signal across the entire water depth range and ontogeny of the species and should therefore be referred to as the Apparent Calcification Depth (ACD). Information about foraminiferal ACDs from the equatorial Pacific are limited. Previous studies from the equatorial Pacific rather focussed on foraminiferal fluxes [*Thunell and Honjo*, 1981; *Fairbanks et al*., 1982; *Thunell et al*., 1983; *Kawahata et al*., 2002; *Yamasaki et al*., 2008]. The few studies reconstructing ACDs have either concentrated on the reconstruction of past oceanic conditions with known ACDs from other ocean basins [*Wara et al.*, 2005; *Russon et al*., 2010], or used surface sediments from the central or EEP [*Faul et al.*, 2000; *Lynch-Stieglitz et al*., 2015; *Nürnberg et al.*, 2015]. However, foraminiferal ACDs have been shown to differ regionally [*Faul et al.,* 2000; *Steph et al.*, 2009]. This is especially true for sub-surface and thermocline species such as *Neogloboquadrina dutertrei*, as the thermocline varies substantially in a highly dynamic system like the EEP [*Loubere,* 2001; *Nürnberg et al*., 2015]. The use of ACDs reconstructed from other ocean basins to target specific water masses is therefore risky and highlights the need for a precise ACD estimation from the equatorial Pacific.

Over the last half a century, it has been revealed that carbon isotope ($\delta^{13}C$) values of foraminifera can be used to reconstruct past ocean circulation and nutrient changes [*Shackleton*, 1974; *Duplessy et al*., 1984; *Zahn et al*., 1991; *Curry and Oppo*, 2005; *Bostock et al*., 2010; *Knudson and Ravelo*, 2015a]. However, due to a variety of factors (see *Chapter 1.4.2*) foraminiferal $\delta^{13}C$ can deviate from the total dissolved inorganic carbon of ambient seawater ($\delta^{13}C_{DIC}$), which might lead to distorted interpretations of past nutrient conditions [*Oppo and Fairbanks,* 1989; *Spero et al*., 1991; *Kroon and Darling,* 1995; *Birch et al*. 2013]. Consequently, a possible foraminiferal $\delta^{13}C$-disequilibrium should be considered when interpreting paleo-data.

Reconstructing past ocean dynamics in the equatorial Pacific is important for regional and global climate, as the EEP is the most important source for marine CO_2 release into the atmosphere under modern conditions [*Takahashi et al*., 2009]. The release of CO_2 from the surface ocean in regions of upwelling is counteracted by carbon fixation of siliceous phytoplankton [*Dugdale and Wilkerson,* 1998]. However, the productivity of these biogenic organisms in the EEP is

hindered by the low availability of $Si(OH)_4$ and iron today [*Broecker and Peng*, 1982; *Dugdale et al.*, 2002; *Sarmiento et al*., 2004; *Ryan et al*., 2006]. The main contributor to equatorial thermocline waters, the SOIW is characterized by high nitrate but low $Si(OH)_4$ concentrations [*Sarmiento et al*., 2004]. During the Last Glacial Maximum (LGM), an enhanced productivity in the EEP suggests that the $Si(OH)_4$ limitation was overcome, requiring the supply of at least three times more $Si(OH)_4$ to the system [*Pichevin et al*., 2009]. Nevertheless, the source of this $Si(OH)_4$ remains enigmatic. On the one hand, it has been suggested that a higher contribution of southern-sourced waters towards the equatorial Pacific thermocline resulted in higher nutrient concentrations [*Pena et al*., 2008]. Supporting evidence for a greater influence of southern-source waters in the Pacific comes from an authigenic mineral study from the Chilean margin that reports higher oxygen concentrations related to an enhanced production of SOIW during glacials [*Muratli et al*., 2010]. In addition, a neodymium isotope (ε_{Nd}) record [*Pena et al*., 2013], and shallow and deep-water radiocarbon activity ($\Delta^{14}C$) reconstructions in the EEP [*de la Fuente et al*., 2015] suggest that relatively old, deep-southern sourced water masses upwell at the equator during glacial boundary conditions. On the other hand, a recent $\delta^{13}C$ and oxygen isotope ($\delta^{18}O$) reconstruction combined with modelling results from the southwest Pacific argue for a decrease in the vertical extent of SOIW during glacial times [*Ronge et al*., 2015]. This reinforced the interpretation from previous stable isotope reconstructions from the southwest Pacific that proposed a reduced production of SOIW under glacial conditions [*Pahnke and Zahn*, 2005] for at least 400 ka [*Elmore et al*., 2015]. In addition to these isotope reconstructions, there is growing debate over whether SOIW was capable of stimulating productivity at the equatorial Pacific. Recent silicon and nitrogen isotope reconstructions argue for a “nutrient-trapping” in the Southern Ocean leaving the northward penetrating intermediate water depleted in nutrients under glacial conditions [*Hendry and Brzezinski*, 2014; *Robinson et al*., 2014; *Rousseau et al*., 2016].

In the North Pacific, a ε_{Nd} record and foraminiferal isotope studies suggest a shift in the formation region of Glacial North Pacific Intermediate Water (GNPIW) from mainly the Sea of Okhotsk towards the northwest Pacific during glacial boundary conditions [*Horikawa et al*., 2010; *Rella et al.,* 2012; *Max et al*., 2014]. Simultaneously, a variety of $\delta^{13}C$ records propose an increased formation and strengthened mid-depth circulation (1000 – 1500 m water depth) in the North Pacific during the last glacial maximum (LGM) [*Duplessy et al*., 1988; *Herguera et al.,* 1992; *Keigwin*, 1998; *Matsumoto et al*., 2002a; *Cook et al.,* 2016]. A recent endobenthic foraminiferal $\delta^{13}C$ study demonstrates that this increased GNPIW formation occurred during glacials at least since the mid-Pleistocene [*Knudson and Ravelo*, 2015a]. The enhanced GNPIW might have expanded further south along the California margin [*Stott et al*., 2000] and the Eastern Tropical North Pacific (ETNP) [*Leduc et al*., 2010]. In the EEP, a very recent Pacific ε_{Nd} data compilation revealed a substantial LGM to Holocene shift in ε_{Nd} values that can only be explained by a higher contribution from northern-sourced waters [*Hu et al.,* 2016]. However, it has not yet been revealed how the proposed diminished SOIW and enhanced GNPIW convection might have influ-

enced the nutrient distribution and biological productivity beyond the northern high latitudes during the LGM and further back in time.

1.4 Planktonic foraminifera as paleo-proxies

1.4.1 Brief overview on planktonic foraminiferal ecology

Planktonic foraminifera are exclusively marine eukaryotic protozoans that are globally distributed in the upper water column of the world's ocean [*Hemleben et al*., 1989]. A prominent feature is the formation of a calcium carbonate shell (= test), on which modern taxonomic classification is based on. Up to 50 extant planktonic foraminiferal species have been identified, which can be divided into spinose and non-spinose species [*Schiebel and Hemleben*, 2005]. Although, planktonic foraminifera are generally heterotrophic [*Hemleben et al*., 1989], some species, in particular spinose species, possess algal symbionts. These symbionts, which are mainly dinoflagellates, produce energy through photosynthesis, which the foraminifera use to drive the calcification process [*Schiebel and Hemleben*, 2005].

The abundance of planktonic foraminiferal species strongly depends on environmental parameters, resulting in a species characteristic biogeographic distribution. Five major faunal provinces were determined: tropic, subtropic, transitional, subpolar and polar [*Bé*, 1977]. The provinciality in modern foraminifers is restricted to global climate belts and hence typically to the thermal structure of the water column [*Bé and Tolderlund*, 1971]. Nevertheless, other factors such as salinity, radiation for symbiont-bearing species, turbidity of the ambient water, food supply and distribution of predators determine the spatial and vertical distribution as well [*Bijma et al*., 1990; *Watkins et al.*, 1996; *Schiebel and Hemleben*, 2005]. Plankton tow analysis revealed that living species are restricted to the euphotic zone and the quantity decreases with increasing water depth. Although changes in salinity play only a marginal role for the foraminiferal depth distribution directly, it affects the density structure of the water column and thereby the accumulation of nutrients in certain depths. As certain species of planktonic foraminifera are often associated with the deep chlorophyll maximum (DCM) where nutrients accumulate [*Fairbanks et al.*, 1982; *Schiebel et al.*, 2001], salinity might therefore affect foraminiferal depth distribution indirectly. Consequently, their distinct distribution is mainly controlled by the prevailing surface hydrography and each species inhabit characteristic ecological niches [*Fairbanks and Wiebe*, 1980; *Schiebel and Hemleben*, 2005].

The formation of calcium carbonate ($CaCO_3$) tests makes planktonic foraminifera an important carbonate producer with an average of 1.3 – 3.2 Gt $CaCO_3$ per year in the global ocean [*Schiebel*, 2002]. During their ontogeny (maturation), the majority of foraminifera migrate through the water column, whilst adding new chambers and covering and thickening the whole pre-existing test by an additional layer of calcite [*Kozdon et al.,* 2009]. Thus, the calcite records the

varying temperatures and salinity of the respective water depth. As each successive chamber is larger and heavier than the previous chamber [*Hemleben and Bijma*, 1994], the shell weight and therefore the geochemical signature of the whole shell, is determined by the last few chambers. During the final phase that is associated with gametogenesis, spinose foraminifera shed their spines, eject the symbionts and secrete a smooth veneer of calcite covering spine holes [*Hemleben et al*., 1989]. Following gametogenesis, planktonic foraminiferal tests sink to the seafloor, constituting 32 – 80 % of the total deep-marine calcite budget [*Schiebel and Hemleben*, 2005]. Due to their global distribution, their specific adaption to environmental conditions, their good fossilization potential and continuous occurrence in the geological record since the Jurassic about 180 Ma ago [*Cifelli,* 1969], planktonic foraminifera tests are frequently used to decrypt past ecological and oceanographic conditions.

1.4.2 General influences on foraminiferal shells

Foraminiferal tests are the by far most commonly analysed carbonates for reconstructing past environmental changes such as the thermal structure of the water column, depth of thermocline, nutrient cycling, circulation changes, and ventilation changes. The application is based on the relationship between foraminiferal calcite and the ambient seawater. However, there are a number of physical, chemical and biological effects on both regional and global scales which may affect the fidelity of foraminiferal calcite to reflect ambient seawater (Figure 1.4) [*Schiebel and Hemleben*, 2005].

1.4.2.1 Stable isotopes

The incorporation of oxygen and carbon isotopes into foraminiferal calcite is affected by isotopic fractionation. Generally, isotopic fractionation is defined as “the partitioning of isotopes between two substances or two phases of the same substance with different isotope ratios” [*Hoefs*, 2009]. In this regard, a distinction is made between equilibrium isotope fractionation and non-equilibrium fractionation. Equilibrium isotope fractionation occurs usually during isotope exchange reactions, e.g. air-sea gas exchange. It involves the forward and backward isotope reaction rates among various well-mixed systems. In contrast, non-equilibrium fractionation is the result of incomplete or unidirectional processes such as kinetic isotope effects in chemical reactions, evaporation, photosynthesis and metabolic effects. This non-equilibrium reactions favour reaction of the lighter isotope compared to the heavier isotope, since light isotopes have a higher mobility [*Zeebe and Wolf-Gladrow*, 2001].

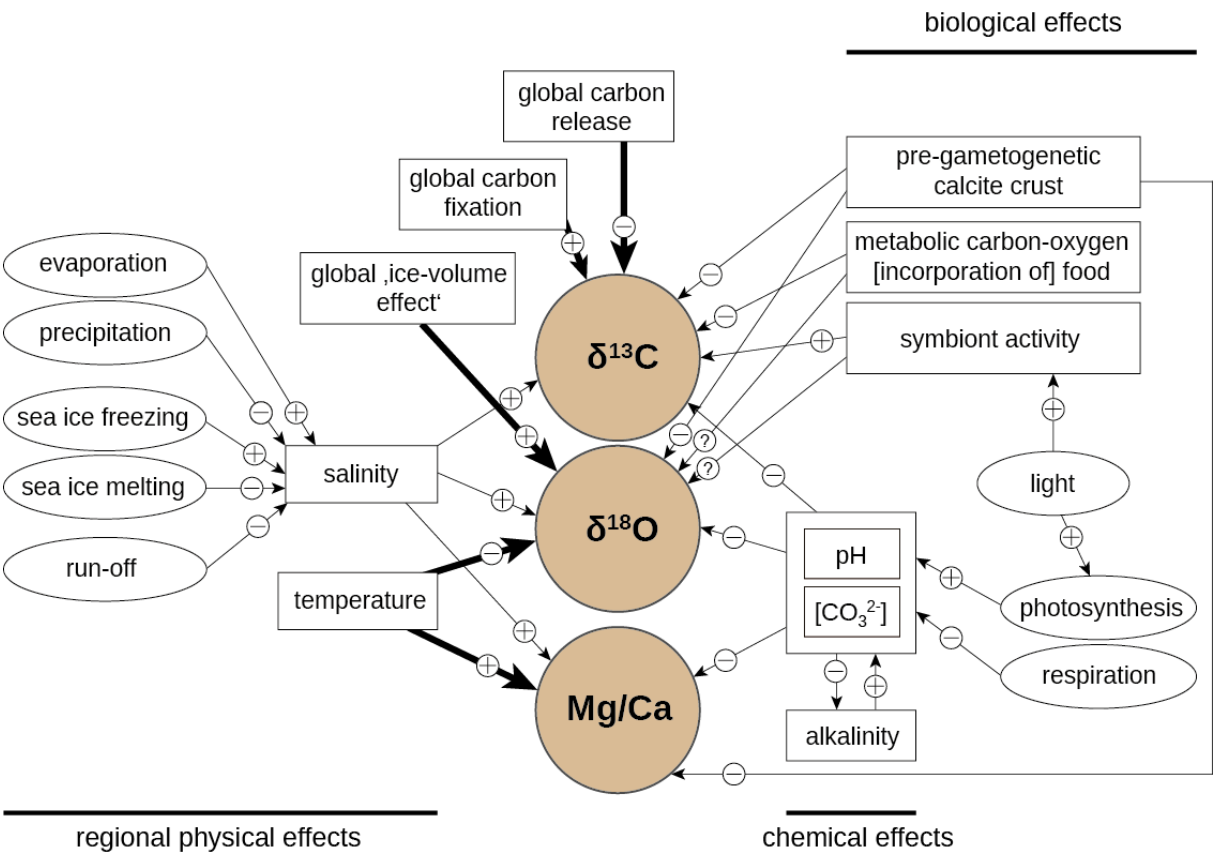

Figure 1.4. Summary of the influencing factors on the stable oxygen ($\delta^{18}O$) and carbon ($\delta^{13}C$) isotope composition as well as on the Magnesium/Calcium (Mg/Ca) ratio of planktonic foraminiferal tests. Bold arrows mark predominant effects. Positive and negative correlations are indicated by [+] and [-], respectively [modified after *Schiebel and Hemleben*, 2005].

Oxygen isotopes

The oxygen isotope composition of the foraminiferal calcite ($\delta^{18}O_{calcite}$) reflects the oxygen isotope composition of the ambient seawater ($\delta^{18}O_{seawater}$) with a temperature-dependent fractionation between ^{18}O and ^{16}O [*McCrea*, 1950]. In this context, at higher temperatures less ^{18}O is incorporated into the calcite shell and vice versa. Besides the dominating role of temperature, there are several processes that affect the $\delta^{18}O_{seawater}$ itself, which have implications for the $\delta^{18}O_{calcite}$. These processes include local changes due to evaporation and precipitation, input of continental freshwater, and storage of light isotopes in continental ice ('ice-volume effect') [*Craig and Gordon*, 1965; *Dansgaard and Tauber*, 1969; *Siegenthaler et al.*, 1979]. The periodic growth and decay of continental ice caps was first described by *Shackleton* [1967] and is now a well-established stratigraphic tool, the so-called Marine Isotope Stages (MIS) [*Emiliani*, 1955]. Furthermore, some species precipitate calcite in disequilibrium from ambient $\delta^{18}O_{seawater}$ due to so-called "vital effects" [*Urey et al.*, 1951; *Wefer*, 1985; *Niebler et al.*, 1999]. These vital effects include ontogenetic effects, symbiont photosynthesis effects, respiration effects and effects of changes in the carbonate ion concentration of seawater (also referred to as pH effect) [*Hemleben*

et al., 1989; *Wefer and Berger*, 1991; *Spero and Lea*, 1993; *Ravelo and Fairbanks*, 1995; *Bijma et al.*, 1999; *Niebler et al*., 1999; *Bemis et al*., 2000; *Birch et al.*, 2013].

Since the pioneer work of *Urey* [1947], the use of $\delta^{18}O_{calcite}$ became a basic tool in paleoceanography. The $\delta^{18}O$-paleotemperature calculations were first established and applied by *Epstein et al*. [1951], *Urey et al.* [1951], and *Emiliani* [1955]. Since then, a number of empirically-derived paleotemperature equations have been developed on both inorganically precipitated carbonates and foraminiferal calcite [*Shackleton*, 1974; *Erez and Luz*, 1983; *Kim and O'Neil*, 1997; *Bemis et al*., 1998; *Anand et al*., 2003; *Mulitza et al*., 2004; *Mohtadi et al.*, 2009]. These foraminiferal-derived equations can be either generic or species-specific, and have been generated using either cultured species, plankton tow samples or living samples from the water column [*Bemis et al*., 1998; *Ganssen and Kroon*, 2000; *Dekens et al*., 2002; *Regenberg et al*., 2009; *Dueñas-Bohórquez et al*., 2011]. They all have basic similarities, but small differences among them can result in different temperature estimates when applying to the same isotope sample (Figure 1.5) [*Bemis et al*., 1998; *King and Howard*, 2005; *Wejnert et al*., 2013].

Another research approach is the use of paleotemperature equations to calculate the predicted theoretical inorganic calcite value ($\delta^{18}O_{equilibrium}$) that is precipitated in isotopic equilibrium with the ambient temperature and $\delta^{18}O_{seawater}$ [*Regenberg et al*., 2009; *Steph et al.*, 2009]. The comparison of measured foraminiferal $\delta^{18}O_{calcite}$ values with predicted $\delta^{18}O_{equilibrium}$ can be used to assess the ACD of a species by integrating the entire calcification history of a specimen.

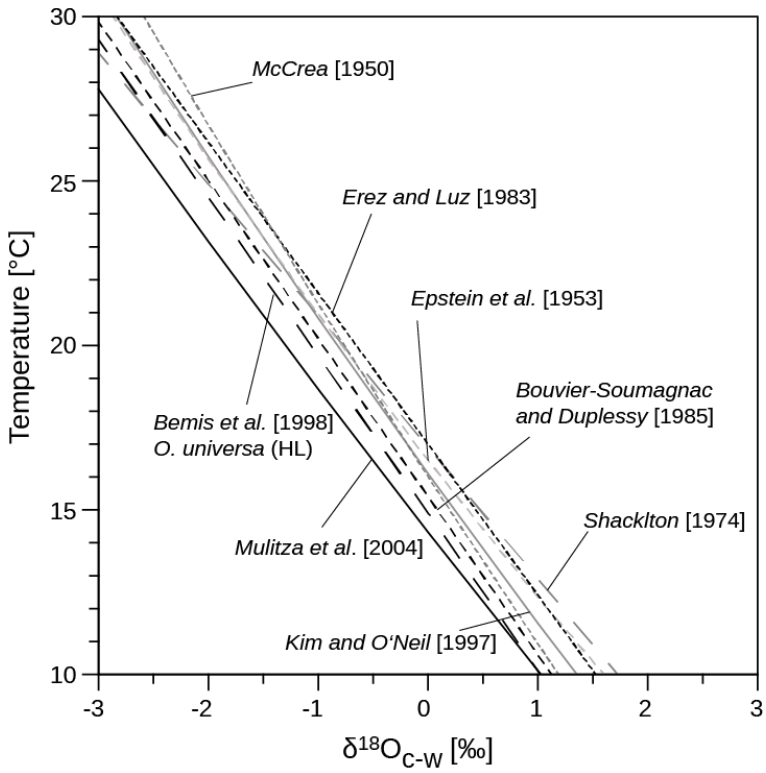

Figure 1.5. Temperature versus $\delta^{18}O_{calcite\ minus\ seawater\ [c\text{-}w]}$ with various published paleotemperature equations [modified after *Bemis et al*., 1998].

Carbon isotopes

Shell formation of foraminifera is closely coupled to the $\delta^{13}C_{DIC}$ of the ambient seawater [*Berger et al.,* 1978*; Spero,* 1992]. Modern ocean $\delta^{13}C_{DIC}$ values typically range from -1 ‰ to +3 ‰. However, the $\delta^{13}C_{DIC}$ is neither distributed uniformly nor is it constant over time. Long-term changes involve the interaction between the atmosphere, ocean and terrestrial biosphere as well as geological reservoirs. Short-term $\delta^{13}C_{DIC}$ modulations involve (a) changes in air-sea fractionation due to thermodynamic effects, which are especially important in cold waters at high latitudes [*Broecker and Maier-Reimer*, 1992; *Lynch-Stieglitz et al*., 1995; *Mackensen*, 2012], (b) the photosynthesis-respiration cycle [*Broecker,* 1982; *Kroopnick*, 1985; *Rohling and Cook*, 1999], (c) whole-ocean variations in the carbonate chemistry of seawater [*Spero et al*., 1997], (d) advective and diffusive mixing processes during water mass circulation, and (e) changes in species habitat or ecology (especially in planktonic species).

Planktonic foraminiferal $\delta^{13}C$ usually varies between -2 ‰ and +2 ‰ [*Wefer and Berger*, 1991] and has been shown to be a reliable tracer for past oceanic circulation and nutrient reconstructions [*Shackleton*, 1974; *Duplessy et al*., 1984; *Curry et al*., 1988; *Oppo and Fairbanks*, 1990; *Zahn et al.,* 1991; *Sarnthein et al*., 1994; *Mackensen et al*., 2001; *Bickert and Mackensen*, 2004; *Curry and Oppo*, 2005; *Bostock et al*., 2010; *Knudson and Ravelo*, 2015a]. However, it should be noted that a number of factors can result in foraminifera secreting their carbonate shell in $\delta^{13}C$ disequilibrium with ambient seawater. Such factors include algal photosynthesis [*Bé et. al*, 1982; *Hemleben et al*., 1989], metabolic fractionation [*Wefer and Berger*, 1991; *Kroon and Darling*, 1995; *Spero et al*., 1997], food availability [*Spero et al.,* 1991; *Ortiz et al*., 1996], and carbonate chemistry of the seawater [*Spero et al*., 1997; *Bijma et al*., 1999]. These factors should be taken into account when interpreting foraminiferal $\delta^{13}C$ to reconstruct past ocean conditions.

1.4.2.2 Mg/Ca paleothermometry

Measuring the elemental composition of Magnesium (Mg) to Calcium (Ca) in foraminiferal calcite enables the reconstruction of past ocean temperatures. The substitution of Ca by the divalent cation Mg is primarily dependent on the temperature of the ambient seawater with high Mg incorporation at high temperatures and vice versa (Figure 1.6) [*Blackmon and Todd*, 1959; *Nürnberg,* 1995*; Nürnberg et al*., 1996; *Lea et al*., 1999]. Culture based [*Nürnberg et al*., 1996; *Lea et al*., 1999; *Dueñas-Bohórquez et al*., 2009, 2011], core-top [*Dekens et al*., 2002; *Elderfield and Ganssen*, 2000; *Elderfield et al*., 2002; *Regenberg et al*., 2009] and sediment trap [*Anand et al.*, 2003; *Mohtadi et al*., 2009; *Friedrich et al.*, 2012] studies have developed species-specific Mg/Ca-paleotemperature equations and established the foraminiferal Mg/Ca paleothermometry as a key paleoceanographic tool for reconstructing past ocean temperatures [*Nürnberg*, 1995; *Nürnberg et al*., 1996, *Rosenthal et al*., 1997; Nürnberg et al., 2000; *Lea et al*., 2000; *Stott et al.*, 2002; *Russell et al*., 2004; *Dueñas-Bohórquez et al*., 2011; *Rosenthal et al*., 2013; *Steinke et al.*, 2014; *Spero et al*., 2015]. Other environmental factors such as salinity or seawater pH have only

a marginal influence due to the relative overpowering control of temperature on foraminiferal Mg [*Lea et al*., 1999; *Kısakürek et al*., 2008; *Yu and Elderfield*, 2008; *Arbuszewski et al*., 2010; *Hönisch et al*., 2013; *Spero et al*. 2015].

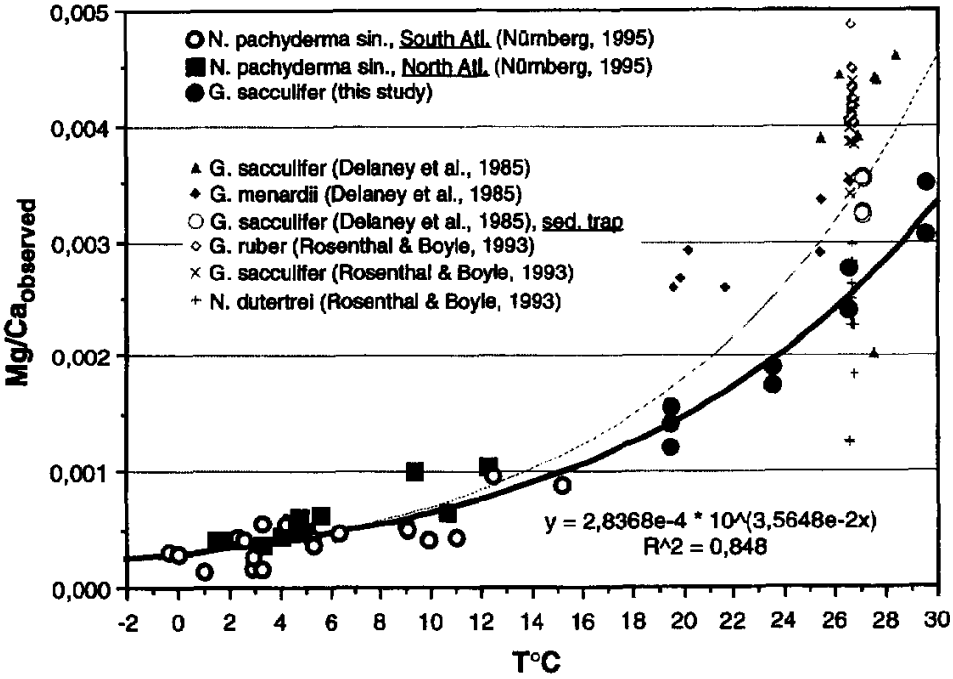

Figure 1.6. Mg/Ca ratios of various planktonic foraminifera species versus water temperature imply an exponential relationship between test chemistry and temperature [figure taken from *Nürnberg et al.*, 1996].

1.5 Aims of the thesis

Understanding the causes and consequences of climate change on glacial-interglacial time-scales are a key goal for global climate research. The equatorial Pacific with the large WPWP and the contrasting EEP upwelling system has been long in the focus of (paleo-)climatic research, as strength and variability of both regions have large effects on global climate. Varying nutrient concentrations in the EEP might have caused changes in the primary productivity and hence, CO_2 concentrations during the last glacial cycles. However, the source for these changes remains elusive. The Southern Ocean has been a focal point in trying to determine the source of glacial-interglacial changes in the equatorial Pacific, as SOIW is the main contributor to the equatorial thermocline today. With new sediment cores available now from the Pacific sector of the Southern Ocean, there is growing debate about the SOIW influence on the equatorial upwelling system during glacials. Detailed information concerning the northern high latitudes mostly focuses on the North Atlantic, as high-resolution records from the North Pacific were relatively scarce. However, more recently, newly recovered sediment material from the Bering Sea and Sea of Okhotsk highlight substantial changes in ocean circulation in the North Pacific. This allows for the first time to compare records from the source region of SOIW and NPIW with equatorial Pacific

records to decipher changes in the relative contribution of extra-tropical intermediate waters on the nutrient distribution of equatorial water masses.

Tracing the water mass signals over time requires reliable paleoproxies. Geochemical studies on planktonic foraminifera are an established tool for paleoceanographic reconstructions, including the reconstruction of water temperatures, salinities as well as productivity and circulation changes (see *Chapter 1.3*). However, using these approaches requires a precise knowledge of the calcification depth of the foraminiferal species.

Thus, the aims of this thesis are:

1) to examine the proxy-generation of planktonic foraminifera in the WPWP and derived from it to determine regional foraminiferal ACDs in order to identify a deep-dwelling planktonic foraminifera, which can serve as a proxy for reconstructing nutrient concentrations in equatorial Pacific sub-thermocline water masses (*Chapter 3*).

2) to determine whether the relative nutrient-inflow from northern-sourced versus southern-sourced waters on tropical intermediate waters and equatorial sub-thermocline changed during the last glacial period (*Chapter 4*).

3) to identify possible implications for equatorial sub-thermocline nutrient variability and biological productivity during the last glacial period (*Chapter 4*).

4) to reconstruct the equatorial long-term variability spanning more than one glacial-interglacial cycles to decipher if the changing end-member contribution is a reoccurring signal during the Pleistocene (*Chapter 5*).

1.6 Author's contribution

Manuscript 1 (Chapter 3)

Nadine Rippert, Dirk Nürnberg, Jacek Raddatz, Edith Maier, Ed Hathorne, Jelle Bijma, and Ralf Tiedemann. *Constraining foraminiferal calcification depths in the Western Pacific Warm Pool.*

I collected water samples for stable isotope measurement from the (Conductivity-Temperature-Depth (CTD) rosette system during the research cruise SO225 on board of the German RV SONNE (November 2012 – January 2013) and helped with the multinet sampling. I performed the multinet sample treatment including the selection of foraminifera from the remaining organic material as well as the identification and counting of foraminiferal species and the subsequent selection of specific foraminifera for stable isotope analyses. Additionally, I selected

and prepared foraminiferal tests for Mg/Ca analyses, and performed the measurements via laser ablation. I wrote the entire manuscript. Dirk Nürnberg, Jacek Raddatz, Edith Maier and Ralf Tiedemann contributed to the interpretation of the data. Ed Hathorne and Jelle Bijma assisted with the preparation, performance and interpretation of the laser ablation. All co-authors reviewed the draft and contributed to the discussion. The paper is published in *Marine Micropaleontology,* doi:10.1016/j.marmicro.2016.08.004.

Manuscript 2 (Chapter 4)

Lars Max, Nadine Rippert, Lester Lembke-Jene, Isabel Cacho, Andreas Mackensen, Dirk Nürnberg, and Ralf Tiedemann. *Evidence for enhanced convection of North Pacific Intermediate Water to the low-latitude Pacific under glacial conditions*.

For this manuscript I selected the deep-dwelling foraminifera *Globorotaloides hexagonus* of sediment core ODP Site 1240 for the first 60 ka. Furthermore, I assessed the ACD of *G. hexagonus* to validate its deep calcification depth. I wrote the material section of ODP Site 1240 and the ACD determination in the methodology chapter. Additionally, I contributed to the interpretation and discussion of the manuscript during the writing process and journal review stages and edited the manuscript in each processing step. The manuscript is under review in *Paleoceanography*.

Manuscript 3 (Chapter 5)

Nadine Rippert, Lars Max, Andreas Mackensen, Isabel Cacho, Patricia Povea, and Ralf Tiedemann. *Alternating influence of northern versus southern-sourced water masses on the equatorial Pacific sub-thermocline during the past 240 ka*.

I extended the record of planktonic foraminifera *Globorotaloides hexagonus* from ODP Site 1240 for stable isotope analyses. I improved the existing age model of ODP Site 1240 by using new benthic isotope data (measured by Patricia Povea). Furthermore, for consistency, I refined previously published age models of South Pacific sediment core SO136-003/MD06-2990 [*Ronge et al*., 2015] and Bering Sea sediment core U1342 [*Knudson and Ravelo*, 2015a]. I wrote the entire manuscript. Lars Max and Ralf Tiedemann contributed to the interpretation of the data. Andreas Mackensen assisted with the stable isotope analyses. Isabel Cacho helped with sampling of sediment core ODP Site 1240 and Patricia Povea provided the benthic stable isotope data of ODP Site 1240. All co-authors reviewed the draft version and contributed to the discussion. The manuscript is in preparation for *Paleoceanography*.

2. Material and Methods

This chapter describes the material and methods that I used to obtain the results shown in the manuscripts presented in *Chapters 3, 4* and *5*. Further materials and methods included in these following chapters were analysed by co-authors of the respective manuscripts and are therefore not considered in this chapter.

2.1 Study material

For this thesis, material from two study sites was analysed. First, samples from the water column of the western equatorial Pacific (Station SO225-21; 3°03.062'S, -165°03.342'W, Manihiki Plateau) [*Werner et al*., 2013] were investigated to assess foraminiferal calcification depths. Second, sediment samples from the eastern equatorial Pacific (Ocean Drilling Program (ODP) Leg 202 Site 1240; 00°01.311'N, 86°27.758'W, 2921 m water depth) were studied to reconstruct past ocean circulation and nutrient distribution (Figure 2.1).

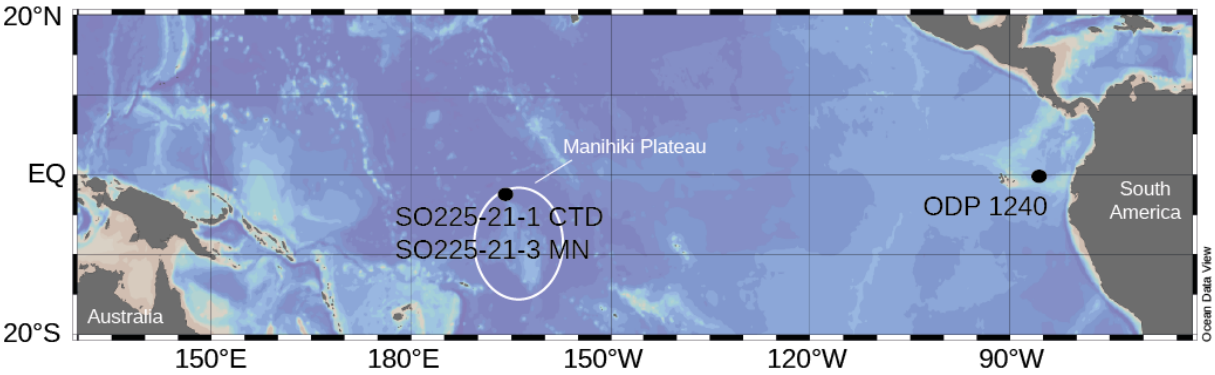

Figure 2.1. Map of the equatorial Pacific with CTD station SO225-21-1, multinet station (MN) SO225-21-3 as well as the location of sediment core ODP Site 1240.

2.1.1 Western equatorial Pacific

At the northernmost edge of the Manihiki Plateau in the WPWP, a multiple open/closing plankton net was used to catch foraminiferal assemblages and to analyse the geochemical signatures of foraminifera in order to determine foraminiferal calcification depths. Furthermore, a CTD profile of the water column was conducted to analyse physical and chemical properties of the water column. Both devices were used during RV SONNE cruise SO225.

In-situ temperature, salinity and oxygen measurements of the 5170 m water column were conducted with a CTD device, which was attached at 24 bottle-rosette system á 10 L (SO225-21-1) [*Werner et al*., 2013]. During the up-cast the bottles of the rosette were systematically closed at 15 selected depths to retrieve the relevant water samples. For each water depth, a 50 ml and a 100 ml subsample was taken and stored in glass bottles for $\delta^{13}C_{DIC}$ and $\delta^{18}O_{seawater}$ analyses, respectively. To prevent biological activity and interaction with air, the water samples for carbon isotope analysis were poisoned with 100 µl of saturated mercuric chloride ($HgCl_2$) solution and sealed with beeswax. Upon measurement, the samples were stored at +4°C.

The multiple open/closing plankton net (SO225-21-3) was used at the same station as the CTD [*Werner et al*., 2013] (Figure 2.1) allowing for stratified vertical sampling of the water column. The net has a square opening of 50 x 50 cm, a 55 µm mesh size, and five net bags. The samples were taken in depths that represent the most commonly investigated upper ocean intervals in paleoceanographic research incorporating the sea surface (0 – 50 m), sub-surface (50 – 100 m), upper thermocline (100 – 200 m), lower thermocline (200 – 300 m) and sub-thermocline (300 – 500 m) as shown by the CTD cast (Figure 2.2) [e.g. *Spero et al*., 2003; *Wara et al*., 2005; *Kiefer et al*., 2006; *Pena et al*., 2008; *Regenberg et* al., 2009; *Nürnberg et al*., 2015]. The relatively large depth intervals were selected to capture enough material for our analyses since the area is known for low primary productivity. Immediately after collection, plankton tow samples were preserved with an Ethanol-Bengal Rose solution and stored at +4°C. In a next step, the foraminifera were wet picked, dried and counted using a reflective light microscope (Zeiss SteREO Discovery.V8). Five species (G*lobigerinoides ruber*, G*lobigerinoides sacculifer, Neogloboquadrina dutertrei, Pulleniatina obliquiloculata* and *Globorotaloides hexagonus*) were selected for further analysis (more details in *Chapter 2.2*).

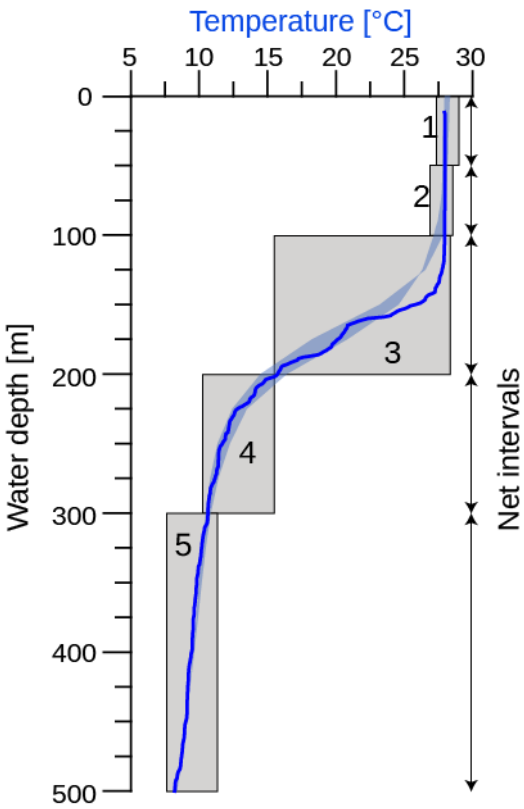

Figure 2.2. Water column temperature record of the uppermost 500 m measured at station SO225-21 (dark blue) together with the five chosen multinet-intervals. In light blue shading indicate long-term seasonal temperature variations [*Locarnini et al*., 2013].

2.1.2 Eastern Equatorial Pacific (EEP)

Material from the EEP was recovered during ODP Leg 202 Site 1240 from the northern flank of the Carnegie Ridge in the Panama Basin (Figure 2.1) [*Mix et al*., 2003]. A 282.9 m sediment sequence was recovered at Site 1240 consisting mainly of nanofossil ooze and diatom-nannofossil ooze and only little of siliciclastic material, mainly clay minerals [*Mix et al*., 2003]. Furthermore, eight ash layers were present in ODP Site 1240. Within the scope of this thesis, only the first 30 m of ODP Site 1240 were investigated spanning the last 300 kyr. Sediment samples had already been washed and separated into sub-fractions at the University of Barcelona. Using a reflective light microscope (Zeiss SteREO Discovery.V8) five specimens of deep-dwelling foraminifera *G. hexagonus* were collected from the 250 – 315 µm size fraction of each selected sediment depth for $\delta^{18}O$ and $\delta^{13}C$ isotope analyses.

2.2 Applied methods

2.2.1 Foraminiferal counting

This study provides the first living foraminiferal abundance analyses from a multiple open/closing plankton net at the Manihiki Plateau. The recovered (coloured) material consisted of plankton from various size fractions (Figure 2.3). Plankton net samples were sieved over nets with a mesh size of 1000 µm and 63 µm to select foraminiferal tests more efficiently. As spinouse species often tend to stuck to larger organic material, the filtered material >1000 µm was examined for foraminiferal tests as well. From the size fraction 125 – 1000 µm intact planktonic foraminifera were wet picked collected using a binocular microscope, and dried afterwards. Foraminifera with coloured cytoplasm in the early chambers were selected, which we infer represent specimens that were collected alive or shortly after they died. This thesis primarily focuses on foraminifera >125 µm. This size fraction is well established in paleoceanographic research, in which many studies focuses on foraminifera in the size the range between 250 and 500 µm [*Dekens et al*., 2002; *Wara et al*., 2005; *Kiefer et al*., 2006; *Knudson and Ravelo*, 2015a; *Nürnberg et al*., 2015]. We enlarged the size fraction slightly to have broad overview over the even smaller sized foraminiferal species. Depending on the amount of material approximately 200 – 400 foraminifera were identified and selected, either in the whole sample or in aliquots. The planktonic foraminiferal taxonomy follows the work of *Parker* [1962], *Bé* [1977] and *Hemleben et al.* [1989].

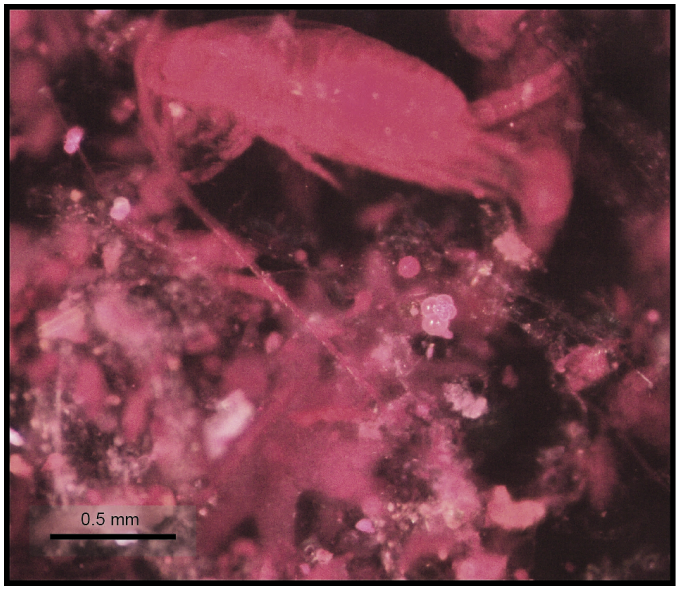

Figure 2.3. Multinet sample from 0 – 50 m water depth show the various size fractions of the recovered material.

Several studies have shown that *Globigerinoides ruber* (white) exists in different morphotypes that dwell in slightly different water depths near the sea surface [e.g. *Wang*, 2000; *Steinke et al*., 2005; *Kuroyanagi et al*., 2008]. The determination of the morphotypes *sensu strictu* (s.s.) and *sensu lato* (s.l.) follows the concept of *Wang* [2000] (Figure 2.4), after which *G. ruber* s.s. has spherical chambers sitting symmetrically over previous sutures with high arched apertus and *G ruber* s.l. corresponds to more compressed subspherical chambers with a small aperture. The morphotype *G. ruber* s.s. has been found to dwell in shallower water depths and was thus selected for the analysis. Nevertheless, due to limited amount of material, specimens of the slightly deeper dwelling *G. ruber* s.l. were also included in our dataset when necessary.

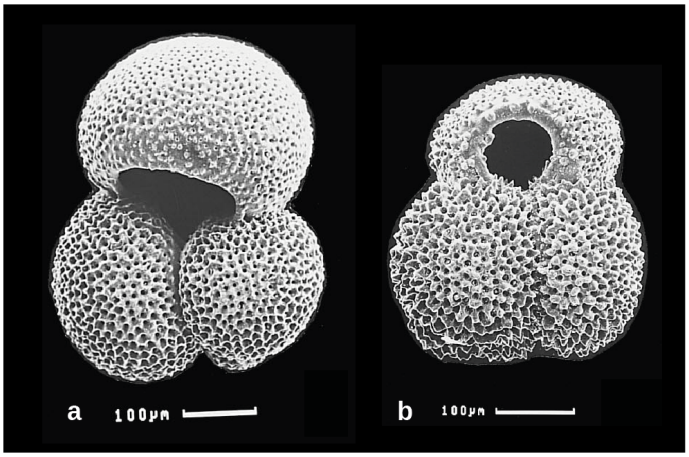

Figure 2.4. The different morphotypes of *Globigerinoides ruber*. a: morphotype *sensu strictu* (s.s) and b: *sensu lato* (s.l.) [figure modified after *Wang*, 2000].

For comparisons with published data, the foraminiferal density in the water column was calculated using the following formula:

$$\rho = \frac{\#}{(a * a) * b} \tag{1}$$

with ρ being the foraminiferal density, a being the multinet opening in meters and b the depth interval the respective net was hauled.

2.2.2 Stable isotope analyses

Foraminiferal stable isotope ratios ($\delta^{18}O$ and $\delta^{13}C$) were carried out at the Alfred-Wegener-Institut, Helmholtz Zentrum für Polar- und Meeresforschung (AWI), Germany, using Finnigan MAT 251 and MAT 253 isotope mass spectrometers that are coupled to automatic carbonate preparation devices Kiel II and IV, respectively. The stable isotope ratios are given in permil (δ)-notation, calibrated via international standard NBS 19 to the Vienna PeeDee Belemnite (VPDB) scale. They are determined as follows:

$$\delta_{sample} = \left[\frac{(\text{heavy isotope}/\text{light isotope})_{sample}}{(\text{heavy isotope}/\text{light isotope})_{VPDB}} - 1 \right] * 1000 \tag{2}$$

The precision of the measurements, determined over a one-year period and based on repeated analysis of an internal laboratory standard (Solnhofen limestone), is ±0.06 ‰ and ±0.08 ‰ (1 σ) for carbon and oxygen isotopes, respectively.

The isotopic composition of seawater samples were determined on a Delta S for the $\delta^{18}O_{seawater}$ and on a Gas Bench II MAS 252 for the $\delta^{13}C_{DIC}$ at the AWI. The $\delta^{18}O_{seawater}$ values were calibrated to the Vienna standard mean ocean water (VSMOW) scale and $\delta^{13}C_{DIC}$ via the international standard NBS 19 to the VPDB scale. The precision based on an internal laboratory standard (Ocean 3 and DML for $\delta^{18}O_{seawater}$ and Solhofen limestone for $\delta^{13}C_{DIC}$) measured over a one-year period is ±0.03 ‰ (1 σ) for $\delta^{18}O_{seawater}$ and ±0.1 ‰ (1 σ) for $\delta^{13}C_{DIC}$.

2.2.3 Determination of trace element ratios

The Mg/Ca ratios of the foraminiferal shells were obtained via laser ablation coupled to a Inductively Coupled Plasma-Mass Spectrometer (LA-ICP-MS). Compared to solution based trace element ICP-MS analyses, LA-ICP-MS requires only very little sample material and only minimal pre-treatment as surface contamination can be removed by pre-ablating samples prior to analysis. Further, it allows to obtain a large range of element concentrations in solid samples and to detect element variabilities within samples.

As many chambers as possible were measured to ensure to have sampled as much test material as possible (Figure 2.5). It has been shown that the large final chamber makes up the bulk

of solution based measurements [*Hemleben and Bijma*, 1994] and average element ratios determined over the whole tests, are in good agreement with published empirical calibrations on bulk foraminifera [*Kunioka et al*., 2006; *Spero et al*., 2015]. Thus, the laser ablation method is ideally suited for the trace element analyses of the multinet samples, which contain only little measureable material.

The geochemical analyses were carried out with the Excimer ArF 193 nm laser ablation system from NEW Wave ESI with a two-volume ablation cell design, coupled to an Agilent 7500cs LA-ICP-MS at GEOMAR, Helmholtz Centre for Ocean Research Kiel, Germany. A more detailed description about the settings for the laser ablation analysis is given in *Chapter 3.2.3*.

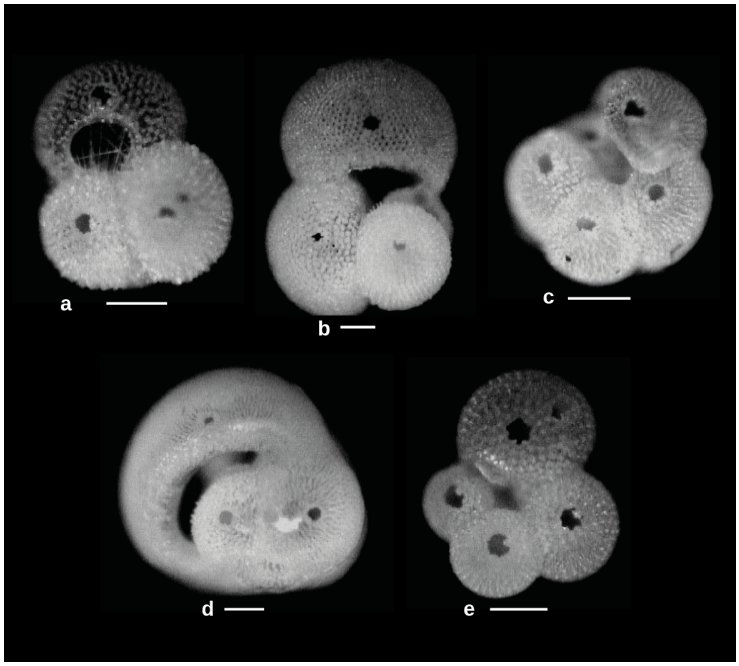

Figure 2.5. Foraminiferal species analysed for Mg/Ca. Holes show the penetration of the laser. White line denotes always 100 µm. a: *Globigerinoides ruber*, b: G*lobigerinoides sacculifer,* c: *Neogloboquadrina dutertrei,* d: *Pulleniatina obliquiloculata* and e: *Globorotaloides hexagonus.*

2.2.3.1 Mg/Ca paleothermometry

Foraminiferal Mg/Ca ratios have become an established proxy to reconstruct past climate system changes over the last decades. The uptake of Mg into biogenic calcite shows an exponential dependency on temperature after:

$$Mg/Ca = B * \exp(A * T) \quad (3)$$

with the pre-exponential and exponential constants given as B and A, respectively, and T denotes the $\delta^{18}O$ calcification temperature [*Nürnberg et al*., 1996; *Lea et al*., 1999; *Elderfield and Gansson*, 2000; *Dekens et al.*, 2002; *Anand et al*., 2003; *Regenberg et al*., 2009; *Friedrich et al.,* 2012]. However, the Mg incorporation into foraminiferal tests is highly biologically mediated

[*Nürnberg et al.,* 1996; *Lea et al*., 1999; *Dueñas-Bohórquez et al*., 2009; 2011]. Due to these so-called "vital effects" species-specific differences in the uptake of Mg into the foraminiferal calcitic test occur. As a consequence, a large number of culture-based, sediment-trap and core-top studies have generated many different generic and species-specific paleotemperature equations that have basic similarities but also differ slightly from each other [*Nürnberg et al.*, 1996; *Dekens et al*., 2002; *Anand et al.,* 2003; *Cléroux et al*., 2008; *Regenberg et al*., 2009]. These small differences might lead to different temperature estimates when applied to the same Mg/Ca ratio. Therefore, different paleotemperature equations were tested (Table S3.5.3) to find the most suitable temperature equation for the planktonic foraminifera from the multinet.

2.3 Assessment of apparent calcification depth (ACD)

The ACDs of foraminiferal species were determined both in the western equatorial Pacific as well as in the EEP. At the Manihiki Plateau two approaches were combined to assess the ACDs of five selected species with improved accuracy. First, measured $\delta^{18}O_{calcite}$ was compared to $\delta^{18}O_{equilibrium}$. To determine the $\delta^{18}O_{equilibrium}$, different paleotemperature equations [*Shackleton*, 1974; *Kim and O'Neil*, 1997; *Bemis et al.*, 1998 (*Orbulina universa* high light); *Mulitza et al*., 2004] were used, in which measured $\delta^{18}O_{seawater}$ and modern temperatures from the CTD data were inserted. Secondly, the determined Mg/Ca-temperatures were associated to in-situ temperatures measured by the CTD at the same station. The water depth in which $\delta^{18}O_{calcite}$ matches $\delta^{18}O_{equilibrium}$ and Mg/Ca temperatures fit in-situ temperatures is taken as the ACD of a species. A more detailed description about the ACD determination at the Manihiki Plateau is given in *Chapter 3.2.5*.

In the EEP, the deep ACD in sub-thermocline waters of *G. hexagonus* was validated by using measured $\delta^{18}O_{calcite}$ of the near core-top sample (10 cm) of ODP Site 1240. These $\delta^{18}O_{calcite}$ values were compared to calculated $\delta^{18}O_{equilibrium}$ values at different water depths and hence, different temperatures. To calculate $\delta^{18}O_{equilibrium}$, several established $\delta^{18}O$-paleotemperature equations [*Epstein et al*., 1953; *Shackleton*, 1974; *Kim and O'Neil*, 1997; *Bemis et al.*, 1998] together with salinity and temperature data from the World Ocean Atlas (WOA09) [*Antonov et al*., 2010; *Locarnini et al.*, 2010] were applied. A more detailed description about the ACD determination in the EEP is given in *Chapter 4.2.2.*

2.4 Stratigraphy of ODP Site 1240

Any paleoceanographic reconstruction is dependent on a sound age model. *Pena et al*. [2008] established the first age model for ODP Site 1240 by a combination of radiocarbon dating and Antarctic ice core stratigraphy. Seventeen monospecific samples of planktonic foraminifer *N. dutertrei* were analysed for radiocarbon, which were calibrated with the marine dataset MA-

RINE 04 in parts younger than 20 kyr and the *Fairbanks et al*. [2005] marine calibration dataset for older sections. For detailed information about the radiocarbon calibration, the reader is referred to *Pena et al*. [2008]. To reconstruct past ocean circulation and nutrient cycling older than MIS 3, the newly generated benthic isotope record (*Cibicidoides* spp., sampled and measured by Patricia Povea, University of Barcelona) was used to refine the existing age model. In this revision, the benthic $\delta^{18}O_{Cibicidoides}$ record was aligned graphically to the global benthic $\delta^{18}O$ reference stack LR04 [*Lisiecki and Raymo*, 2005] using the software AnalySeries 2.0 [*Paillard et al*., 1996]. Beyond the benthic isotope record of ODP Site 1240, the newly generated $\delta^{18}O$ record of deep-dwelling planktonic foraminifera *G. hexagonus* and the existing record of surface-dwelling planktonic species *G. ruber* [*Pena et al.,* 2008] were also graphically tuned to the LR04 stack. In addition, the ash layer “L” with a previously estimated age of 230±10 kyr [*Ninkovich and Shackleton*, 1975] was considered as well.

In *Chapter 5*, the long-term *G. hexagonus* record of ODP Site 1240 was compared to a published data set from a Bering Sea sediment core (U1342; 54.83°N, 176.92°E, 818 m) [*Knudson and Ravelo*, 2015a] and a published sediment record from the South Pacific (SO136-003/MD06-2990; 42.19°S, 169.55°E, 943 m) [*Ronge et al.,* 2015]. The age models of both cores were again refined using radiocarbon dates (where available) and visual alignment to the global benthic stack LR04. A more detailed description about the revised stratigraphy and the newly generated age points for all three sediment cores is given in *Chapter 5.2.2* and Table S5.7.1.

3. Manuscript I

Constraining foraminiferal calcification depths in the Western Pacific Warm Pool

Nadine Rippert[1*], Dirk Nürnberg[2], Jacek Raddatz[2,3], Edith Maier[1], Ed Hathorne[2], Jelle Bijma[1], and Ralf Tiedemann[1]

[1]Alfred-Wegener-Institut, Helmholtz Zentrum für Polar- und Meeresforschung, Postfach 12 01 61, 27515 Bremerhaven, Germany
[2]GEOMAR, Helmholtz Centre for Ocean Research Kiel, Wischhofstr. 1-3, 24148 Kiel, Germany
[3]Goethe University Frankfurt, Institute of Geosciences, Altenhöferallee 1, 60438 Frankfurt am Main, Germany
*corresponding email: Nadine.Rippert@awi.de

Marine Micropaleontology 128, 14-27
doi:10.1016/j.marmicro.2016.08.004

Abstract

Insight into past changes of upper ocean stratification, circulation, and nutrient signatures rely on our knowledge of the Apparent Calcification Depth (ACD) and ecology of planktonic foraminifera, which serve as archives for paleoceanographic relevant geochemical signals. The ACD of different species varies strongly between ocean basins, but also regionally. We constrained foraminiferal ACDs in the Western Pacific Warm Pool (Manihiki Plateau) by comparing stable oxygen and carbon isotopes ($\delta^{18}O_{calite}$, $\delta^{13}C_{calcite}$) as well as Mg/Ca ratios from living planktonic foraminifera to *in-situ* physical and chemical water mass properties (temperature, salinity, $\delta^{18}O_{seawater}$, $\delta^{13}C_{DIC}$). Our analyses point to *Globigerinoides ruber* as the shallowest dweller, followed by *Globigerinoides sacculifer*, *Neogloboquadrina dutertrei*, *Pulleniatina obliqui-loculata* and *Globorotaloides hexagonus* inhabiting increasingly greater depths. These findings are consistent with other ocean basins; however, absolute ACDs differ from other studies. The

uppermost mixed-layer species *G. ruber* and *G. sacculifer* denote mean calcification depths of ~95 m and ~120 m, respectively. These western Pacific ACDs are much deeper than in most other studies and most likely relate to the thick surface mixed layer and the deep chlorophyll maximum in this region. Our results indicate that *N. dutertrei* appears to be influenced by mixing waters from the Pacific Equatorial Divergence, while *P. obliquiloculata* with an ACD of ~160 m is more suitable for thermocline reconstructions. ACDs of *G. hexagonus* reveal a deep calcification depth of ~450 m in oxygen-depleted, but nutrient-rich water masses, consistent to other studies. As the $\delta^{13}C$ of *G. hexagonus* is in near-equilibrium with ambient seawater, we suggest this species is suitable for tracing nutrient conditions in equatorial water masses originating in extra-topical regions.

3.1 Introduction

Geochemical signals of planktonic foraminifera shells (= tests) are frequently used for paleoceanographic studies as they well reflect past environmental conditions [e.g. *Shackleton*, 1974; *Ravelo and Fairbanks*, 1992; *Nürnberg*, 1995; *Nürnberg et al*., 1996; *Bemis et al.,* 1998; *Elderfield and Ganssen*, 2000; *Lea et al.*, 2000]. Many species, however, are known to migrate through the water column during their life cycle and thus, their implemented geochemical signals most likely provide an integrated signal across both the entire water depth range and the entire ontogenetic (calcification) cycle of the species [e.g. *Hemleben and Bijma*, 1994]. Hence, the foraminiferal habitat depths determined by these geochemical signals are best described by the term Apparent Calcification Depth (ACD). It should be noted that the shell weight and therefore the chemical signature of the shell as a whole is mainly determined by the chemical composition of the last few chambers.

Approaches using planktonic foraminifers as biotic carriers of geochemical signals generally emphasize the importance of the knowledge of foraminiferal ACDs. Since the first plankton tow studies of *Bé* [1959, 1962], efforts were launched to most reliably define the foraminiferal depth habitat [*Thunell and Honjo*, 1981; *Fairbanks et al*., 1982; *Thunell et al*., 1983]. With the development of geochemical analysis on foraminiferal tests, it was further possible to assess foraminiferal ACD [*Emiliani*, 1955; *Shackleton*, 1974; *Nürnberg*, 1995; *Faul et al.*, 2000; *King and Howard*, 2005; *Regenberg et al*., 2009; *Steph et al*., 2009; *Wilke et al*., 2009; *Birch et al*., 2013; *Wejnert et al*., 2013]. These studies reveal significant regional intraspecific differences in the ACD [*Faul et al*., 2000; *Steph et al*., 2009]. The species *Globigerinoides ruber*, for example, is often referred to as a “surface dweller”, i.e. living within the upper 30 m of the water column [*Hemleben et al*., 1989*; Faul et al*., 2000; *Steph et al*, 2009; *Birch et al*., 2013]. However, in cases of high sea-surface temperatures (SST) and a deep chlorophyll maximum (DCM), it has been shown to descend and calcify in deeper waters [*Fairbanks et al*., 1982; *Wejnert et al*., 2013]. Contrary, the ACDs of *Neogloboquadrina dutertrei* scatter within 40 – 200 m water depth range [*Hemleben et al*., 1989; *Dekens et al.*, 2002; *Steph et al*., 2009; *Faul et al*., 2000; *Nürnberg et al*., 2015].

Particularly, during strong upwelling the ACD depth can shoal from within the thermocline to distinctly shallower waters [*Loubere*, 2001]. As the studies are scattered over the world oceans, reliable estimations of the ACDs of planktonic foraminifera in a specific area remains a challenge, which is further hampered by logistical difficulties.

The Western Pacific Warm Pool (WPWP) is the largest warm water area on Earth with SSTs consistently higher than 28°C (Figure 3.1a) [*Yan et al*., 1992]. The WPWP deep thermocline (~175 – 300 m in the centre of the WPWP) [*Andreason and Ravelo*, 1997] allows for a large heat capacity, making it the major source of heat and moisture transfer from low to high latitudes. In contrast, in the eastern equatorial Pacific (EEP) the thermocline reaches depths as shallow as

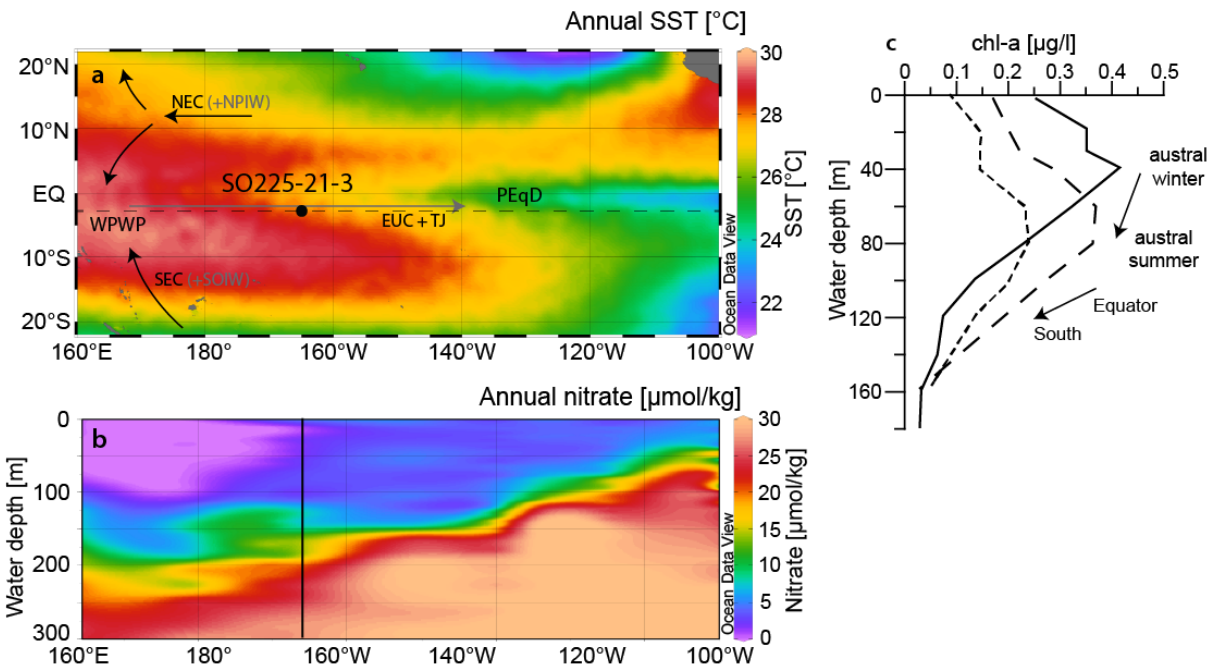

Figure 3.1. Upper ocean conditions of the equatorial Pacific. a: Annual sea-surface temperatures (SSTs) with multinet position SO225-21-3 and selected profile line shown in *b* (dashed line). WPWP denotes the Western Pacific Warm Pool, PEqD the Pacific Equatorial Divergence. Major surface (black) and intermediate (grey) currents are indicated with arrows; NEC = North Equatorial Current fed by the NPIW = North Pacific Intermediate Water, SEC = South Equatorial Current fed by the SOIW = Southern Ocean Intermediate Water, and EUC + TJ = Equatorial Undercurrent and Tsuchiya Jets [after *Tomczak and Godfrey*, 1994; *Firing et al*., 1998; *Rowe et al*., 2000]. b: Longitudinal depth section of annual nitrate along 3°S (see dashed line in *a*) with multinet position SO225-21-3 (black vertical line). Temperature map and section were generated with Ocean Data View [*Schlitzer*, 2012] using World Ocean Atlas 13 Data [a; *Locarnini et al*., 2013] and GLODAP bottle data [b; *Key et al.*, 2004]. c: Chlorophyll-a concentration of the upper 200 m showing a seasonal and latitudinal change in the depth of the deep chlorophyll maximum. Profiles taken from *FLUPAC* cruise (black line, 0°, 164°W, October 1994) [*Blain et al*., 1997], *Alizé 2* cruise at 0°, 165°W (wide strippled line, February 1991) [*Reverdin et al*., 1991] and *Alizé 2* cruise at 2.5°S, 168°W (narrow strippled line, February 1991) [*Reverdin et al*., 1991], respectively.

30 m [*Locarnini et al*., 2013]. This asymmetric behaviour is also clearly seen in the zonal nitrate section (Figure 3.1b), which points towards overall oligotrophic conditions in the WPWP and contrasting with fertile conditions in the EEP. Fluctuations in size and temperature of the WPWP are important drivers for the El Niño Southern Oscillation (ENSO), the Asian monsoon system and, through atmospheric teleconnections, the global climate system [*Sagawa et al*., 2012]. Despite the importance of the WPWP in the climate system, only little information about foraminiferal ACDs are available. To-date, the limited number of studies from the WPWP have concentrated on reconstructing upper ocean conditions with known ACDs from different regions [e.g. *Wara et al.*, 2005; *Russon et al*., 2010] or focused on foraminiferal assemblages from the center of the WPWP near New Guinea [*Kawahata et al.*, 2002; *Yamasaki et al*., 2008], or on plankton tows and surface sediments from the central equatorial Pacific [*Watkins et al.*, 1996; *Lynch-Stieglitz et al*., 2015].

Our multinet study from the Manihiki Plateau attempts for the first time to define the modern ACDs of selected planktonic foraminifera at the south-eastern margin of the WPWP. Five modern planktonic foraminiferal species are studied: *G. ruber* (white), *Globigerinoides sacculifer*, *N. dutertrei*, *Pulleniatina obliquiloculata* and *Globorotaloides hexagonus*. We measured stable oxygen and carbon isotopes ($\delta^{18}O_{calcite}$, $\delta^{13}C_{calcite}$) as well as Mg/Ca ratios on the foraminiferal calcite and compared these data to *in-situ* physical and chemical seawater characteristics (temperature, salinity, $\delta^{18}O_{seawater}$, dissolved inorganic carbon $\delta^{13}C_{DIC}$). By doing so, we were able to better constrain species-specific ACD in an area with the thickest and warmest mixed layer on Earth and to determine the species-specific carbon-isotope disequilibrium. By doing so, we developed a great understanding of regional foraminiferal ACDs in the WPWP. We were then able to define to what extent the geochemical measurements deviate from predictions based on empirical relationships. Our study can be used to inform on what species to use for upper ocean water mass reconstructions of WPWP internal dynamics.

3.1.1 Foraminiferal ecological preferences and hydrographic setting

The abundance of planktonic foraminiferal species is strongly affected by environmental parameters such as, the thermal structure of the water column, salinity, and food supply [e.g. *Bijma et al*., 1990; *Watkins et al*., 1996; *King and Howard*, 2003; *Žarić et al*., 2005]. Culture experiments and surface-sediment samples indicate temperature as one of the major environmental parameters affecting the foraminiferal biogeographic distribution [*Bé and Tolderlund*, 1971; *Bijma et al*., 1990; *Morey et al*., 2005]. Even though most planktonic foraminifera have a large temperature tolerance of about 14 – 32°C [*Bijma et al*., 1990*; Mulitza et al*., 1998], they all have an individual, far more restricted optimum temperature (e.g. 23.5°C for *G. sacculifer*) at which chamber formation, gametogenesis, and food acceptance is highest [*Bijma et al*., 1990]. In contrast, the salinity tolerance range in planktonic species is wider than variations encountered in the open oceans (e.g. 24 – 47 in *G. sacculifer*) [*Bijma et al.,* 1990],

thus, salinity plays most likely a marginal role for the foraminiferal distribution. Salinity, however, can influence the vertical distribution of planktonic foraminifera indirectly by changing the density structure of the water column and thereby restricting vertical movement and the accumulation of nutrients in certain depths [*Bijma et al.*, 1990].

The WPWP at the Manihiki Plateau is characterized by high annual SSTs and sea-surface salinities (SSS) of 28 ± 0.2°C and 35 ± 0.03 (psu), respectively [*Locarnini et al*., 2013; *Zweng et al.,* 2013]. Sediment trap results from the WPWP reveal that despite the small seasonal SST range of ±0.2°C, planktonic foraminifera are not present all year round in high abundances [*Kawahata et al*., 2002; *Lin et al*., 2004]. The production is rather controlled by local nutrient availability and light intensity [*Kawahata et al.,* 2002]. As a consequence of the oligotrophic surface waters in the WPWP, with nutrient concentrations of <0.1 mM NO_3^- and <0.2 mM PO_4 [*Blanchot et al*., 2001; *Le Borgne et al.*, 2002; *Rafter and Sigman*, 2015], primary production is low and foraminiferal fluxes are modest (mean 171 shells m^{-2} day^{-1}) [*Kawahata et al*., 2002]. In contrast, the high-nutrient low-chlorophyll (HNLC) region of the Pacific Equatorial Divergence is enriched in macronutrients (>3 mM NO_3^-; >0.4 mM PO_4) and foraminiferal fluxes are higher (up to 430 shells m^{-2} day^{-1}) [*Thunell and Honjo*, 1981]. Through a complex and highly dynamic current system [e.g. *Wyrtki and Kilonski*, 1984; *Fine et al.*, 1994; *Tomczak and Godfrey*, 1994; *Johnson and Moore*, 1997; *Rowe et al*., 2000; *Goodman et al*., 2005; *Grenier et al*., 2011], including the South Equatorial Current (SEC), the persistent eastward-directed sub-surface Equatorial Undercurrent (EUC) and the Tsuchiya Jets [after *Tsuchiya*, 1972], nutrients are transported via intermediate and mode waters from the extra-tropical HNLC regions to the thermocline of the western equatorial Pacific and upwell along the equator in the Pacific Equatorial Divergence.

In the vicinity of the nutricline, chlorophyll-a concentrations reach a maximum between 40 and 90 m water depths in the WPWP indicating the DCM (Figure 3.1c). Planktonic foraminifera respond to the distribution of chlorophyll and high abundances are often associated with the DCM [*Fairbanks et al*., 1982; *Schiebel et al*., 2001]. Even though the depth of the DCM does not change significantly from east to west [*La Borgne et al*., 2002], it changes meridionally. Upwelling decreases away from the equator and, as a consequence, the DCM deepens. The DCM depth also varies seasonally: while the DCM at the equator is situated at ~60 m (range ~40 – 80 m, values >0.3 mg m^{-3}) during austral summer, it shoals during autumn and reaches its shallowest position during austral winter (25 – 70 m, maximum 40 m) [*Le Borgne et al*., 2002].

Variations in upper ocean temperatures, depth of the thermocline and hence, nutrients in the upper water column, are influenced by the ENSO climate phenomenon [*Collins et al.*, 2010]. Nevertheless, the Oceanic Niño Index (ONI), a standard for identifying El Niño and La Niña events through averaging SST anomalies, was only slightly increased (0.2 – 0.4°C) from August to December 2012 [*NOAA*, 2015a], thus indicating only a tendency for a very weak El Niño (ONI >0.5°C).

3.2 Material and Methods

3.2.1 Sample material

During the RV SONNE cruise SO225, *in-situ* temperature, salinity and oxygen measurements were conducted with a Conductivity-Temperature-Depth (CTD) device equipped with a 24 in each case 10 L bottle-rosette system (SO225-21-1; 3.05°S, -165.056°W) [*Werner et al*., 2013]. The water column was sampled at 15 depths, and for each water depth a 50 ml and a 100 ml subsamples was taken and stored in glass bottles for $\delta^{13}C$ and $\delta^{18}O_{seawater}$ measurements, respectively. Water samples for carbon isotope analysis were poisoned with 100 µl of saturated $HgCl_2$ solution to prevent biological activity and sealed with beeswax to prevent interaction with air.

At the same location where SO225-21-1 was recovered, a multiple open/closing plankton net was run during the night at the northernmost edge of the Manihiki Plateau in the WPWP (SO225-21-3) [*Werner et al*., 2013] (Figure 3.1a). The multinet (HydroBios, Kiel) with a square mouth opening of 50 x 50 cm, 55 µm mesh size, and five net bags allowed stratified vertical sampling in five depth intervals within the first 500 m of the water column. The depths were selected after viewing the CTD cast and thus, included the sea surface (0 – 50 m), sub-surface (50 – 100 m), upper thermocline (100 – 200 m), lower thermocline (200 – 300 m) and sub-thermocline (300 – 500 m). These depth intervals are often investigated in paleoceanographic research [e.g. *Spero et al*., 2003; *Wara et al*., 2005; *Kiefer et al*., 2006; *Pena et al*., 2008; *Regenberg et al*., 2009; *Nürnberg et al.*, 2015], highlighting the need to better understand the ACD of the species calcifying in these depths. Since the area is known for low primary production, we selected relatively large net depth intervals to capture enough material for our analyses. Immediately after collection, plankton tow samples were preserved with an Ethanol-Bengal Rose solution.

3.2.2 Handling foraminiferal assemblage counts

In the laboratory, plankton net samples were sieved over 1000 µm and 63 µm. Material >1000 µm was analysed for spinose species attached to particulate organic matter. Within the fraction 63 – 1000 µm intact planktonic foraminifera >125 µm were wet picked using a binocular microscope and dried afterward. As all individuals contained coloured cytoplasm in the early chambers, we infer that the samples were collected alive or shortly after they died. Smaller-sized planktonic foraminifera are more difficult to define taxonomically. As we primarily focus on size fractions well established for paleoceanographic purposes (>250 µm), only foraminifera >125 µm were counted. Depending on the amount of material, samples were either quantitatively split into aliquots and approximately 200 – 400 foraminifera were identified or the whole sample was counted (Supplement Table S3.5.1). Further, we calculated the density of different species over the netted depth range using the formula: # / (a*a)*b; with # being the number of counted

specimen, *a* being the multinet-opening in meters and *b* the depth interval the respective net was hauled.

Planktonic foraminiferal taxonomy follows the work of *Parker* [1962], *Bé* [1977] and *Hemleben et al.* [1989]. We are aware that *G. ruber* (white) exists in different morphotypes. The determination of the morphotypes *sensu strictu* (s.s.) and *sensu lato* (s.l.) follows the concept of *Wang* [2000], in which *G. ruber* s.s. has spherical chambers sitting symmetrically over previous sutures with high arched apertus and *G ruber* s.l. corresponds to more compressed subspherical chambers with a small aperture. These different morphotypes have been shown to dwell at slightly different water depths, yet always at the sea surface [e.g. *Wang*, 2000; *Steinke et al*., 2005; *Kuroyanagi et al*., 2008]. For our analyses we selected mainly the morphotype *s.s.*, but due to limited amount of material, we also included some specimen of the slightly deeper-dwelling morphotype *s.l.* for the isotope analyses when necessary.

3.2.3 Determination of Mg/Ca ratios and calculation of water temperatures

Mg/Ca ratios of planktonic foraminiferal calcite were measured to assess the water temperature during test growth. Prior to the analysis, the cytoplasm within the test was removed by treating the foraminiferal shells with 7 % sodium hypochlorite (NaClO) before rinsing with deionised water. Intact specimens were selected from the 320 – 760 µm size fraction as a narrower size range was prevented by the rather low amount of material (Table 3.1).

The geochemical analyses were obtained with the Excimer ArF 193 nm laser ablation system from NEW Wave ESI with a two-volume ablation cell design, coupled to an Agilent 7500cs Inductively Coupled Plasma-Mass Spectrometer (LA-ICP-MS) at GEOMAR. This micro-analytical technique enables the measurement of element/Ca through the shell wall of individual chambers. However, for the habitat assessment we use the mean Mg/Ca ratios of all the chambers in the final whorl of each shell that could be targeted with the laser. *Hemleben and Bijma* [1994] demonstrated that the vast majority of the shell mass and therefore most of the geochemical signal is contained in the last few chambers. Measuring as many chambers as possible is important as Mg/Ca seems to vary randomly from chamber to chamber in cultures under constant environmental conditions [*de Nooijer et al*., 2014]. Thus, we analysed as many chambers as possible to ensure that we have sampled as much of the shell as possible. Culturing studies have investigated the difference between whole-test calibrations and Mg/Ca-temperature equations based on Mg/Ca measurements of the last chambers and found no significant difference between them [*Kunioka et al*., 2006; *Dueñas-Bohórquez et al*., 2009, 2011; *Spero et al*., 2015]. The laser was targeted on the test surface, ablating through the test wall with a 50 µm diameter spot size, and stopped when the wall was penetrated. Ablations were conducted in a He atmosphere and the laser energy density was between 0.97 and 1.85 J/cm^2 with a laser repetition rate of 5 Hz. The ablation was done on as many chambers as possible (f to f-4), always proceeding from the

Table 3.1. Overview of net collections of five paleoceanographically important foraminiferal species. The depth ranges from which the foraminifera were selected, species abundances, foraminiferal shell sizes, number of tests measured as well as geochemical analyses are given.

Species	Net depth [m]	#/m^3	Shell size [range in µm]	Number of tests measured	Accomplished measurement		
					$\delta^{18}O_{calcite}$ [‰]	$\delta^{13}C_{calcite}$ [‰]	Mean Mg/Ca [mmol/mol]
G. ruber	0 – 50	5.60	150 – 250	18	-2.25 ± 0.012	-0.04 ± 0.009	
	0 – 50	5.60	250 – 300	11	-2.17 ± 0.01	0.71 ± 0.008	
	50 – 100	6.00	150 – 250	17	-2.68 ± 0.02	0.02 ± 0.006	
	50 – 100	6.00	250 – 300	14	-2.40 ± 0.004	0.46 ± 0.007	
	50 – 100	6.00	300 – 350	9	-2.47 ± 0.05	0.79 ± 0.025	
	100 – 200	0.84	~410	1			4.71 ± 0.4
	300 – 500	0.12	~320	1			5.10 ± 0.8
G. sacculifer	0 – 50	11.04	300 – 350	7	-2.30 ± 0.008	1.18 ± 0.008	
	0 – 50	11.04	350 – 500	4	-2.31 ± 0.007	1.31 ± 0.004	
	0 – 50	11.04	~520	1			4.27 ± 0.6
	0 – 50	11.04	~520	1			4.50 ± 0.4
	50 – 100	9.84	300 – 350	5	-2.33 ± 0.05	0.83 ± 0.025	
	50 – 100	9.84	350 – 500	4	-2.32 ± 0.006	1.00 ± 0.006	
	50 – 100	9.84	350 – 500	4	-1.89 ± 0.01	1.34 ± 0.008	
	50 – 100	9.84	>500	2	-2.27 ± 0.01	1.53 ± 0.007	
	100 – 200	6.64	300 – 350	6	-2.39 ± 0.01	0.56 ± 0.007	
	100 – 200	6.64	350 – 500	5	-2.43 ± 0.01	1.02 ± 0.009	
	100 – 200	6.64	350 – 500	5	-1.94 ± 0.01	0.73 ± 0.005	
	100 – 200	6.64	>500	3	-2.11 ± 0.04	0.99 ± 0.018	
	200 – 300	0.40	>500	2	-2.15 ± 0.02	1.29 ± 0.023	
	300 – 500	0.40	~750	1			4.88 ± 0.2
N. dutertrei	50 – 100	8.00	250 – 300	12	-1.90 ± 0.02	-0.14 ± 0.017	
	50 – 100	8.00	300 – 350	9	-2.15 ± 0.02	-0.08 ± 0.008	
	50 – 100	8.00	350 – 500	6	-2.21 ± 0.01	0.03 ± 0.006	
	100 – 200	4.32	~360	1			3.21 ± 0.2
P. obliquiloculata	50 – 100	20.64	>500	2	-1.75 ± 0.04	-0.01 ± 0.028	
	50 – 100	20.64	~520	1			3.16 ± 0.05
	100 – 200	20.48	350 – 500	4	-1.62 ± 0.01	0.06 ± 0.004	
	100 – 200	20.48	350 – 500	4	-1.83 ± 0.01	-0.01 ± 0.003	
	100 – 200	20.48	>500	2	-1.54 ± 0.004	0.26 ± 0.016	
	100 – 200	20.48	>500	2	-1.49 ± 0.01	0.25 ± 0.012	
	100 – 200	20.48	~675	1			3.11 ± 0.1
	200 – 300	0.52	>500	2	-1.60 ± 0.03	0.11 ± 0.008	
	200 – 300	0.52	>500	2	-1.42 ± 0.01	0.41 ± 0.004	
	300 – 500	0.20	~640	1			2.85 ± 0.3
G. hexagonus	300 – 500	1.76	250 – 300	10	1.39 ± 0.05	-0.06 ± 0.01	
	300 – 500	1.76	300 – 350	9	1.59 ± 0.01	0.22 ± 0.003	
	300 – 500	1.76	350 – 500	6	1.49 ± 0.005	0.24 ± 0.006	
	300 – 500	1.76	~400	1			1.36 ± 0.4

outside of the test towards the inside. Time-resolved signals of ^{24}Mg were selected for integration and the mean background intensities (gas blank) were subtracted. Signal intensities were internally standardised to ^{43}Ca to account for variations in ablation yield. Mg/Ca intensity ratios were calibrated with analyses of the international reference NIST 610 and NIST 612 glasses after

every 10 sample spots [using values from *Jochum et al*., 2011], which were ablated with a higher energy density (around 2.65 J/cm^2). A powder pellet of the powdered reference material JCp-1 (*Porites* sp.) was ablated like a sample and the repeated measurements during the analytical session (n = 6) gave a relative standard deviation of 7.4 % (1 σ) for Mg/Ca with an average value of ~3.707 mmol/mol that is 11 % less than the solution ICP-MS consensus value from *Hathorne et al*. [2013] (4.199 mmol/mol).

Core top and culture studies point towards a species-specific dependency of the Mg incorporation into foraminiferal tests due to the interplay of biological processes and ecological behaviour [e.g. *Nürnberg et al*., 1996; *Lea et al*., 1999; *Regenberg et al.*, 2009; *Nehrke et al*., 2013; *Mewes et al*., 2015]. As a consequence, various species-specific calibrations have been established that have all basic similarities, but produce significantly different temperature estimates when applied to the same Mg/Ca ratios. Hence, the accurate selection of the applied calibration curve is crucial. To find the most reliable calibration curve for each investigated foraminiferal species from the multinet samples, we converted the measured whole-shell foraminiferal Mg/Ca ratios (Supplement Table S3.5.2) into temperatures using generic and species-specific equations if available (Supplement S3.5.3, Supplement Table S3.5.3). At the depth interval in which a species was found in highest abundance on the Manihiki Plateau (see *Chapter 3.3.2*), we determined the mean temperature during sampling time from both CTD data and the seasonal range in temperature from the WOA13 data [*Locarnini et al*., 2013] at the same location. By comparing the *in-situ* temperatures with the Mg/Ca-derived temperatures, we identified the most suitable calibration equation for each species at our study site (Table 3.2, Supplement S3.5.3).

Table 3.2. Equations used to convert foraminiferal Mg/Ca into temperatures and to calculate equilibrium $\delta^{18}O_{equilibrium}$.

Species	Type of sample	Water mass	Equation			Reference
			Mg/Ca = B*exp(A*T)			
			B	A		
G. ruber	Surface sediment (0 – 1 cm)	Sea-surface and sub-surface (0 – 100 m)	0.40	0.09		*Regenberg et al.* [2009]
G. sacculifer	Surface sediment (0 – 1 cm)	Sea-surface and sub-surface (0 – 100 m)	0.37	0.09		*Dekens et al.* [2002]
N. dutertrei	Surface sediment (0 – 1 cm)	Upper thermocline (100 – 200 m)	0.65	0.065		*Regenberg et al.* [2009]
P. obliquiloculata	Sediment-trap	Upper thermocline (100 – 200 m)	0.18	0.12		*Anand et al.* [2003]
G. hexagonus	Surface sediment (0 – 1 cm)	Sub-surface (300 – 500 m)	0.52	0.10		*Elderfield and Ganssen* [2000]
			$T = a+b(\delta^{18}O_{calcite} - \delta^{18}O_{seawater}) - c(\delta^{18}O_{calcite} - \delta^{18}O_{seawater})^2$			
			a	b	c	
	Inorganic	Sub-thermocline (300 – 500 m)	16.1	-4.64	0.09	*Kim and O'Neil* [1997]
	Living foraminifera	Sea-surface to upper thermocline (0 – 200 m)	14.32	-4.28	0.07	*Mulitza et al.* [2004]

3.2.4 Stable isotope analyses

Stable oxygen and carbon isotope ratios ($\delta^{18}O_{calcite}$ and $\delta^{13}C_{calcite}$) of the foraminiferal tests (Table 3.1) were determined to estimate the ACD by comparing measured $\delta^{18}O_{calcite}$ to predicted $\delta^{18}O_{calcite}$ as well as to assess the deviation from prediction based on empirical relationships. The isotope ratios were measured on a ThermoScientific MAT 253 mass spectrometer coupled to an automatic carbonate preparation device Kiel CARBO IV at AWI. The isotope measurements were calibrated via the international standard NBS 19 to the VPDB scale. All results are given in the common δ-notation *versus* VPDB. The precision of the measurements, determined over a one-year period and based on repeated analysis of an internal laboratory standard (Solnhofen limestone), is ±0.06 ‰ and ±0.08 ‰ (1 σ) for carbon and oxygen isotopes, respectively.

Measurements of the oxygen isotope composition of seawater ($\delta^{18}O_{seawater}$) were performed on a ThermoScientific Delta S mass spectrometer and those for the seawater dissolved inorganic carbon isotope composition ($\delta^{13}C_{DIC}$) were made with a ThermoScientific MAT 252 coupled to a Gas Bench II at AWI. The $\delta^{18}O_{seawater}$ values are given in δ-notation *versus* VSMOW and $\delta^{13}C_{DIC}$ values *versus* VPDB. The precision determined over a one-year period is ±0.03 ‰ (1 σ) for $\delta^{18}O_{seawater}$ and ±0.1 ‰ (1 σ) for $\delta^{13}C_{DIC}$.

3.2.5 Estimation of the apparent calcification depth

We constrained the ACDs of selected planktonic foraminiferal species by combining two approaches. This enables us to assess the ACD with improved accuracy. First, we compared the measured foraminiferal $\delta^{18}O_{calcite}$ to calculated $\delta^{18}O_{equilibrium}$ values at different water depths and hence, different temperatures. The water depth from which $\delta^{18}O_{calcite}$ matches $\delta^{18}O_{equilibrium}$ is taken as the isotope ACD (Table 3.3). The expected $\delta^{18}O_{equilibrium}$ values were calculated using paleotemperature-equations of *Shackleton* [1974], *Kim and O'Neil* [1997], *Bemis et al*. [1998; *Orbulina universa* high light], and *Mulitza et al*. [2004] (Supplement Table S3.5.4). In them, we inserted our measured variables foraminiferal $\delta^{18}O_{calcite}$, seawater $\delta^{18}O$ (converted into VPDB by subtracting -0.27 ‰) [*Hut,* 1987], and modern temperatures from CTD data. Different equations were tested to show that relative species order in the water column is independent of the $\delta^{18}O$-paleotemperature equation. The absolute isotope-ACDs, however, differ with each equation (Supplement Table S3.5.4). In cases where $\delta^{18}O_{calcite}$ values were lower than predicted $\delta^{18}O_{equilibrium}$ values at the sea surface, ACDs of 5 m water depth were assigned (Supplement Table S3.5.4). ACDs derived by *Shackleton* [1974] and *Kim and O'Neil* [1997] are similar at the sea surface. In deeper waters, *Shackletons*' [1974] equation produces markedly shallower isotope-ACDs than *Kim and O'Neils'* [1997]. On the other hand, the equations of *Bemis et al*. [1998] and *Mulitza et al*. [2004], that were both generated using planktonic foraminifera, yield deeper isotope-ACDs at all depths. Nevertheless, using *Mulitza et al.* [2004] for upper-ocean dwelling species (0 – 220 m), the number of samples with measured $\delta^{18}O_{calcite}$ that are lower than

Table 3.3. Specification of Apparent Calcification Depth (ACD) of foraminiferal species at Manihiki Plateau using (1) measured $\delta^{18}O_{calcite}$ values that were placed at water depths corresponding to theoretical $\delta^{18}O_{equilibrium}$ values depending on water temperature and salinity. (2) Mg/Ca derived temperature estimates placed at water depths corresponding to *in-situ* measured austral summer temperatures [*Werner et al*., 2013] and seasonal World Ocean Atlas 2013 temperature ranges [*Locarnini et al.,* 2013]. Each line represents one single analysed sample.

Species	ACD [m water depth]						Combined isotope and temperature ACD [m water depth]	
	using $\delta^{18}O_{eq}$ Dec. 2012	using seasonal $\delta^{18}O_{eq}$		using Temperature during sampling (Dec. 2012)	using seasonal temperature		ACD range	Mean ACD
		Shallowest	Deepest		Shallowest	Deepest		
G. ruber	152	106	126					
	154	113	137					
	77	65	66					
	138	91	105					
	124	85	96					
				136	92	109		
				5	5	16		
	mean isotope ACD: 109			mean temperature ACD: 61			5 – 154	95 ± 44
G. sacculifer	151	101	118					
	151	100	118					
	151	98	115					
	151	99	117					
	161	140	156					
	152	104	124					
	141	93	107					
	132	89	101					
	159	135	154					
	156	119	145					
	154	115	140					
				141	100	112		
				126	67	105		
				5	5	5		
	mean isotope ACD: 129			mean temperature ACD: 74			5 – 161	117 ± 39
N. dutertrei	160	140	156					
	154	115	140					
	153	110	132					
				154	140	150		
	mean isotope ACD: 140			mean temperature ACD: 148			110 – 160	142 ± 16
P. obliquilo-culata	163	151	160					
	166	154	164					
	162	146	158					
	168	156	166					
	169	157	168					
	167	154	164					
	171	159	170					
				158	145	155		
				159	146	156		
				160	151	161		
	mean isotope ACD: 162			mean temperature ACD: 155			145 – 171	159 ± 7

Table 3.3. *continued.*

G. hexagonus	431	427	435					
	498	509	514					
	467	469	473					
				375	396	403		
	mean isotope ACD: 469			mean temperature ACD: 391			375 – 514	450 ± 46

the respective $\delta^{18}O_{equilibrium}$ at the sea surface is minimised. In deeper waters, however, the equation of *Mulitza et al*. [2004] yield isotope-ACDs of up to 660 m (Supplement Table S3.5.4), and these are deeper than the nets were hauled. As a consequence, we selected the equation by *Kim and O'Neil* [1997], which was calibrated using inorganic calcite, for sub-thermocline waters (220 – 500 m, Table 3.2). Seasonal variations in $\delta^{18}O_{equilibrium}$ due to varying temperature are considered by using temperature data from the WOA13 database to account for temperature variationsduring the foraminiferal life cycle (Table 3.3) [*Locarnini et al*., 2013]. To assess the influence of species-specific offsets from $\delta^{18}O_{equilibrium,}$ we corrected the measured $\delta^{18}O_{calcite}$ values for disequilibrium effects [values are taken from *Niebler et al.*, 1999 and *Steph et al.*, 2009] and recalculated the $\delta^{18}O$-derived ACDs with the *Mulitza et al*. [2004] and *Kim and O'Neil* [1997] equations (Supplement Table S3.5.4).

In a second step, we compared the temperatures converted from the average Mg/Ca of living specimens (Table 3.1) to the ocean temperatures prevailing during the time of sampling (December 2012) at the sample location and placed the temperature-ACD at the according water depth (Table 3.3). To account for seasonal variations in the temperature record, we also compared the derived Mg/Ca temperatures to austral winter and austral summer temperatures (data from WOA13) (Table 3.3) [*Locarnini et al.*, 2013].

In a last step, we combined both ACD approaches and determined the mean ACD. We are aware, that we have an uneven distribution between $\delta^{18}O$ and Mg/Ca measurements (Table 3.1). Thereby, more credit is given towards the $\delta^{18}O$-derived ACD. To validate the combined mean ACD, we used the mean temperature and mean $\delta^{18}O_{calcite}$ of the respective species and calculated the $\delta^{18}O_{water}$. For this purpose we selected different paleotemperature equations (Supplement S3.5.5, Supplement Table S3.5.5) and rearranged the equations for the $\delta^{18}O_{water}$. The $\delta^{18}O_{water}$ was then compared to the measured $\delta^{18}O_{seawater}$ (Supplement S3.5.5). It demonstrates that the calculated $\delta^{18}O_{water}$ displays the measured $\delta^{18}O_{seawater}$ curve and hence, supports the use of a combined isotope and Mg/Ca approach.

3.3 Results and Discussion

3.3.1 Hydrological conditions in the upper ocean water column

At the time of multinet sampling (December 2012) at station SO225-21 the mixed layer was characterized by a SST of 27.9°C, a SSS of 35.5, an oxygen concentration > 170 µmol/l and a $\delta^{18}O_{seawater}$ of +0.5 ‰ (Figure 3.2). The SST and SSS agree well with the long-term WOA13 dataset [*Locarnini et al*., 2013] showing a deep surface mixed layer (SML) extending to 105 m water depth, below which temperature decreases steadily. The main thermocline is located between 130 m and 230 m water depth and reflects an overall temperature decline of ~16°C (from 28°C to ~12°C).

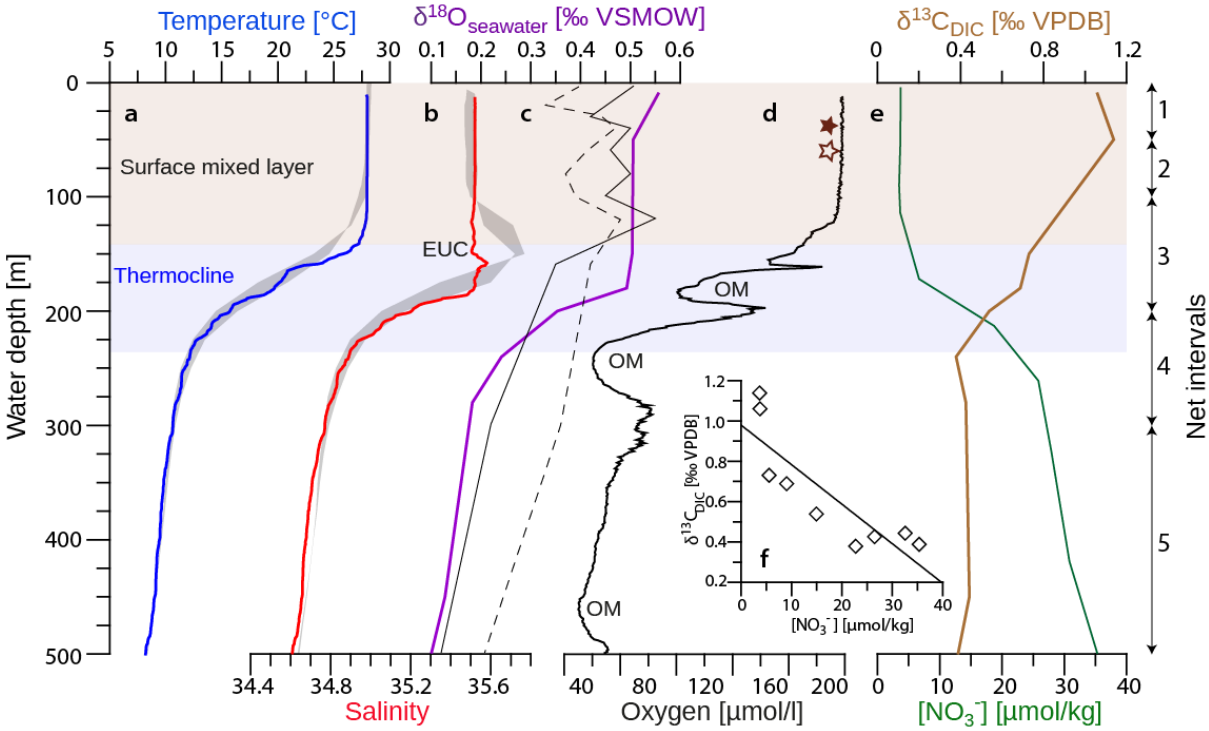

Figure 3.2. Water column characteristics of the uppermost 500 m at multinet station SO225-21-03 along the towed net intervals. a: Temperature and b: salinity profile from CTD casts in December 2012 (SO225-21-01) [*Werner et al*., 2013]. Blue/red curves show the temperature/salinity during the time of multinet sampling with the position of the Equatorial Undercurrent (EUC). Grey shaded areas delineate long-term seasonal temperature and salinity variations [*Locarnini et al*., 2013; *Zweng et al*., 2013]. c: Measured $\delta^{18}O_{seawater}$ from CTD station SO225-21-01 (purple, this study); solid/dashed black lines indicate $\delta^{18}O_{seawater}$ at 160°W/168°W, respectively, using the *Schmidt et al*. [1999] database. d: Oxygen concentration from CTD cast in December 2012 [*Werner et al*., 2013] showing three oxygen minima (OM). Dark brown stars indicate the chlorophyll-a maxima during austral winter (filled symbol) [*Blain et al.,* 1997] and austral summer (open symbol) [*Reverdin et al*., 1991] (data shown in Figure 3.1c), e: $\delta^{13}C_{DIC}$ values measured on water samples from CTD casts (brown, this study) and nitrate concentration of the water column (green) obtained from GLODAP bottle data [*Key et al*., 2004]. f:

Covariance between $\delta^{13}C_{DIC}$ and $[NO_3^-]$ at 3°S and 168°W yields a relationship of $\delta^{13}C_{DIC}$= -0.02 * $[NO_3^-]$ + 0.98 (r^2 = 0.73). Arrows and numbers on the right denote the five net intervals of the multinet collection with sea surface (1), sub-surface (2), upper thermocline (3), lower thermocline (4) and sub-thermocline (5).

At the top of the thermocline, however, both temperature and salinity deviate from the long-term average (Figure 3.2a and b). The temperatures are up to 2°C warmer between 125 and 150 m. Salinities are significantly reduced between 125 and 160 m. These changes may indicate changes in the source area and speed of the EUC as a consequence of weaker trade winds in December 2012. In contrast, the comparison between $\delta^{18}O_{seawater}$ values from the sampling site to 1991-profiles at 160°W and 168°W [*Schmidt et al*., 1999] reveals up to 0.2 ‰ heavier values (Figure 3.2c). As in the open ocean, $\delta^{18}O_{seawater}$ is mainly affected by the evaporation/precipitation balance [*Dansgaard*, 1964] with heavier values attributed to higher evaporation, we assume an increase in evaporation probably related to stronger trade winds from 1991 until December 2012. This agrees with model experiments that show an acceleration of Pacific trade winds due to the intensification of the Walker circulation over the period 1992 – 2011 [*McGregor et al*., 2014]. Consequently, it seems that over the last decade trade wind strength and hence evaporation increased, but in December 2012 wind strength dropped for a short time, leading to a decrease in upwelling and thus to warmer and less saline waters at the top of the thermocline. Further support comes from the equatorial Pacific Zonal Wind field models in November – December 2012 [*NOAA*, 2015b] and from the slightly increased Oceanic Niño Index (ONI) that indicates a very weak El Niño (ONI >0.5°C) and consequently weaker prevailing winds (see also *Chapter 3.1.1*) [*NOAA*, 2015a].

Associated with the thermo- and halocline, oxygen concentrations decline in two steps, which points to two oxygen minima (OM) located at ~180 m and ~250 m (Figure 3.2d). Possibly both OM belong to one expansive OM that is separated by a chlorophyll maximum in which oxygen is produced. However, to verify this hypothesis a deeper chlorophyll-a profile extending to at least 300 m water depth is needed. Oxygen concentrations further decline below the thermocline towards a less pronounced OM in ~450 m with concentrations of 57 µmol/l. The strongest OM in December 2012 (concentration of 44 µmol/l) is located at ~660 m water depth below the hauled nets.

At the multinet sampling site, the overall range in $\delta^{13}C_{DIC}$ is from ~0.4 ‰ to ~1.1 ‰, achieving a maximum in the surface waters (Figure 3.2e). The $\delta^{13}C_{DIC}$ data start to decline below ~50 m and gradually decrease throughout the thermocline in response to remineralisation processes and the release of ^{12}C to the ambient seawater. The overall shape of the $\delta^{13}C_{DIC}$ profile is anticorrelated to the GLODAP $[NO_3^-]$ profile [*Key et al.*, 2004]. With increasing nitrate concentrations, the $\delta^{13}C_{DIC}$ values decrease simultaneously due to the concurrent uptake of ^{12}C and nutrients during photosynthesis. The slope of this relationship depends on the fractionation of

$\delta^{13}C$ during photosynthesis. Our $\delta^{13}C_{DIC}$:[NO_3^-] comparison yield a relationship of: $\delta^{13}C_{DIC}$ = -0.02 * [NO_3^-] + 0.98 (r^2 = 0.73) (Figure 3.2f).

3.3.2 Vertical distribution of planktonic foraminifers in the water column

A total number of 20 taxa have been identified in the net collection from the Manihiki Plateau of which 16 could be identified on the species level (Supplement Table S3.5.1). Most common and abundant species (>10 %) are: *Globorotalia menardii* (mean relative abundance (MRA) 22.7 %, range 7.8 % – 26.4 %), *Pulleniatina obliquiloculata* (MRA 15.4 %, range 5.2 – 19.6 %), *Globigerinita glutinata* (MRA 13.8 %, range 5.7 – 30.1 %), *Globigerinella* spp. (MRA 12.8 %, range 3.6 – 16 %) and *Globorotalia* spp. (MRA 10 %, range 3.6 – 10.8 %). Less abundant species (2 – 10 %) are *Globigerinoides sacculifer* (MRA 7.2 %, range 3.6 – 9.8 %), *Neogloboquadrina dutertrei* (MRA 5.1 %, range 2.6 – 6.3 %), *Globigerinoides ruber* (white) (MRA 2.9 %, range 0.8 – 5 %) and *Globoquadrina conglomerata* (MRA 2.1 %, range 1 – 2.8 %). All other taxa occur in very low abundances (MRA <2 %). For further analyses, we selected four species often used in paleoceanographic research (*G. ruber, G. sacculifer, N. dutertrei,* and *P. obliquiloculata*) [e.g. *Spero et al*., 2003; *Kiefer et al*., 2006; *Pena et al.*, 2008; *Leduc et al*., 2009; *Nürnberg et al*., 2015; *Rippert et al.,* 2015], although other species had a higher abundance in the water column during our expedition. The highest abundances (in #/m^3) of the selected species were found between 0 and 100 m water depth (Figure 3.3). This is the depth interval with highest chlorophyll-a vertical concentrations (Figure 3.1c), supporting the idea that nutrient distribution mainly determines the vertical distribution of foraminiferal species [*Hemleben et al.*, 1989; *Schiebel et*

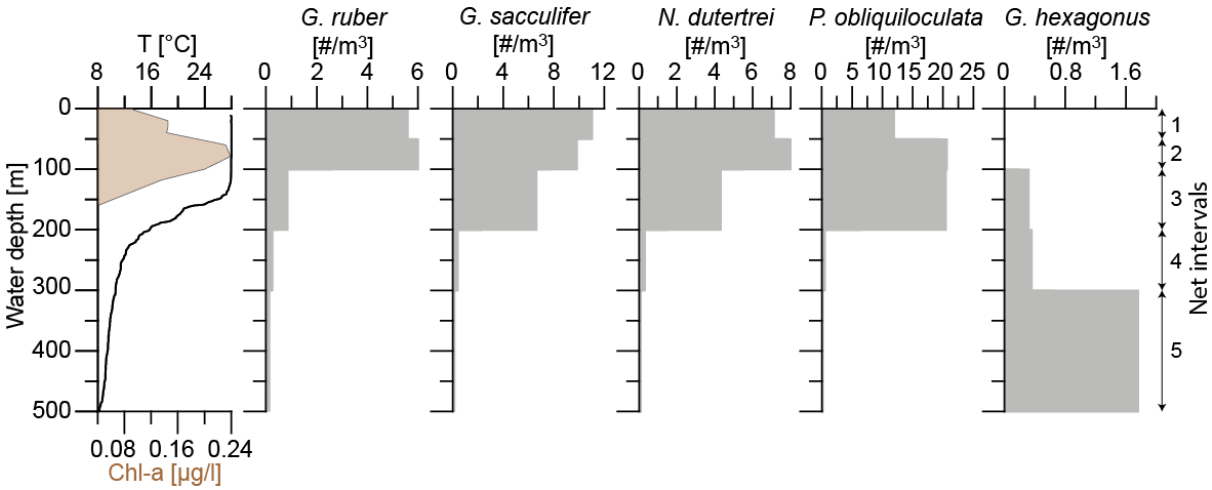

Figure 3.3. Planktonic foraminiferal abundances (in specimen/m^3) for five paleoceanographically important species in this study plotted with (on the left) *in-situ* data of temperature [*Werner et al.,* 2013] and chlorophyll-a (brown) [*Reverdin et al*., 1991]. Arrows and numbers on the right denote the five net intervals of the multinet collections with sea surface (1), sub-surface (2), upper thermocline (3), lower thermocline (4) and sub-thermocline (5).

al., 2001; *Schiebel and Hemleben*, 2005].

Sediment trap and surface sediment studies from tropical areas indicate that *G. sacculifer* and *G. ruber* dominate the foraminiferal abundances with >5 % and >10 %, respectively, with similar abundances in the Atlantic and Pacific for *G. sacculifer* (~10 %) and higher abundances of *G. ruber* in the Atlantic compared to the Pacific (~40 to ~18 %, respectively) [*Thunell and Honjo*, 1981; *Ravelo et al.*, 1990; *Kawahata et al*., 2002; *Schmuker and Schiebel*, 2002; *Yamasaki et al*., 2008]. Our MRAs, however, show abundances of these species of <10 % in December 2012. This is in agreement with sediment trap analyses from the West Caroline Basin (New Guinea) deployed over a one year interval that revealed a seasonal bias in foraminiferal shell flux with lowest fluxes for *G. ruber* and *G. sacculifer* in December [*Kawahata et al*., 2002]. Further, our study site at the northernmost rim of the Manihiki Plateau is situated at the transition from the WPWP to the Pacific Equatorial Divergence [*Le Borgne et al*., 2002]. High SSTs at the sampling site suggest the dominant influence from the WPWP. On the other hand, surface nitrate concentrations of 3.6 ± 0.1 µmol/kg (168.7°W, -3°S, 168°W) [*Key et al*., 2004] are higher than nitrate concentrations typically characteristic for the WPWP (<0.1 µmol kg^{-1}) [*Blanchot et al*., 2001; *Rafter and Sigman*, 2015] and rather suggest a presumably slight increased influence of the Pacific Equatorial Divergence. Additionally, repeated station analyses on nitrate concentrations along the equator also reveal increasing nitrate concentrations at the base of the SML during austral summer [*Rafter and Sigman*, 2015]. Since the hydrographic data record a general decrease in upwelling (Figure 3.2), higher nutrient concentrations probably result from increased diapycnal mixing [*Rafter and Sigman*, 2015]. As a consequence of these higher nutrient concentrations primary production was increased, which can be seen in the higher chlorophyll-a concentrations determined from Ocean Colour Data during sampling [*NASA Ocean Biology*, 2015]. The resulting higher amounts of nutrients and food most likely explain the relatively high abundances of *G. menardii*, *P. obliquiloculata,* and *G. glutinata*, which are often associated within or are found at the border of fertile tropical areas [*Watkins et al*., 1998]. A higher abundance of these species, in turn, will compete with *G. ruber* and *G. sacculifer*, and thereby, decrease their abundance as seen in our multinet analyses.

Despite the low MRA of 1.7 %, *G. hexagonus* dominates the foraminiferal assemblage with roughly 45 % at 300 – 500 m water depth (Supplement Table S3.5.1). Therefore, we included this species in our analyses as well. The high numbers below 300 m demonstrate its adaptation to deeper, colder waters. To date, there is only sparse information about the seasonal and the reproductive cycle of this species. Time series sediment traps from the Peru-Chile Current indicate that in contrast to most other deep-dwelling species, *G. hexagonus* is present year-round [*Marchant et al*., 1998]. Taking the preference for an ecologically more uniform habitat with smaller seasonal variations (compared to the shallow ocean) into account, the reproductive cycle of *G. hexagonus* could be similar to other deep-dwelling species (possibly once per year) [*Schiebel and Hemleben*, 2005]. However, more studies on their depth and seasonal distribution as well as their ecology are required to infer a specific calcification depth.

3.3.3 Foraminiferal apparent calcification depth

By combining the isotope-based ACDs (Figure 3.4a) with the Mg/Ca-based ACDs (Figure 3.4b), we can reliably infer the overall range of species-specific ACDs (Figure 3.4c, Table 3.3). Relative ACDs within a foraminifera assemblage point to *G. ruber* as the shallowest dweller, followed with increasing depth by *G. sacculifer*, *N. dutertrei*, *P. obliquiloculata* and *G. hexagonus* being the deepest dwelling species. The ACDs of these species are similar to that shown for other ocean basins [e.g. *Ravelo and Fairbanks*, 1992; *Dekens et al*., 2002; *Regenberg et al.,* 2009; *Steph et al*., 2009; *Rincón-Martínez et al*., 2011; *Birch et al.*, 2013; *Lynch-Stieglitz et al*., 2015]. However, absolute values differ between and within ocean basins. Furthermore, a large discrepancy between the $\delta^{18}O$-derived ACDs and the Mg/Ca temperature-derived ACDs can sometimes be observed. This is possibly the result of a combination of various effects:

1) Mg/Ca was measured on different and sometimes larger tests than tests used for isotope measurements due to logistical obstacles (Table 3.1). The test sizes used for the Mg/Ca ablation of this study are unusually large for Mg/Ca analyses that often concentrate on test sizes between 250 and 500 µm [e.g. *Dekens et al.*, 2002; *Anand et al*., 2003]. However, as we were limited by the amount of foraminiferal tests within the net samples for the measurements, we had to enlarge the size fraction. Studies have shown that there might be a size-related control on the incorporation of Mg into the foraminiferal shell with decreasing Mg/Ca values with increasing size possibly due to the additional formation of gametogenic calcite [*Elderfield et al*., 2002; *Ni et al.,* 2007; *Friedrich et al.,* 2012]. However, it was also shown that the amount of gametogenic calcite was constant (ca. 4 µg) independent of size [*Hamilton et al*., 2008]. The fact that the foraminifera we analysed often still had their spines or remains thereof indicates that gametogenetic calcite was not present. Nonetheless, isotope and Mg/Ca samples from a similar size range (Table 3.1) show comparable ACDs (Table 3.3) and thus, we consider the large size Mg/Ca-derived ACD estimations as reliable.

2) For laser ablation, only one single foraminiferal test was needed, but for isotope measurements more than one shell per species was used (Table 3.1). Thereby, the inter-sample variability was lower in isotope measurements, which could have led to less variability in ACD estimates.

3) The $\delta^{18}O$-paleotemperature equations applied in this study provide an additional reason for varying ACDs between the measurements. This holds true especially for mixed layer species as they are exposed to greater variability of water characteristics and thus, tend to have more ecology-related chemical effects. Mg/Ca was converted into temperatures using species-specific calibration equations (Table 3.2). For the determination of $\delta^{18}O_{equilibrium}$, we used the general equations of *Mulitza et al*. [2004] that was developed using four foraminiferal species reflecting both surface and sub-surface species and the equation of *Kim and O'Neil* [1997] that was derived from inorganic calcite (see *Chapter 3.2.5*).

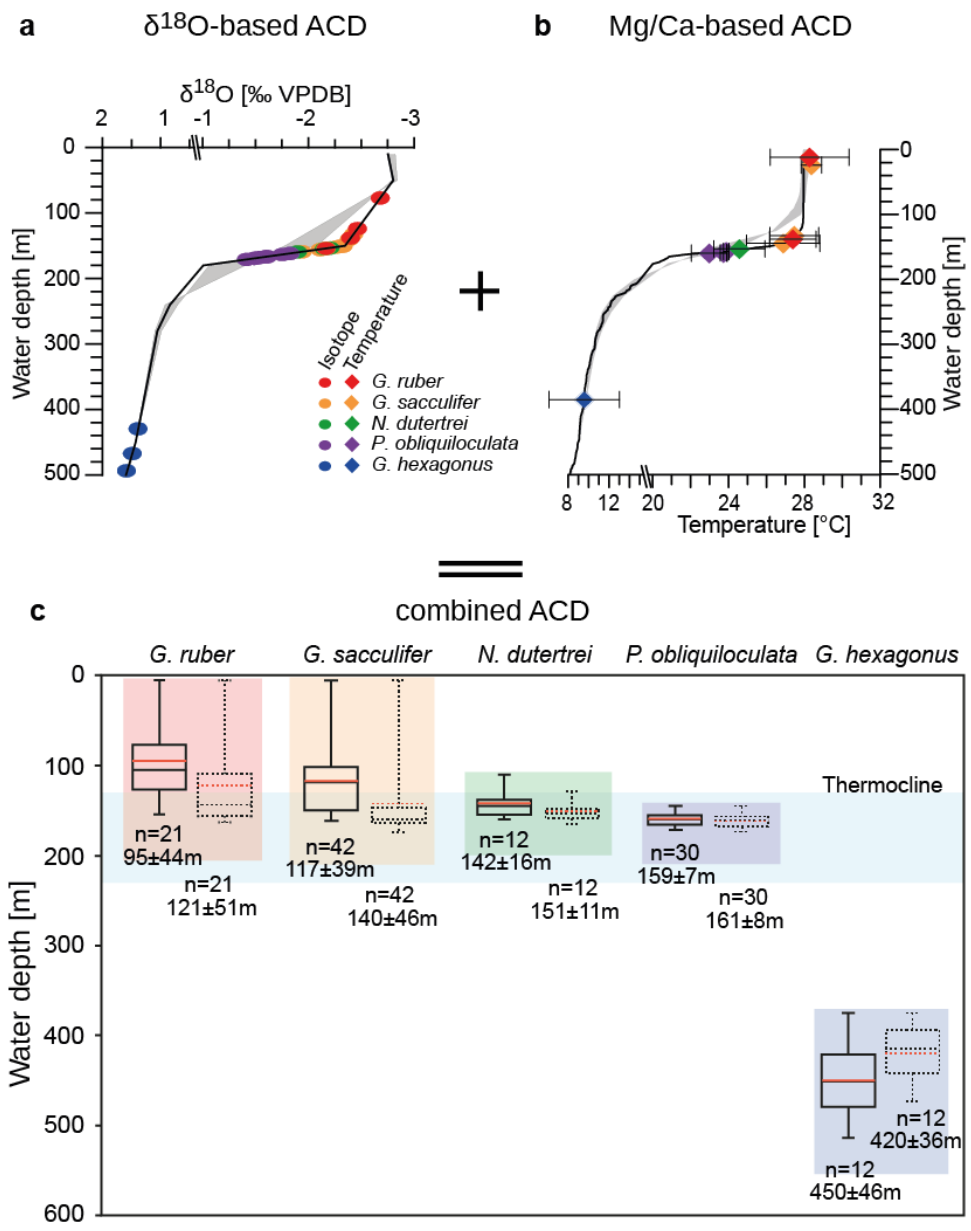

Figure 3.4. Assessment of Apparent Calcification Depths (ACD) for selected color-coded planktonic foraminiferal species from multinet station SO225-21. ACD is inferred from two approaches: a: measured foraminiferal $\delta^{18}O_{calcite}$ values were compared to $\delta^{18}O_{equilibrium}$ values, which were calculated using the water temperatures during sampling time (black) and seasonal temperatures [grey, *Locarnini et al.*, 2013] (see *Chapter 3.2.5* for detailed information), b: Mg/Ca derived species-specific temperature (with standard deviations) estimates were placed at water depths with the corresponding *in-situ* measured austral summer temperatures [*Werner et al.*, 2013] and seasonal temperature range [grey; *Locarnini et al.*, 2013] (see *Chapter 3.2.5*). c: Combined ACDs for each species. Each box plot represents the ACD of one species; the dashed box represents the ACD of each species corrected for $\delta^{18}O$-disequilibrium effects. Each box comprises 50 % of determined ACDs, ranging from quartile Q 0.25 to Q 0.75. The two lines within the box mark the median (black line) and the mean (red line, values and standard deviation is given below the box plot) and allow to decipher the skewness of the ACD distribution. The whiskers (vertical lines) denote the minimum and maximum values. The number of measurements (n) is given below the box plot.

3.3.3.1 Apparent calcification depths of *G. ruber* and *G. sacculifer*

At multinet station SO225-21-3, *G. ruber* and *G. sacculifer* calcified over a broad depth range ranging from the sea surface down to ~160 m water depth (Figure 3.4, Table 3.3). This mirrors the thick SML in the WPWP and supports the notion of these species being surface-dwellers [*Fairbanks et al.*, 1982; *Bé et al*., 1985; *Ravelo and Fairbanks*, 1992; *Watkins et al*., 1996; *Steph et al.*, 2009; *Rincón-Martínez et al*., 2011; *Lynch-Stieglitz et al*., 2015; *Nürnberg et al.*, 2015].

Most studies point to a habitat of *G. ruber* within the first 30 m of the water column [*Fairbanks et al*., 1982; *Bé et al.*, 1985; *Faul et al.,* 2000; *Mohtadi et al*., 2009] and *G. sacculifer* within the first 80 m [*Fairbanks et al*., 1982; *Bé et al*, 1985; *Watkins et al*., 1996; *Steph et al*., 2009]. Our study revealed that in December 2012, highest *G. ruber* abundances were found in the nets of 50 – 100 m (Figure 3.3) and the ACD estimate showed that 50 % of *G. ruber* calcified between 70 and 125 m (Figure 3.4). The depth agrees well to the optimum temperature preference of ~27°C [*Mulitza et al*., 1998]. Various studies point towards varying calcification depths for different morphotypes of *G. ruber* [*Wang*, 2000; *Steinke et al*., 2005; *Kuroyanagi et al.*, 2008] and a seasonal bias in *G. ruber* abundances [e.g. *Kawahata et al*., 2002; *Stott et al*., 2002; *Lin et al.*, 2004; *Žarić et al*., 2005]. However, with the present dataset we are not able to address this issue.

The determined ACDs of *G. sacculifer* are commonly deeper than the ACDs of *G. ruber* (Table 3.3), which corroborates Central Pacific core-top studies that recorded heavier $\delta^{18}O$ values and thus, a generally deeper ACD for *G. sacculifer* in comparison to *G. ruber* [*Lynch-Stieglitz et al*., 2015]. Furthermore, a plankton tow study from the South Atlantic revealed that in areas with a thick mixed layer, *G. sacculifer* often exhibits deeper ACDs than *G. ruber*, whereas in areas with a shallow thermocline, both species dwell at similar depths [*Kemle-von Mücke and Oberhänsli*, 1999]. This observation agrees with the slightly cooler optimum temperature range in *G. sacculifer* compared to *G. ruber* [*Bijma et al.*, 1990]. Fifty percent of *G. sacculifer*'s ACDs fall in the depth range between 100 and 150 m, which is deeper than the highest abundances of this species, which is found in the nets in 0 – 50 m. However, it has been shown that *G. sacculifer* migrates to deeper water depths later in its ontogeny [*Hemleben and Bijma*, 1994]. As small individuals outnumber larger specimens due to the high mortality rate, highest total abundances of this species are much shallower than ACDs determined on larger specimens [*Hemleben and Bijma*, 1994]. Furthermore, a stratified plankton-tow study from the Red Sea showed that specimens from the 350 – 500 µm size fraction accumulate in a narrow depth range [*Bijma and Hemleben*, 1994] similar to our results. This also explains why tests selected from deeper habitats depths (100 – 200 m for *G. sacculifer* and 300 – 500 m for *G. ruber*) also record ACDs within the SML and not from the net depth range they were selected from (Tables 3.1 and 3.3). Hence, calcification of these tests happened within the SML. Just before net sampling, these specimens possibly died and sank down to the to the depth in which we caught them.

The SML at the study site extended deeper than the SML recorded by the long-term average at the same position (Figure 3.2a). This could explain why the ACDs of *G. ruber* and *G. sacculifer*

are deeper than ACDs estimated from seasonally varying temperatures (Table 3.3). Using seasonal temperatures, both species record shallowest ACDs in austral winter and deepest during austral summer, possibly also as a result of changes in the depth of the DCM (Figure 3.1c). Despite the fact that both species host symbionts and are therefore highly dependent on light availability [*Hemleben and Bijma*, 1994; *Schiebel and Hemleben*, 2005], the data suggest that these species possibly descend to deeper waters in oligotrophic environments to exploit the DCM for food as proposed by e.g. *Fairbanks et al.* [1982], *Schiebel et al*. [2001], *Schiebel and Hemleben* [2005], and *Steph et al*. [2009].

Species-specific vital-effects can alter the ACD assessment, as the deviation from isotopic equilibrium might result in too-deep or too-shallow calculated ACDs. In symbiont-bearing species vital effects have been shown to be large [*Niebler et al*., 1999]. Correcting the measured $\delta^{18}O_{calcite}$ data for a disequilibrium of -0.4 ‰ and -0.6 ‰ [*Niebler et al.,* 1999] for *G. ruber* and *G. sacculifer*, respectively, results in <23 % deeper ACDs for *G. ruber* and <10 % deeper ACDs for *G. sacculifer* that would point to a calcification within the thermocline (Figure 3.4, Supplement Table S3.5.3). However, as the highest abundances of these species were found in surface waters similar to other studies, we find these deep vital-corrected ACDs rather unlikely.

In summary, it seems that ACDs determined by using measured temperatures during sampling (December 2012) or seasonal temperatures do not differ substantially. However, using vital-corrected ACDs might lead to different results as foraminifera might be placed into different water masses. Thus, to make realistic ACD-reconstructions, one needs to consider the combination of determined ACD, the local hydrography, local foraminiferal abundance data, and to take into account that the last few chambers determine the majority of the chemical signature of the shell.

3.3.3.2 Apparent calcification depths of *N. dutertrei* and *P. obliquiloculata*

The ACD assessment at the sampling site for *N. dutertrei* and *P. obliquiloculata* reveals calcification in a very narrow depth range at the top and within the upper thermocline, which is in broad agreement with ACD studies [e.g. *Ravelo and Fairbanks*, 1992; *Faul et al.,* 2000; *Regenberg et al.,* 2009; *Steph et al.,* 2009]. The mean ACD of ~140 ± 16 m (*N. dutertrei*) and ~160 ± 7 m (*P. obliquiloculata*) (Table 3.3) are somewhat deeper than in other studies, possibly due to the comparatively deep thermocline in the western equatorial Pacific. As the thermocline was warmer during sampling than the long-term average (see *Chapter 3.3.1*), we also calculated the ACDs using seasonal temperature data [*Locarnini et al*., 2013]. The estimated seasonal ACDs are, however, within the ACD range determined by the combined stable isotope and temperature approach (Table 3.3). Furthermore, both species are also affected by isotopic disequilibrium. Correcting the measured $\delta^{18}O_{calcite}$ values of *N. dutertrei* and *P. obliquiloculata* for disequilibrium of -0.2 ‰ and -0.1 ‰ [*Niebler et al*., 1999], respectively, only small shifts towards

deeper water depths of <3 % for *N. dutertrei* and <1 % for *P. obliquiloculata* occur (Figure 3.4; Supplement Table S3.5.3).

The net collection from this study has the highest abundance of *N. dutertrei* in 50 – 100 m water depth within the DCM (Figure 3.3). This agrees with the general view that *N. dutertrei* inhabits a shallow water depth close to the DCM [*Fairbanks et al*., 1982; *Bé et al*., 1985; *Hemleben et al*., 1989; *Ravelo and Fairbanks*, 1992; *Dekens et al*., 2002; *Schmuker and Schiebel*, 2002; *Sadekov et al.*, 2013]. Our study site at the Manihiki Plateau is at the border of the Pacific Equatorial Divergence (see also *Chapter 3.3.2*). As the longitudinal transition between WPWP and Pacific Equatorial Divergence varies between ~150°E and 150°W [*Le Borgne et al.,* 2002] depending on the wind strength and surface currents, it is expected that *N. dutertrei* changes its habitat and calcification depth depending on the prevailing environmental setting. This is supported by calcification-depth studies from the highly dynamic eastern equatorial Pacific that reveal variable habitats depending on the strength of the coastal upwelling with shallower habitats in cases of strong upwelling [*Nürnberg et al*., 2015, and discussion therein].

Our ACD estimates for *P. obliquiloculata* correspond well with the observations: all specimens, regardless of the net depth the foraminifera were taken from, calcified between 145 m and 170 m and highest abundances of adult specimen were found in nets of 100 – 200 m water depths. Consequently, this species might be more appropriate for thermocline reconstructions. This is in line with previous studies showing that *P. obliquiloculata* is associated with the base of the upper thermocline in other ocean basins [e.g. *Ravelo and Fairbanks*, 1992; *Faul et al*., 2000; *Mohtadi et al*., 2009; *Rincón-Martínez et al.*, 2011].

3.3.3.3 Apparent calcification depths of *G. hexagonus*

Both $\delta^{18}O$-derived and Mg/Ca-derived ACDs display a deep habitat for *G. hexagonus* ranging from 375 to 515 m water depth (mean ACD: 450 m ± 46 m) (Figure 3.4, Table 3.3) below the thermocline. As seasonal temperature variations are <0.4°C in 300 – 500 m water depth, the ACD of *G. hexagonus* varies by maximal 30 m. Most deep-dwelling foraminifera calcify close to isotopic equilibrium with small positive deviations [*Niebler et al*., 1999]. Applying a +0.1 ‰ disequilibrium-correction to the $\delta^{18}O_{calcite}$ values (Supplement Table S3.5.3) results in an up to 30 m shallower ACD, which is still clearly below the thermocline (Figure 3.4). Overall, the assessed ACDs correspond well to the highest abundances from the net collection in 300 – 500 m water depth (Figure 3.3).

Depth assignments from other studies are rare, as this species is endemic for the Indo-Pacific [*Schiebel and Hemleben*, 2005] and hardly ever exceeds a relative abundance of 2 % in sediment assemblages [*Beiersdorf et al*., 1996; *Hilbrecht*, 1996]. Our depth assessment, nevertheless, is similar to a study from the North Pacific with an estimated calcification depth of 330 – 390 m below the thermocline [*Ortiz et al.*, 1996]. However, our estimated ACD is deeper than the calcification depth reported from a core-top study from the western tropical Indian Ocean

that places the calcification depth between ~100 – 160 m, i.e. within the mid-thermocline [*Birch et al*., 2013]. These differences are probably the result of an interaction of four different effects:

1) In the Indian Ocean, *Birch et al*. [2013] used a different size window ranging from 125 to 300 µm, whereas the test selected for this study range from 250 to 400 µm. Although smaller individuals often inhabit shallower waters than larger individuals [*Fairbanks et al*., 1982; *Bijma and Hemleben*, 1994; *Kroon and Darling*, 1995], our smallest size fraction still records far deeper habitats than largest specimen derived from Indian Ocean samples. Thus, the size effect on the different ACDs is assumed to be rather small.

2) *Birch et al*. [2013] applied the paleotemperature equation of *Erez and Luz* [1983], which was calibrated using symbiont-bearing *G. sacculifer*. As *G. hexagonus* does not harbour symbionts [*Parker*, 1962], this symbiotic equation may result in erroneous temperatures. Symbionts increase ambient pH and [CO_3^{2-}] and hence decrease shell $\delta^{18}O$ [*Spero et al.,* 1997; *Bijma et al*., 1999], leading to an over-estimation of the real calcification temperature and hence would infer a calcification depth that is too shallow. By recalculating the ACD of *G. hexagonus* in the Indian Ocean with the equation by *Kim and O'Neil* [1997], the resulting ACD is deeper, between 110 and 180 m. Nevertheless, this re-calculated ACD still lies within the western tropical Indian Ocean thermocline, highlighting the need for further explanations for varying ACDs of *G. hexagonus*.

3) *Ortiz et al*. [1996] argue that *G. hexagonus* is a sub-thermocline species well adapted to its deep habitat, which is associated with the NPIW in the North Pacific. This water mass is characterized by elevated nutrient and particulate organic matter concentrations [e.g. *Yamanaka and Tajika*, 1996; *Sarmiento et al*., 2004]. In contrast, sub-thermocline Indian Ocean water masses are less nutrient-rich than in the North Pacific. Furthermore, deep-dwelling (non-spinose) foraminifera such as *Globorotalia tuncatulinoides* or *Globorotalia hirsuta* are mainly herbivores [*Hemleben et al*., 1989; *Schiebel and Hemleben*, 2005]. The sub-thermocline species *Globorotalia scitula*, for example, feeds on detrital, particulate organic material [*Itou et al*., 2001]. As *G. hexagonus* inhabits a similar depth range to that of *G. tuncatulinoides* and *G. scitula*, we hypothesize that *G. hexagonus* is also a herbivore, feeding on particulate organic material. Consequently, *G. hexagonus* possibly calcifies in shallower water masses in the western Indian Ocean within the thermocline, where nutrients and particulate organic material accumulate. At our sampling site, the majority of Pacific equatorial sub-surface waters originate from outside the tropics and feed the equatorial sub-surface current system. The ACD determined for *G. hexagonus* corresponds to the depth of the Tsuchiya Jets that transport nutrients and particulate organic material originating in the extra-tropical regions along the equatorial Pacific (Figure 3.1a) [*Johnson and Moore*, 1997; *Rowe et al*., 2000]. Thus, we conclude, that *G. hexagonus* favours water masses enriched in nutrients.

4) Another important factor might be the insensitivity of *G. hexagonus* to changing oxygen concentrations in the water column [*Birch et al*., 2013]. In the Indian Ocean, *G. hexagonus*

calcifies in relatively low oxygen concentrations of 100 – 130 µmol/kg, just above the OM [*Birch et al.*, 2013]. Similarly, at our sampling site, the ACDs in 375 – 500 m water depth correspond to decreasing oxygen concentrations (~60 µmol/kg) (Figure 3.2d) towards the OM at 450 m water depth. Hence it seems, that *G. hexagonus* prefers to calcify in cool, oxygen-depleted and nutrient-rich water masses and consequently, might be most suitable for reconstructing the variability in extra-tropical nutrient inflow into the equatorial current system.

3.3.4 Foraminiferal carbon isotope disequilibrium

In order to evaluate modern species-specific $\delta^{13}C$-disequilibrium effects at certain growth stages, we measured the $\delta^{13}C_{calcite}$ values on various size fractions. The overall $\delta^{13}C_{calcite}$ values range from -0.14 ‰ in *N. dutertrei* to a maximum value of +1.53 ‰ in *G. sacculifer* (Figure 3.5, Table 3.4). Generally, deeper dwelling species record lower $\delta^{13}C_{calcite}$ values (concomitant with higher $\delta^{18}O_{calcite}$ values) than SML species. A variety of parameters including algal photosynthesis [*Bé et. al.*, 1982; *Hemleben et al.*, 1989], metabolic fractionation [*Wefer and Berger,* 1991; *Kroon and Darling*, 1995; *Spero et al.*, 1997], food availability [*Spero et al.*, 1991; *Ortiz et al.*, 1996], and carbonate chemistry of the seawater [*Spero et al.*, 1997; *Bijma et al.*, 1999] influence foraminiferal $\delta^{13}C_{calcite}$ values.

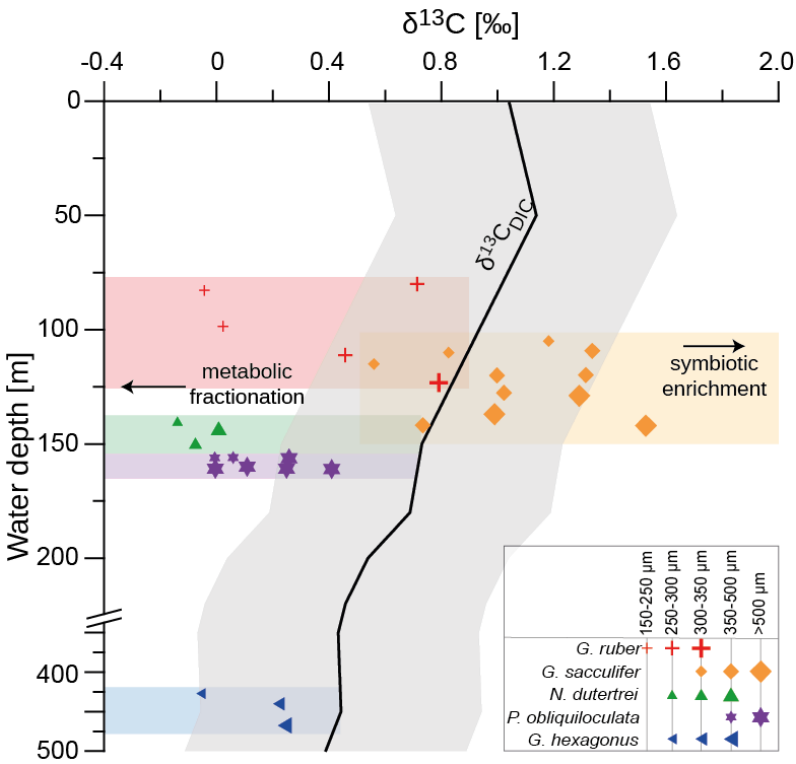

Figure 3.5. Measured $\delta^{13}C_{calcite}$ of selected living planktonic foraminifera in comparison to the *in-situ* measured $\delta^{13}C_{DIC}$ (black line) measured at multinet station SO225-21-3. Each symbol corresponds to a single species. The size of the symbol characterizes the specific test-size spectrum. Instrumental standard deviation is smaller than symbol sizes (±0.01 ‰), therefore not shown. Coloured-boxes

illustrate the depths at which 50 % of each species calcify (Figure 3.4c). Values more negative than the equilibrium line are mostly affected by metabolism and respired light carbon, more positive values are possibly affected by symbiotic activity. Grey shaded area represents the ±0.5 ‰ inter-sample $\delta^{13}C_{calcite}$ variability ('$\delta^{13}C_{calcite}$-envelope') expected in foraminiferal analyses.

Table 3.4. Foraminiferal $\delta^{13}C_{calcite}$ values with the determined $\delta^{13}C$-disequilibrium and $\delta^{13}C$-disequilibrium values using vital-corrected ACDs. Each line represents one measurement of the respective species.

Species	Shell size [range in µm]	Number of tests measured	$\delta^{13}C_{calcite}$ [‰]	Disequilibrium [‰]	Disequilibrium 'vital-corrected' [‰]
G. ruber	150 – 250	18	-0.04	-1.1	-0.9
	150 – 250	17	0.02	-1.0	-0.9
	250 – 300	11	0.71	-0.3	-0.2
	250 – 300	14	0.46	-0.6	-0.4
	300 – 350	9	0.79	-0.2	-0.1
G. sacculifer	300 – 350	7	1.18	0.5	0.5
	300 – 350	5	0.83	-0.1	0.1
	300 – 350	6	0.56	-0.4	-0.2
	350 – 500	4	1.31	0.6	0.6
	350 – 500	4	1.00	0.3	0.3
	350 – 500	4	1.34	0.6	0.6
	350 – 500	5	1.02	0.3	0.3
	350 – 500	5	0.73	-0.2	-0.01
	>500	2	1.53	0.8	0.8
	>500	3	0.99	0.3	0.3
	>500	2	1.29	0.6	0.6
N. dutertrei	250 – 300	12	-0.14	-0.9	-0.9
	300 – 350	9	-0.08	-0.9	-0.8
	350 – 500	6	0.03	-0.8	-0.7
P. obliquiloculata	350 – 500	4	0.06	-0.7	-0.7
	350 – 500	4	-0.01	-0.7	-0.7
	>500	2	-0.01	-0.7	-0.7
	>500	2	0.26	-0.5	-0.5
	>500	2	0.25	-0.5	-0.5
	>500	2	0.11	-0.6	-0.6
	>500	2	0.41	-0.3	-0.3
G. hexagonus	250 – 300	10	-0.06	-0.5	-0.5
	300 – 350	9	0.22	-0.2	-0.2
	350 – 500	6	0.24	-0.2	-0.2

Using the determined ACDs in which 50 % of the species calcify (between quartile Q 0.25 and Q 0.75) (Figure 3.4c), we attempted to infer the species-specific $\delta^{13}C$-disequilibrium from ambient seawater at the study site. We did not determine the carbonate chemistry at the study site and

hence, we cannot correct for the carbonate ion effect. Nevertheless, the measured $\delta^{13}C_{calcite}$ reveals a distinct size-dependent deviation from $\delta^{13}C_{DIC}$ values that generally agrees with other studies, such as *Oppo and Fairbanks* [1989], *Spero et al*. [1991], *Spero and Lea* [1993], *Kroon and Darling* [1995], and *Birch et al*. [2013]. The offset from ambient seawater for most species is even more pronounced than the added ±0.5 ‰ $\delta^{13}C$-uncertainty (the '$\delta^{13}C$-envelope') that might be expected in measured foraminiferal values to account for inter-sample variability expected in foraminiferal analysis [*Birch et al*., 2013]. We also used 'vital-effect' corrected ACDs for the $\delta^{13}C$-disequilibrium assessment. However, following this approach only results in little, if any, change in the ACD of the respective species (Table 3.4).

Large individuals of symbiont-bearing *G. ruber* and *G. sacculifer* are influenced by algal photosymbiosis. The symbionts preferentially incorporate light carbon into the organic matter leaving the microenvironment the foraminifera calcifies from enriched in ^{13}C. Hence, ^{13}C-enriched chambers are produced [*Spero and Lea*, 1993]. Since the symbiont density increases with shell size [*Spero and Parker*, 1985], the $\delta^{13}C_{calcite}$ values become more positively offset from ambient seawater $\delta^{13}C_{DIC}$ with up to +0.8 ‰ in *G. sacculifer*. However, small individuals of SML and thermocline species have a large surface-to-volume ratio, tend to grow more rapidly, and possibly show a larger impact of depleted, respired CO_2 due to higher metabolic activity [*Berger et al*., 1978; *Wefer and Berger*, 1991; *Spero et al*., 1997]. As a result, foraminiferal $\delta^{13}C_{calcite}$ is often negatively offset from equilibrium by up to -1.1 ‰ (in *G. ruber*) (Table 3.4). As an individual grows, the influence of symbiont-isotopic fractionation increases and dominates over the impact of respiration [*Berger et al*., 1978; *Wefer and Berger*, 1991; *Spero et al*., 1997].

Deep-dwelling asymbiotic *G. hexagonus* generally reveals a disequilibrium fractionation of ≤ -0.5 ‰, which is in the range of the $\delta^{13}C_{DIC}$–uncertainty. Only small tests of this species are slightly negatively depleted in $\delta^{13}C_{calcite}$, probably due low metabolic rates as a consequence of low temperatures. Nevertheless, the near-equilibrium calcification is supported by a study from the tropical Indian Ocean [*Birch et al.,* 2013], highlighting *G. hexagonus* as a reliable recorder of $\delta^{13}C$ in sub-surface water masses.

3.4 Conclusions

The quality of paleoceanographic reconstructions of upper-ocean water mass conditions is tied to our precise knowledge of the ACDs of the studied foraminiferal species. The comparison between $\delta^{18}O_{calcite}$ and Mg/Ca-derived temperatures measured on five living planktonic species with *in-situ* physical and chemical water mass properties enables us to enhance our knowledge about the species-specific ACDs.

The WPWP experiences a pronounced year-round thick SML that still extends deeper during December 2012 down to ~130 m water depth. Determined ACDs of symbiont-bearing species *G. ruber* and *G. sacculifer* using both seasonal temperature data and temperatures during

sampling indicate mean calcification depth of ~95 m and ~120 m, respectively, corresponding to the base of the SML. These ACDs are deeper than in other ocean basins due to the hydrographic conditions of the WPWP, and the optimum temperature preference of these foraminifera. As vital effects further affect symbiont-bearing species, a combined approach of foraminiferal abundances, determined ACDs and hydrography provides most reliable ACD reconstructions.

Below the SML *N. dutertrei* and *P. obliquiloculata* calcified in a very narrow depth range of 140 – 160 m, corresponding to the top and within the thermocline, regardless of the temperature data used (seasonal or during sampling). The same holds true for vital effect corrections. The agreement between our ACD of *P. obliquiloculata* and other studies, suggest that *P. obliquiloculata* is most suitable for thermocline reconstructions.

The species *G. hexagonus* records mean ACDs of ~450 m and is thus the deepest dwelling species from the analysed species of this study. It calcifies its test in oxygen-depleted, but nutrient-rich water masses. The same trend has been observed in other studies from different ocean basins. Temperature and seawater chemistry are more stable in sub-surface waters compared to surface water conditions. As a consequence, *G. hexagonus* calcifies in $\delta^{13}C$-equilibrium with ambient seawater, and hence, this species serves as an archive for tracing nutrient variations in equatorial Pacific mode and intermediate water masses being sourced in extra-tropical regions.

Acknowledgements.

This work was funded by the German Ministry for Education and Research (BMBF - Bundesministerium für Bildung und Forschung) in the framework of the joint project Manihiki II (03G0225B). We thank the captain, crew and participants of RV SONNE cruise SO225 for retrieving the studied material. B. Donner and M. Kucera are acknowledged for helping with foraminiferal identification. We are grateful to B. Glückselig, J. Voigt, L. Schönborn, G. Meyer and A. Mackensen for helping with sample preparation, Mg/Ca evaluation and isotope analyses. We express our thanks to J. Roberts for language assistance. We thank the editor Frans Jorissen and two anonymous reviewers for their help in improving the quality of the manuscript. The data of this study are available at PANGEA (URL: http://www.pangaea.de).

Appendix A. Species list

Globigerinella spp. [Cushman 1927], *Globigerinita glutinata* [Egger 1893], *Globigerinoides ruber* var. white [d'Orbigny 1839], *Globigerinoides sacculifer* [Brady 1877], *Globoquadrina conglomerata* [Schwager 1866], *Globorotalia hirsuta* [d'Orbigny, 1839], *Globorotalia menardii* [d'Orbigny 1865], *Globorotalia scitula* [Brady, 1882], *Globorotalia truncatulinoides* [d'Orbigny, 1839], *Globorotalia* spp. [Cushman 1927], *Globorotaloides hexagonus* [Natland 1938], *Neogloboquadrina dutertrei* [d'Orbigny 1839], and *Pulleniatina obliquiloculata* [Parker and Jones 1862].

Appendix B. Supplementary data

Supplementary data to this article can be found online at http://dx.doi.org/10.1016 /j.marmicro.2016.08.004.

3.5 Supplementary data

To:

Rippert, N., Nürnberg, D., Raddatz, J., Maier, E., Hathorne, E., Bijma, J., Tiedemann, R., 2016. Constraining foraminiferal calcification depths in the western Pacific warm pool. Marine Micropaleontology 128, 14-27. doi:10.1016/j.marmicro.2016.08.004.

Table S3.5.1. Foraminiferal assemblage counting at station SO225-21 in December 2012. Values of zeros were omitted for a clearer view.

Net depth	*G. ruber*	*G. sacculifer*	*N. dutertrei*	*P. obliquiloculata*	*G. menardii*	*G. truncatulinoides*	*G. crassaformis*	*G. tumida*	*Globorotalia* spp.	*O. universa*	*G. bulloides*	*G. glutinata*	*G. hexagonus*	*Globoturborotalita* spp.	*H. pelagica*	*G. conglomerata*	*G. conglobatus*	*Globigerinella* spp.	*G. minuta*	*Turborotalita* spp.	others	Total
countings																						
0 – 50	70	138	89	149	275			12	152	24		296		4	4	40		140			16	1409
50 – 100	75	123	100	258	386			12	164	16	4	316		8		24		208			16	1710
100 – 200	21	166	108	512	688			48	280	24		160	8	56	16	56		416			48	2607
200 – 300	6	10	8	13	16		1		9		4	62	9	7	5	5	3	14	16	11	7	206
300 – 500	6	7	5	10	26			1	7		1	11	88		21	2		7	1		1	194
																						6126
relative abundance																						
0 – 50	4.97	9.79	6.32	10.57	19.52			0.85	10.79	1.70		21.01		0.28	0.28	2.84		9.94			1.14	
50 – 100	4.39	7.19	5.85	15.09	22.57			0.70	9.59	0.94	0.23	18.48		0.47		1.40		12.16			0.94	
100 – 200	0.81	6.37	4.14	19.64	26.39			1.84	10.74	0.92		6.14	0.31	2.15	0.61	2.15		15.96			1.84	
200 – 300	2.91	4.85	3.88	6.31	7.77		0.49		4.37		1.94	30.10	4.37	3.40	2.43	2.43	1.46	6.80	7.77	5.34	3.40	
300 – 500	3.09	3.61	2.58	5.15	13.40			0.52	3.61		0.52	5.67	45.36		10.82	1.03		3.61	0.52		0.52	
MRA	2.91	7.25	5.06	15.38	22.71		0.02	1.19	9.99	1.04	0.15	13.79	1.71	1.22	0.75	2.07	0.05	12.81	0.28	0.18	1.44	
specimen/m3																						
0 – 50	5.6	11.04	7.12	11.92	22			0.96	12.16	1.92		23.68		0.32	0.32	3.2		11.2			1.28	112.7
50 – 100	6	9.84	8	20.64	30.88			0.96	13.12	1.28	0.32	25.28		0.64		1.92		16.64			1.28	136.8
100 – 200	0.84	6.64	4.32	20.48	27.52			1.92	11.2	0.96		6.4	0.32	2.24	0.64	2.24		16.64			1.92	104
200 – 300	0.24	0.4	0.32	0.52	0.64				0.36		0.16	2.48	0.36	0.28	0.2	0.2		0.56	0.64	0.44	0.28	8.2
300 – 500	0.12	0.14	0.1	0.2	0.52			0.02	0.14		0.02	0.22	1.76		0.42	0.04		0.14	0.02		0.02	3.9

Table S3.5.2. Mg/Ca values of single measurements.

Nr of Foraminifera	Species	Net depth [m]	Shell size [range in µm]	Chamber number	Mg/Ca [mmol/mol]	Mean Mg/Ca [mmol/mol]
1	*G. ruber*	100 – 200	410	Final	4.30	4.71
				F-1	4.66	
				F-2	5.16	
2	*G. ruber*	300 – 500	320	Final	4.23	5.10
				F-1	5.63	
				F-2	5.43	
3	*G. sacculifer*	0 – 50	520	Final	3.61	4.27
				F-1 (2)	4.45	
				F-2	4.76	
4	*G. sacculifer*	100 – 200	645	Final	4.05	4.50
				F-1	4.89	
				F-2	4.55	
5	*G. sacculifer*	300 – 500	750	Final	4.67	4.88
				F-1	4.89	
				F-2	5.06	
6	*N. dutertrei*	100 – 200	360	Final	3.50	3.21
				F-1	2.93	
				F-2	3.02	
				F-3	3.30	
				F-4	3.30	
7	*P. obliquiloculata*	0 – 50	520	Final	3.12	3.16
				F-1	3.16	
				F-2	3.21	
8	*P. obliquiloculata*	100 – 200	675	Final	3.07	3.11
				F-1	3.15	
9	*P. obliquiloculata*	300 – 500	640	Final	2.61	2.85
				F-1	2.80	
				F-2	3.14	
10	*G. hexagonus*	300 – 500	400	Final	0.95	1.36
				F-1	1.16	
				F-2	1.48	
				F-3	1.84	

S3.5.3. Evaluation of various Mg/Ca-temperature calibrations

Mg incorporation into foraminiferal tests is highly biologically mediated [*Nürnberg et al*., 1996; *Rosenthal et al*., 1997; *Lea et al*., 1999; *Dueñas-Bohórquez et al*., 2009; 2011]. Due to these so-called "vital effects" there are species-specific differences in the uptake of Mg into the foraminiferal calcitic test. As a consequence, separate Mg/Ca thermometer calibrations for different species of planktonic foraminifera have been developed either on core top samples or culture experiments [*Nürnberg et al*., 1996; *Dekens et al*., 2002; *Anand et al*., 2003; *Cléroux et al*., 2008; *Regenberg et al*., 2009]. All equations have basic similarities, but slight differences might lead to significantly different temperatures estimates when applied to the same Mg/Ca ratio. To find the most applicable calibration equation for each investigated planktonic foraminiferal species from the multinet samples, we converted the measured foraminiferal Mg/Ca ratios into temperatures using generic and species-specific equations if available (Table S3.5.3, Figure S3.5.3). We analysed as many chambers as possible to minimize random variations in Mg/Ca within a test [*de Nooijer et al*., 2014]. Previous culturing studies have investigated the difference between whole-test calibrations and Mg/Ca-temperature equations based on Mg/Ca measurements of the last four chambers and found no significant difference between them [*Dueñas-Bohórquez et al*., 2009; *Spero et al*., 2015]. Further, *Hathorne et al.* [2003] and *Reichart et al*. [2003] found that Mg/Ca data from both single-chamber and multiple-shells are similarly correlated to temperature. At the depth interval in which a species was found in highest abundance per m^3 at the Manihiki Plateau (Table S3.5.1), we determined the mean temperature during sampling time from both CTD data and the seasonal range in temperature from the WOA13 data [*Locarnini et al*., 2013] at the same location. By comparing these *in-situ* temperatures with the Mg/Ca-derived temperatures, we identified the most suitable calibration equation for each species at our study site.

G. sacculifer was found most abundant per m^3 in 0 – 100 m water depth. The calibration of *Anand et al*. [2003] gives the warmest temperatures, which are consistently higher than the seasonal range and result in temperatures of up to 32°C. A similar result derives using the equation by *Nürnberg et al*. [2000]. Thus, we neglect these calibrations. Using the calibration by *Dueñas-Bohórquez et al*. [2011, whole chamber] results in coldest temperature. The temperatures derived by *Dekens et al.* [2002] deviate from the average temperatures by only up to 0.8°C. As this calibration was deduced using surface sediment samples from the equatorial Pacific, we found this equation most applicable for our *G. sacculifer* calibration.

G. ruber is analysed frequently in paleoceanographic research to reconstruct past sea surface temperatures, hence many species-specific calibrations are available. The net collections indicate that *G. ruber* appears most abundant per m^3 in water depths between 0 – 100 m. The comparison between the calculated and *in-situ* temperatures from that depth interval shows that the species-specific calibration of *Lea et al*. [2000] results in the warmest temperatures of >30°C, which outreaches the *in-situ* temperatures and the seasonal range by far. Thus, we reject this

calibration curve to minimize an overestimation of our temperatures. The calibration of *Mohtadi et al.* [2009] gives the coldest temperatures for *G. ruber*, even colder than the seasonal temperature range. Calibration equations of *Dekens et al*. [2002], *Regenberg et al*. [2009], and *Anand et al*. [2003] are similar and differ only by ~1°C. Both *Dekens et al.* [2002] and *Regenberg et al*. [2009] calibrated their equation with material from the low latitudes. As *Regenberg et al*. [2009] used *G. ruber* shells from a similar size fraction (355 – 400 µm) as our analysed foraminifera (320 – 425 µm), we selected this species-specific calibration equation for further analyses of *G. ruber*.

Neogloboquadrina dutertrei and *P. obliquiloculata* were both found in major abundances per m^3 between 50 – 100 m water depth. However, we compared the Mg/Ca-derived temperatures to *in-situ* temperatures from 100 – 200 m water depth, as most large foraminifers of these species were found at this depth. As this depth interval collides with the thermocline, a very large seasonal range exists. For *N. dutertrei* we applied three species-specific and one generic calibration equation. The various calibrations show a large scatter within the calculated temperature with coldest temperatures derived from *Elderfield and Ganssen* [2000] and warmest temperatures with the equation of *Anand et al.* [2003]. *Elderfield and Ganssen* [2000] used a combination of 8 different species for its equation and thus, is not species-specific. We also reject the calibration of *Dekens et al*. [2002], despite the fact that the calculated temperatures lies well within the seasonal range. However, *Dekens et al*. [2002] assumed for its equation a habitat depth of their adult species of 50 m for *N. dutertrei*. Due to the varying habitat of this species [e.g. *Nürnberg et a*l., 2015], the authors itself denote the limit of their equation for *N. dutertrei*. Most applicable for our *N. dutertrei* Mg/Ca estimates is the calibration of *Regenberg et al*. [2009]. This calibration yields temperatures most similar to the mean temperature between 100 – 200 m water depth.

For *P. obliquiloculata* we tested two species-specific equations and additionally consulted two generic equations. The species-specific calibration of *Cléroux et al*. [2008] results in very high temperatures. This calibration was developed using core-top samples from the North Atlantic. Further the derived temperatures of up to 29°C outreach even the seasonal range of sea-surface temperatures of 27.8 – 28.4°C. Thus, this equation was discarded. The *Elderfield and Ganssen* [2000] calibration reveals the coolest temperatures. Although these calculated temperatures are within the seasonal range of the temperatures at 100 – 200 m water depth, it is far colder than the mean temperature at 100 – 200 m water depth in December 2012. The equations of *Anand et al.* [2003] and the 'warm-water' species calibration of *Regenberg et al.* [2009] seem more promising. Both are very similar and differ only by ~0.3°C. Unfortunately, *Regenberg et al*. [2009] did not analyse *P. obliquiloculata.* The applied calibration is a combination of three warm-water species (*G. ruber* pink and white, *G. sacculifer*) and two species associated with the thermocline (*G. menardii* and *N. dutertrei*). All these foraminifers are thought to host symbionts [*Kucera*, 2007], while *P. obliquiloculata* is only facultative symbiotic [*Hemleben et al.,* 1989]. Hence, we apply the species-specific calibration of *Anand et al.* [2003] for the *P. obliquiloculata* analyses.

No species-specific calibration exists for the Indo-Pacific species *G. hexagonus* so far. *G. hexagonus* was found most frequently in nets of 300 – 500 m water depth. The mean temperatures in this depth interval is 9.4°C. Using the general calibration of *Anand et al.* [2003], which was calibrated by using 10 planktonic species, reveals the warmest temperatures of 14.2°C. Similar to *G. hexagonus, G. truncatulinoides* is frequently hauled from deep waters below the thermocline [*Hemleben et al.,* 1989]. Therefore, we also applied the species-specific equation of *G. truncatulinoides* [*Anand et al*., 2003] to our *G. hexagonus* Mg/Ca values. However, this results in even higher temperatures of 14.8°C. As a consequence, we reject both equations. We further tested a *G. bulloides* equation from the North Atlantic [*Cléroux et al.*, 2008] as both *G. hexagonus* and *G. bulloides* are symbiont-barren [*Hemleben et al.,* 1989], and the 'cold–water' species equation of *Regenberg et al.* [2009]. Both Mg/Ca calculated temperatures are colder than the mean and seasonal temperatures at the Manihiki Plateau. *Regenberg et al*. [2009] used a mixture of the deep-dwelling foraminifera *G. truncatulinoides* and *G. crassaformis* for their 'cold-water' equation. During their ontogeny both *G. truncatulinoides* and *G. crassaformis* sink to deeper water depths and build a thick calcite crust that reflects the colder waters [*Schiebel and Hemleben*, 2005]. This might be the reason for the colder temperatures calculated from our *G. hexagonus* Mg/Ca values. Most suitable for our calculation is the general calibration of *Elderfield and Ganssen* [2000]. The eight planktonic species used for this calibration mirror the broad range of foraminiferal habitats. The resulting calculated temperature of 9.6°C fit well with our measured mean *in-situ* temperature of 9.4°C and is therefore assumed to be the most suitable calibration for the *G. hexagonus* Mg/Ca values from the Manihiki Plateau.

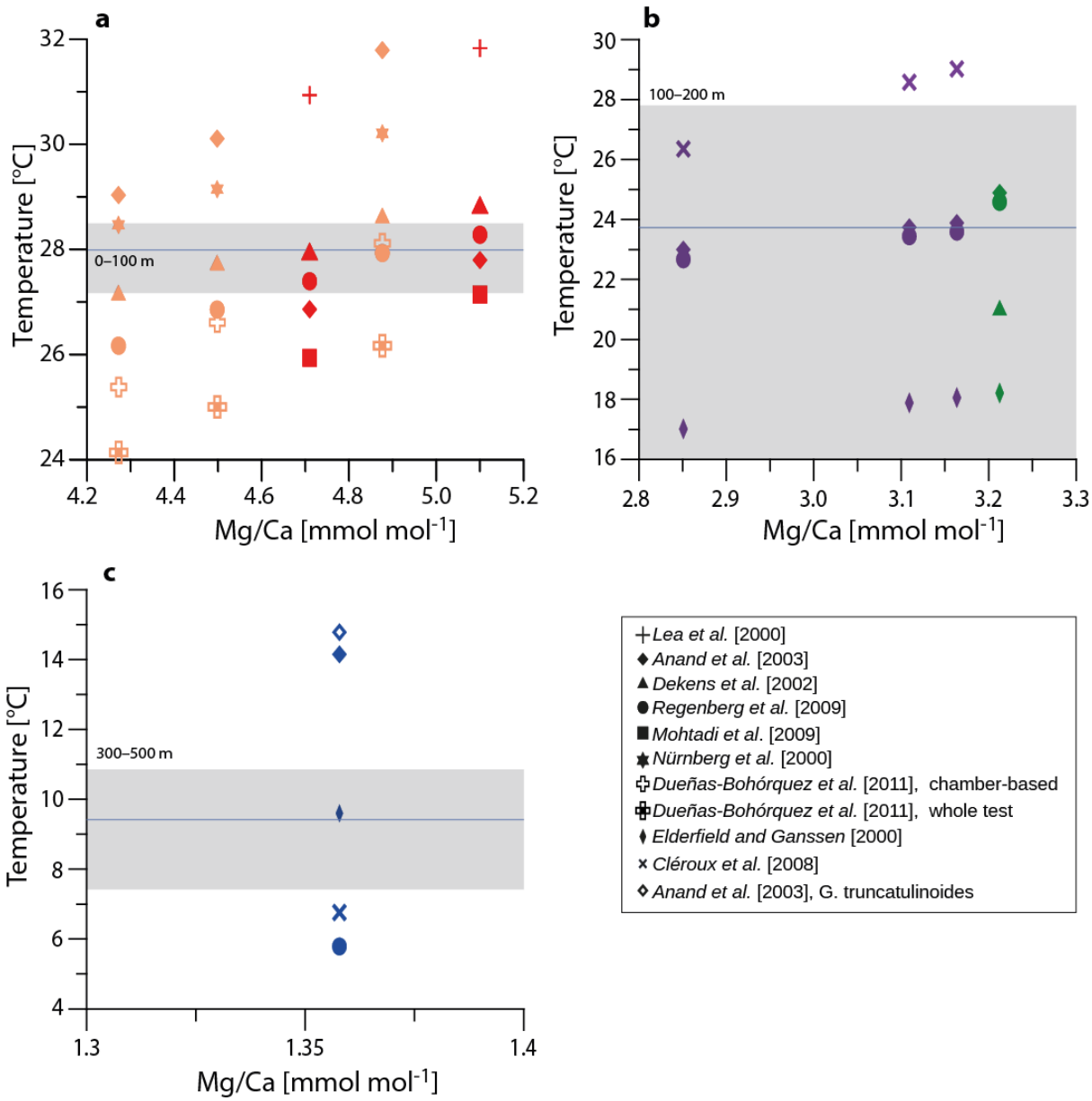

Figure S3.5.3. Foraminiferal Mg/Ca derived temperatures for mean Mg/Ca values determined over a whole test using various calibration equations for a: *G. sacculifer* (orange) and *G. ruber* (red), b: *P. obliquiloculata* (purple) and *N. dutertrei* (green), and c: *G. hexagonus* (blue). Each vertical sequence of symbols denotes one specimen whereas each symbol represents a different calibration equation from various authors (see also Table S3.5.3). The blue line represents the mean temperatures in December 2012 over the depth interval each foraminifera were found most abundant in the net collections. The grey bar shows the seasonal temperature range derived from the WOA13 Data [*Locarnini et al., 2013*].

Table S3.5.3. Calibration equations tested to convert measured Mg/Ca values into temperatures.

Species	Source	Mg/Ca = B*exp (A*T)		Reference
		y- Intercept B	Slope A	
Globigerinoides ruber	Surface sediment (equatorial Pacific)	0.30	0.089	*Lea et al*. [2000]
	Sediment trap (North Atlantic)	0.48	0.085	*Anand et al*. [2003]
	Surface sediment (equatorial Pacific)	0.38	0.09	*Dekens et al*. [2002]
	Surface sediment (Caribbean and tropical Atlantic)	0.40	0.09	*Regenberg et al*. [2009]*
	Sediment traps (Indo-Pacific Warm Pool)	0.85	0.066	*Mohtadi et al.* [2009]
Globigerinoides sacculifer	Sediment trap (North Atlantic)	1.06	0.048	*Anand et al*. [2003]
	Surface sediment (equatorial Pacific)	0.37	0.09	*Dekens et al.* [2002]*
	Culture experiments	0.491	0.033	*Nürnberg et al.* [2000]
	Surface sediment (Caribbean and tropical Atlantic)	0.60	0.075	*Regenberg et al*. [2009]
	Culture experiments (whole chamber)	0.55-0.0001*MSD[1]	0.089	*Dueñas-Bohórquez et al.* [2011]
	Culture experiments (last four chambers	0.55-0.0002*MSD[1]	0.089	*Dueñas-Bohórquez et al.* [2011]
Neogloboquadrina dutertrei	Sediment trap (North Atlantic)	0.342	0.09	*Anand et al.* [2003]
	Surface sediment (Caribbean and tropical Atlantic)	0.65	0.065	*Regenberg et al.* [2009]*
	Surface sediment (equatorial Pacific)	0.60	0.08	*Dekens et al. [2002]*
	Surface sediment (North Atlantic) 8 planktonic species	0.52	0.10	*Elderfield and Ganssen,* [2000]
Pulleniatina obliquiloculata	Surface sediment (North Atlantic)	1.02	0.039	*Cléroux et al*. [2008]
	Sediment trap (North Atlantic)	0.18	0.12	*Anand et al.* [2003]*
	Surface sediment (Caribbean and tropical Atlantic); 'warm-water' multispecies calibration	0.22	0.113	*Regenberg et al*. [2009]
	Surface sediment (North Atlantic) 8 planktonic species	0.52	0.10	*Elderfield and Ganssen,* [2000]
Globorotaloides hexagonus	Sediment trap (North Atlantic) 10 planktonic species	0.38	0.09	*Anand et al.* [2003]
	Sediment trap (North Atlantic) *G. truncatulinoides* calibration	0.359	0.09	*Anand et al.* [2003]
	Surface sediment (North Atlantic) 8 planktonic species	0.52	0.10	*Elderfield and Ganssen*, [2000]*
	Surface sediment (North Atlantic) *G. bulloides* calibration	0.78	0.082	*Cléroux et al.* [2008]
	Surface sediment (Caribbean and tropical Atlantic); 'cold-water' multispecies calibration	0.84	0.083	*Regenberg et al*. [2009]

*equation being applied in this study
[1]MSD = maximum shell diameter

Table S3.5.4. Apparent Calcification Depths (ACDs) of selected planktonic foraminiferal species used in this study determined by the comparison between the measured oxygen isotope values ($\delta^{18}O_{calcite}$) with that theoretically expected at various water depths ($\delta^{18}O_{equilibrium}$) in dependence of temperature and salinity. $\delta^{18}O_{equilibrium}$ was calculated using $\delta^{18}O$-paleotemperature equations of *Shackleton* [1974] (sha), *Bemis et al.* [1998] (bem), *Kim and O'Neil* [1997] (kim) and *Mulitza et al*. [2004] (mul). Seasonal data were taken from the World Ocean Atlas database [*Locarnini et al.,* 2013]. To correct for disequilibrium effects, isotope values were corrected with disequilibrium values of -0.6 ‰ for *G. sacculifer*, -0.4 ‰ for *G. ruber*, -0.2 ‰ for *N. dutertrei* and -0.1 ‰ for *P. obliquiloculata.* Deep-dwelling foraminifera calcify close to equilibrium. For *G. hexagonus* we assume a calcification depth between *G. tumida* and *G. crassaformis* and hence corrected our values for a disequilibrium of +0.1 ‰. Mean and ± standard deviation is given for each species and equation.

Species	$\delta^{18}O_{calcite}$ [‰]	ACDs using				seasonal ACDs after kim & mul		disequilibrium corr. after
		sha	kim	bem	mul	shallowest	deepest	kim & mul
G. ruber	-2.25	5	50	103	152	106	126	161
G. ruber	-2.168	49	59	122	154	113	137	163
G. ruber	-2.68	5	5	5	77	65	66	153
G. ruber	-2.4	5	5	70	138	91	105	158
G. ruber	-2.465	5	5	55	124	85	96	156
mean ± stdev		14 ± 20	25 ± 27	71 ± 45	129 ± 31	92 ± 19	106 ± 28	158 ± 4
G. sacculifer	-2.303	5	5	92	151	101	118	164
G. sacculifer	-2.306	5	5	91	151	100	118	164
G. sacculifer	-2.329	5	5	86	151	98	115	164
G. sacculifer	-2.316	5	5	89	151	99	117	164
G. sacculifer	-1.886	112	126	154	161	140	156	174
G. sacculifer	-2.266	5	5	100	152	104	124	165
G. sacculifer	-2.388	5	5	73	141	93	107	163
G. sacculifer	-2.428	5	5	63	132	89	101	162
G. sacculifer	-1.942	99	113	152	159	135	154	173
G. sacculifer	-2.112	61	73	135	156	119	145	169
G. sacculifer	-2.152	52	63	126	154	115	140	168
mean ± stdev		33 ± 42	37 ± 48	106 ± 31	151 ± 8	108 ± 17	127 ± 19	166 ± 4
N. dutertrei	-1.899	109	123	154	160	140	156	165
N. dutertrei	-2.151	52	63	126	154	115	140	159
N. dutertrei	-2.205	5	5	114	153	110	132	158
mean ± stdev		55 ± 52	64 ± 59	131 ± 21	156 ± 4	122 ± 16	143 ± 12	161 ± 4
P. obliquiloculata	-1.753	142	151	157	163	151	160	166
P. obliquiloculata	-1.622	152	153	160	166	154	164	168
P. obliquiloculata	-1.826	125	140	155	162	146	158	164
P. obliquiloculata	-1.535	154	156	162	168	156	166	170
P. obliquiloculata	-1.488	155	157	163	169	157	168	171
P. obliquiloculata	-1.596	153	155	161	167	154	164	169
P. obliquiloculata	-1.415	157	159	165	171	159	170	173
mean ± stdev		148 ± 11	153 ± 6	160 ± 3	167 ± 3	154 ± 4	164 ± 4	169 ± 3

Species	$\delta^{18}O_{calcite}$ [‰]	ACDs using				seasonal ACDs after kim & mul		disequilibrium corr. after
		sha	kim	bem	mul	shallowest	deepest	kim & mul
G. hexagonus	1.388	277	431	618	569	556	558	386
G. hexagonus	1.587	353	498	776	662	644	649	467
G. hexagonus	1.486	312	467	686	612	600	602	430
mean ± stdev		314 ± 38	465 ± 34	693 ± 79	614 ± 47	600 ± 44	603 ± 46	428 ± 41

S3.5.5: $\delta^{18}O_{water}$ calculation to validate combined ACD approach

The measured Mg/Ca data and $\delta^{18}O$ data enable us to calculate of the $\delta^{18}O$ of the water. The calculated $\delta^{18}O_{water}$ can be compared to the measured $\delta^{18}O_{seawater}$ (Figure 3.2c). This will enable us to further validate the combined ACD approach, if the calculated $\delta^{18}O_{water}$ values are close to the $\delta^{18}O_{seawater}$ curve. To calculate the $\delta^{18}O_{water}$, different paleotemperature equations were selected (Table S3.5.5) and rearranged for $\delta^{18}O_{water}$. Mean temperature from Mg/Ca and mean $\delta^{18}O_{calcite}$ of the respective species were inserted. The $\delta^{18}O_{water}$ was then compared to the measured $\delta^{18}O_{seawater}$. Figure S3.5.5 displays the calculated $\delta^{18}O_{water}$ of the respective species in comparison to the measured $\delta^{18}O_{seawater}$. It demonstrates that the calculated $\delta^{18}O_{water}$ mirrors the measured $\delta^{18}O_{seawater}$ curve.

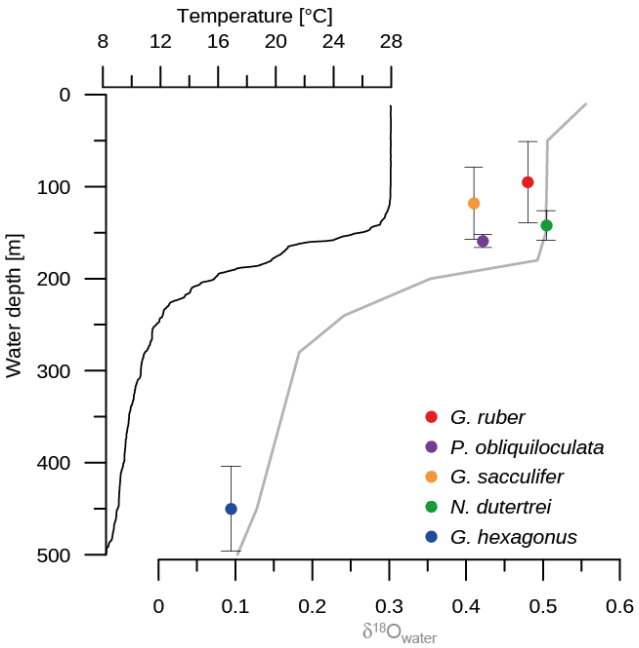

Figure S3.5.5. Calculated $\delta^{18}O_{water}$ of the five respective species used in this study in comparison to measured $\delta^{18}O_{seawater}$ (grey). The vertical bars denote the standard deviation of the mean ACD assessment (Table 3.3).

Table S3.5.5. Equations used to calculate $\delta^{18}O_{water}$ of the respective foraminiferal species using mean Mg/Ca temperatures and mean $\delta^{18}O_{calcite}$ values.

Species	Mean Mg/Ca-temperature	Mean $\delta^{18}O_{calcite}$	$\delta^{18}O_{water}$ [VSMOW][1]	Equation		Source	Reference
				$T= a+b(\delta^{18}O_{calcite}-\delta^{18}O_{seawater})$			
				a	b		
G. ruber	27.84	-2.39	0.4803	15.4	-4.78	*G. ruber*	*Farmer et al.* [2007]
G. sacculifer	27.86	-2.22	0.4102	16.2	-4.94	*G. sacculifer*	*Farmer et al.* [2007]
N. dutertrei	24.58	-2.09	0.5047	13.1	-4.95	*G. tumida*	*Farmer et al.* [2007]
P. obliquiloculata	23.54	-1.61	0.4218	14.6	-5.09	*N. dutertrei*	*Farmer et al.* [2007]
G. hexagonus	9.6	1.49	0.0944	17.0	-4.59	*G. sacculifer*	*Erez and Luz* [1983]

[1] $\delta^{18}O_{water}$ [VPDB] was converted to VSMOW by adding +0.27 [for *Farmer et al.*, 2007] and +0.22 [for *Erez and Luz*, 1983].

4. Manuscript II

Evidence for enhanced convection of North Pacific Intermediate Water to the low-latitude Pacific under glacial conditions

Lars Max[1*], **Nadine Rippert**[1], Lester Lembke-Jene[1], Andreas Mackensen[1], Dirk Nürnberg[2], and Ralf Tiedemann[1]

[1]Alfred Wegener Institute, Helmholtz Centre for Polar and Marine Research, Bremerhaven, Am Alten Hafen 26, D-27568 Bremerhaven, Germany

[2]GEOMAR, Helmholtz Centre for Ocean Research Kiel, Wischhofstr. 1-3, D-24148 Kiel, Germany

*corresponding author: Lars Max (Lars.Max@awi.de)

***Under review* in Paleoceanography**

Abstract

We provide high-resolution foraminiferal stable carbon isotope ($\delta^{13}C$) records from the subarctic Pacific and Eastern Equatorial Pacific (EEP) to investigate circulation dynamics between the extra-tropical and tropical North Pacific during the past 60 kyr. We measured the $\delta^{13}C$ composition of the epibenthic foraminiferal species *Cibicides lobatulus* (*C. lobatulus)* from a shallow sediment core recovered from the western Bering Sea (SO201-2-101KL; 58°52.52'N, 170°41.45'E, 630 m water depth) to reconstruct past ventilation changes close to the source region of Glacial North Pacific Intermediate Water (GNPIW). Information regarding glacial changes in the $\delta^{13}C$ of sub-thermocline water masses in the EEP is derived from the deep-dwelling planktonic foraminifera *Globorotaloides hexagonus* (*G. hexagonus*) at ODP Site 1240 (00°01.31'N, 82°27.76'W, 2921 m water depth). Apparent similarities in the long-term evolution of $\delta^{13}C$ between GNPIW, intermediate waters in the eastern tropical North Pacific and sub-thermocline water masses in the EEP suggest the expansion of relatively ^{13}C-depleted, nutrient-enriched, and northern-sourced intermediate waters to the equatorial Pacific under glacial conditi-

ons. Further, it appears that additional influence of GNPIW to the tropical Pacific is consistent with changes in nutrient distribution and biological productivity in surface-waters of the glacial EEP. Our findings highlight potential links between North Pacific mid-depth circulation changes, nutrient cycling, and biological productivity in the equatorial Pacific under glacial boundary conditions.

4.1 Introduction

The high latitudes of the North Pacific and the Southern Ocean play an essential role in regulating the exchange of CO_2 between the ocean and the atmosphere [*Takahashi et al.*, 2002]. In both regions, vertical mixing brings nutrient- and CO_2-rich deep waters into the euphotic zone and facilitates the biological pump, which sequesters atmospheric CO_2 back into the deeper ocean interior [e.g. *Honda et al.*, 2002]. In the modern North Pacific, however, the further exposure of nutrient- and CO_2-rich sub-surface waters to the surface ocean is largely hampered by a permanent halocline [*Haug et al.*, 1999]. In both regions, intermediate water masses are formed that re-circulate excess nutrients from the high-latitude oceans towards the low latitude-regions of the Pacific Ocean (Figure 4.1). North Pacific Intermediate Water (NPIW) is formed in the sub-surface of the Northwest Pacific via mixing of high-nutrient sub-surface waters and intermediate water masses produced in coastal polynyas through brine rejection during wintertime sea-ice production in the Okhotsk Sea [*Talley*, 1993; *Shcherbina et al.*, 2003]. Today, NPIW circulates within the upper ~300 – 800 m and is mainly restricted to the subtropical North Pacific regions between ~20°N – 40°N, however a tongue of NPIW also spreads into the Celebes Sea in the western tropical Pacific [*Talley*, 1993; *Bostock et al.*, 2010]. In the Southern Ocean Antarctic Intermediate Water (AAIW) is produced at the surface ocean from upwelled nutrient- and CO_2-enriched Circumpolar Deep Water (CDW). AAIW ventilates into the Subtropical Gyre known as “ocean tunnelling” and thereby affects the equatorial current system (Figure 4.1). An important difference between northern- and southern-sourced intermediate waters is that sub-surface formation of NPIW largely prevents the biologically driven re-setting of deep ocean nutrient ratios that happens at the surface ocean during formation of AAIW. It is for this reason that NPIW is characterized by higher silicic acid to nitrate supply ratios compared to southern-sourced intermediate waters (Figure 4.1) [*Sarmiento et al.*, 2004]. On the other hand, as carbon fixation is dominated by siliceous phytoplankton at the surface-ocean near the formation region of modern AAIW, southern-sourced intermediate waters are characterized by high nitrate, but low silicic acid concentrations (Figure 4.1) [*Sarmiento et al.*, 2004].

Under modern conditions, mainly southern-sourced water masses (AAIW) are injected into the eastward-directed Equatorial Undercurrent (EUC) and the Equatorial Pacific Intermediate Water (EqPIW) via the South Equatorial Current and the New Guinea Coastal Undercurrent [*Dugdale et al.*, 2002]. The dominant role of AAIW on equatorial intermediate waters was also verified by a geochemical tracer analyses that suggests that EqPIW are primarily a combination of AAIW and

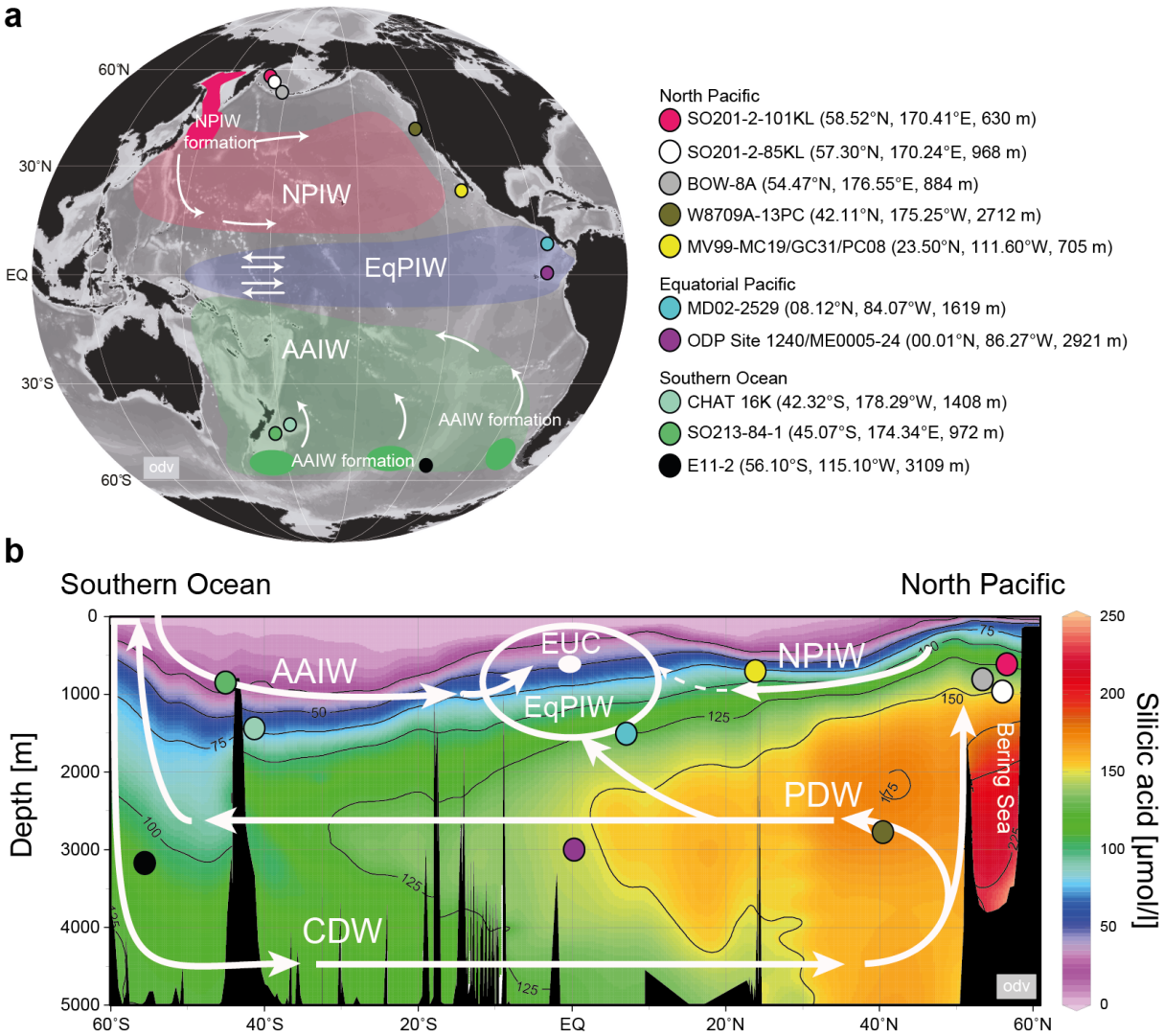

Figure 4.1. a: Bathymetric chart of the Pacific Ocean with locations of proxy records in the North Pacific (SO201-2-101KL, *this study*; SO201-2-85KL, *Max et al.*, 2012; BOW-8A, *Horikawa et al.*, 2010; W8709A-13PC, *Lund and Mix*, 1998; MV99-MC19/GC31/PC08, *Basak et al.*, 2010), the Equatorial Pacific (MD02-2529, *Leduc et al.*, 2010; ODP Site 1240, *Pichevin et al.*, 2009; *this study*; ME0005-24, *Kienast et al.*, 2007), and the Southern Ocean (CHAT 16K, *Noble et al.*, 2013; SO213-84-1, *Ronge et al.*, 2015; E11-2, *Robinson et al.*, 2014) considered in this study. White arrows denote major circulation pattern of intermediate water masses in the North Pacific and Southern Ocean: Magenta and green spots indicate formation regions of AAIW and NPIW, shaded magenta and green areas mark modern lateral extent of intermediate waters in the Pacific Ocean. b: Latitudinal profile of present-day silicic acid concentrations from the North Pacific to the Southern Ocean [*Garcia et al.*, 2010] and major modern mid-depth to deep-water masses (white arrows): AAIW = Antarctic Intermediate Water; CDW = Circumpolar Deep Water; EUC = Equatorial Undercurrent; EqPIW = Equatorial Pacific Intermediate Water; NPIW = North Pacific Intermediate Water; PDW = Pacific Deep Water [modified after *Bostock et al.*, 2010]. This figure was generated with Ocean Data View [*Schlitzer*, 2015].

Pacific Deep Water (PDW) with only a very minor contribution of NPIW today (Figure 4.1) [*Bostock et al.*,2010]. As the intermediate water masses flow towards the east, they supply nutrients via diapycnal mixing to the overlying waters masses. As a consequence of the high southern-sourced contribution today, carbon fixation by siliceous phytoplankton is limited by low silicic acid and iron availability in the Eastern Equatorial Pacific (EEP) making this region a significant net source of CO_2 to the atmosphere [*Dugdale et al.*, 2002].

Information regarding past ocean circulation changes can be reconstructed from the stable carbon isotopic composition ($\delta^{13}C$) measured on benthic foraminiferal tests. During the past thirty years, this proxy has been successfully used to investigate glacial to interglacial changes in water mass geometry and ocean circulation [e.g. *Duplessy et al.*, 1984; *Curry et al.*, 1988; *Mix et al.*, 1991; *Curry et al.*, 2005; *Bostock et al.*, 2010; *Knudson and Ravelo*, 2015a]. In the modern ocean, high(low) values of $\delta^{13}C$ of the Dissolved Inorganic Carbon (DIC) are indicative of low(high) nutrient concentrations and large-scale oceanic water mass circulation patterns [*Kroopnick*, 1985]. For $\delta^{13}C$ reconstructions of intermediate- and deep-water mass circulation changes the initial $\delta^{13}C$, where water masses are subducted into the ocean interior, has to be taken into account. The initial $\delta^{13}C$ value of a water mass is affected by air-sea gas exchange at the surface-ocean, which in turn is temperature-dependent. After isolation from the surface-ocean, the $\delta^{13}C$ of a given water mass is mainly altered by in-situ addition of CO_2 through respiration of sinking organic material. Today, a $\delta^{13}C_{DIC}$ of about 1 ‰ characterize surface waters of the North Atlantic where North Atlantic Deep Water (NADW) is formed. As it flows to the circum-Antarctic Ocean interior the continuous degradation of sinking organic particles reduces the original $\delta^{13}C_{DIC}$ of NADW to about 0.5 ‰. In the Southern Ocean deep-water further re-circulates to the Indian and Pacific Ocean and lowest values of ~ -0.6 ‰ $\delta^{13}C_{DIC}$ are observed today in the deep subarctic Pacific. Since $\delta^{13}C$ of epibenthic foraminifera is closely related to the $\delta^{13}C_{DIC}$ of ambient seawater, past differences in nutrient content and water mass circulation patterns can be reconstructed from benthic foraminiferal tests preserved in marine sediments [e.g. *Duplessy et al.*, 1984].

Combined evidence of $\Delta^{14}C$ deep-water ventilation ages and benthic foraminiferal $\delta^{13}C$ records suggest changes in mid-depth circulation (the upper 1000 to ~2000 m water depth) of the North Pacific Ocean under glacial conditions [*Duplessy et al.*, 1988; *Herguera et al.*, 1992; *Keigwin*, 1998; *Matsumoto et al.*, 2002a; *Okazaki et al.*, 2012]. Accordingly, the mid-depth circulation of the North Pacific was strengthened by formation of Glacial North Pacific Intermediate Water (GNPIW). In contrast to today, it has been proposed that the Bering Sea formed intermediate waters during glacial times and played an important role in formation of GNPIW [e.g. *Tanaka and Takahashi*, 2005; *Horikawa et al.*, 2010]. Evidence for additional cold and well-oxygenated intermediate water in the glacial Bering Sea has been provided from a study based on changes in radiolarian assemblages [*Tanaka and Takahashi*, 2005]. Based on a neodymium isotope record (ε_{Nd}) it has been argued that Bering Sea intermediate water was a principal component of GNPIW during the glacial period [*Horikawa et al.*, 2010]. The formation of

glacial Bering Sea intermediate waters was explained by changes in high-latitude hydrological processes such as enhanced brine rejection and the resulting salinity increase favouring the subduction of cold surface waters to the mid-depth in the Bering Sea as important precursor of GNPIW [*Rella et al.*, 2012]. A recent study based on endobenthic foraminiferal stable oxygen ($\delta^{18}O$) and $\delta^{13}C$ records from the Bering Sea indicates that enhanced GNPIW formation was not only restricted to the Last Glacial Maximum (LGM), but also recurred during extreme glacial intervals of the last 1.2 Myr [*Knudson and Ravelo*, 2015a].

In the Southern Hemisphere there is so far no consensus about the amount of AAIW production during glacial boundary conditions. Based on $\delta^{13}C$ and $\delta^{18}O$ analyses on benthic foraminifera from the Australian margin it has been suggested that a colder and fresher water mass ventilated at intermediate depth, which was linked to a shift in the frontal zonation within the Southern Ocean [*Lynch-Stieglitz et al*., 1994]. Furthermore, a study based on authigenic minerals from the Chilean margin found higher oxygen concentrations during glacial times, which were linked to an enhanced production of AAIW [*Muratli et al*., 2010]. On the contrary, it has been proposed that stronger water column stratification in the Southern Ocean led to a reduced production of AAIW under glacial conditions [*Pahnke and Zahn*, 2005]. Accordingly, periods of increased intermediate water formation were linked to Southern Hemisphere warm episodes through a tight coupling between climate warming and intermediate water production at the high southern latitudes. A recent study combined benthic $\delta^{13}C$ and $\delta^{18}O$ records off New Zealand with modelling results and reconstructed the vertical extent of AAIW over the last 350 kyr [*Ronge et al.*, 2015]. These results showed that the vertical extent of AAIW changed on glacial-interglacial timescales with a significantly shallower AAIW subduction under glacial conditions. The shallower subduction of glacial AAIW has been related to an advanced winter sea-ice edge as well as enhanced freshwater flux from sea-ice melting that induced a salinity anomaly and resulted in formation of less dense intermediate waters in the Southern Ocean.

Studies based on ε_{Nd} records as well as $\Delta^{14}C$ shallow- and deep-water ventilation ages from the equatorial Pacific suggest a dominant role of the Southern Ocean in transferring climatic signals from the high latitudes towards the tropical regions during late Marine Isotope Stage (MIS) 2 [*Pena et al.*, 2013; *de la Fuente et al.*, 2015]. Accordingly, available reconstructions of changes in water mass signatures of the equatorial Pacific suggest a principal southern-source for tropical Pacific intermediate water masses during glacial times similar to today. In a recent study, *Carriquiry et al.* [2015] analysed $\delta^{13}C$ records at the western Baja California Margin and relates changes in mid-depth nutrient distribution to a larger influence of glacial AAIW to the tropical North Pacific. In contrast, *Leduc et al.* [2010] explained anomalies in glacial $\delta^{13}C$ of intermediate waters in the Eastern Tropical North Pacific (ETNP) by a switch from southern nutrient-poor to northern nutrient-enriched intermediate water masses due to a sustained formation of GNPIW. This notion is supported by a very recent ε_{Nd} data compilation from 55 core sites around the Pacific [*Hu et al*., 2016] that revealed a significant offset in EEP ε_{Nd} signature values between LGM and Holocene values (by 1 – 2 epsilon units lower than during the

Holocene), which can only be explained by a higher contribution from northern-sourced waters [*Hu et al*., 2016]. The enhanced penetration of northern-sourced water masses is in agreement with evidence for enhanced glacial mid-depth circulation reconstructed from $\delta^{13}C$ records of California margin sediment cores, however these records also point to spatial and temporal complexity in the ventilation history of the Northeast Pacific [*Stott et al.*, 2000]. Together, these results point to a more prominent role of GNPIW in shaping the mid-depth water mass characteristics of the glacial North Pacific. On the other hand, it still remains illusive how strengthened GNPIW circulation shaped the mid-depth water mass characteristics of the glacial North Pacific and whether GNPIW might have influenced the nutrient distribution, biological productivity and export patterns far beyond the northern high latitudes.

In this study, we report on stable isotope measurements derived from sedimentary records of the western subarctic Pacific (Bering Sea) and EEP to investigate spatiotemporal changes in GNPIW circulation and its influence on low-latitude Pacific water mass characteristics during the past 60 kyr. We chose a sediment core from the western Bering Sea located on Shirshov Ridge (SO201-2-101KL; 58°52.52'N, 170°41.45'E, 630 m water depth, Figure 4.1) and measured the $\delta^{13}C$ composition of the epibenthic foraminifera *Cibicides lobatulus* (*C. lobatulus*) as an indicator for past ventilation changes close to the source-region of GNPIW [*Max et al.*, 2014]. Today the western Bering Sea is poorly ventilated due to the absence of local intermediate water formation and water masses bathing core site SO201-2-101KL are dominated by upwelling of nutrient-rich PDW (Figure 4.1b). Additional $\delta^{13}C$ data of deep-dwelling planktonic foraminifera *Globorotaloides hexagonus* (*G. hexagonus*) from Ocean Drilling Program (ODP) Site 1240 (00°01.31'N, 82°27.76'W, 2921 m water depth, Figure 4.1) provide information about glacial changes of sub-thermocline water mass characteristics in the EEP. Modern water mass signatures of sub-thermocline waters at ODP Site 1240 are linked to the lower branch of the EUC, which brings nutrients to the surface ocean of the EEP (Figure 4.1b). By comparing water mass signatures of intermediate- to deep-water masses of the Pacific Ocean and Southern Ocean with sub-thermocline to mid-depth water masses in the tropical Pacific we examine whether (1) the influence of northern-sourced versus southern-sourced water masses on tropical Pacific intermediate- and sub-thermocline water masses of the EEP changed during the last glacial period and (2) discuss potential implications for sub-thermocline nutrient availability and biological productivity in the equatorial Pacific in the past.

4.2 Materials and Methods

4.2.1 Stable carbon ($\delta^{13}C$) and oxygen ($\delta^{18}O$) isotope measurements from benthic and deep-dwelling planktonic foraminifera

We measured the $\delta^{13}C$ and $\delta^{18}O$ isotope composition of epibenthic foraminifera *C. lobatulus* selected from sediment samples of western Bering Sea sediment core SO201-2-101KL and

deep-dwelling planktonic foraminifera *G. hexagonus* from samples of ODP Site 1240 in the Panama Basin (Figure 4.1; Supplementary Table S4.4.1 and S4.4.2). Sedimentation rates of 11 – 16 cm kyr^{-1} have been reported for core SO201-2-101KL from Shirshov Ridge [*Riethdorf et al.*, 2013] and 6.4 – 25.2 cm kyr^{-1} for ODP Site 1240 [*Pena et al.*, 2008]. According to our sampling scheme we achieved a millennial to centennial-scale resolution of proxy-data in this study with an average temporal resolution of ~0.25 kyr for core SO201-2-101KL and ~0.23 kyr for the last 60 kyr of ODP Site 1240, respectively. Stable isotope analyses in core SO201-2-101KL were made on samples of two to three specimens of *C. lobatulus* picked from the 250 – 400 µm size fractions. The stable isotopic composition of *G. hexagonus* of ODP Site 1240 were determined using five specimens per sample picked from the 250 – 315 µm size fraction.

It has been proposed that *C. lobatulus* preferentially lives attached to hard substrate on or slightly above the sediment surface and studies on living specimen indicated that this species faithfully records the $\delta^{13}C_{DIC}$ of ambient seawater [*Schweizer et al.*, 2009]. Some investigators have observed a positive offset in the $\delta^{13}C$ of *C. lobatulus* with regard to ambient bottom water $\delta^{13}C_{DIC}$ in some high-latitude settings of the North Atlantic Ocean [*Mackensen et al.*, 2000]. However, this effect was caused by high seasonal variability of the original ambient $\delta^{13}C_{DIC}$-signal, confirmed by time-series measurements of water column $\delta^{13}C_{DIC}$ and related to the calcification of *C. lobatulus* during time intervals of maximum ventilation [*Mackensen et al.*, 2000]. We thus regard the $\delta^{13}C$-signal *C. lobatulus* to reliably reflect $\delta^{13}C$ of ambient seawater.

Isotopic compositions of *C. lobatulus* and *G. hexagonus* were measured at the Alfred Wegener Institute, Helmholtz Centre for Polar and Marine Research, Germany, using a Thermo Fisher MAT 253 mass spectrometer coupled to a Kiel IV automatic carbonate preparation device. All stable isotope measurements were calibrated via the NBS-19 international standard and results are reported in δ-notation versus VPDB scale. Overall long-term analytical reproducibility of measurements based on internal laboratory standard (Solnhofen limestone) together with samples over a one-year period is better than ±0.06 ‰ for $\delta^{13}C$ and ±0.08 ‰ for $\delta^{18}O$.

4.2.2 Stable oxygen isotope composition ($\delta^{18}O$) and apparent calcification depth of deep-dwelling planktonic foraminifera *G. hexagonus*

Information regarding apparent calcification depth (ACD) of the planktonic foraminifera *G. hexagonus* is still sparse. We make a first attempt to determine the ACD at ODP Site 1240 to validate the depth habitat of *G. hexagonus* in the EEP. The ACD-estimation was done by comparing measured foraminiferal $\delta^{18}O_{calcite}$ from a near core-top sample (at 10 cm) to a theoretically expected equilibrium $\delta^{18}O$ values of calcite ($\delta^{18}O_{equilibrium}$) that foraminifera would incorporate in dependence of modern water temperature, salinity and $\delta^{18}O$ values of seawater ($\delta^{18}O_{seawater}$). In order to calculate $\delta^{18}O_{seawater}$, the $\delta^{18}O_{seawater}$-salinity relationships given by *Leduc et al.* [2007] for 0 – 40 m water depth:

$$\delta^{18}O_{seawater}\ (‰) = 0.253*S-8.52,$$

and for >40 m water depth:

$$\delta^{18}O_{seawater}\ (‰) = 0.471*S-16.15$$

were used in conjunction with annual salinity data derived from World Ocean Atlas 2009 [*Antonov et al.*, 2010].

Several established $\delta^{18}O$-paleotemperature equations [*Epstein et al.*, 1953; *Shackleton*, 1974; *Kim and O'Neil*, 1997; *Bemis et al.*, 1998] were considered for $\delta^{18}O_{calcite}$ as absolute ACD estimation strongly depends on the applied temperature equation [*Wejnert et al.*, 2013] (Figure 4.2). Modern temperatures are derived from the World Ocean Atlas 2009 [*Locarnini et al.*, 2010], and $\delta^{18}O_{seawater}$ were included after correcting $\delta^{18}O_{seawater}$ to the VPDB scale by subtracting the $\delta^{18}O_{seawater}$-conversion factor given in *Bemis et al.* [1998]. The water depth showing the best match between $\delta^{18}O_{calcite}$ and $\delta^{18}O_{equilibrium}$ is taken as the ACD of *G. hexagonus* (Figure 4.2).

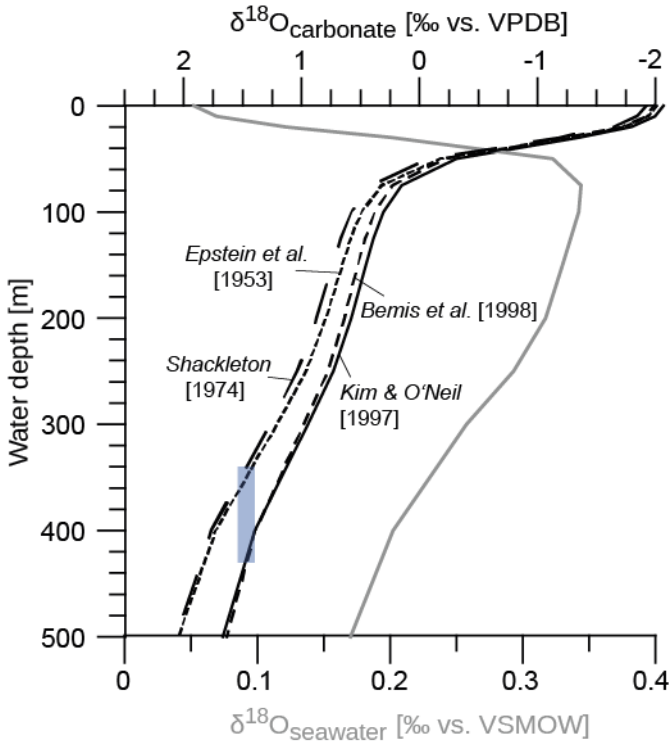

Figure 4.2. Apparent Calcification Depth (ACD) of planktonic foraminifera *G. hexagonus* in the Eastern Equatorial Pacific. ACD of *G. hexagonus* at ODP Site 1240 was inferred from best match between measured foraminiferal $\delta^{18}O_{calcite}$ values and corresponding calculated theoretically present $\delta^{18}O_{equilibrium}$ value, which were determined using various paleotemperature equations (black partly dashed lines), modern water temperatures [*Locarnini et al.*, 2010] and $\delta^{18}O_{seawater}$ (gray line). The blue bar indicates the ACD range of *G. hexagonus* considering all used equations.

The calculated ACD suggests that *G. hexagonus* dwells below the thermocline in 340 – 430 m water depth similar to estimated depth habitats defined by *Ortiz et al.* [1996] in the North Pacific.

Further support comes from a very recent ACD assessment from the western equatorial Pacific, which concludes that deep-dwelling *G. hexagonus* is a suitable proxy for tracing properties of equatorial sub-thermocline water masses [*Rippert et al*., 2016, *this thesis*]. Hence, the stable isotopic composition of *G. hexagonus* is considered to reflect the water mass properties of sub-thermocline waters of the EEP.

4.2.3 Stratigraphic approach and age models

The stratigraphic framework of western Bering Sea core SO201-2-101KL was constructed using a multi-proxy approach described in detail in *Riethdorf et al.* [2013]. Briefly, information derived from high-resolution X-ray fluorescence (XRF) and spectrophotometric logging data (color b*) of core SO201-2-101KL were used for correlation to millennial-scale variability preserved in the NGRIP ice core [*Andersen et al.*, 2004] according to the GICC05 timescale [*Svensson et al.*, 2008] (Figure 4.3a). The tuning of core SO201-2-101KL to NGRIP was further validated by five planktonic radiocarbon ages spanning the time interval from the onset of MIS 2 to the time interval of the last glacial termination (Figure 4.3a) [see *Max et al.*, 2012].

We adopted the established age scale of ODP Site 1240 described in the work of *Pena et al.* [2008]. The stratigraphic framework of ODP Site 1240 was constructed from 17 AMS ^{14}C ages based on monospecific samples of the planktonic foraminifera *Neogloboquadrina dutertrei* (*N. duterteri*) and tuning of the initiation of *N. duterteri* $\delta^{13}C$ minima at ODP Site 1240 to the CO_2 increase in the Vostok CO_2, as shown by *Spero and Lea* [2002]. Graphical correlation of planktonic foraminiferal Mg/Ca derived sea surface temperatures (SST) from ODP Site 1240 to Antarctic Vostok deuterium records was used to get additional age controls for deeper parts of the core [see supplement of *Pena et al.*, 2008 for more details] (Figure 4.3b).

4.3 Results

Under modern conditions, the western Bering Sea is poorly ventilated due to the absence of local intermediate water formation. Today, water masses bathing core site SO201-2-101KL are dominated by upwelling of nutrient-rich PDW with very low $\delta^{13}C$ signatures of ~ -0.6 ‰ (Figures 4.1 and 4.4). The nutrient-rich and ^{13}C-depleted signature of PDW results from its long isolation from the sea surface and continuous respiration of organic matter along its path from the Southern Ocean into the North Pacific [*Herguera et al.*, 2010]. The reconstructed glacial (60 – 20 ka) $\delta^{13}C$ values show a pronounced variability on millennial timescales, in particular during MIS 3, and vary between -0.8 – 0.2 ‰ (Figure 4.4). Upon millennial-scale variability a long-term trend towards increased $\delta^{13}C$ of Bering Sea intermediate water since the beginning of MIS 3 is clearly visible in core SO201-2-101KL, which culminated during early MIS 2 (~29 ka) with $\delta^{13}C$ signatures of up to ~0.3 ‰ (Figure 4.4). During MIS 2 $\delta^{13}C$ values show a long-term decrease with $\delta^{13}C$ signatures reaching ~ -0.2 ‰ at the beginning of the last deglaciation (~17 ka).

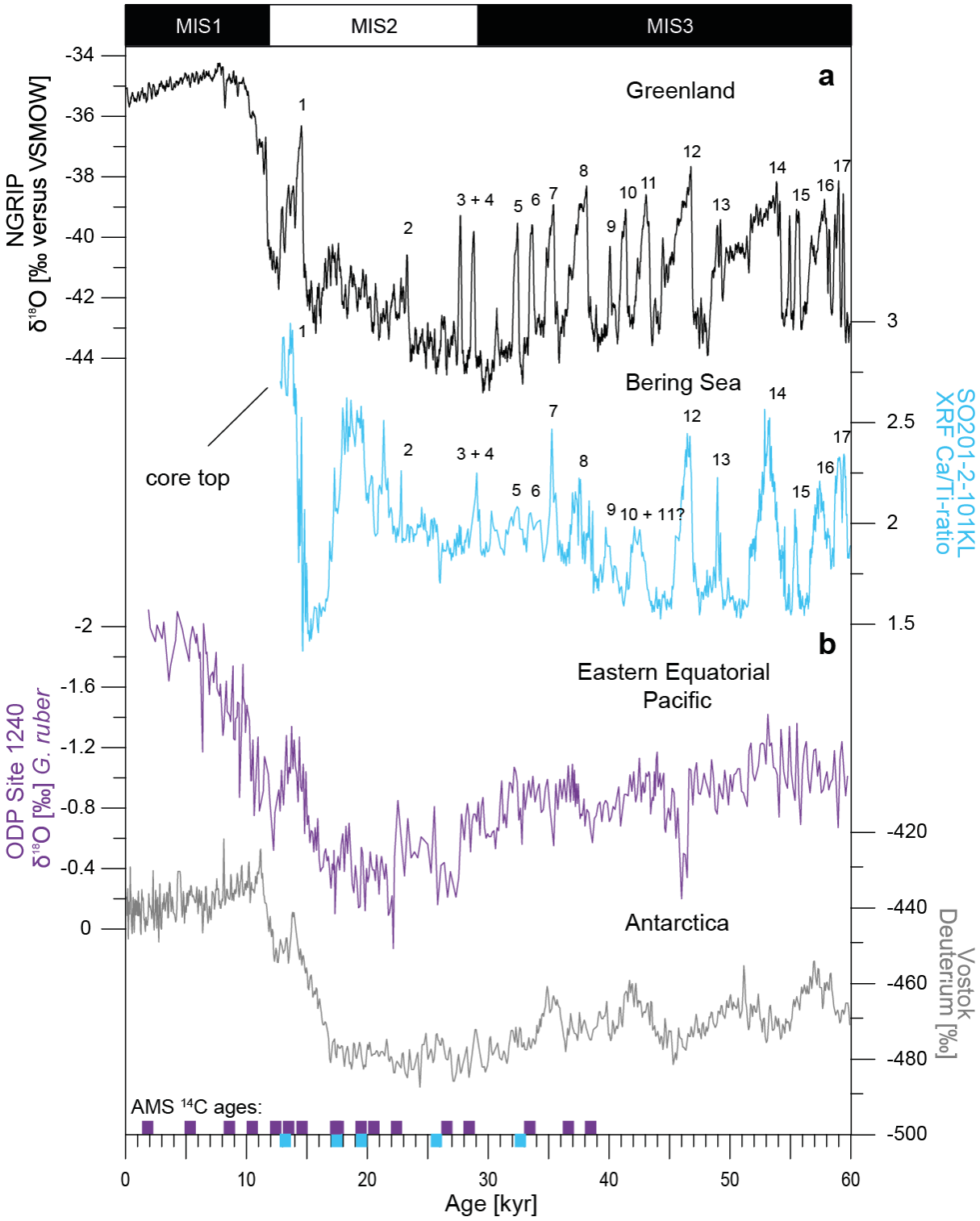

Figure 4.3. a: Comparison of high-resolution XRF core-logging data (Ca/Ti-ratio) from core SO201-2-101KL to NGRIP ice-core record. Numbers indicate Dansgaard-Oeschger Interstadials in NGRIP [*Andersen et al.*, 2004] and SO201-2-101KL [*this study*] during the past 60 kyr [*Riethdorf et al.*, 2013]. b: The stratigraphic framework of ODP Site 1240 based on 17 AMS ^{14}C ages and graphical tuning deeper parts of the cores to the Vostok ice core record [*Petit et al.*, 1999; *Pena et al.*, 2008]. Available AMS-^{14}C dating's derived from core SO201-2-101KL and ODP Site 1240 are given by blue and purple squares at the bottom.

The deep-dwelling planktonic foraminifera *G. hexagonus* record from ODP Site 1240 serves as proxy for changes in $\delta^{13}C$ signatures of sub-thermocline water masses upwelled in the EEP (Figure 4.4). Under modern conditions, water mass upwelling to the surface of the EEP happens via the lower branch of the EUC with modern $\delta^{13}C$ signatures of ~0.1 ‰ (Figures 4.1 and 4.4). During MIS 3 (~60 – 30 ka) the *G. hexagonus* $\delta^{13}C$ proxy record indicates the presence of relatively ^{13}C-enriched (nutrient-depleted) water masses with $\delta^{13}C$ signatures of 0.1 – 0.2 ‰ and relatively low variability in $\delta^{13}C$ of sub-thermocline waters (Figure 4.4). A first switch to relatively ^{13}C-depleted sub-thermocline water masses in the EEP is apparent during early MIS 2, and most ^{13}C-depleted values of ~ -0.4 ‰ are found at the beginning of the last deglaciation (~17 ka).

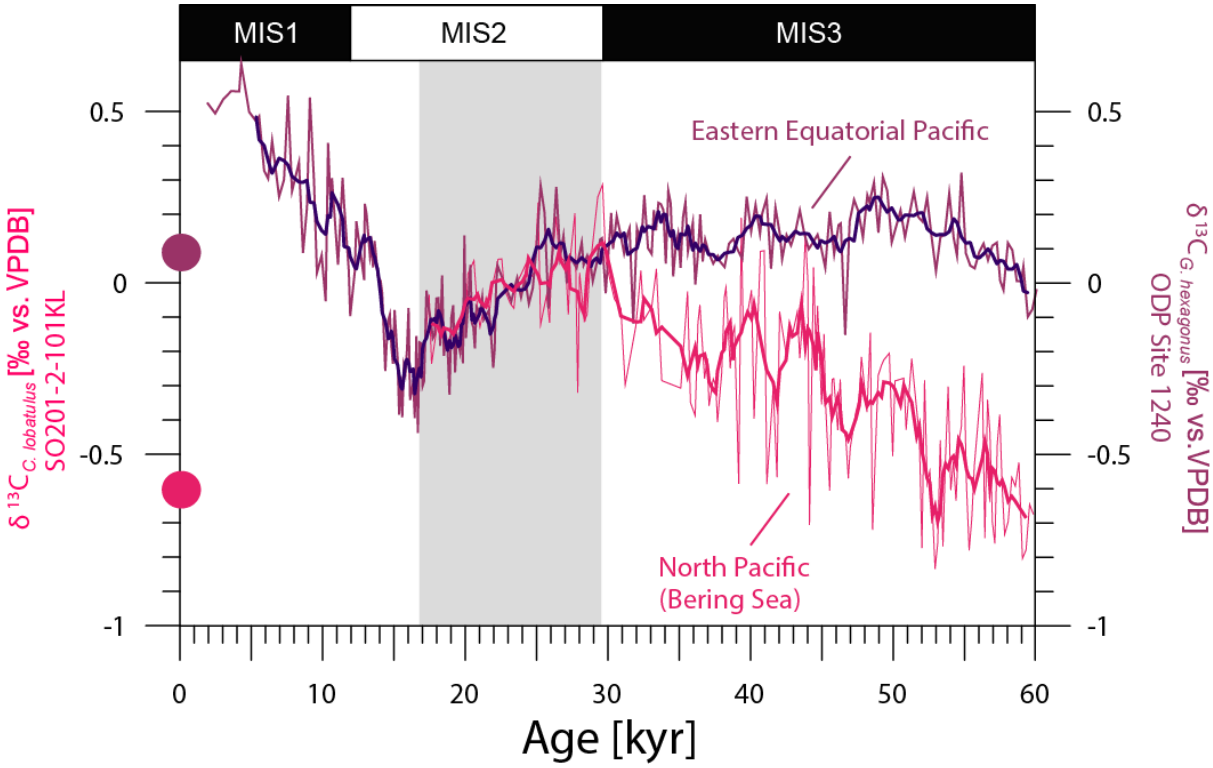

Figure 4.4. Detailed comparison of mid-depth benthic $\delta^{13}C$ record from sediment core SO201-2-101KL from the subarctic Pacific (Bering Sea) with $\delta^{13}C$ record of deep-dwelling (sub-thermocline) planktonic foraminifera *G. hexagonus* derived from ODP Site 1240 in the Eastern Equatorial Pacific during the past 60 kyr. Grey shaded area marks times of convergence between the given $\delta^{13}C$ records during MIS 2. Coloured circles indicate $\delta^{13}C_{DIC}$ composition of water masses bathing the respective core sites under modern conditions [*Key et al.*, 2004].

4.4 Discussion

Based on proxy data of marine productivity and benthic foraminiferal stable isotope records a recent study suggested that the long-term increase in $\delta^{13}C$ Bering Sea intermediate water was related to local formation of waters masses with lower salinity and higher oxygen content under glacial conditions [*Schlung et al.*, 2013]. *Rella et al.* [2012] argued that an eastward displacement of the Aleutian Low and a shift to predominantly northerly winds over the Bering Sea created favourable conditions for active polynya formation and brine rejection coupled to sea-ice formation, which led to intermediate water production as one potential source-region of GNPIW during the glacial period. However, changes in thermodynamic (temperature-dependent) equilibration between the surface ocean $\delta^{13}C_{DIC}$ and the atmospheric CO_2 also influence isotopic fractionation, whereby surface ocean $\delta^{13}C_{DIC}$ increases by 0.1 ‰ with each 1°C decrease in surface ocean temperature [*Mook et al.,* 1974]. Given that glacial production of intermediate waters in the western Bering Sea was supposedly linked to sea-ice formation during winter, when surface ocean temperature were always close to the freezing point, temperature-dependent changes in air-sea gas exchange of western Bering Sea surface waters should have had a minor effect on the $\delta^{13}C_{DIC}$ signal. A recent study showed that during stadial periods of the deglaciation most of the western Bering Sea was covered by seasonal sea ice [*Méheust et al.*, 2016], thus providing favourable conditions for intermediate water formation. Moreover, benthic $\delta^{13}C$ data from proximal core SO201-2-85KL point to a decline in $\delta^{13}C$ and reduced ventilation during deglacial warm stages and the early Holocene when sea-ice cover was substantially reduced [*Max et al.*, 2012; *Max et al.*, 2014].

4.4.1 Glacial contribution of northern- *versus* southern-sourced water masses in the Eastern Tropical North Pacific (~8°N)

In a first step, we compare the benthic $\delta^{13}C$ of mid-depth records from the Southern Ocean (SO213-84-1; *Ronge et al.*, 2015), the subarctic Pacific (SO201-2-101KL; *this study*) and a deep-water benthic $\delta^{13}C$ record from the Northeast Pacific (W8709A-13PC; *Lund and Mix,* 1998) with mid-depth $\delta^{13}C$ signatures derived from sediment core MD02-2529 [*Leduc et al.*, 2010] located in the ETNP to assess the influence of northern- versus southern-sourced water masses on EqPIW characteristics during the past 60 kyr (Figures 4.1 and 4.5a). The core site of MD02-2529 in the ETNP is situated at the modern confluence of northern oxygen-poor and southern oxygen-rich waters, and thus is ideally located to investigate past changes in the respective latitudinal extents of northern versus southern-sourced water masses in the past [*Leduc et al.*, 2010].

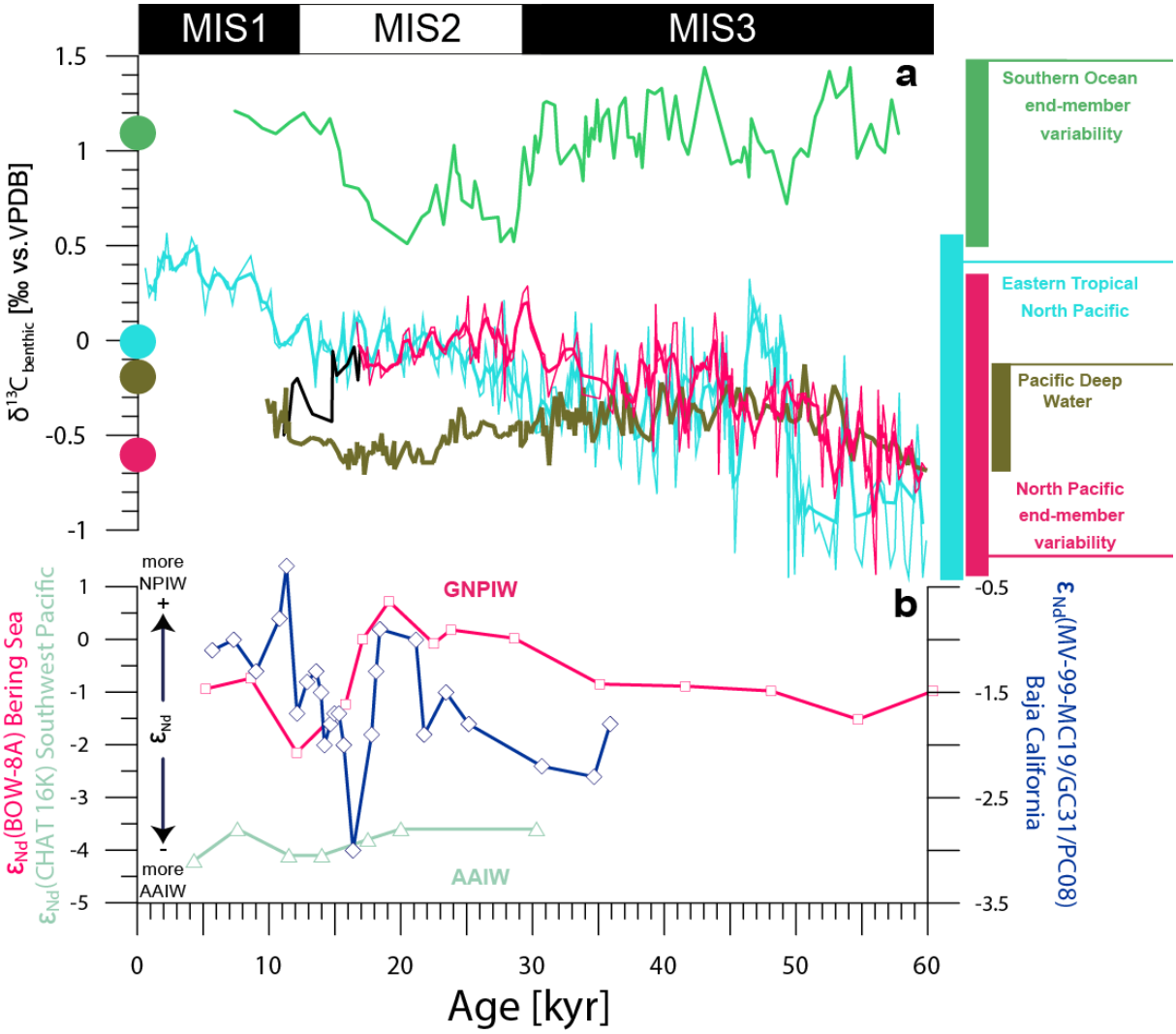

Figure 4.5 Benthic $\delta^{13}C$ records and ε_{Nd} signatures from intermediate waters of the North Pacific (GNPIW), off Baja California, the Eastern Tropical North Pacific (EqPIW) and the Southern Ocean (AAIW) compared to benthic $\delta^{13}C$ deep-water (PDW) variability for the last 60 kyr. a: Benthic $\delta^{13}C$ record from Southern Ocean core SO213-84-1 (AAIW, in green) [*Ronge et al.*, 2015], benthic $\delta^{13}C$ record from MD02-2529 located in the Eastern Tropical North Pacific (in light blue) [*Leduc et al.*, 2010], benthic intermediate-water $\delta^{13}C$ record from Bering Sea core SO201-2-101KL (in magenta) [*this study*] and SO201-2-85KL (in black) [*Max et al.*, 2014], deep-water benthic $\delta^{13}C$ record from core W8709A-13PC (in brown) [*Lund and Mix*, 1998). b: End-member intermediate-water mass ε_{Nd} records from southern Bering Sea core BOW-8A (GNPIW, in magenta) [*Horikawa et al.*, 2010] and southwest Pacific core CHAT 16K (AAIW, in light green) [*Noble et al.*, 2013] together with ε_{Nd} signatures derived from sediment cores off Baja California (in blue) [*Basak et al.*, 2010]. Coloured vertical bars indicate total variability in measured $\delta^{13}C$ at respective core sites. Coloured circles indicate $\delta^{13}C_{DIC}$ composition of water masses bathing respective core sites under modern conditions [*Key et al.*, 2004].

The glacial $\delta^{13}C$ end-member variability of AAIW is reflected by sediment core SO213-84-1 off New Zealand [*Ronge et al.*, 2015] (Figure 4.5a). There, glacial $\delta^{13}C$ signatures of AAIW range between ~0.5 – 1.4 ‰ and characterizing southern-sourced intermediate water masses. The

long-term evolution of $\delta^{13}C$-signatures between AAIW and intermediate waters in the North Pacific and ETNP reveals remarkable differences in temporal variability under glacial conditions (Figure 4.5a). Moreover, huge gradients in $\delta^{13}C$ (up to 2 ‰) between Southern Ocean core SO213-84-1 and MD02-2529 from the ETNP [*Leduc et al.*, 2010] clearly separate ^{13}C-enriched (more nutrient-depleted) signatures of AAIW from ^{13}C-depleted (more nutrient-enriched) signatures of EqPIW under glacial conditions (Figure 4.5a). Evidence for a weakened production or shoaling of glacial AAIW has been inferred from $\delta^{13}C$-records off New Zealand [*Pahnke and Zahn*, 2005; *Ronge et al.*, 2015], which generally points to a glacial change in relative contribution of intermediate waters from the Southern Ocean to the tropical Pacific. However, large gradients and the discrepancy in temporal evolution of $\delta^{13}C$ signatures of EqPIW and AAIW cannot be explained by $\delta^{13}C$ variability of southern-sourced intermediate waters alone and point to additional water masses influencing the glacial mid-depth tropical Pacific.

Next, we compare our new benthic $\delta^{13}C$ record from the mid-depth subarctic Pacific (SO201-2-101KL) and the benthic $\delta^{13}C$ record of PDW from the Northeast Pacific (W8709A-13PC) [*Lund and Mix*, 1998] with EqPIW $\delta^{13}C$ water mass characteristics (MD02-2529) [*Leduc et al.*, 2010] during the past 60 kyr (Figures 4.1 and 4.5a). Millennial-scale variability superimposed on the long-term $\delta^{13}C$ trend of EqPIW is more pronounced compared to the $\delta^{13}C$-signal recorded in SO201-2-101KL (GNPIW) or W8709A-13PC (PDW) during early MIS 3 (55 – 45 ka). In addition EqPIW $\delta^{13}C$ values oscillate between $\delta^{13}C$ signatures of GNPIW and PDW during MIS 3 (60 – 30 ka). During this time, there is no clear relationship to northern- or southern-sourced intermediate waters, and rather admixing of different source water masses to EqPIW is likely. On the other hand, clear similarities in the long-term evolution in $\delta^{13}C$ between the intermediate water records derived from subarctic Pacific core SO201-2-101KL and sediment core MD02-2529 from the ETNP are observed since at least ~29 ka (Figure 4.5a). Moreover, glacial gradients in $\delta^{13}C$ between GNPIW and EqPIW are relatively small and vary between 0.2 – 0.5 ‰. In contrast, absolute $\delta^{13}C$ signatures as well as the temporal evolution of EqPIW and PDW differs substantially such as $\delta^{13}C$ of EqPIW increases steadily, whereas $\delta^{13}C$ of PDW shows a long-term trend to more depleted ^{13}C signatures during MIS 2 (Figure 4.5a). Accordingly, available deep-water ventilation ages as well as the long-term trend in deep-water $\delta^{13}C$ of the North Pacific indicate that glacial PDW was similar or even less well ventilated than today [*Lund and Mix*, 1998; *Galbraith et al.*, 2007; *Lund et al.*, 2011] and the ventilation history different to the mid-depth circulation dynamics of the North Pacific [*Kennett and Ingram*, 1995; *Stott et al.*, 2009]. Altogether, our results indicate that intermediate waters in the subarctic Pacific and ETNP (GNPIW and EqPIW) share similar glacial $\delta^{13}C$ signatures, which are indicative for the presence of nutrient-enriched intermediate water masses, but are apparently different to $\delta^{13}C$ signatures of AAIW or PDW (Figure 4.5a). Given that GNPIW features slightly higher $\delta^{13}C$ signatures compared to EqPIW masses our results point to the advection of northern-sourced intermediate water masses towards the tropical Pacific. Thus, from similarities in long-term evolution of $\delta^{13}C$ between the North Pacific and ETNP intermediate water records we argue that relatively nutrient-

enriched GNPIW generally extended further south to the tropical Pacific under glacial conditions. During the last deglaciation (~17 – 15 ka), however, intermediate water $\delta^{13}C$-signals at the ETNP and North Pacific starts to diverge substantially. The $\delta^{13}C$ signatures in the ETNP increase, while the $\delta^{13}C$ values decrease at site SO201-2-85KL in the subarctic Pacific (Figure 4.5a).

Independent evidence for enhanced glacial influence of northern-sourced intermediate waters to the low-latitude Pacific comes from the comparison of available ε_{Nd} records of the Bering Sea and off Baja California [*Basak et al.*, 2010; *Horikawa et al.*, 2010] (Figure 4.5b). In particular, ε_{Nd} data at the intermediate depth in the Bering Sea show radiogenic values explicitly indicating that Bering Sea surface water masses (marked by more radiogenic ε_{Nd} signatures) were subducted to intermediate depths under glacial conditions [*Horikawa et al.*, 2010]. At the same time, glacial ε_{Nd} values derived from a sediment record off Baja California point to the presence of more radiogenic intermediate water masses, which has been linked to admixture of dominantly northern-sourced intermediate waters [*Basak et al.*, 2010]. Furthermore, available information of glacial ε_{Nd} signatures from a sediment core in the southwest Pacific [*Noble et al.*, 2013] clearly distinguish less radiogenic ε_{Nd} signatures of AAIW from signals of more radiogenic intermediate water masses found in the Bering Sea or off Baja California (Figure 4.5b). Altogether, results from ε_{Nd} records are in line with enhanced glacial advection of northern-sourced intermediate water masses towards the tropical Pacific (Figures 4.1 and 4.5b). However, rapid changes in Bering Sea and Baja California ε_{Nd} signatures are visible during the last deglaciation that point to a switchback to reduced influence of northern-sourced intermediate water masses to the low-latitude Pacific since ~17 ka (Figure 4.5b).

The combined evidences from $\delta^{13}C$ and ε_{Nd} proxy data of the subarctic Pacific, the eastern North Pacific (Baja California), the ETNP and Southern Ocean suggest that northern-sourced intermediate waters extended further south to the ETNP under glacial conditions (Figures 4.5a and b). This is in agreement with a scenario proposed by *Herguera et al.* [2010], in which a deepening of the main thermocline and cooling of the high-latitude North Pacific would lead to a south-eastward expansion of GNPIW circulation and greater glacial influence of northern-sourced intermediate water on the tropical Pacific. Therefore, we propose that glacial changes in the relative contribution of intermediate waters from both the Southern Ocean and North Pacific are important in re-circulating excess nutrients from the high-latitude oceans towards the low latitude-regions of the Pacific Ocean. We suggest that the observed glacial changes in $\delta^{13}C$-signatures of tropical intermediate waters in the ETNP are linked to additional contribution of northern-sourced intermediate waters. Increased glacial contribution from relatively nutrient-enriched, northern-sourced intermediate water (relative to AAIW) to the low-latitude Pacific is also in line with a regional pattern of elevated marine productivity observed along the tropical North Pacific [*Arellano-Torres et al.*, 2011]. Altogether, our results further confirm considerations of a southward expansion of GNPIW to explain the $\delta^{13}C$ signatures found in the mid-depth tropical Pacific during MIS 2 [*Herguera et al.*, 2010].

4.4.2 Evidence for increased GNPIW influence on the Eastern Equatorial Pacific since MIS 2?

To assess whether GNPIW expanded further south to the equatorial upwelling system, we compare the variability in $\delta^{13}C$ of GNPIW and AAIW with a new sub-thermocline $\delta^{13}C$ proxy record of the deep-dwelling planktonic foraminifera *G. hexagonus* from ODP Site 1240. Glacial variations in $\delta^{13}C$ of sub-thermocline water masses are interpreted as both changes in incoming nutrients and export productivity in the surface ocean of the EEP. During MIS 3 (~60 – 30 ka) the *G. hexagonus* $\delta^{13}C$ proxy record indicates the presence of relatively ^{13}C-enriched (nutrient-depleted) water masses with low variability in $\delta^{13}C$ of sub-thermocline waters of the EEP (Figure 4.6a). At the same time, GNPIW shows distinctly lower (more-nutrient-rich) $\delta^{13}C$ values with higher temporal variability than EEP sub-surface waters. However, apparent similarities are observed since ~29 ka at the beginning of MIS 2, where absolute $\delta^{13}C$ values as well as the long-term trend indicate more nutrient-enriched sub-thermocline water masses recorded in $\delta^{13}C$ of *G. hexagonus* at ODP Site 1240, which closely follows the temporal evolution of the $\delta^{13}C$ signature advected towards the tropical Pacific via GNPIW (Figure 4.6a).

Interestingly, another rapid switch to monotonically increasing $\delta^{13}C$ of *G. hexagonus* is visible during the last deglaciation, which suggests a decoupling from northern-sourced intermediate waters between ~17 – 15 ka. The transition from ^{13}C-depleted (more nutrient-enriched) to rather ^{13}C-enriched (more nutrient-depleted) sub-surface water implies another significant change in characteristics of source water masses along with changes in biological productivity in the EEP during the last deglaciation (Figures 4.6a and b). Simultaneously, intermediate waters in the North Pacific became further ^{13}C-depleted and seems to be decoupled from sub-thermocline waters in the EEP. This is in line with a recent study on surface ocean productivity at ODP Site 1240, which showed that southern-sourced intermediate waters played a more dominant role for the nutrient redistribution in the EEP since the early deglaciation [e.g. *Calvo et al.*, 2011]. Dissimilar trends are also evident between northern-sourced intermediate water and mid-depth water masses in the ETNP, probably due to a reduced lateral extent of GNPIW during the last deglaciation (Figure 4.5a). Since then, mid-depth waters in the ETNP seems to follow the temporal variability of southern-sourced intermediate water that imply a larger influence of ^{13}C-enriched (more nutrient-depleted) AAIW in the tropical Pacific. However, we note that large gradients between $\delta^{13}C$ of sub-thermocline waters in the EEP and AAIW are also visible during the last deglaciation and Holocene. Still, available benthic $\delta^{13}C$ records from the mid-depth to deep North Pacific do not cover the whole Holocene and impede further interpretation of $\delta^{13}C$ variability in the ETNP during this time.

Past changes in sub-thermocline water mass signatures in the EEP have been usually linked to differences in advection and/or source-water mass characteristics of Southern Ocean water masses to the tropical Pacific. Rapid changes in meridional transport of southern-sourced intermediate water towards the tropical regions have been proposed from proposed from ε_{Nd}

records over the last 30 kyr [*Pena et al.*, 2013]. A recent study investigating Southern Ocean and EEP shallow- and deep-water ventilation ages suggest that relatively old water masses (PDW/UCDW) upwelled to EEP thermocline waters and proposed a dominant deep southern-source during late MIS 2 [*de la Fuente et al.*, 2015]. A study reconstructing radiocarbon activity of mid-depth waters from sediment cores off Baja California also pointed to the presence of slightly older intermediate waters in the eastern North Pacific during the latter part of the glacial period [*Marchitto et al.*, 2007], which might also explain glacial age anomalies in the surface ocean of the EEP. Thus, we explain changes in $\delta^{13}C$ of sub-thermocline water masses of the EEP between MIS 3 and MIS 2 by changes in source water masses characteristics probably due to variable ocean interior transport pathways reaching the equatorial Pacific under glacial conditions. Based on the apparent similarities between $\delta^{13}C$-signatures of northern-sourced intermediate waters, mid-depth waters in the Panama basin of the ETNP and sub-thermocline waters in the EEP (Figures 4.5a and 4.6a), we argue for additional intrusion of GNPIW into sub-thermocline water masses of the EEP during MIS 2.

4.4.3 "North Pacific Nutrient Leakage"

We provide the first evidence that relatively ^{13}C-depleted (nutrient-enriched) GNPIW influenced glacial EEP sub-thermocline waters during MIS 2 and discuss further potential implications on marine productivity of the equatorial Pacific regions at that time (Figures 4.6a - c). Nitrogen and silicon isotopes are often used as diagnostic tools for reconstructing past nutrient cycling. With higher nutrient consumption, both substrate (dissolved nutrients) and products generated from it become progressively enriched in heavier isotopes. Indeed several studies of sediment cores in the EEP found evidence for changes in marine productivity and nutrient utilization during MIS 2 [*Kienast et al.*, 2007; *Pichevin et al.*, 2009; *Robinson et al.*, 2009; *Dubois et al.,* 2011] (Figure 4.6b). Overall similarities between these records demonstrate that they are not primarily influenced by local processes at the deposition site, but rather reflect a robust signal of regional changes in nutrient delivery and biological productivity in the EEP [*Dubois et al.,* 2011]. *Pichevin et al.* [2009] found that the glacial biological carbon pump in the EEP was more efficient due to a relaxation of nutrient limitation and speculated about its contribution to lower atmospheric CO_2 conditions during MIS 2.

Glacial relaxation of nutrient limitation and concurrent maxima in biological productivity in the EEP have been usually related to the redistribution of excess nutrients (mainly silicic acid) from the Southern Ocean via "ocean tunnelling" as proposed by the Silicic Acid Leakage Hypothesis [*Matsumoto et al.,* 2002b]. At the same time, changes in the contribution of northern-sourced intermediate waters are often neglected e.g. by assuming that the relative contribution from northern- and southern-sourced water did not change significantly in the past [e.g. *Dubois et al.,* 2011; *Pena et al.*, 2013]. However, studies using diatom-bound silicon and nitrogen isotopes as proxies for nutrient utilization suggested enhanced glacial drawdown of silicic acid and nitrate

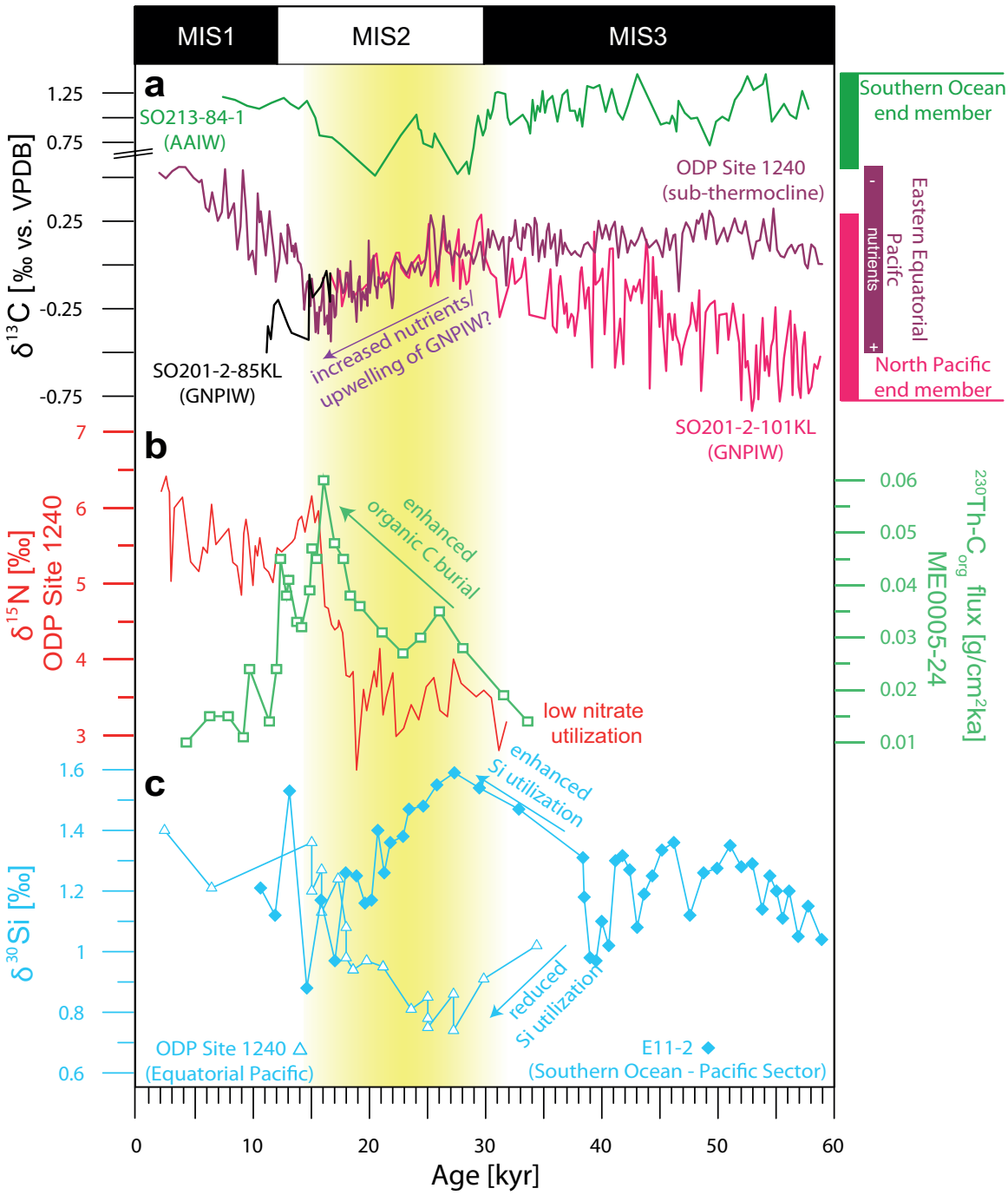

Figure 4.6. Reconstructed $\delta^{13}C$ variability of GNPIW versus AAIW compared to glacial changes in $\delta^{13}C$ of sub-thermocline waters, biological productivity and nutrient utilization in the Eastern Equatorial Pacific (EEP) and Southern Ocean. a: $\delta^{13}C$ record of GNPIW (SO201-2-85KL, *Max et al.*, 2014; SO201-2-101KL; *this study*) compared to $\delta^{13}C$ composition of AAIW (SO213-84-1, *Ronge et al.*, 2015) and deep-dwelling planktonic foraminifera $\delta^{13}C$ record of *G. hexagonus* (ODP Site 1240, *this study*) during the past 60 kyr. b: $\delta^{15}N$ record at ODP Site 1240 in the EEP [*Pichevin et al.*, 2009] together with ^{230}Th-normalized C_{org} flux of neighbouring core ME0005-24 [*Kienast et al.*, 2007]. c: $\delta^{30}Si_{Diatom}$ isotope composition of ODP Site 1240 in the EEP [*Pichevin et al.*, 2009] compared to $\delta^{30}Si_{Diatom}$ composition derived from core E11-2 [*Robinson et al.*, 2014] located in the Pacific Zone of the Southern Ocean. Yellow shaded bar marks times of increased GNPIW contribution to sub-thermocline waters of the EEP during MIS 2.

along with higher glacial opal fluxes in the Pacific Subantarctic Zone of the Southern Ocean during MIS 2 [*Bradtmiller et al.*, 2009; *Robinson et al.*, 2005, 2014]. These results show that, in contrast to the EEP, silicic acid and nitrate have been utilized more efficiently and became rather "trapped" north of the Antarctic Polar Front in the glacial deep Southern Ocean (Figures 4.6b and c). However, it has been also shown that average glacial opal fluxes were less than during the Holocene south of the Antarctic Polar Front [*Bradtmiller et al.*, 2009]. Whether the glacial Southern Ocean provides sufficient nutrients via "ocean tunnelling" to enhance marine productivity at the EEP as predicted by the Silicic Acid Leakage Hypothesis is still discussed controversial [*Hendry and Brzezinski*, 2014*; Robinson et al.*, 2014].

Interestingly, times of enhanced organic carbon flux rates and low nutrient utilization (silicic acid and nitrate) in the EEP are visible since the beginning of MIS 2 and generally coincided with the proposed changes in additional contributions of relatively nutrient-rich GNPIW to equatorial Pacific sub-thermocline water masses (Figures 4.6b and c). Invoking an additional export of unutilized (preformed) nutrients from the high-latitude North Pacific via nutrient-enriched GNPIW (here named as "North Pacific Nutrient Leakage") thus might be another, yet unconsidered, process to explain relieved nutrient limitation and a stimulated biological pump in the EEP during MIS 2. Unfortunately, less is known about glacial changes in utilization of major nutrients, such as silicon or iron in the source region of GNPIW. Some studies propose low biological productivity and nutrient utilization (nitrate) in the Bering Sea due to a decrease in productivity, or an increase in nitrate availability through changes in vertical mixing under glacial conditions [*Riethdorf et al.*, 2013; *Schlung et al.*, 2013]. Other studies point to near-complete nutrient utilization (nitrate) in the Bering Sea and western subarctic Pacific during glacial times [*Brunelle et al.,* 2007, 2010]. A recent study emphasizes the role of strong physical stratification of the glacial subarctic Pacific surface waters, which prevented additional flux of nitrate from underlying water, such that available surface nitrate was used to near completion [*Knudson and Ravelo*, 2015b]. Our results propose that additional influence of nutrient-rich North Pacific mid-depth waters to the tropical Pacific via GNPIW might hold new clues about glacial productivity changes in the EEP, but need to be further evaluated in order to understand the role of enhanced influence of GNPIW to the low-latitude Pacific under glacial conditions.

During the deglaciation, the resumption of intense overturning within the Southern Ocean led to a higher injection of relatively nutrient-depleted southern-sourced water masses into the EqPIW. As a consequence, decreasing nutrient concentrations and increasing nutrient consumption are recorded in the EqPIW (Figure 4.6). However, we can only speculate about the offset in timing between the onset of EqPIW $\delta^{13}C$ changes (shown by *G. hexagonus*) and the increase in $\delta^{15}N$ in ODP Site 1240. The switch in relative end-member contribution during the deglaciation possibly causes variations in intermediate water suboxia and hence water column denitrification [*Robinson et al*., 2009]. This would affect the nitrogen isotopes only as *G. hexagonus* seems to be more insensitive to varying oxygen concentrations [*Rippert et al*.,

2016, *this thesis*]. Nonetheless, the discrepancy in timing needs to be further investigated in combination with $\delta^{15}N$ studies from the high latitudes.

4.5 Conclusions

Here we report on new foraminiferal $\delta^{13}C$ records from the western subarctic Pacific (Bering Sea) and EEP spanning the past 60 kyr. Combined evidence of $\delta^{13}C$ from core SO201-2-101KL and ε_{Nd} records of the Bering Sea points to a long-term increase in GNPIW formation since the onset of MIS 3, which culminated early in MIS 2 (~29 ka). The comparison between benthic foraminiferal $\delta^{13}C$ records of SO201-2-101KL and marine sediment core MD02-2529 from the Panama Basin as well as ε_{Nd} records of the Bering Sea and eastern North Pacific reveals remarkable similarities in the long-term evolution between GNPIW and EqPIW signatures in the tropical North Pacific during the glacial period. These results support the notion that northern-sourced intermediate water extended further south to the tropical Pacific region than today under glacial boundary conditions. Glacial changes in $\delta^{13}C$ of sub-thermocline water masses in the EEP were derived from deep-dwelling planktonic foraminiferal species *G. hexagonus* at ODP Site 1240 and indicate significant changes in sub-thermocline water mass characteristics during MIS 2. Notably, the proposed times of additional influence of GNPIW to the tropical Pacific coincides with changes in nutrient availability and biological productivity in the glacial EEP. Overall, our new findings indicate that past changes in North Pacific mid-depth circulation might have played a crucial role in glacial nutrient availability and biological productivity in the EEP, but needs to be further constrained by future studies investigating glacial changes in utilization of major nutrients, such as silicon or iron in the subarctic Pacific.

Acknowledgments and Data

The Helmholtz Climate Initiative REKLIM (Regional climate change) funded this study. NR, LLJ and RT received funding through research projects Manihiki II (03G0225B) and SiGePAX (03F0704A) by the Bundesministerium für Bildung und Forschung (BMBF). This research used samples provided by BMBF-project KALMAR, and the International Ocean Discovery Program (IODP). IODP was sponsored by the U.S. National Science Foundation (NSF) and participating countries under the management of Joint Oceanographic Institutions (JOI), Inc. We gratefully acknowledge the Master and crew of R/V SONNE cruises SO201-2 (KALMAR) and thank for their professional support on board. We express our thanks to L. Schönborn and G. Meyer for conducting stable isotope measurements at the AWI stable isotope lab. The authors thank Isabel Cacho for helpful comments and suggestions. Supplementary data are available at PANGAEA Data Publisher for Earth & Environmental Science.

4.6 Supplementary data

To:

Max, L., Rippert, N., Lembke-Jene, L., Tiedemann, R., Cacho, I., Mackensen, A., Nürnberg, D., Evidence for enhanced convection of North Pacific Intermediate Water to the low-latitude Pacific under glacial conditions. *Under review* at Paleoceanography.

Table S4.4.1. Stable isotope data ($\delta^{13}C$) of epibenthic foraminifera *Cibicides lobatulus* from sediment core SO201-2-101KL (58°52'N, 170°41'E).

Depth (cm)	Age (ka)	$\delta^{13}C_{C.lobatulus}$ (‰VPDB)	Depth (cm)	Age (ka)	$\delta^{13}C_{C.lobatulus}$ (‰VPDB)	Depth (cm)	Age (ka)	$\delta^{13}C_{C.lobatulus}$ (‰VPDB)	Depth (cm)	Age (ka)	$\delta^{13}C_{C.lobatulus}$ (‰VPDB)
83	16.66	0.095	255	31.20	-0.298	430	45.54	-0.606	650	56.60	-0.341
85	16.82	-0.019	260	31.96	-0.125	433	45.71	-0.282	655	56.77	-0.438
90	17.21	-0.156	263	32.30	0.036	435	45.82	-0.279	660	56.94	-0.698
93	17.46	-0.034	265	32.52	-0.108	440	46.11	-0.429	665	57.11	-0.760
95	17.63	-0.236	270	33.06	-0.070	443	46.28	-0.282	670	57.29	-0.469
100	18.06	-0.116	273	33.39	0.041	445	46.39	-0.401	675	57.46	-0.384
103	18.31	-0.050	275	33.77	-0.285	450	46.67	-0.455	680	57.63	-0.596
105	18.48	-0.198	280	35.10	-0.307	453	46.84	-0.570	685	57.80	-0.734
110	18.91	-0.159	283	35.58	-0.025	455	46.98	-0.481	690	58.05	-0.696
113	19.16	-0.134	285	35.78	-0.349	460	47.37	-0.378	695	58.30	-0.567
115	19.33	-0.144	290	36.11	-0.387	463	47.61	-0.338	700	58.55	-0.593
120	19.76	-0.113	293	36.31	-0.116	465	47.76	-0.216	705	58.80	-0.524
123	20.01	-0.117	295	36.44	-0.064	470	48.15	-0.377	710	59.05	-0.804
125	20.18	0.026	300	36.77	-0.279	473	48.39	-0.145	715	59.30	-0.779
130	20.60	0.065	303	36.96	-0.220	475	48.55	-0.720	720	59.55	-0.646
133	20.86	-0.085	305	37.08	-0.358	480	48.94	-0.270	725	59.82	-0.675
135	21.03	-0.129	310	37.38	-0.280	483	49.17	-0.240	730	60.11	-0.859
140	21.45	-0.043	313	37.56	-0.299	485	49.33	-0.225			
143	21.71	-0.079	315	37.67	-0.406	490	49.72	-0.205			
145	21.88	-0.012	320	37.97	-0.261	493	49.96	-0.505			
150	22.30	0.069	323	38.15	-0.043	495	50.11	-0.286			
153	22.56	0.070	325	38.27	-0.013	500	50.50	-0.281			
155	22.73	-0.017	330	38.57	-0.249	503	50.74	-0.278			
160	23.15	-0.060	333	38.75	-0.149	505	50.90	-0.428			
163	23.41	-0.074	335	38.87	-0.128	510	51.29	-0.221			
165	23.58	-0.004	340	39.16	-0.586	515	51.64	-0.371			
170	24.00	0.033	343	39.34	0.190	520	51.82	-0.445			
173	24.25	0.056	345	39.46	-0.112	525	52.00	-0.773			
175	24.42	0.007	350	39.79	-0.087	530	52.19	-0.284			
180	24.85	0.031	353	40.06	-0.021	535	52.37	-0.586			
183	25.10	0.234	355	40.24	-0.396	540	52.56	-0.549			
185	25.27	-0.122	360	40.68	0.092	545	52.74	-0.661			
190	25.70	-0.035	363	40.95	0.094	550	52.92	-0.834			
193	25.90	-0.116	365	41.13	-0.587	555	53.11	-0.760			
195	26.04	0.043	370	41.58	-0.307	560	53.29	-0.459			
200	26.37	0.193	373	41.85	-0.567	565	53.48	-0.768			
203	26.56	0.087	375	42.03	-0.084	570	53.66	-0.507			
205	26.69	0.076	380	42.47	-0.204	575	53.84	-0.303			
210	27.02	0.059	383	42.74	-0.121	580	54.03	-0.604			
213	27.22	-0.092	385	42.92	-0.152	585	54.21	-0.521			
215	27.35	0.070	390	43.27	-0.084	590	54.39	-0.635			
220	27.68	0.203	393	43.44	-0.219	595	54.58	-0.465			
223	27.88	-0.320	395	43.55	-0.152	600	54.76	-0.421			
225	28.01	0.029	400	43.84	0.145	605	54.95	-0.242			
230	28.34	-0.111	403	44.01	0.005	610	55.13	-0.593			
233	28.53	-0.092	405	44.12	-0.706	615	55.31	-0.780			
235	28.71	0.032	410	44.40	0.045	620	55.50	-0.688			
240	29.28	0.250	413	44.58	-0.191	625	55.68	-0.531			
243	29.62	0.287	415	44.69	-0.067	630	55.87	-1.025			
245	29.85	0.062	420	44.97	-0.354	635	56.05	-1.234			
250	30.45	-0.047	423	45.14	-0.149	640	56.23	-0.263			
253	30.90	-0.075	425	45.26	-0.357	645	56.42	-0.744			

Table S4.4.2. Stable isotope data ($\delta^{13}C$) of deep-dwelling planktic foraminifera *Globorotaloides hexagonus* from ODP Site 1240 (00°01'N, 82°27'W).

Depth (cm)	Age (ka)	$\delta^{13}C_{G.hexagonus}$ (‰VPDB)	Depth (cm)	Age (ka)	$\delta^{13}C_{G.hexagonus}$ (‰VPDB)	Depth (cm)	Age (ka)	$\delta^{13}C_{G.hexagonus}$ (‰VPDB)
1	1.91	0.53	187	15.26	-0.22	316	22.16	-0.004
5	2.47	0.50	189	15.36	-0.38	318	22.26	0.051
9	3.03	0.54	191	15.47	-0.27	324	23.22	-0.053
13	3.59	0.56	193	15.58	-0.391	326	23.36	-0.030
17	4.15	0.56	195	15.69	-0.240	328	23.63	0.015
18	4.29	0.64	197	15.80	-0.262	330	23.91	-0.041
22	4.85	0.50	199	15.91	-0.195	332	24.18	0.013
26	5.34	0.47	201	16.02	-0.073	334	24.46	-0.060
29	5.55	0.49	203	16.13	-0.341	336	24.73	-0.014
34	5.90	0.33	207	16.35	-0.289	338	25.00	0.112
38	6.18	0.31	209	16.46	-0.394	340	25.28	0.284
42	6.46	0.42	211	16.57	-0.155	342	25.55	0.205
49	6.95	0.25	213	16.67	-0.437	344	25.83	-0.074
54	7.29	0.30	215	16.78	-0.173	346	26.10	0.091
58	7.57	0.55	217	16.89	-0.176	348	26.38	0.280
62	7.85	0.27	219	17.00	-0.300	350	26.65	0.079
69	8.34	0.35	221	17.11	-0.286	352	26.88	0.137
73	8.62	0.09	227	17.28	-0.022	354	27.11	0.000
77	8.90	0.22	233	17.46	-0.080	356	27.34	0.078
82	9.11	0.54	235	17.59	-0.112	360	27.80	0.044
89	9.39	0.30	237	17.72	-0.161	364	28.16	0.118
94	9.60	0.03	239	17.85	-0.151	366	28.29	0.053
102	9.93	0.08	241	17.98	-0.045	370	28.55	0.080
109	10.21	-0.05	243	18.11	-0.044	374	28.80	0.047
113	10.38	0.41	245	18.24	-0.183	376	28.93	0.006
117	10.54	0.24	247	18.37	0.022	380	29.19	0.055
118	10.65	0.31	249	18.50	-0.212	384	29.45	0.127
122	11.08	0.05	251	18.63	-0.153	386	29.58	0.131
125	11.40	0.31	253	18.76	-0.192	390	29.84	-0.029
126	11.50	0.23	255	18.89	-0.325	396	30.22	0.204
129	11.83	0.04	257	19.02	-0.101	398	30.35	0.100
130	11.93	-0.10	259	19.15	-0.065	402	30.61	0.195
133	12.25	0.03	261	19.28	-0.260	406	30.87	0.145
134	12.36	0.18	263	19.41	-0.154	410	31.13	0.087
137	12.68	0.08	265	19.52	-0.177	414	31.38	0.144
141	12.91	0.01	267	19.62	-0.199	416	31.51	0.160
142	12.95	0.23	269	19.73	-0.136	420	31.77	-0.118
145	13.08	0.20	271	19.83	-0.234	424	32.03	0.159
151	13.32	0.08	273	19.94	0.139	426	32.16	0.137
153	13.43	0.11	275	20.04	-0.160	430	32.42	0.170
155	13.53	0.05	281	20.36	0.053	432	32.55	0.256
157	13.64	0.12	283	20.46	-0.116	436	32.80	0.102
159	13.75	0.08	285	20.57	-0.129	440	33.06	0.085
161	13.85	0.02	287	20.67	-0.190	442	33.21	0.213
165	14.07	0.01	289	20.78	-0.069	444	33.36	0.154
167	14.17	-0.03	293	20.98	-0.082	446	33.53	0.234
171	14.39	-0.26	295	21.08	-0.073	448	33.71	0.230
173	14.49	-0.17	297	21.19	-0.042	450	33.88	0.213
175	14.60	-0.11	299	21.29	-0.106	452	34.05	0.057
177	14.71	-0.09	306	21.65	-0.080	454	34.22	0.269
179	14.82	-0.19	308	21.75	-0.119	456	34.40	0.232
181	14.93	-0.24	312	21.95	-0.247	458	34.57	0.020
183	15.04	-0.08	314	22.06	-0.193	460	34.74	0.103

Depth (cm)	Age (ka)	$\delta^{13}C_{G.hexagonus}$ (‰VPDB)	Depth (cm)	Age (ka)	$\delta^{13}C_{G.hexagonus}$ (‰VPDB)	Depth (cm)	Age (ka)	$\delta^{13}C_{G.hexagonus}$ (‰VPDB)
462	34.91	0.142	568	42.20	0.1	687	51.44	0.3
464	35.09	0.045	572	42.51	0.1	691	51.75	0.2
466	35.26	0.192	576	42.82	0.1	695	52.06	0.2
468	35.43	0.236	580	43.14	0.2	699	52.37	0.3
470	35.60	0.093	584	43.45	0.2	703	52.68	0.1
472	35.77	0.135	588	43.76	0.1	707	52.99	0.035
474	35.95	0.176	592	44.07	0.1	711	53.2978	0.134
476	36.12	-0.004	596	44.38	0.1	715	53.6081	0.142
478	36.29	0.078	600	44.69	0.1	719	53.9184	0.262
480	36.46	0.200	603	44.92	0.1	723	54.2287	0.132
482	36.64	0.063	607	45.23	0.0	726	54.46	0.08
484	36.81	0.127	611	45.54	0.2	730	54.7717	0.322
488	37.06	0.089	615	45.85	0.1	734	55.0821	0.087
496	37.38	0.057	619	46.16	0.2	738	55.3924	0.051
504	37.69	0.1	621	46.32	0.2	742	55.7027	0.043
508	37.85	0.1	625	46.63	-0.2	746	56.01	0.09
516	38.17	0.0	629	46.94	0.2	750	56.3233	0.115
520	38.48	0.1	633	47.25	0.2	754	56.6336	0.067
524	38.79	0.1	637	47.56	0.2	758	56.9439	0.109
528	39.10	0.1	641	47.87	0.1	762	57.2543	0.118
532	39.41	0.1	645	48.18	0.3	765	57.49	0.007
536	39.72	0.3	647	48.33	0.2	768	57.7197	-0.02
540	40.03	0.2	651	48.64	0.3	772	58.03	0.117
544	40.34	0.2	655	48.95	0.1	776	58.3403	0.096
548	40.65	0.1	659	49.26	0.3	780	58.6507	0.006
550	40.81	0.2	663	49.57	0.3	784	58.961	0.005
554	41.12	0.2	667	49.88	0.1	786	59.12	0.048
558	41.43	0.0	673	50.35	0.2	790	59.4264	-0.098
562	41.74	0.2	675	50.50	0.2	794	59.7368	-0.077
566	42.05	0.1	679	50.82	0.1	798	60.0471	-0.018

5. Manuscript III

Alternating influence of northern versus southern-sourced water masses on the equatorial Pacific sub-thermocline during the past 240 ka.

Nadine Rippert[1*], Lars Max[1], Andreas Mackensen[1], Isabel Cacho[2], Patricia Povea[2], and Ralf Tiedemann[1]

[1]Alfred-Wegener-Institut, Helmholtz Zentrum für Polar- und Meeresforschung, Postfach 12 01 61, 27515 Bremerhaven, Germany

[2]Grup de Recerca Consolidat en Geociències Marines, Dept. de Dinàmica de la Terra i de l'Oceà, Universitat de Barcelona, C/Martí Franques, 08028 Barcelona, Spain

*corresponding author: Nadine Rippert (Nadine.Rippert@awi.de)

***to be submitted to* Paleoceanography**

Abstract

The Eastern Equatorial Pacific (EEP) is a key area to understand past oceanic processes that control atmospheric CO_2 concentrations. Many studies argue for higher past nutrient concentrations in the EEP by enhanced transfer of nutrients via Southern Ocean Intermediate Water (SOIW) to the low-latitude Pacific. Latest studies, however, argue against SOIW as a nutrient source at least during Marine Isotope Stage 2 (MIS 2) as proxy-data indicate that nutrients are better utilized in the Southern Ocean under glacial conditions. Whereas, recent results from the subarctic Pacific suggest that enhanced ventilation of nutrient-rich Glacial North Pacific Intermediate Water (GNPIW) contribute to the nutrient concentration in equatorial Pacific sub-thermocline water masses during MIS 2. However, the interplay between SOIW versus GNPIW and its influence on the nutrient distribution in the EEP spanning more than one glacial cycle are still not understood. We present a carbon isotope ($\delta^{13}C$) study of sub-thermocline waters derived from deep

dwelling planktonic foraminifera *Globorotaloides hexagonus* in the EEP (ODP Site 1240), which is compared with published $\delta^{13}C$ records around the Pacific. Results indicate an enhanced influence of GNPIW during MIS 2 and MIS 6 compared to today and largest contributions of northern-sourced intermediate waters during glacial maxima. These observations suggest that changes in EEP nutrient concentrations are possibly related to the relative contributions between northern and southern intermediate waters. A switch from increased GNPIW – decreased SOIW to diminished GNPIW – enhanced SOIW influence on equatorial sub-thermocline waters is recognized during glacial terminations and marks substantial changes in nutrient concentrations and biological productivity in the EEP.

5.1 Introduction

The modern Eastern Equatorial Pacific (EEP) acts as the most important source for marine carbon dioxide (CO_2) to the atmosphere [*Takahashi et al*., 2009]. The elevated pCO_2 has been attributed to the upwelling of nutrient-rich waters in combination with low productivity by siliceous phytoplankton that sequesters CO_2 during photosynthesis [*Dugdale and Wilkerson,* 1998]. However, primary productivity of these organisms is nowadays hindered by the low availability of silicic acid ($Si(OH)_4$) and iron in the EEP [*Broecker and Peng*, 1982; *Dugdale et al.*, 2002; *Sarmiento et al*., 2004; *Ryan et al*., 2006]. Other macronutrients such as nitrate are not fully utilized and remain high [*Robinson et al.,* 2009]. Southern Ocean Intermediate Water (SOIW), which is the main contributor of Equatorial Pacific Intermediate Water (EqPIW) under modern conditions [*Goodman et al.*, 2005; *Qu et al.*, 2009; *Bostock et al*., 2010], only contains depleted $Si(OH)_4$ concentrations relative to other macronutrients, as diatoms blooming in the formation area of SOIW remove $Si(OH)_4$ out of the surface waters [*Hendry and Brzezinski*, 2014]. These low-silicon SOIW are then fed into the low-latitude thermocline [*Qu and Lindstrom*, 2004]. As a result, SOIW contributes about half of the nitrate supply but only roughly 30 % of the total modern equatorial $Si(OH)_4$ supply into the EEP upwelling system [*Sarmiento et al*., 2004; *Dugdale et al*., 2002]. Its northern counterpart, the nutrient-elevated North Pacific Intermediate Water (NPIW), is nowadays mostly bound to about 20°N but extends further south in the western Pacific [*Bostock et al*., 2010]. Thereby, the imprint of NPIW reaches the equatorial Pacific, where it accounts for ~70 % of the $Si(OH)_4$ supply today [*Sarmiento et al*., 2004].

Under glacial conditions, changes in nutrient utilization based on silicon isotope records showed that the EEP recieved three times more $Si(OH)_4$, thereby removing the $Si(OH)_4$-limitation within the EEP [*Pichevin et al.*, 2009]. *Brzezinski et al*. [2002] and *Matsumoto et al*. [2002b] assumed that excess $Si(OH)_4$ has been delivered via enhanced SOIW to the EEP as described in the Silicic Acid Leakage Hypothesis (SALH). This caused diatoms to displace coccolithophores at low latitudes and consequently, weakened the carbonate pump and lowered glacial atmospheric pCO_2 [*Brzezinski et al*., 2002]. Stable isotope analyses [*Pena et al., 2008*], biomarkers [*Calvo et al*., 2011], planktonic foraminiferal abundances [*Yu et al.,* 2012], neodymium isotope records (ε_{Nd})

[*Pena et al.,* 2013], and radiocarbon data [*de la Fuente et al*., 2015] further support the increasing influences of southern-sourced waters on the equatorial upwelling waters. However, the potential of SOIW in delivering more nutrients to the low-latitude Pacific under glacial conditions is still under debate. Recent studies found increased glacial productivity in the Southern Ocean, which potentially leave surface waters rather nutrient depleted, and leads to “nutrient-trapping” in the Southern Ocean [*Loubere et al.*, 2011; *Hendry and Brzezinski*, 2014; *Robinson et al.*, 2014; *Rousseau et al*., 2016]. Furthermore, there is growing debate on the amount of SOIW formed during glacial maxima. An authigenic mineral study found higher oxygen concentrations along the Chilean margin during glacials and correlated these to an increased SOIW production [*Muratli et al*., 2010]. In contrast, a benthic carbon isotope ($\delta^{13}C$) record from the southwest Pacific [*Pahnke and Zahn*, 2005] and ε_{Nd} values from the tropical Atlantic [*Pahnke et al*., 2008; *Huang et al*., 2014] both suggest a reduced production of SOIW during glacial conditions, possibly related to stronger water column stratification. More recently, results from benthic $\delta^{13}C$ records, which form an intermediate to deep water transect at the New Zealand margin, suggest in combination with model results a shoaling of the SOIW / Upper Circumpolar Deep Water (UCDW) boundary during glacials due to an increased freshwater flux into SOIW by melting sea ice [*Ronge et al.,* 2015].

In the subarctic Pacific, benthic foraminiferal $\delta^{13}C$ records point to increased formation of Glacial North Pacific Intermediate Water (GNPIW) [*Duplessy et al.*, 1988; *Keigwin*, 1998; *Matsumoto et al.*, 2002a]. In comparison with the modern situation, a ε_{Nd} record proposes a glacial shift in the formation area from mainly the Sea of Okhotsk towards the northwest Bering Sea [*Horikawa et al*., 2010], which was further supported by foraminiferal isotope studies [*Rella et al., 2012*; *Max et al.*, 2014; *Knudson and Ravelo*, 2015a; *Max et al*., under review, *this thesis*] and reconstructions based on radiolarian assemblages [*Matul et al*., 2015]. Evidence for strengthened mid-depth circulation in the North Pacific has been further noticed along the California margin to the Eastern Tropical North Pacific (ETNP) [*Stott et al.,* 2000; *Leduc et al.*, 2010] and as far as the equatorial Pacific, where benthic $\delta^{13}C$ signatures and trends show apparent similarities between Bering Sea records and EEP sub-thermocline waters during glacial boundary conditions [*Knudson and Ravelo*, 2015a; *Max et al*., under review, *this thesis*].

First studies indicate reoccurring signals during the Pleistocene with a shallower penetration of SOIW in the southern hemisphere and at the same time higher GNPIW ventilation in the North Pacific [*Elmore et al*., 2015; *Knudson and Ravelo*, 2015a; *Ronge et al*., 2015]. However, the interplay between SOIW versus NPIW and its influence on past nutrient distribution in the EEP spanning more than one glacial cycle are not well constrained, but important for our understanding of past ocean processes and past atmospheric CO_2 fluctuations. This study provides new insights into the dynamic behaviour by comparing $\delta^{13}C$ records from the equatorial sub-thermocline Pacific, the Pacific Sector of the Southern Ocean and the North Pacific to further disentangle the varying sources of nutrient-injections into the equatorial Pacific sub-thermocline over the past 240 ka.

5.1.1 Modern oceanography and hydrography

The modern EEP is one of the largest high-nitrate low-chlorophyll (HNLC) areas in the world oceans [e.g. *Dugdale and Wilkerson,* 1998; *Le Borgne et al.,* 2002]. Delivery of nutrients towards the EEP happens through the eastward flowing Equatorial Undercurrent (EUC) that is formed in the western equatorial Pacific by the South Equatorial Current (SEC), New Guinea Coastal Undercurrent (NGCUC) and the North Equatorial Counter Current (NECC) (Figure 5.1a) [*Fine et al.*, 1994; *Dugdale et al*., 2002]. As the EUC flows eastward across the equatorial Pacific its upper branch shoals parallel with the thermocline providing nutrients to the euphotic zone and thereby, stimulating primary productivity [*Dugdale et al*., 2002; *Ryan et al*., 2006]. The lower branch of the EUC does not upwell along the equator, but as it travels across the equator it receives nutrients from the underlying EqPIW and at the same time provides nutrients to the upper EUC by diapycnal mixing [*Dugdale et al*., 2002; *Qu et al.*, 2009; *Rafter and Sigman*, 2015].

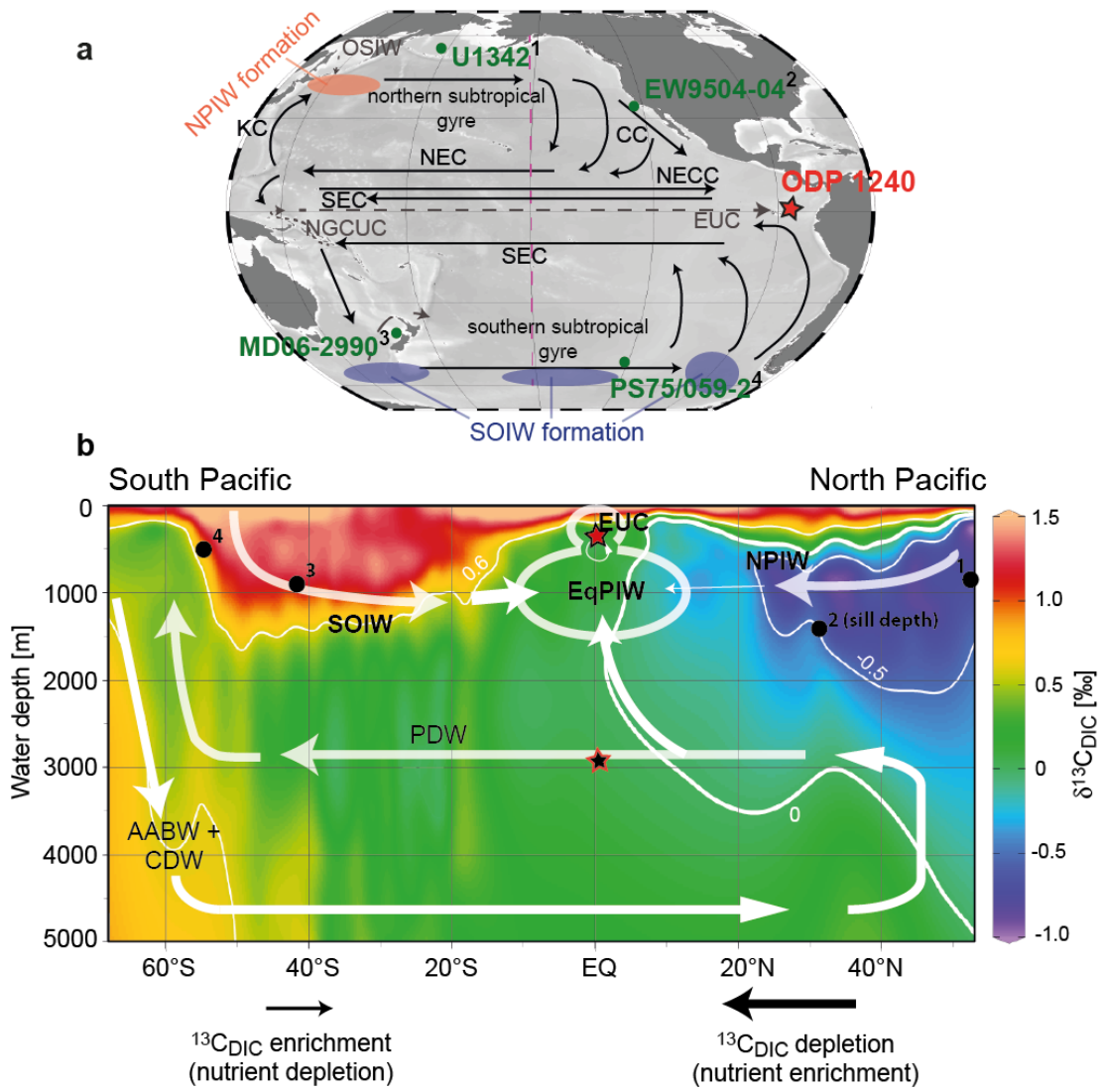

Figure 5.1. Overview of Pacific Ocean current system and hydrography. a: Major surface (solid line) and subsurface (dashed line) currents that are mentioned in the text [after *Tchernia*, 1980; *Tomczak*

and Godfrey, 2005; *Kessler,* 2006]. Formation areas of North Pacific Intermediate Water (NPIW) and Southern Ocean Intermediate Water (SOIW) are given in colored circles [after *Talley*, 1993; *Bostock et al*., 2013]. Location of sediment core ODP Site 1240 [*this study*] is shown with a red star, other $\delta^{13}C$ reference cores with green spots. The red line in (a) denotes the transect shown in (b). b: Meridional carbon isotope transect across the Pacific Ocean with major mid-depth to deep water masses (white arrows): Equatorial Pacific Intermediate Water (EqPIW) and Equatorial Undercurrent (EUC), NPIW and SOIW, PDW = Pacific Deep Water, AABW = Antarctic Bottom Water and CDW = Circumpolar Deep Water. The red star indicates the location of ODP Site 1240 benthic (open) and ODP Site 1240 *G. hexagonus* (full). Black dots denote the reference sediment cores from (a) (assignment through small numbers). Maps and transect were generated using Ocean Data View [*Schlitzer*, 2015] using data from *Schmitter et al*. [2013].

In HNLC areas, including the EEP primary productivity is stimulated by the input of iron [e.g. *Martin et al*., 1994; *Coale et al*., 1998]. A variety of iron sources in the formation region of the EUC have been identified to increase the iron concentration within the EUC including hydrothermal venting [*Gordon et al*., 1997], riverine input and direct interaction of NGCUC with continental shelf areas [*Mackey et al*., 2002] as well as atmospheric dust input along the equator [*Winckler et al*., 2008]. A nutrient analysis by *Dugdale et al*. [2002] revealed that concentrations of other macronutrients such as nitrate and $Si(OH)_4$ are not only asymmetrically distributed along the equator but also differ meridional. North of the equator within the NECC both $Si(OH)_4$ and nitrate are in about equal proportions. Contrary, the NGCUC has low $Si(OH)_4$ to nitrate ratios, a signal originating in its source water – the SOIW (Table 5.1) [*Dugdale et al*., 2002]. SOIW comprises Subantarctic Mode Water (SAMW) and Antarctic Intermediate Water (AAIW) [after *Pena et al*., 2013]. SAMW occupies ~300 – 800 m water depth and is formed in wintertime by vigorous deep mixing along the Subantarctic Front [*McCartney*, 1977; *Bostock et al*., 2013]. The densest of the circumpolar SAMW is the AAIW, which sinks to 800 – 1400 m water depth [*McCartney*, 1977; *Bostock et al.*, 2013], although characterized by a prominent salinity minimum [*McCartney*, 1977].

On the other hand, NPIW, which is the main contributor for NECC [*Fine et al.*, 1994], is never exposed to the surface thereby nutrient-depletion by biological productivity is marginal and nutrient levels remain high [*Sarmiento et al*., 2004]. Instead, modern NPIW-formation is tightly coupled to Okhotsk Sea Intermediate Water (OSIW) that is formed in coastal polynyas during wintertime sea-ice formation within the Sea of Okhotsk [*Shcherbina et al*., 2003]. The fresh and cold OSIW merges with the northward flowing warm and less dense Kuroshio Current (KC) and forms a mixture of these two water masses east of Japan in the northwest Pacific [*Talley*, 1993]. The nutrient-elevated NPIW spreads at depths of approximately 300 – 800 m southwards and eastward across the North Pacific (Table 5.1) and feeds the near-surface flowing California Current (CC) as well as North Equatorial Current (NEC) and NECC [*Reid*, 1965; *Talley*, 1993].

Equatorial Pacific Intermediate Water that provides nutrients to the overlying EUC is mainly made up of SOIW and Pacific Deep Water (PDW) under modern conditions [*Bostock et al.,*

2010]. PDW formed initially in the North Pacific via upwelling and diffusion of Circumpolar Deep Water (CDW) and Antarctic Bottom Water (AABW) (Figure 5.1) [*Tomczak and Godfrey*, 2005]. The deep northern-south water mass is the oldest water mass on Earth, characterized by low oxygen and high nutrient concentrations with a pronounced silicate maximum as well as elevated CO_2 concentrations (Table 5.1) [*Fiedler and Talley*, 2006].

Table 5.1. Modern geochemical characteristics for different intermediate and deep water-masses at their origin.

Tracer	NPIW	EUC + EqPIW[a]	SOIW	PDW	AABW
Salinity[1,2]	33.9 – 34.1	34.5 – 34.7	34.3 – 34.5	34.6 – 34.7	34.6 – 34.8
Average potential density [σ_θ][1,3,4]	26.8	26.6 – 27.0	27.1	27.7 – 27.8	>27.8
Oxygen [µmol/kg][4]	0 – 150	0 – 80	150 – 250	100 – 135	190 – 210
Nitrate [µmol/kg][4]	25 – 45	30 – 40	20 – 35	37 – 40	31 – 34
Silicate [µmol/kg][4]	60 – 150	20 – 50	5 – 50	150 – 170	110 – 125
Phosphate [µmol/kg][4]	2.0 – 3.2	1.9 – 2.7	1.4 – 2.3	2.4 – 2.8	2.1 – 2.3
$\delta^{13}C$ [‰][5]	-0.7	0 – 0.1	1.1	-0.1	0.4

[a]values determined for 300 – 500 m water depth
[1]values from *Bostock et al*. [2010]
[2]values from *Locarnini et al*. [2013]
[3]values from *Fiedler and Talley* [2006]
[4]values from *Key et al*. [2004]
[5]values from *Schmitter et al*. [2013]

5.2 Materials and Methods

5.2.1 Material and stable isotope analyses

We measured stable oxygen ($\delta^{18}O$) and carbon ($\delta^{13}C$) isotopes of deep-dwelling planktonic foraminifera *Globorotaloides hexagonus* from ODP Site 1240 at the northern flank of Carnegie Ridge in the Panama Basin (0°01.31´N, 86°27.76´W, 2,921 m water depth) [*Mix et al*., 2003] (Figure 5.1). For stable isotope analyses, five specimens of *G. hexagonus* were picked from the 250 – 315 µm size fraction in each sample. The measurements were conducted on a Thermo Fisher Scientific MAT 253 mass spectrometer coupled to an automatic carbonate preparation device Kiel CARBO IV at AWI. The isotope measurements were calibrated via the international standard NBS 19 and all results are given in δ-notation versus VPDB. The precision of the measurements, determined over a one-year period and based on repeated analysis of an internal laboratory standard (Solnhofen limestone), is ±0.06 ‰ and ±0.08 ‰ for carbon and oxygen isotopes, respectively.

To validate the depth habitat of *G. hexagonus* we determined its Apparent Calcification Depth (ACD) using the uppermost core top sample (at 10 cm) [details described in *Max et al.,* under

review, *this thesis*]. The ACD assessment indicates an ACD of 340 – 430 m water depth that agrees with studies from the central equatorial Pacific [*Rippert et al*., 2016, *this thesis*] and North Pacific [*Ortitz et al*., 1996].

We further used published benthic $\delta^{18}O$ and $\delta^{13}C$ records from Bering Sea sediment core U1342 (54.83°N, 176.92°E, 818 m) [*Knudson and Ravelo*, 2015a] and from South Pacific sediment core SO136-003/MD06-2990 (in the later only termed MD06) (42.19°S, 169.55°E, 943 m) [*Ronge et al*., 2015].

5.2.2 Stratigraphic approach

We improved existing age models of the first 29 meters composite depth (m.c.d.) from ODP Site 1240 [*Pena et al*., 2008], MD06 [*Ronge et al*., 2015] and U1342 [*Knudson and Ravelo*, 2015a] by a combination of published radiocarbon dating (if available) and $\delta^{18}O$ correlation to the global benthic $\delta^{18}O$ stack LR04 [*Lisiecki and Raymo*, 2005] (Figure 5.2). For the age model of ODP Site 1240, we used the established age model from *Pena et al*. [2008] for the first 5.2 m.c.d based on 17 Accelerator Mass Spectrometry (AMS) ^{14}C dates that cover the first ~38 ka. For the sediment depth interval between 5.2 m.c.d. and ~19 m.c.d we used a new benthic $\delta^{18}O_{Cibicidoides}$ record and $\delta^{18}O$ record of deep-dwelling planktonic foraminifera *G. hexagonus* [both *this study*], which were aligned graphically to the LR04 record [*Lisiecki and Raymo*, 2005]. Beyond the range of the $\delta^{18}O_{Cibicidoides}$ record (~19 m.c.d. – 29.4 m.c.d), we took the *G. hexagonus* record and visually tuned it to the LR04 stack. As the *G. hexagonus* record has a only low-resolution during that time interval, we additionally used the surface-dwelling planktonic species *Globigerinoides ruber* record of ODP Site 1240 [*Pena et al.,* 2008] to constrain the developed age model (Figure 5.2). Furthermore, the ash layer “L” [*Ninkovich and Shackleton*, 1975] was considered as well that is located at 125.71 m.c.d. [*Pena et al.*, 2008]. Our age model estimation yields an age of the ash layer “L” of 235.83 ka, which is in the range of the previously estimated age of 230 ± 10 ka [*Ninkovich and Shackleton*, 1975].

For the age model of site MD06 we used the six ^{14}C dates of *Ronge et al*. [2015] dating back ~25 ka and beyond that graphically tuned the benthic *Cibicidoides wuellerstorfi* $\delta^{18}O$ record to the LR04 record. For U1342 we used the $\delta^{18}O$ values measured on *Uvigerina peregrina* [*Knudson and Ravelo,* 2015a] and graphically aligned them to LR04.

As a result, the sediment record from 0 – 29.4 m.c.d. of ODP Site 1240 comprises the time interval of the last 300 kyrs. The sampling distance provides an average time resolution of 0.23 kyr for the first 60 ka and 1.4 kyr for 60 – 240 ka. The upper 9.4 m of sediment core MD06 and the upper 39.4 m of U1342 (core composite depth below seafloor, CCSF-A) cover the time interval of the last 351.7 kyr and 1260 kyr with an average temporal resolution of 0.91 kyr and 1.16 kyrs, respectively (Figure 5.2). Supplementary Table S5.7.1 summarizes all age control points used for site ODP Site 1240, MD 06, and U1342.

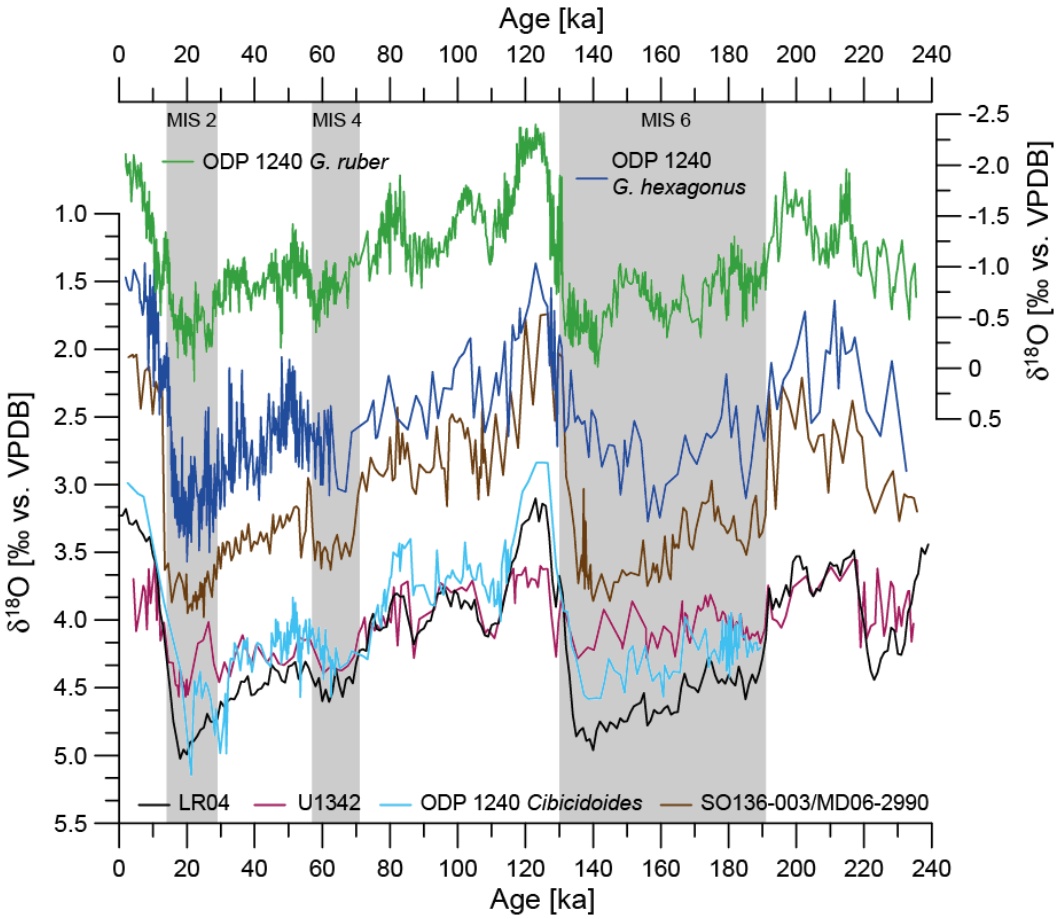

Figure 5.2. Stratigraphic correlation of published and newly generated $\delta^{18}O$ records with respect to the benthic $\delta^{18}O$ reference stack (LR04, black) [*Lisiecki and Raymo*, 2005]. ODP Site 1240 *G. ruber* (green) [*Pena et al*., 2008], ODP Site 1240 *G. hexagonus* (dark blue) [*this study*], SO136-003/MD06-2990 *C. wuellerstorfi* (brown) [*Ronge et al*., 2015], ODP Site 1240 *Cibicidoides* spp. (light blue) [*this study*] and U1342 *U. peregrina* (purple) [*Knudson and Ravelo*, 2015a].

5.3 Carbon isotopes as proxy for nutrient concentrations

Over the past decades it has been shown that the $\delta^{13}C$ signature of specific benthic foraminiferal tests is closely related to the $\delta^{13}C_{DIC}$ signature of ambient seawater [*Berger et al.,* 1978*; Duplessy et al.,* 1988]. This makes foraminiferal $\delta^{13}C$ a widely applied proxy to trace past changes in circulation and nutrient conditions in the global ocean [*Duplessy et al*., 1984; *Oppo and Fairbanks*, 1990; *Mix et al.,* 1991; *Zahn et al.,* 1991; *Keigwin*, 1998; *Stott et al*., 2000; *Matsumoto et al*., 2002a; *Curry and Oppo*, 2005; *Rickaby and Elderfield*, 2005; *Bostock et al.*, 2010; *Knudson and Ravelo*, 2015a].

In this study we compare the epibenthic *C. wuellerstorfi* and infaunal *U. peregrina* with the sub-thermocline dwelling planktonic species *G. hexagonus*. Differences in species habitat or ecology might affect the $\delta^{13}C$ interpretation. *C. wuellerstorfi* lives epibenthic or elevated above the sediment surface [*Lutze and Thiel*, 1989] and its calcitic test has been shown to reliably record

the $\delta^{13}C_{DIC}$ signal without significant fractionation of carbon isotopes [*Duplessy et al*., 1984]. The influence of seasonal depositions of phytodetritus layers might affect the $\delta^{13}C$ of benthic foraminifera [*Mackensen et al.*, 1993]. However, this influence was excluded for MD06 due to negligible glacial-interglacial changes in paleoproductivity [*Ronge et al*., 2015]. In contrast, infaunal *U. peregrina* was found to correlate with accumulation rates of organic carbon, which leads to a disequilibrium from bottom water $\delta^{13}C_{DIC}$ [*Zahn et al*., 1986]. In this study, we used the corrected *U. peregrina* values from *Knudson and Ravelo* [2015a], who converted the $\delta^{13}C_{U.peregrina}$ values to $\delta^{13}C_{C.wuellerstorfi}$ values by using a constant adjustment of +0.9 ‰. However, this offset was shown to be highly variable ranging from +1.1 ‰ during the Holocene to +0.1 ‰ during MIS 2 around New Zealand [*McCave et al*., 2008]. It was found to be even larger (+1.4 to +0.76 ‰) in a more recent study from the same area [*Elmore et al*., 2015]. Nevertheless, an adjusted correction factor would change the amplitude but not the direction of the curve. Given, that there are no studies available from the subarctic Pacific that determine the variable offset between *Cibicidoides* and *Uvigerina,* we refrained from using a variable $\delta^{13}C$ offset factor and used the correction for *U. peregrina* values given by *Knudson and Ravelo* [2015a]. For planktonic *G. hexagonus* we assume a constant calcification depth over time. Further, we do not correct $\delta^{13}C$ values of *G. hexagonus* for disequilibrium effects as the few available studies infer an only marginal carbon isotope offset to ambient $\delta^{13}C_{DIC}$ [*Birch et al*., 2013; *Rippert et al*., 2016, *this thesis*].

Intermediate and deep water masses from different end-members have a characteristic $\delta^{13}C_{DIC}$ signature (Figure 5.1b, Table 5.1), depending on the biological cycle and thermodynamically driven gas exchange between the surface ocean and the atmosphere [*Mackensen et al*., 1993; *Rohling and Cooke*, 1999; *Lisiecki*, 2010; *Mackensen*, 2012]. The latter is particularly important in the source region of intermediate waters; with each 1°C drop in temperature, the $\delta^{13}C_{DIC}$ decreases by 0.1 ‰ [*Broecker and Maier-Reimer*, 1992; *Mackensen*, 2012]. In the Southern Ocean, the glacial drop in $\delta^{13}C$ of intermediate waters is similar to the $\delta^{13}C$ drop recorded in UCDW, thus it was assumed that the thermodynamic effect influences the $\delta^{13}C$ record only insignificantly [*Ronge et al*., 2015]. In the subarctic Pacific, the modern and glacial formation of intermediate waters is linked to sea-ice formation when surface-ocean temperatures are close to the freezing point [*Rella et al*., 2012]. Given that the formation conditions are nearly congruent during glacial-interglacials, a change in the air-sea gas exchange is assumed to have an only minor effect on the $\delta^{13}C$ signal of the Bering Sea.

Nevertheless, instead of using absolute $\delta^{13}C$ values, we adopted the approach by *Knudson and Ravelo* [2015a] and used the comparisons between ODP Site 1240 with $U1342_{U.peregrina\ (corr.)}$ [*Knudson and Ravelo*, 2015a] and MD06 [*Ronge et al*., 2015] as a proxy for relative nutrient injections of northern-sourced and southern-sourced waters on equatorial sub-thermocline. Thus, as a proxy for assessing GNPIW-nutrient influence we calculate $\Delta\delta^{13}C_{NP\text{-}EQ_{G.hex}}$ ($\delta^{13}C$ at site U1342 minus $\delta^{13}C_{G.hex}$ at ODP Site 1240) and for SOIW-nutrient influence the $\Delta\delta^{13}C_{EQ_{G.hex}\text{-}SP_{SW}}$ (the $\delta^{13}C_{G.hex}$ at site ODP Site 1240 minus $\delta^{13}C$ at MD06). In the modern ocean, U1342 is located in 818 m water depth within the oxygen minimum zone, which is characterized by very low $\delta^{13}C$

values (Figure 5.1b). On the other hand, *G. hexagonus* of ODP Site 1240 is situated in ^{13}C enriched (nutrient-depleted) waters that are mainly fed from southern-sourced waters today [*Bostock et al.*, 2010]. Consequently, modern $\Delta\delta^{13}C_{NP\text{-}EQ_{G.hex}}$ values are extremely negative. If the oxygen minimum zone at site U1342 is replaced by well-ventilated GNPIW, the benthic foraminifers would bath in relatively high $\delta^{13}C_{DIC}$ signatures. If GNPIW expands its influence southward into the EEP upwelling system, the equatorial and the subarctic $\delta^{13}C$ values would approach each other. A full control of GNPIW on equatorial sub-surface water would result in a small but still positive difference ($\Delta\delta^{13}C_{NP\text{-}EQ_{G.hex}}$), allowing for the aging effect on the $\delta^{13}C$ signal. To investigate the SOIW- influence we use the same approach. In the modern ocean SOIW has relatively high $\delta^{13}C_{DIC}$ values (Figure 5.1b) and the $\delta^{13}C$ difference between equatorial sub-thermocline and SOIW is relatively small. If the injection of SOIW into the EEP upwelling system would cease, we would expect an increased difference in $\delta^{13}C$ (large $\Delta\delta^{13}C_{EQ_{G.hex}\text{-}SP_{SW}}$).

5.4 Results

Over the last 240 ka carbon isotope data from North Pacific core U1342, equatorial sub-thermocline (ODP Site 1240 *G. hexagonus*) and South Pacific record MD06 oscillate between -0.68 ‰ and +1.38 ‰ with high $\delta^{13}C$ and thus, nutrient-depleted values in the South Pacific and low $\delta^{13}C$ (nutrient-elevated) values in the North Pacific (Figure 5.3).

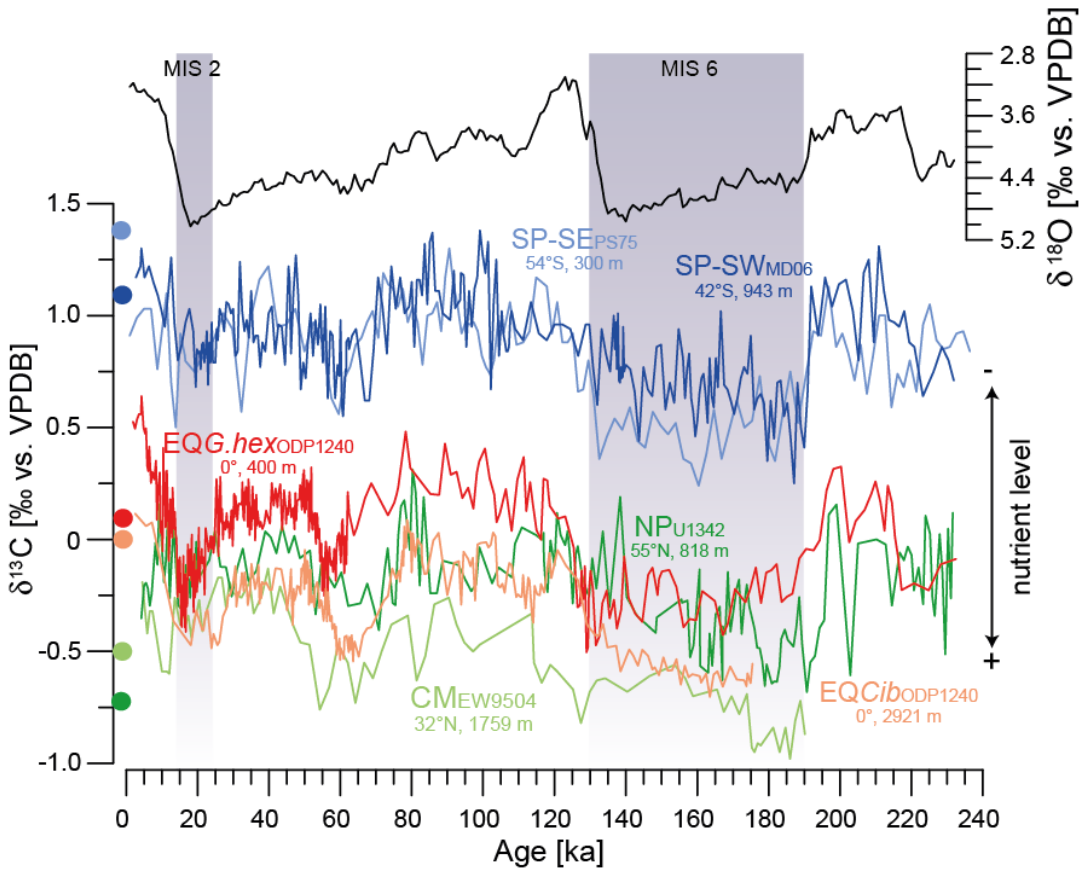

Figure 5.3. Compilation of Pacific carbon isotope records: MD06 (South Pacific) (dark blue) [*Ronge et al.*, 2015], PS75/059-2 (light blue) [*Tapia*, 2016], equatorial ODP Site 1240 *G. hexagonus* (red) and

Cibicidoides (orange) [*this study*], U1342$_{corr.}$ (North Pacific) (dark green) [*Knudson and Ravelo*, 2015a] and EW9504-04 (California margin (CM), light green) [*Stott et al.*, 2000]. Benthic $\delta^{18}O$ stack [*Lisiecki and Raymo*, 2005] is shown for stratigraphic orientation. Coloured circles denote modern $\delta^{13}C_{DIC}$ at core location. Grey bars mark glacial Marine Isotope Stages 2 and 6.

The $\delta^{13}C$ amplitude in all three records is similar (0.99 – 1.14 ‰) and do not differ significantly. In every record, glacials are characterized by lower and interglacial by higher $\delta^{13}C$ values displaying the 0.32 ‰ changes in the terrestrial biosphere and consequently storage in the deep ocean [*Gebbie et al.,* 2015] as well as additional changes in the ocean interior. Equatorial sub-thermocline $\delta^{13}C$ variations are assumed to reflect both nutrient injections and export productivity in the surface ocean of the EEP. Late Holocene equatorial sub-thermocline values largely follow South Pacific signatures and drift apart from North Pacific values (Figure 5.3). Contrary, equatorial sub-thermocline $\delta^{13}C$ values show an apparent similarity with North Pacific $\delta^{13}C$ record during glacial periods and particularly during the glacial maxima MIS 2 and MIS 6.

5.5 Discussion

The carbon isotope comparisons ($\Delta\delta^{13}C$) between the North Pacific and EEP sub-thermocline as well as between EEP sub-thermocline and the South Pacific allow us to identify relative changes in the nutrient input into equatorial sub-thermocline waters. Modern $\Delta\delta^{13}C_{EQ_{G.hex}-SP_{SW}}$ values are very negative (-1.0 ‰) albeit SOIW largely contributes to equatorial sub-thermocline waters under modern conditions [*Bostock et al*., 2010]. Contrary, modern $\Delta\delta^{13}C_{NP-EQ_{G.hex}}$ values are slightly more positive than $\Delta\delta^{13}C_{EQ_{G.hex}-SP_{SW}}$, although northern-sourced waters only subsidize minor to equatorial sub-thermocline waters today. This contrasting picture might be explained by the additional contribution of $\delta^{13}C$-depleted PDW on equatorial sub-thermocline that would decrease equatorial $\delta^{13}C$ values [*Bostock et al*., 2010]. During the past 240 ka and particularly during late MIS 2 (16 – 19 ka) and late MIS 6 (128 – 140 ka) both $\Delta\delta^{13}C$ curves show large-scale fluctuations (Figures 5.4c and d), which indicate that the source water-mass contribution might have been different in the past.

5.5.1 Reduced SOIW-nutrient contribution on equatorial sub-thermocline during peak glacials

In a first step, we investigated the relative nutrient-contribution of southern-sourced water masses on equatorial sub-thermocline, as the majority of modern equatorial waters are fed by SOIW [*Bostock et al*., 2010]. The $\delta^{13}C$ difference between the southwestern South Pacific and equatorial sub-thermocline record ($\Delta\delta^{13}C_{EQ_{G.hex}-SP_{SW}}$) increased from -1.0 ‰ under modern conditions to -1.2 ‰ during glacial maxima (Figure 5.4). This increasing $\delta^{13}C$ difference suggests that southern-sourced water masses are either more nutrient-depleted compared to today or that the

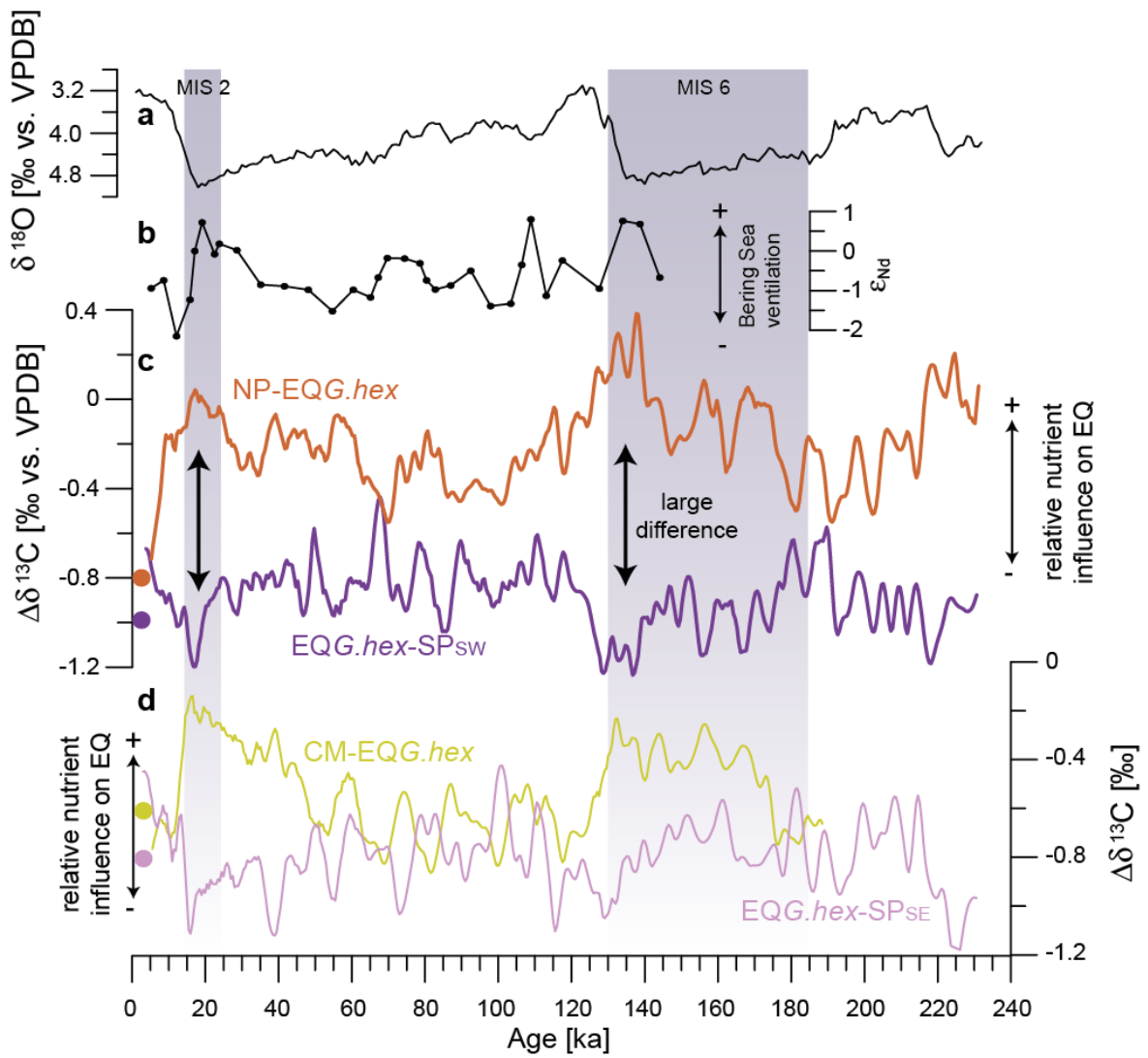

Figure 5.4. Comparison of different $\delta^{13}C$ records from the Pacific. a: Global benthic $\delta^{18}O$ stack [*Lisiecki and Raymo*, 2005] for stratigraphic reference, b: ε_{Nd} record from Bering Sea core BOW-8A [*Horikawa et al.,* 2010], c: 5pt moving average of $\delta^{13}C$ comparison between North Pacific sediment core U1342 (NP) [*Knudson and Ravelo*, 2015a] and California Margin (CM) record EW9504-04 [*Stott et al.,* 2000] minus ODP Site 1240 *G. hexagonus* values. d: 5pt moving average of $\delta^{13}C$ comparison between ODP Site 1240 *G. hexagonus* values minus southeast Pacific record PS75-59-2 (SP_{SE}) [*Tapia,* 2016] and southwest Pacific MD06 (SP_{SW}) [*Ronge et al.,* 2015]. Colored circles denote $\Delta\delta^{13}C$ values using modern water mass characteristics for the respective comparisons. Grey bars denote glacial Marine Isotope Stages 2 and 6.

nutrient-injection from SOIW derived in the southwestern Pacific into the equatorial intermediate water is reduced during peak glacials. However, different formation regions of SOIW exist in the South Pacific (Figure 5.1a) with the bulk of SOIW formed in the southeast Pacific off Chile [*Bostock et al*., 2013]. This southeast-SOIW is slightly younger and fresher than the SOIW-counterpart in the southwest Pacific [*Bostock et al*., 2013]. Higher glacial oxygen concentrations along the Chilean margin were correlated to an enhanced SOIW formation in the SE Pacific dur-

ing the Last Glacial Maximum (LGM) [*Muratil et al*. [2010]. Unfortunately, hardly any sediment cores from intermediate depths recording long-term variations in intermediate water $\delta^{13}C_{DIC}$ exist from the southeast Pacific. We therefore considered a central South Pacific $\delta^{13}C$ record from the deep-dwelling planktonic foraminifera *Globorotalia inflata* (core PS75/059–2; 54°13'S, 125°256'W, 3.613 m water depth; *Tapia* [2016]), that calcifies in 300 – 800 m water depth and thus, within SOIW (Figure 5.1c) [*Elderfield and Ganssen*, 2000; *Tapia,* 2016]. Carbon isotope values were corrected by +0.3 ‰ as *G. inflata* calcifies in disequilibrium with ambient seawater [*King and Howard*, 2004; *Shiraldi et al*., 2014]. The $\delta^{13}C$ values of PS75/059-2 (SP-SE_{PS75}) display comparable values as $\delta^{13}C_{MD06}$ (Figure 5.3). This indicates that the nutrient composition of intermediate waters from the eastern and western sector of the South Pacific is rather similar across the Pacific Sector of the Southern Ocean. Accordingly, the $\delta^{13}C$ difference of $\Delta\delta^{13}CEQ_{G.hex}$-$SP_{SE}$ shows a similar pattern as $\Delta\delta^{13}CEQ_{G.hex}$-$SP_{SW}$ (Figure 5.4d).

The $\delta^{13}C$ values of the penultimate glacial in both southeast and southwest Pacific cores are lower than the respective $\delta^{13}C$ values of MIS 2 (Figure 5.3). In the southwest Pacific, the $\Delta\delta^{13}CEQ_{G.hex}$-$SP_{SW}$ values display comparable signatures during MIS 2 and MIS 6 (Figure 5.4). In contrast, in the southeast Pacific the $\Delta\delta^{13}CEQ_{G.hex}$-$SP_{SE}$ values are offset by ~0.2 ‰ between MIS 2 and MIS 6. Only during peak MIS 2 and peak MIS 6, they display similar values. A local salinity reconstruction from the central south Pacific estimated that contrasting conditions prevailed in the Southern Ocean between MIS 2 and MIS 6 with water masses saltier than during the Holocene during MIS 6 and contrasting fresher-than-Holocene conditions during MIS 2 [*Tapia et al*., 2015]. To what extent this might influence the nutrient concentration between the southeast and southwest Pacific Ocean remains elusive as information regarding major nutrient cycles are missing during MIS 6. Nevertheless, the last peak glacial and the penultimate glacial shows an increased difference between equatorial sub-thermocline waters and SOIW waters compared to modern values.

Our analyses point to a reduced southern nutrient-contribution on equatorial sub-thermocline during high glacials. This notion is supported by $\delta^{13}C$ studies from New Zealand, that highlight a shoaling of the SOIW/UCDW boundary from ~2000 m to ~1100 m water depth [*Elmore et al*., 2015; *Ronge et al*., 2015]. This shoaling possibly reflect a reduced production of SOIW due to increased freshwater flux by melting sea ice in the formation area of SOIW [*Pahnke and Zahn*, 2005; *Ronge et al*., 2015]. Further support comes from nutrient studies in the Southern Ocean that found increased opal accumulation rates in the Subantarctic Zone (SAZ) during glacials, which was explained by an increased upwelling due to enhanced wind stress in the SAZ and thus, a higher supply of nutrients to the euphotic zone [*Hendy and Brzezinski*, 2014; *Robinson et al*., 2014]. As a consequence, the nutrient-concentration of SOIW decreased during glacials. Thus, it seems questionable whether nutrient-depleted SOIW was able to stronger enhance productivity at the equator during late MIS 2 and late MIS 6 as suggested by proxies indicative of changes in biological productivity. Opal flux and productivity reconstructions in the EEP infer a

greater nutrient contribution during glacials [e.g. *Dugdale et al.*, 2004; *Loubere et al.*, 2003, 2007; *Calvo et al.*, 2011; *Loubere et al.*, 2011], which suggest that sub-thermocline waters in the EEP experienced substantial changes in its chemistry. Thus, the largest $\delta^{13}C$ difference between the EEP and Southern Ocean $\delta^{13}C$ values argues for a relative reduced contribution of nutrient-depleted southern-sourced waters on equatorial sub-thermocline during extreme glacials (Figure 5.5).

5.5.2 Northern-sourced nutrient influence on EqPIW during peak glacials

Here we consider two possible sourced from the North Pacific, PDW and NPIW. The change in $\delta^{13}C_{G.hexagonus}$ values during the peak glacials might be explained by an enhanced upwelling of PDW at the equator. A recent ε_{Nd} data comparison between LGM and Holocene values reveals substantial reduced glacial ε_{Nd} values in the EEP, which was explained by a more invigorated deep circulation and higher contribution from deep northern-sourced waters [*Hu et al.*, 2016]. Sediment core ODP Site 1240 was retrieved from ~2900 m water depth and thus, the benthic $\delta^{13}C$ of ODP Site 1240 reports variability in PDW waters (Figure 5.1). The comparison between the *G. hexagonus* record and the benthic record of ODP Site 1240 yields an offset of ~0.2 ‰ during late MIS 2 and MIS 6, when the $\delta^{13}C$ differences between the equatorial sub-thermocline and the Southern Ocean is greatest (Figure 5.3). The $\delta^{13}C_{G.hexagonus}$ and $\delta^{13}C_{Cibicidoides}$ values approach each other only during the Termination I and II. They indicate even similar values during Termination II (126 – 132 ka) after the maximum $\delta^{13}C$ difference between the EqPIW and SOIW occurred (Figures 5.3 and 5.4). Thus, we argue that the glacial PDW contribution into the sub-thermocline might not have changed substantially from today's (Figure 5.5). Only during the deglaciation, the contribution from deep water masses on the equatorial sub-thermocline might have been enhanced. This notion is supported by a recent $\delta^{13}C$ comparison between EqPIW and PDW during the past 60 ka, which indicates a substantially different temporal evolution in $\delta^{13}C$ values of EqPIW and PDW during MIS 2 [*Max et al.*, under review, *this thesis*]. Furthermore, recent analyses of radiocarbon activity show maximal benthic ^{14}C offsets to atmospheric values during the LGM [*Skinner et al.*, 2010; *de la Fuente et al.*, 2015; *Skinner et al.*, 2015; *Ronge et al.*, 2016]. At 15 ka, within the termination when both our determined $\delta^{13}C_{EQ_{G.hex}-SP}$ offsets decrease (Figure 5.3), the old glacial carbon pool between 2000 – 4300 m was eroded [*Ronge et al.*, 2016]. The decreasing ventilation ages were explained by the deglacial breakdown of the Southern Ocean stratification in relation to enhanced Southern Ocean upwelling [*Ronge et al.*, 2016]. Also within the EEP, a ventilation age reconstruction from ODP Site 1240 estimated that the largest benthic-planktonic ^{14}C offset (B-P) occurred during peak MIS 2, which decreased to modern values from 15 ka onward [*de la Fuente et al.*, 2015]. These combined evidences argue against a higher PDW contribution to EEP sub-thermocline waters during peak glacials and rather suggests a more invigorated role of northern-sourced intermediate waters.

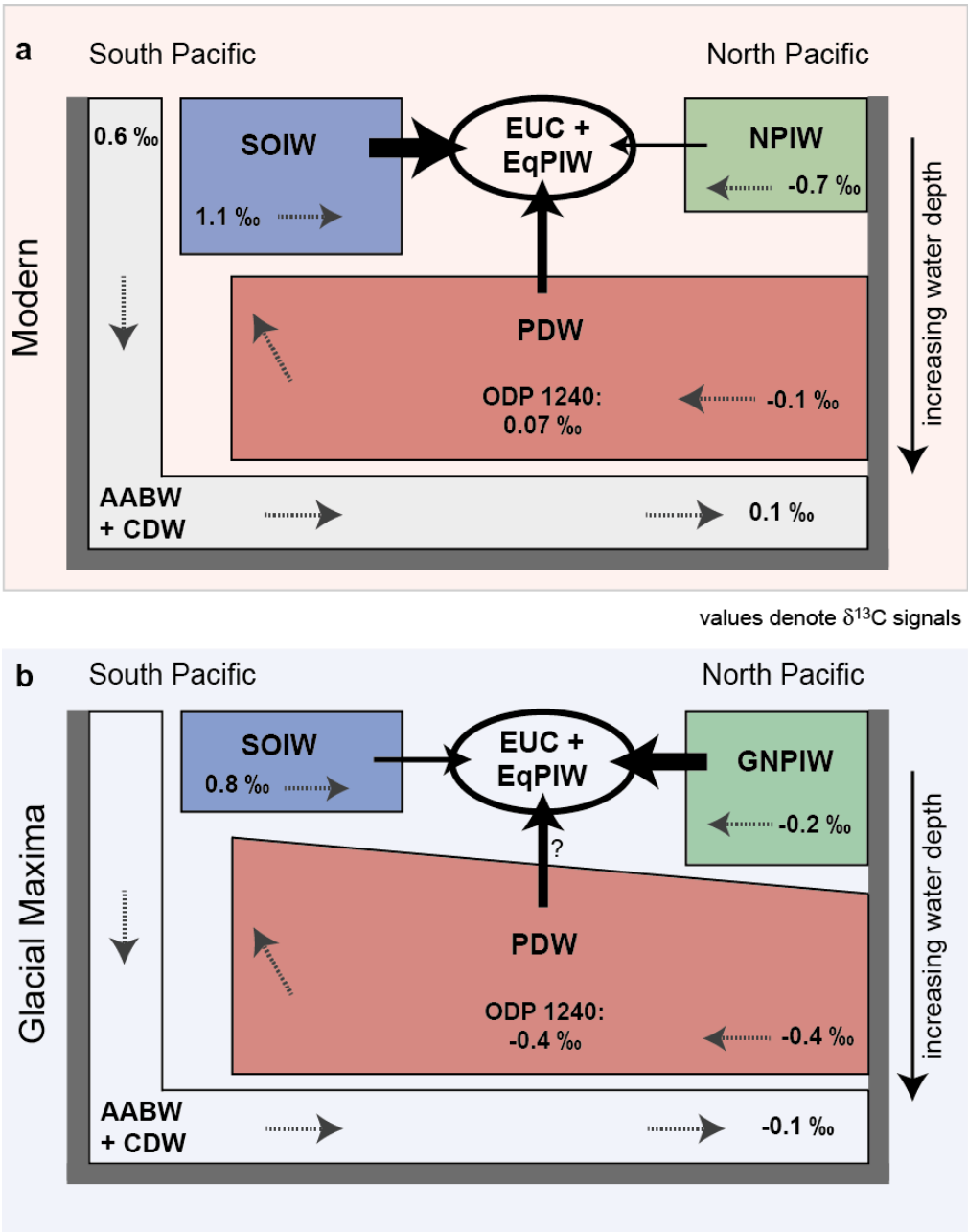

Figure 5.5. Schematic illustration of changing end-member contributions on EEP upwelling waters during a: interstadials and b: glacial maxima. EUC + EqPIW = Equatorial Undercurrent + Equatorial Pacific Intermediate Water, SOIW = Southern Ocean Intermediate Water, (G)NPIW = (Glacial) North Pacific Intermediate Water, PDW = Pacific Deep Water, CDW + AABW = Antarctic Bottom Water + Circumpolar Deep Water. Black arrows represent possible contributions of end-members and dashed arrows show current flow. Given values represent $\delta^{13}C$ values that were determined using data from GLODAP [*Key et al*., 2004], *Peterson et al*. [2014], and from sediment cores analyzed in this study.

In a next step, we compared the $\delta^{13}C$ sub-thermocline values to a record from the Bering Sea (U1342) to investigate a possible contribution of GNPIW. Our $\delta^{13}C$ comparison reveals that the difference between the Bering Sea and EEP $\delta^{13}C$ values ($\Delta\delta^{13}C_{NP\text{-}EQ_{G.hex}}$) diminishes substantially during glacials and both $\delta^{13}C$ records approach similar values during late MIS 2 and late

MIS 6. Most interestingly, the smallest offset between $\delta^{13}C_{NP}$ and $\delta^{13}CEQ_{G.hex}$ values happen simultaneously to the largest offset between $\delta^{13}CEQ_{G.hex}$ and $\delta^{13}C_{SP}$ signatures (Figure 5.4). This might indicate a relatively higher GNPIW contribution than today on the equatorial $\delta^{13}C$. Given that GNPIW evinces slightly higher $\delta^{13}CEQ_{G.hex}$ values, the $\Delta\delta^{13}CNP\text{-}EQ_{G.hex}$ are slightly positive during glacial maxima. Similar to the increased $\Delta\delta^{13}CNP\text{-}EQ_{G.hex}$ from Bering Sea core U1342 during extreme glacials, a recent high-resolution $\delta^{13}C$ comparison between western Bering Sea (Shirshov Ridge) core SO201-2-101KL and ODP Site 1240 *G. hexagonus* over the past 60 ka [*Max et al.,* under review, *this thesis*] indicates a close resemblance of sub-thermocline waters to North Pacific waters during MIS 2.

Rella et al. [2012] argue that the formation of GNPIW was initiated in the Bering Sea by the closure of the Bering Strait and an easternmost position of the Aleutian Low. This pooled relatively fresh water within the Bering Sea and fostered a strengthened pycnocline [*Riethdorf et al.*, 2016]. The newly formed intermediate water with high oxygen content and low salinities was present in the subarctic Pacific from ~60 ka until the beginning of Termination I [*Schlung et al*., 2013]. Further support comes from a ε_{Nd} study indicating that intermediate waters from the Bering Sea were a principle component of GNPIW during MIS 2 and MIS 6 [*Horikawa et al*., 2010] and seems to be a reoccurring feature during the past 1.2 Ma [*Knudson and Ravelo*, 2015a]. The enhances stratification prevented upwelling of nutrients from below and as a consequence, isolated the available nitrate at the surface [*Knudson and Ravelo*, 2015b; *Riethdorf et al*., 2016]. High nitrogen isotopes indicate an enhanced nutrient utilization in the Bering Sea during MIS 2 and MIS 6 [*Galbraith et al.*, 2008; *Brunelle et al*., 2010; *Knudson and Ravelo*, 2015b; *Riethdorf et al*., 2016]. However, it was reported that productivity and export production remained low during glacial maxima [*Kienast et al*., 2004; *Jaccard et al*., 2005; *Gebhardt et al*., 2008; *Brunelle et al*., 2010; *Kim et al*., 2011]. The combined evidence for an increased GNPIW formation but reduced primary productivity in the subarctic Pacific and a decreased $\delta^{13}C$ difference between the Bering Sea core and EEP sub-thermocline argues for an enhanced nutrient-injection of GNPIW into equatorial sub-thermocline waters during peak glacials. This nutrient-injection was higher than today. Thereby it confirms a previous $\delta^{13}C$ compilation, which postulates increased North Pacific mid-depth circulation that expands southward and eastward between 700 – 2600 m water depth in the subarctic Pacific [*Matsumoto et al*., 2002a].

The penultimate glacial maximum (MIS 6) shows larger $\Delta\delta^{13}CNP\text{-}EQ_{G.hex}$ values than MIS 2 (Figure 5.4), which suggests an even higher nutrient-contribution from northern-sourced waters into the equatorial upwelling waters. A model simulation investigates the extension of past glaciations and found colder MIS 6 conditions with an extensive Eurasian ice sheet compared to MIS 2 [*Colleoni et al*., 2016]. Furthermore, in the Sea of Okhotsk ice-rafted debris accumulation was 2 – 3 times higher due to extensive mountain glaciers during MIS 6 compared to the LGM [*Nürnberg et al*., 2011]. Together with the change from seasonal to still mobile perennial sea ice cover [*Nürnberg et al*., 2011], GNPIW formation could have been further intensified during MIS 6. As persistent stratification and nearly complete surface nutrient utilization prevailed during that time

[*Riethdorf et al*., 2016], the nutrient-injection into equatorial sub-thermocline waters might have been enhanced and possibly explains the larger $\Delta\delta^{13}C_{NP\text{-}EQ_{G.hex}}$ during MIS 6 compared to MIS 2.

An expanded GNPIW circulation could also explain the increased ventilation along the California margin during MIS 6 as well as MIS 3 and MIS 2 [*Stott et al*., 2000]. Therefore, we compared ODP Site 1240 and EW9504-04 (32°17'N, 118°24'W, 1759 m water depth, 1400 sill depth) (Figure 5.1) [*Stott et al*., 2000] to investigate possible $\delta^{13}C$ modifications along the flow path of GNPIW. The carbon isotope comparison between EW9504-04 and ODP Site 1240 ($\Delta\delta^{13}C_{CM\text{-}EQ_{G.hex}}$) yields a similar pattern as $\Delta\delta^{13}C_{NP\text{-}EQ_{G.hex}}$ with small differences during glacials and high differences during past interglacials due to very low $\delta^{13}C$ values at the Californian margin (Figure 5.4d). The amplitude of $\Delta\delta^{13}C_{CM\text{-}EQ_{G.hex}}$ is less pronounced compared to the $\Delta\delta^{13}C_{NP\text{-}EQ_{G.hex}}$ record, possibly because regional circumstances such as sill depths and local productivity along the California margin modify the $\delta^{13}C$ of EW9504-04 slightly [*Stott et al*., 2000]. Nevertheless, these regional differences do not influence the general pattern, as $\delta^{13}C$ comparisons between $\delta^{13}C_{G.hexagonus}$ of ODP Site 1240 and benthic $\delta^{13}C$ records cores from additional sediment cores of the California margin (ODP Site 1012, *Andreasen et al.* [2000] and ODP Site 1014, *Hendy and Kennet* [2000], here termed CM_{add}, both not shown) indicate a very similar pattern as $\Delta\delta^{13}C_{CM\text{-}EQ_{G.hex}}$ with higher $\Delta\delta^{13}C_{CM_{add}\text{-}EQ_{G.hex}}$ values during glacial maxima and lower $\Delta\delta^{13}C_{CM_{add}\text{-}EQ_{G.hex}}$ values during interglacials. It thereby supports an earlier Pacific carbon isotope study that found a relatively larger contribution of well-oxygenated (ventilated) waters between 1000 – 2600 m water depth originating in the North Pacific [*Duplessy et al*., 1988]. A more recent stable isotope analyses off the Baja California margin by *Herguera et al*. [2010] concluded that the observed $\delta^{13}C$-enriched intermediate waters are the result of a changed thermohaline circulation with a possibly enhanced GNPIW formation mode. Further south in the ETNP, a carbon isotope study by *Leduc et al.* [2010] proposed that GNPIW spreads at least till 8°N during the last glacial. Hence, it seems as if the enhanced ventilated GNPIW is progressively expanding southward, and thereby reaches the California margin and ETNP at the start of the glaciations. During glacial maxima, the volume of GNPIW expanded even further south reaching the equatorial sub-thermocline waters (Figure 5.5). Thereby, it possibly also changed the chemistry of the equatorial sub-thermocline waters, which is consistent with findings of *Loubere et al*. [2003, 2011], and *Max et al.* [under review, *this thesis*].

Our $\delta^{13}C$ comparisons together with previously published results show that large-scale reorganization in the formation area of GNPIW and SOIW took place during glacial stages that amplified during glacial maxima. In the western equatorial Pacific, these high latitude intermediate waters are incorporated into the equatorial current system. Thus, glacial/interglacial changes in this area affect the relative contribution of extra-tropical intermediate waters within the EqPIW as well. An idealized layer modeling shows that with the reduction of the Indonesian Throughflow during glacial conditions the proportion of GNPIW that was deflected into the tropical EqPIW increased [*McCreary and Lu*, 2001] and thus reaches the EEP sub-thermocline during glacial maxima. Fur-

thermore, under modern conditions the NECC, which in turn also feeds the EUC, is fed from both hemispheres (see *Chapter 5.1.2*). Only during the Northwest Monsoon, the SEC is prevented from injecting into the NECC, and thus, the NECC is only fed from the north [*Tomczak and Godfrey*, 2005]. A hydrogen isotope record together with regional modeling reconstructed a southward position of the mean Intertropical Convergence Zone (ITCZ) and an intensification of Northeast trade winds during the last glacial [*Pahnke et al*., 2007]. The glacial southward shift of the ITCZ is further verified by nitrogen isotopes and organic carbon records [*Dubois and Kienast*, 2011], biomarker analysis [*Shaari et al.*, 2013], and by nannofossil assemblages [*Staines-Urías et al*., 2015]. The resulting stronger northeast trades might have reduced the northward penetration and contribution of SOIW to the NECC and possibly also the EqPIW. Thereby, it provides a possible scenario for our proposed relatively enhanced contribution of northern-sourced waters on the equatorial Pacific sub-thermocline during late MIS 2 and late MIS 6.

5.5.3 Deglacial and interglacial change in EEP nutrient-concentration

The $\delta^{13}C$ comparisons between high latitude and EEP upwelling waters yield rapid changes within the Termination I and II. The $\delta^{13}C$ difference between the Bering Sea and ODP Site 1240 increases towards modern values (Figure 5.4), which suggests decreasing nutrient-injections from northern-sourced intermediate waters into EqPIW. The GNPIW retreat is supported by the deposits of laminated sediments around the subarctic Pacific that indicates less well ventilated intermediate waters and the expansion of the oxygen minimum zone in the subarctic Pacific [*Kuehn et al.,* 2014]. The increasing temperatures and the opening of the Bering Strait triggered a change in productivity [*Riethdorf et al*., 2016]. Low nitrogen isotopes indicate enhanced productivity that was explained by a change towards seasonal sea ice, decreased upper ocean stratification and subsequent enhanced nutrient supply to the euphotic zone by mixing and renewed riverine input [*Gebhardt et al.*, 2008; *Knudson and Ravelo*, 2015b; *Riethdorf et al*., 2016]. Consequently, the increasing $\delta^{13}C$ difference between the Bering Sea and the EEP during warm periods suggests that northern-sourced intermediate water masses were depleted in nutrients during interglacials compared to glacials and more confined to the modern extent.

On the other hand, the both $\Delta\delta^{13}C_{EQ_{G.hex}-SP}$ records show increasing values from the glacial maxima towards the interglacials. This argues for an intensified southern-sourced nutrient-injection into the equatorial sub-thermocline. Silicon isotopes from the Southern Ocean indicate elevated $Si(OH)_4$ concentrations at mode and intermediate depths in the SAZ [*Rousseau et al*., 2016]. The excess dissolved silicon is then transported equatorwards as described by the SALH [*Hendry and Brzezinski*, 2014]. *Loubere et al.* [2003, 2007] found that the re-establishment of deep EUC waters with a mainly southern-sourced water mass occurred roughly at 18 ka. This is in harmony with a stable isotope study from the EEP showing an increased inflow of SOIW at the onset of the terminations [*Pena et al.*, 2008; 2013; *Bova et al*., 2015]. The intensified SOIW ventilation expanded further north into the ETNP, where $\delta^{13}C$ records and ε_{Nd} signatures show compa-

rable values to southern Ocean signatures within the deglaciation [*Leduc et al.*, 2010; *Basak et al.*, 2010].

5.6 Conclusions

This study investigates the varying influence of extra-tropical intermediate waters on EEP sub-thermocline. The carbon isotope comparisons indicate decreasing $\Delta\delta^{13}C$ ratios between the Equatorial sub-thermocline and the Southern Ocean records during peak glacials, which imply a diminishing relative nutrient influence from SOIW. On the other hand, the $\delta^{13}C$ comparisons between EEP sub-thermocline record and sediment cores within the pathway of GNPIW indicate minor $\delta^{13}C$ differences between the regions during peak glacials. This argues for enhanced GNPIW ventilation and subsequently relative enhanced nutrient contribution on equatorial sub-thermocline waters during late MIS 2 and late MIS 6.

The signal of relative increasing GNPIW influence on equatorial sub-thermocline would have large effects on biological productivity, as GNPIW is nutrient elevated compared to SOIW. Given that the modern EEP acts as one of the biggest CO_2 source on Earth today, past changes in the biological pump of the equatorial Pacific might have affected the balance between oceanic and atmospheric CO_2 concentrations. There is growing debate, whether the EEP turned into a sink for atmospheric CO_2 during at least the last glacial [*Sanyal and Bijma*, 1999; *Martínez-Botí et al.*, 2015]. The expansion of nutrient-rich GNPIW might be another piece of the puzzle to further understand atmospheric CO_2 variations during the Pleistocene and in particular during peak glacial periods.

Acknowledgments and Data

This research used samples provided by the Ocean Drilling Program (ODP). ODP is sponsored by the U.S. National Science Foundation (NSF) and participating countries under the management of Joint Oceanographic Institutions (JOI), Inc. We are grateful to L. Schönborn and G. Meyer for conducting stable isotope measurements at the AWI stable isotope lab. NR was funded by the German Ministry for Education and Research (BMBF – Bundesministerium für Bildung und Forschung) in the framework of the joint project Manihiki II (03G0225B). LM received funding through the Helmholtz Climate Initiative REKLIM (Regional climate change). The data of this study are available at PANGEA (URL: http://www.pangaea.de).

5.7 Supplementary data

To:

Rippert, N., Max L., Mackensen, A., Cacho, I., Povea, P., Tiedemann, R., Alternating influence of northern versus southern-sourced water masses on the equatorial Pacific sub-thermocline during the past 240 ka. *In preparation* for Paleoceanography.

Table S5.7.1. Age control points for analysed sediment cores.

ODP Site 1240			SO136-003/MD06-2990		
Core depth (m.c.d.)	Age (ky)	Pointer Type	Core depth (m)	Age (ky)	Pointer Type
0.01	1.91	14C Marine04[1]	0.03	3.35	14C Marine04[2]
0.25	5.27	14C Marine04[1]	0.07	4.50	14C Marine04[2]
0.77	8.9	14C Marine04[1]	0.15	9.48	14C Marine04[2]
1.17	10.54	14C Marine04[1]	0.25	13.93	14C Marine04[2]
1.38	12.79	14C Marine04[1]	0.35	19.33	14C Marine04[2]
1.51	13.32	14C Marine04[1]	0.73	25.85	14C Marine04[2]
1.75	14.6	14C Marine04[1]	1.13	38.46	Cib $\delta^{18}O$ vs LR04
2.23	17.22	14C Marine04[1]	1.28	45.64	Cib $\delta^{18}O$ vs LR04
2.31	17.33	14C Marine04[1]	1.69	59.48	Cib $\delta^{18}O$ vs LR04
2.63	19.41	14C Marine04[1]	1.13	38.46	Cib $\delta^{18}O$ vs LR04
2.91	20.88	14C Marine04[1]	1.28	45.64	Cib $\delta^{18}O$ vs LR04
3.18	22.26	14C Marine04[1]	1.69	59.48	Cib $\delta^{18}O$ vs LR04
3.5	26.65	14C Fairbanks05[1]	1.81	61.62	Cib $\delta^{18}O$ vs LR04
3.62	28.03	14C Fairbanks05[1]	2.98	62.27	Cib $\delta^{18}O$ vs LR04
4.42	33.19	14C Fairbanks05[1]	3.01	63.55	Cib $\delta^{18}O$ vs LR04
4.86	36.98	14C Fairbanks05[1]	3.26	79.34	Cib $\delta^{18}O$ vs LR04
5.16	38.17	14C Fairbanks05[1]	3.46	86.42	Cib $\delta^{18}O$ vs LR04
5.65	44.63	Cib $\delta^{18}O$ vs LR04	3.59	93.40	Cib $\delta^{18}O$ vs LR04
6.43	49.32	Cib $\delta^{18}O$ vs LR04	3.91	105.56	Cib $\delta^{18}O$ vs LR04
7.59	52.72	Cib $\delta^{18}O$ vs LR04	4.05	108.22	Cib $\delta^{18}O$ vs LR04
9.81	64.00	Cib $\delta^{18}O$ vs LR04	4.24	128.65	Cib $\delta^{18}O$ vs LR04
10.21	75.64	Cib $\delta^{18}O$ vs LR04	4.28	130.63	Cib $\delta^{18}O$ vs LR04
10.91	80.20	Cib $\delta^{18}O$ vs LR04	4.38	136.56	Cib $\delta^{18}O$ vs LR04
11.39	87.95	Cib d18O vs LR04	4.60	139.76	Cib $\delta^{18}O$ vs LR04
12.72	109.57	Cib d18O vs LR04	4.86	156.01	Cib $\delta^{18}O$ vs LR04
13.74	118.74	Cib $\delta^{18}O$ vs LR04	5.21	165.94	Cib $\delta^{18}O$ vs LR04
14.09	126.24	Cib $\delta^{18}O$ vs LR04	5.62	185.33	Cib $\delta^{18}O$ vs LR04
14.89	130.79	Cib $\delta^{18}O$ vs LR04	5.76	191.84	Cib $\delta^{18}O$ vs LR04
17.35	155.79	G.hex $\delta^{18}O$ vs LR04	5.89	204.31	Cib $\delta^{18}O$ vs LR04
18.53	166.23	Cib $\delta^{18}O$ vs LR04	6.13	221.39	Cib $\delta^{18}O$ vs LR04
18.94	173.24	*G.hex* $\delta^{18}O$ vs LR04	6.17	227.48	Cib $\delta^{18}O$ vs LR04
20.63	185.53	*G.hex* $\delta^{18}O$ vs LR04	6.21	231.52	Cib $\delta^{18}O$ vs LR04
22.02	198.82	*G.hex* $\delta^{18}O$ vs LR04	6.45	242.92	Cib $\delta^{18}O$ vs LR04
22.86	208.38	*G.ruber* $\delta^{18}O$ vs LR04	6.66	251.62	Cib $\delta^{18}O$ vs LR04
24.44	217.52	*G.ruber* $\delta^{18}O$ vs LR04	7.09	268.35	Cib $\delta^{18}O$ vs LR04
24.92	227.40	*G.ruber* $\delta^{18}O$ vs LR04	7.35	281.91	Cib $\delta^{18}O$ vs LR04
27.08	250.54	*G.ruber* $\delta^{18}O$ vs LR04	7.58	291.43	Cib $\delta^{18}O$ vs LR04
27.75	270.39	*G.ruber* $\delta^{18}O$ vs LR04	8.15	303.82	Cib $\delta^{18}O$ vs LR04
28.64	291.11	*G.ruber* $\delta^{18}O$ vs LR04	8.31	307.69	Cib $\delta^{18}O$ vs LR04
29.39	299.34	*G.ruber* $\delta^{18}O$ vs LR04	8.51	316.58	Cib $\delta^{18}O$ vs LR04
25.71	235.83	Ash layer	8.65	318.69	Cib $\delta^{18}O$ vs LR04
			9.00	339.06	Cib $\delta^{18}O$ vs LR04
			9.24	346.93	Cib $\delta^{18}O$ vs LR04

U1342					
Core depth (CCSF-A)	Age (ky)	Pointer type	Core depth (CCSF-A)	Age (ky)	Pointer type
0.3	12.33	Uvi (corr to cib) $\delta^{18}O$ vs LR04	21.44	639.45	Uvi (corr to cib) $\delta^{18}O$ vs LR04
0.49	17.49	Uvi (corr to cib) $\delta^{18}O$ vs LR04	22.1	689.37	Uvi (corr to cib) $\delta^{18}O$ vs LR04
0.94	20.28	Uvi (corr to cib) $\delta^{18}O$ vs LR04	22.34	700.94	Uvi (corr to cib) $\delta^{18}O$ vs LR04
2.1	56.74	Uvi (corr to cib) $\delta^{18}O$ vs LR04	22.66	727.15	Uvi (corr to cib) $\delta^{18}O$ vs LR04
2.46	70.41	Uvi (corr to cib) $\delta^{18}O$ vs LR04	23.6	745.43	Uvi (corr to cib) $\delta^{18}O$ vs LR04
3.12	80.69	Uvi (corr to cib) $\delta^{18}O$ vs LR04	26.19	793.12	Uvi (corr to cib) $\delta^{18}O$ vs LR04
3.29	87.1	Uvi (corr to cib) $\delta^{18}O$ vs LR04	26.87	817.53	Uvi (corr to cib) $\delta^{18}O$ vs LR04
3.49	93.2	Uvi (corr to cib) $\delta^{18}O$ vs LR04	27.86	849.57	Uvi (corr to cib) $\delta^{18}O$ vs LR04
3.76	105.45	Uvi (corr to cib) $\delta^{18}O$ vs LR04	28.47	866.26	Uvi (corr to cib) $\delta^{18}O$ vs LR04
3.94	109.3	Uvi (corr to cib) $\delta^{18}O$ vs LR04	28.9	892.7	Uvi (corr to cib) $\delta^{18}O$ vs LR04
3.99	115.24	Uvi (corr to cib) $\delta^{18}O$ vs LR04	29.07	909.96	Uvi (corr to cib) $\delta^{18}O$ vs LR04
4.8	126.78	Uvi (corr to cib) $\delta^{18}O$ vs LR04	29.36	917.25	Uvi (corr to cib) $\delta^{18}O$ vs LR04
5.05	131.07	Uvi (corr to cib) $\delta^{18}O$ vs LR04	30.19	955.99	Uvi (corr to cib) $\delta^{18}O$ vs LR04
5.17	134.73	Uvi (corr to cib) $\delta^{18}O$ vs LR04	30.92	973.72	Uvi (corr to cib) $\delta^{18}O$ vs LR04
5.27	140.59	Uvi (corr to cib) $\delta^{18}O$ vs LR04	31.24	993.19	Uvi (corr to cib) $\delta^{18}O$ vs LR04
5.41	155.43	Uvi (corr to cib) $\delta^{18}O$ vs LR04	31.41	1014.92	Uvi (corr to cib) $\delta^{18}O$ vs LR04
5.6	165.97	Uvi (corr to cib) $\delta^{18}O$ vs LR04	31.59	1021.77	Uvi (corr to cib) $\delta^{18}O$ vs LR04
6.35	184.09	Uvi (corr to cib) $\delta^{18}O$ vs LR04	31.68	1032.05	Uvi (corr to cib) $\delta^{18}O$ vs LR04
6.62	191.25	Uvi (corr to cib) $\delta^{18}O$ vs LR04	35.02	1133.3	Uvi (corr to cib) $\delta^{18}O$ vs LR04
7.22	217.41	Uvi (corr to cib) $\delta^{18}O$ vs LR04	35.23	1147.62	Uvi (corr to cib) $\delta^{18}O$ vs LR04
7.69	227.48	Uvi (corr to cib) $\delta^{18}O$ vs LR04	36.12	1206.8	Uvi (corr to cib) $\delta^{18}O$ vs LR04
7.9	233.05	Uvi (corr to cib) $\delta^{18}O$ vs LR04	36.45	1216.01	Uvi (corr to cib) $\delta^{18}O$ vs LR04
8.53	240.34	Uvi (corr to cib) $\delta^{18}O$ vs LR04	39.24	1257.17	Uvi (corr to cib) $\delta^{18}O$ vs LR04
8.69	249.8	Uvi (corr to cib) $\delta^{18}O$ vs LR04			
8.98	255.81	Uvi (corr to cib) $\delta^{18}O$ vs LR04			
10.53	282.62	Uvi (corr to cib) $\delta^{18}O$ vs LR04			
11.27	299.64	Uvi (corr to cib) $\delta^{18}O$ vs LR04			
12.41	328.83	Uvi (corr to cib) $\delta^{18}O$ vs LR04			
14.53	396.69	Uvi (corr to cib) $\delta^{18}O$ vs LR04			
15.39	410	Uvi (corr to cib) $\delta^{18}O$ vs LR04			
15.72	433.2	Uvi (corr to cib) $\delta^{18}O$ vs LR04			
16.37	455.49	Uvi (corr to cib) $\delta^{18}O$ vs LR04			
17.92	489.11	Uvi (corr to cib) $\delta^{18}O$ vs LR04			
19.64	548.68	Uvi (corr to cib) $\delta^{18}O$ vs LR04			
20.27	576.81	Uvi (corr to cib) $\delta^{18}O$ vs LR04			
20.3	582.25	Uvi (corr to cib) $\delta^{18}O$ vs LR04			
20.9	597.65	Uvi (corr to cib) $\delta^{18}O$ vs LR04			

6. Conclusion and Outlook

6.1 Conclusion

The overall aim of this thesis was to investigate long-term variations in the upper ocean nutrient circulation in the Pacific Ocean. The emphasis of this work was the equatorial Pacific sub-thermocline and its relationship to increased intermediate water ventilation in the North Pacific. The assessment of precise regional foraminiferal ACDs is another important aspect of this thesis, as planktonic foraminifera generally serve as a tool to reconstruct past upper-ocean conditions. For this purpose, multiple different proxies were applied including the measurements of physical and chemical water properties, Mg/Ca ratios of planktonic foraminifera and benthic and planktonic $\delta^{18}O$ and $\delta^{13}C$ values, as well as the determination of foraminiferal abundances. The obtained results of this thesis together with relevant published records from the Pacific, archives profound outcomes concerning the raised research questions that given in C*hapter 1.5*.

The comparison between in-situ physical and chemical water mass properties with $\delta^{18}O_{calcite}$ values and Mg/Ca-derived temperatures measured on five living planktonic foraminifera species enabled species-specific ACDs and $\delta^{13}C$-disequilibrium in the WPWP to be obtained (*Chapter 3*). It was shown that the relative order of *G. ruber* as the shallowest dweller, followed by *G. sacculifer*, *N. dutertrei*, *P. obliquiloculata* and *G. hexagonus* inhabiting increasingly greater depths, is similar to other ocean basins. However, the relatively deep SML in the WPWP during the period of sampling (reaching a maximum depth of ~130 m) resulted in the ACD of *G. ruber* and *G. sacculifer* of ~95 m and ~120 m respectively, which is deeper than in other ocean basins. As vital effects further affect symbiont-bearing species, a combined approach of foraminiferal abundances, local hydrography and determined ACDs provides the most reliable ACD reconstructions for these SML dwellers. At the top of and within the thermocline in the WPWP, both *N. dutertrei* and *P. obliquiloculata* calcify in water depths of ~140 m and ~160 m, respectively. We found that for the reconstruction of thermocline conditions, *P. obliquiloculata* seems to be most promising at the Manihiki Plateau. Most significantly, the ACD assessment reveals that *G. hexagonus* prefers to calcify in cooler, more oxygen-depleted and nutrient-rich sub-thermocline water masses at ~450 m. This species seems to have only negligible $\delta^{13}C$-disequilibrium with ambient seawater and thus, *G. hexagonus* was found to be most suitable for reconstructing the long-term variability in extra-tropical nutrient injections into the equatorial current system.

Furthermore, GNPIW ventilation and the variable influence of northern-sourced versus southern-sourced water masses in the eastern tropical Pacific was reconstructed using the newly generated benthic foraminiferal $\delta^{13}C$ data from the Bering Sea and the new sub-thermocline $\delta^{13}C$ record from the EEP (*Chapter 4 and 5*). An increased formation of GNPIW was observed since the onset of MIS 3 by combining $\delta^{13}C$ records and ε_{Nd} evidence from the Bering Sea. The resemblance between our Bering Sea sediment core (SO201-2-101KL) and a previously published benthic $\delta^{13}C$ record from the Panama Basin (MD02-2529) suggests a southward expansion of GNPIW into the tropical North Pacific during glacial boundary conditions (*Chapter 4*). This finding is supported by a ε_{Nd} comparison between the Bering Sea and the eastern North Pacific, which indicates that the enhanced GNPIW ventilation during glacials reached Baja California. The southward penetration of GNPIW culminated early in MIS 2 (~29 ka). During that time $\delta^{13}C$ measured on deep-dwelling planktonic species *G. hexagonus* at ODP Site 1240 reveals remarkable similarities with SO201-2-201 KL. These similarities are accompanied by changes in marine productivity and nutrient utilization in the EEP. This likely suggests nutrient leakage from northern-sourced waters on equatorial Pacific sub-thermocline water masses during MIS 2.

So far, environmental changes within the EEP have only been correlated to SOIW due to the large contribution of southern-sourced water masses on EqPIW today. To investigate long-term changes spanning more than one glacial cycle, we compared the sub-thermocline $\delta^{13}C$ record of ODP Site 1240 to records from the Bering Sea (U1342), the eastern North Pacific (EW9504-04), the southwest Pacific (SO136-003/MD06-2990) and the southeast Pacific (PS75/059-2) (*Chapter 5*). The comparison of carbon isotope records indicates that $\delta^{13}C$ values between the North Pacific and the equatorial sub-thermocline are nearly identical during peak MIS 2 and late MIS 6. At the same time, the largest offset is recorded in the $\delta^{13}C$ values between EqPIW and SOIW. In agreement with the evidence for a reduced production and/or shallower penetration of SOIW and the enhanced North Pacific mid-depth circulation, the results of this thesis argue for repeated episodes of enhanced nutrient-injection of GNPIW coupled with diminished contribution from southern-sourced waters into the EqPIW during Pleistocene peak glacials.

6.2 Outlook

To ensure paleoceanographic reconstructions as precisely as possible, it is essential to accurately determine the ACD of each species. It has been proven that ACDs vary regionally, but also seasonally [e.g. *Kawahata et al,* 2002; *Steph et al*., 2009]. The multinet study shown in *Chapter 3* presents for the first time foraminiferal ACDs from the south-eastern margin of the equatorial Pacific. It should be noted that this study was conducted during a single season at one location. For the western equatorial Pacific there exist no spatial ACD assessments, although chlorophyll data suggest a deeper chlorophyll maximum north and south of the equator. In addition, a one-year sediment trap analyses from the western equatorial Pacific highlights a seasonal difference in planktonic foraminifera abundance, which might be related to the varying strength of trade winds

and the associated nutrient concentrations [*Kawahata et al*., 2002]. Consequently, for a more reliably spatial-refined ACD assessment and to prevent a seasonally biased interpretation of paleo-data, additional multinet studies distributed within the WPWP and the EEP are needed. This thesis demonstrates the suitable application of sub-thermocline dwelling *G. hexagonus* to trace varying nutrient concentrations in equatorial Pacific sub-thermocline waters. *Marchant et al*. [1998] showed that, at least in the Peru-Chile current, the abundance of *G. hexagonus* did not differ seasonally. However, studies of this species are scarce. Indeed, different ACDs have been reported from the Pacific Ocean and the Indian Ocean (*Chapter 3.3.3.3*) Hence, more detailed information concerning regional calcification depths in the WEP and EEP, seasonal variations in abundances, feeding and the reproduction cycle would aid the use of *G. hexagonus* as an archive for sub-thermocline water masses.

The climate phenomenon ENSO causes large variations of the SSTs, large changes in precipitation, and a change in the depth of the thermocline and the associated availability of nutrients. El Niño events occur with a periodicity of 3 – 8 years and a duration of ~6 months. This periodicity is typically too short to be resolved by most sedimentary records, especially at the Manihiki Plateau where sedimentation rates are low (1 – 3 cm/kyr) [*Beiersdorf et al*., 1995; *Raddatz et al*., submitted (*abstract in the appendix*)]. Despite the difficulty in resolving such short time periods, it has often been discussed whether glacial climate prevailed in a more El Niño-like state [e.g. *López-Otálvaro et al*., 2008; *Li et al*., 2011; *Sadekov et al*., 2013] or La Niña-like conditions [e.g. *Beaufort et al*., 2001; *Staines-Urías et al.,* 2015]. These different climate modes could cause a shift in the ACD of especially SML- and thermocline-dwelling species. Consequently, ACD assessments during El Niño and La Niña events are needed to better constrain past glacial-interglacial oceanic and climate changes.

Our new downcore reconstructions indicate that past changes in North Pacific mid-depth circulation influenced the carbon signature of equatorial sub-thermocline water masses during peak glacial conditions. To record the long-term evolution of equatorial Pacific sub-thermocline waters, the $\delta^{13}C$ record of *G. hexagonus* was compared to the $\delta^{13}C$ record of Bering Sea sediment core U1342. The latter was measured on infaunal benthic *U. peregrina* that was corrected with a modern constant offset of +0.9 ‰ with respect to bottom water $\delta^{13}C_{DIC}$ [*Duplessy et al*., 1984; *Knudson and Ravelo*, 2015a]. However, a number of studies have shown that this offset is highly variable on glacial-interglacial timescales [*Pahnke and Zahn*, 2005; *McCave et al*., 2008; *Ronge et al.*, 2015], decreasing our confidence in the utility of *U. peregrina* as a tracer of past bottom water $\delta^{13}C_{DIC}$. This is particularly important as the contribution of Bering Sea Intermediate Water to GNPIW during glacial conditions, remains enigmatic [*Tanaka and Takahashi*, 2005; *Horikawa et al.*, 2010; *Rella et al*., 2012; *Max et al*., 2014; *Matul et al*., 2015; *Cook et al*., 2016]. Thus, it would be beneficial to compare a high-resolution record of epibenthic *Cibicidoides* from the Bering Sea and the Sea of Okhotsk, which covers more than one glacial-interglacial cycle, to equatorial intermediate waters. This would enable a more accurately determination of the specific North Pacific end-member signature and contribution to equatorial upwelling waters during glacials and

across the terminations. In addition, it would allow more accurate constraints to be place on the timing of the switch from northern- to southern-sourced water masses feeding into the equatorial Pacific.

This thesis also revealed that GNPIW might have changed glacial equatorial nutrient availability by providing preformed nutrients to EqPIW, which we defined as the 'North Pacific Nutrient Leakage' hypothesis. This nutrient leakage from the north argues for a relaxation of the nutrient limitation in the EEP. To date, there is no consistent information regarding glacial equatorial productivity [*Loubere et al*., 2003; *Bradtmiller et al*., 2006; *Pichevin et al*., 2009; *Robinson et al*., 2009; *Arellano-Torres et al*., 2011; *Calvo et al*., 2011; *Dubois et al*., 2011], but a north-south dichotomy in the primary productivity within the EEP during MIS 2 emerges [Bova, personal communication]. Whether this reflects atmospheric shifts in the position of the ITCZ and thus variations in upwelling, or variations in the contribution of nutrients from the different end-members, remains uncertain. To elucidate this matter, necessary information about utilization processes of major nutrients in the GNPIW formation region are needed. Recent studies from the Bering Sea hint to low glacial mass accumulation rates of biogenic opal and decreased glacial nitrate utilization [*Schlung et al*., 2013; *Knudson and Ravelo*, 2015b]. However, information on other major nutrients such as silicon and iron are absent. As northern-sourced water inject ~70 % of the modern $Si(OH)_4$ into equatorial upwelling waters [*Sarmiento et al*., 2004], more information on glacial-interglacial variations in this input are required. For example, silicon isotopes in the formation region of GNPIW combined with published records from the Southern Ocean would possibly allow us to infer the sources of productivity changes at the equator during glacials.

Understanding the causes of productivity changes in the equatorial Pacific would enable scientists to make more accurate estimations about the role of the equatorial Pacific within the past global CO_2 budget. To date, there is no real consensus about the emission of CO_2 to the atmosphere during glacials. A boron isotope study from the EEP proposes that the glacial oceanic CO_2 emission was even larger than today [*Sanyal and Bijma*, 1999]. In contrast, a more recent boron isotope study from the same area calculated that the EEP turned from a carbon source towards a CO_2 sink in the last glacial [*Martínez-Botí et al*., 2015]. Supporting evidence for an environmental change towards a glacial CO_2 sink comes from a diatom-bound carbon isotope calculation from the tropical western Pacific [*Xiong et al*., 2013]. In summary, a more coherent understanding of past changes in the equatorial Pacific will enable us to more accurately infer potential future ocean dynamics in this climatically sensitive region, improving future global climate predictions.

Acknowledgement

First of all, I want to thank my supervisor Ralf Tiedemann for giving me the opportunity to do my PhD and supported me along the way. Also I want to thank Gerhard Bohrmann for reviewing this thesis and appreciate all the helpful comments from all the members of my thesis committee. Special thanks also to Isabel Cacho for giving me the opportunity to work at ODP Site 1240 and supporting me during my stay in Barcelona.

I am particularly grateful for everyone who has helped me along my way. My gratitude goes to Dirk Nürnberg and Lars Max for their support, constructive comments, discussions and reviews. And special thanks to all the co-authors for their great help and ideas during writing and editing.

I really appreciate also the technical help of Antje Mewes, Birgit Glückselig, Günter Meyer, Janette Voigt, Lisa Schönborn, Susanne Wiebe, Rita Fröhlking-Teichert and Ute Bock. Without your silent support it would have been impossible to do this work. Furthermore, great thanks goes to Michal Kucera and Barbara Donner for their guidance during foraminiferal identification and sample preparation. And many thanks to my office mate Jenny for language assistance.

Special thanks to Edith for her amazing support and coffee times. Without you I could not have imagined publishing the papers and doing this! Special thanks also for Sarah and Verena for your comments, open ears and fun times in and outside the office.

Muchas gracias a mis amigos Patri, Olia, Albert y Mercé. I really appreciate all your support with work, bureaucracy, Catalan language and great times in Barcelona. It's been amazing getting to know you.

Also special thanks to all other PhD students from the Marine Geology Department at AWI, and from all the different other AWI departments. It was great meeting so many others along the way. Furthermore, I thank the people from Urbino 2014 for the laughter, fun and experiences in and outside of science.

Additionally, I want to thank the members of the DokTeam and the graduate school POLMAR for their support and this great experience being a DokTeam member. It really pushed me forwards working together with you.

The most personal and special thanks for all the help and support during this exciting, challenging and demanding times goes to my family and my freak. I could not have done it without your open ear and your encouragement!

Data Handling

All data presented in this thesis will be stored electronically and will be available online in the PANGAEA-database at www.pangaea.de.

References

Abelmann, A., Gersonde, R., Cortese, G., Kuhn, G., Smetacek, V., 2006. Extensive phytoplankton blooms in the Atlantic sector of the glacial Southern Ocean. Paleoceanography 21(1), PA1013. doi:10.1029/2005PA001199.

Anand, P., Elderfield, H., Conte, M.H., 2003. Calibration of Mg/Ca thermometry in planktonic foraminifera from a sediment trap time series. Paleoceanography 18, 1050. doi:10.1029/2002PA000846.

Andersen, K.K., Azuma, N., Barnola, J.M., Bigler, M., Biscaye, P., Caillon, N., Chappellaz, J., Clausen, H.B., Dahl-Jensen, D., Fischer, H., Fluckiger, J., Fritzsche, D., Fujii, Y., Goto-Azuma, K., Gronvold, K., Gundestrup, N.S., Hansson, M., Huber, C., Hvidberg, C.S., Johnsen, S.J., Jonsell, U., Jouzel, J., Kipfstuhl, S., Landais, A., Leuenberger, M., Lorrain, R., Masson-Delmotte, V., Miller, H., Motoyama, H., Narita, H., Popp, T., Rasmussen, S.O., Raynaud, D., Rothlisberger, R., Ruth, U., Samyn, D., Schwander, J., Shoji, H., Siggard-Andersen, M.L., Steffensen, J.P., Stocker, T., Sveinbjornsdottir, A.E., Svensson, A., Takata, M., Tison, J.L., Thorsteinsson, T., Watanabe, O., Wilhelms, F., White, J.W.C., N.G.I.C. Project, 2004. High-resolution record of Northern Hemisphere climate extending into the last interglacial period. Nature 431(7005), 147-151. doi:10.1038/nature02805.

Andreasen, D.J., Ravelo, A.C., 1997. Tropical Pacific Ocean thermocline depth reconstructions for the Last Glacial Maximum. Paleoceanography 12(3), 395-413. doi:10.1029/97PA00822.

Andreasen, D.H., Flower, M., Harvey, M., Chang, S., Ravelo, A.C., 2000. Data Report: late Pleistocene oxygen and carbon isotopic records from Sites 1011, 1012, and 1018. In: Lyle, M., Koizumi, I., Richter, C., Moore, T.C. (Eds.), Proceedings of the Ocean Drilling Program, Scientific Results 167, College Station, Texas, pp 1-4.

Antonov, J.I., Seidov, D., Boyer, T.P., Locarnini, R.A., Mishonov, A.V., Garcia, H.E., Baranova, O.K., Zweng, M.M., Johnson, D.R., 2010. World Ocean Atlas 2009, Volume 2: Salinity. In: Levitus, S. (Ed.), NOAA Atlas NESDIS 69. U.S. Government Printing Office, Washington D.C., pp. 184.

Arbuszewski, J., deMenocal, P., Kaplan, A., Farmer, E.C., 2010. On the fidelity of shell-derived δ^{18}Oseawater estimates. Earth and Planetary Science Letters 300(3-4), 185-196. doi:10.1016/j.epsl.2010.10.035.

Arellano-Torres, E., Pichevin, L.E., Ganeshram, R.S., 2011. High-resolution opal records from the eastern tropical Pacific provide evidence for silicic acid leakage from HNLC regions during glacial periods. Quaternary Science Reviews 30(9-10), 1112-1121. doi:10.1016/j.quascirev.2011.02.002.

Basak, C., Martin, E.E., Horikawa, K., Marchitto, T.M., 2010. Southern Ocean source of superset of ^{14}C-depleted carbon in the North Pacific Ocean during the last deglaciation. Nature Geoscience 3(11), 770-773. doi:10.1038/ngeo987.

Bé, A.W.H., 1959. Ecology of recent planktonic foraminifera. Part 1.- Areal distribution in the western North Atlantic. Micropaleontology 5, 77-100.

Bé, A.W.H., 1962. Quantitative multiple opening-and-closing plankton samplers. Deep-Sea Research 6, 373-392.

Bé, A.W.H., 1977. An ecological, zoogeographic and taxonomic review of recent planktonic foraminifera. In: Ramsay, A.T.S. (Ed.), Oceanic Micropaleontology. Academic Press, London, pp. 1-100.

Bé, A.W.H., Tolderlund, D.S., 1971. Distribution and ecology of living planktonic foraminifera in surface waters of the Atlantic and Indian Oceans. In: Funnel, B.M., Riedel, W.R. (Eds.), The

Micropaleontology of Oceans. University Press, Cambridge, pp. 105-149.

Bé, A.W.H., Spero, H.J., Anderson, O.R., 1982. Effects of symbiont elimination and reinfection on the life processes of the planktonic foraminifer *Globigerinoides sacculifer*. Marine Biology 70, 73-86.

Bé, A.W.H., Bishop, J.K.B., Sverdlove, M.S., Gardner, W.D., 1985. Standing stock, vertical distribution and flux of planktonic foraminifera in the Panama Basin. Marine Micropaleontology 9, 307-333.

Beaufort, L., de Garidel-Thoron, T., Mix, A.C., Pisias, N.G., 2001. ENSO-like Forcing on Oceanic Primary Production During the Late Pleistocene. Science 293(5539), 2440-2444. doi:10.1126/science.293.5539.2440.

Beiersdorf, H., Bickert, T., Cepek, P., Fenner, J., Petersen, N., Schönfeld, J., Weiss, W., Won, M.Z., 1995. High-resolution stratigraphy and the response of biota to late Cenozoic environmental changes in the central equatorial Pacific Ocean (Manihiki Plateau). Marine Geology 125, 29-59.

Bemis, B.E., Spero, H.J., Bijma, J., Lea, D.W., 1998. Reevaluation of the oxygen isotopic composition of planktonic foraminifera: Experimental results and revised paleotemperature equations. Paleoceanography 13(2), 150-160. doi:10.1029/98PA00070.

Bemis, B.E., Spero, H.J., Lea, D.W., Bijma, J., 2000. Temperature influence on the carbon isotopic composition of *Globigerina bulloides* and *Orbulina universa* (planktonic foraminifera). Marine Micropaleontology 38(3-4), 213-228. doi:10.1016/S0377-8398(00)00006-2.

Berger, W.H., Killingley, J.S., Vincent, E., 1978. Stable isotopes in Deep-Sea carbonates — box core Erdc-92, West Equatorial Pacific. Oceanologica Acta 1, 203-216.

Bickert, T., Mackensen, A., 2004. Last Glacial to Holocene changes in South Atlantic deep water circulation. In: Wefer, G., Mulitza, S., Rathmeyer, V., (Eds.), The South Atlantic in the Late Quaternary-Reconstruction of Material Budget and Current Systems. Springer, Berlin Heidelberg, pp 671-693.

Bijma, J., Hemleben, C., 1994. Population dynamics of the planktonic foraminifer *Globigerinoides sacculifer* (Brady) from the central Red Sea. Deep Sea Research Part I: Oceanographic Research Papers 41, 485-510.

Bijma, J., Faber, W.W., Hemleben, C., 1990. Temperature and salinity limits for growth and survival of some planktonic foraminifers in laboratory cultures. Journal of Foraminiferal Research 20, 95-116.

Bijma, J., Spero, H.J., Lea, D.W., 1999. Reassessing foraminiferal stable isotope geochemistry: Impact of the oceanic carbonate system (experimental results). In: Fischer, G., Wefer, G. (Eds.), Use of Proxies in Paleoceanography. Springer, Berlin Heidelberg, pp. 489-512.

Birch, H., Coxall, H.K., Pearson, P.N., Kroon, D., O'Regan, M., 2013. Planktonic foraminifera stable isotopes and water column structure: Disentangling ecological signals. Marine Micropaleontology 101(0), 127-145. doi:10.1016/j.marmicro.2013.02.002.

Blackmon, P.D., Todd, R., 1959. Mineralogy of some foraminifera as related to their classification and ecology. Journal of Paleontology 33(1), 1-15.

Blain, S., Leynaert, A., Tréguer, P., Chretiennot-Dinet, M.-J., Rodier, M., 1997. Biomass, growth rates and limitation of Equatorial Pacific diatoms. Deep Sea Research Part I: Oceanographic Research Papers 44, 1255-1275.

Blanchot, J., André, J.M., Navarette, C., Neveux, J., Radenac, M.H., 2001. Picophytoplankton in the equatorial Pacific: vertical distributions in the warm pool and in the high nutrient low chlorophyll conditions. Deep Sea Research Part I: Oceanographic Research Papers 48(1), 297-314. doi:10.1016/S0967-0637(00)00063-7.

Bostock, H.C., Opdyke, B.N., Williams, M.J.M., 2010. Characterising the intermediate depth waters of the Pacific Ocean using $\delta^{13}C$ and other geochemical tracers. Deep Sea Research Part I: Oceanographic Research Papers 57(7), 847-859. doi:10.1016/j.dsr.2010.04.005.

Bostock, H.C., Sutton, P.J., Williams, M.J.M., Opdyke, B.N., 2013. Reviewing the circulation and mixing of Antarctic Intermediate Water in the South Pacific using evidence from geochemical tracers and Argo float trajectories. Deep Sea Research Part I: Oceanographic Research Papers 73, 84-98. doi:10.1016/j.dsr.2012.11.007.

Bouvier-Saumagnac, Y., Duplessy, J.-C., 1985. Carbon and oxygen isotopic compositian of planktonic foraminifera from Iabaratory culture, plankton tows and recent sediment: implications for the reconstruction of paleoclimatic conditions and of the global carbon cycle. Journal of Foraminiferal Research 15, 302-320.

Bova, S.C., Herbert, T., Rosenthal, Y., Kalansky, J., Altabet, M., Chazen, C., Mojarro, A., Zech, J., 2015. Links between eastern equatorial Pacific stratification and atmospheric CO_2 rise during the last deglaciation. Paleoceanography 30(11), 1407-1424. doi:10.1002/2015PA002816.

Bradtmiller, L.I., Anderson, R.F., Fleisher, M.Q., Burckle, L.H., 2006. Diatom productivity in the equatorial Pacific Ocean from the last glacial period to the present: A test of the silicic acid leakage hypothesis. Paleoceanography 21(4), PA4201. doi:10.1029/2006PA001282.

Bradtmiller, L.I., Anderson, R.F., Fleisher, M.Q., Burckle L.H., 2009. Comparing glacial and Holocene opal fluxes in the Pacific sector of the Southern Ocean. Paleoceanography 24, PA2214, doi:10.1029/2008PA001693.

Broecker, W., 1982. Glacial to interglacial changes in ocean chemistry. Progress in Oceanography 11, 151-197.

Broecker, W.S., Maier-Reimer, E., 1992. The influence of air and sea exchange on the carbon isotope distribution in the sea. Global Biogeochemical Cycles 6(3), 315-320. doi:10.1029/92GB01672.

Broecker, W.S., Peng, T.H., 1982. Tracers in the Sea. Lamont-Doherty Geological Observatory, Columbia University, pp 702.

Brunelle, B.G., Sigman, D.M., Cook, M.S., Keigwin, L.D., Haug, G.H., Plessen, B., Schettler, G., Jaccard, S.L., 2007. Evidence from diatom-bound nitrogen isotopes for subarctic Pacific stratification during the last ice age and a link to North Pacific denitrification changes. Paleoceanography 22, PA1215. doi:10.1029/2005PA001205.

Brunelle, B.G., Sigman, D.M., Jaccard, S.L., Keigwin, L.D., Plessen, B., Schettler, G., Cook, M.S., Haug, G.H., 2010. Glacial/interglacial changes in nutrient supply and stratification in the western subarctic North Pacific since the penultimate glacial maximum. Quaternary Science Reviews 29(19-20), 2579-2590. doi:10.1016/j.quascirev.2010.03.010.

Brzezinski, M.A., Pride, C.J., Franck, V.M., Sigman, D.M., Sarmiento, J.L., Matsumoto, K., Gruber, N., Rau, G.H., Coale, K.H., 2002. A switch from $Si(OH)_4$ to NO^{3-} depletion in the glacial Southern Ocean. Geophysical Research Letters 29(12), 5164. doi:10.1029/2001GL014349.

Calvo, E., Pelejero, C., Pena, L.D., Cacho, I., Logan, G.A., 2011. Eastern Equatorial Pacific productivity and related-CO_2 changes since the last glacial period. Proceedings of the National Academy of Sciences of the United States of America 108(14), 5537-5541. doi:10.1073/pnas.1009761108.

Carriquiry, J.D., Sanchez, A., Leduc, G., 2015. Southern Ocean influence on the Eastern Tropical North Pacific's intermediate depth circulation during the last glacial maximum. Paleoceanography 30, 1132-1151. doi:10.1002/2014PA002766.

Chase, Z., McManus, J., Mix, A.C., Muratli, J., 2014. Southern-ocean and glaciogenic nutrients control diatom export production on the Chile margin. Quaternary Science Reviews 99, 135-145. doi:10.1016/j.quascirev.2014.06.015.

Cifelli, R., 1969. Radiation of Cenozoic Planktonic Foraminifera. Systematic Zoology 18, 154-168.

Cléroux, C., Cortijo, E., Anand, P., Labeyrie, L., Bassinot, F., Caillon, N., Duplessy, J.-C., 2008. Mg/Ca and Sr/Ca ratios in planktonic foraminifera: Proxies for upper water column temperature reconstruction. Paleoceanography 23(3), PA3214. doi:10.1029/2007PA001505.

Coale, K.H., Johnson, K.S., Fitzwater, S.E., Blain, S.P.G., Stanton, T.P., Coley, T.L., 1998. IronEx-I, an in situ iron-enrichment experiment: Experimental design, implementation and results. Deep Sea Research Part II: Topical Studies in Oceanography 45(6), 919-945. doi:10.1016/S0967-0645(98)00019-8.

Colleoni, F., Wekerle, C., Näslund, J.-O., Brandefelt, J., Masina, S., 2016. Constraint on the penultimate glacial maximum Northern Hemisphere ice topography (≈140 kyrs BP). Quaternary Science Reviews 137, 97-112. doi:10.1016/j.quascirev.2016.01.024.

Collins, M., An, S.-I., Cai, W., Ganachaud, A., Guilyardi, E., Jin, F.-F., Jochum, M., Lengaigne, M., Power, S., Timmermann, A., Vecchi, G., Wittenberg, A., 2010. The impact of global warming on the tropical Pacific Ocean and El Nino. Nature Geoscience 3, 391-397. doi:10.1038/ngeo868.

Cook, M.S., Ravelo, A.C., Mix, A., Nesbitt, I.M., Miller, N.V., 2016. Tracing subarctic Pacific water masses with benthic foraminiferal stable isotopes during the LGM and late Pleistocene. Deep Sea Research Part II: Topical Studies in Oceanography 125-126, 84-95. doi:10.1016/j.dsr2.2016.02.006.

Craig, H., Gordon, L.I., 1965. Deuterium and oxygen 18 variations in the ocean and the marine atmosphere. Symposium on Marine Geochemistry. University of Rhode Island Publication Vol. 3, 277-374.

Curry, W.B., Oppo, D.W., 2005. Glacial water mass geometry and the distribution of $\delta^{13}C$ of ΣCO_2 in the western Atlantic Ocean. Paleoceanography 20(1), PA1017. doi:10.1029/2004PA001021.

Curry, W.B., Duplessy, J.C., Labeyrie, L.D., Shackleton, N.J., 1988. Changes in the distribution of $\delta^{13}C$ of deep water ΣCO_2 between the Last Glaciation and the Holocene. Paleoceanography 3, 317-341.

Dansgaard, W., 1964. Stable isotopes in precipitation. Tellus 16, 436-468.

Dansgaard, W., Tauber, H., 1969. Glacier oxygen-18 content and Pleistocene ocean temperatures. Science 166, 499-502.

de la Fuente, M., Skinner, L., Calvo, E., Pelejero, C., Cacho, I., 2015. Increased reservoir ages and poorly ventilated deep waters inferred in the glacial Eastern Equatorial Pacific. Nature Communications 6(7420). doi:10.1038/ncomms8420.

de Nooijer, L.J., Hathorne, E.C., Reichart, G.J., Langer, G., Bijma, J., 2014. Variability in calcitic Mg/Ca and Sr/Ca ratios in clones of the benthic foraminifer *Ammonia tepida*. Marine Micropaleontology 107, 32-43. doi:10.1016/j.marmicro.2014.02.002.

Dekens, P.S., Lea, D.W., Pak, D.K., Spero, H.J., 2002. Core top calibration of Mg/Ca in tropical foraminifera: Refining paleotemperature estimation. Geochemistry, Geophysics, Geosystems 3(4), 1-29. doi:10.1029/2001GC000200.

Dickson, R., Hurrell, J., Bindoff, N., Wong, A., Arbic, B., Oweens, B., Imawaki, S., Yashayaev, I., 2000. The world during WOCE. In: Siedler, G., Chrurch, J., Gould, J. (Eds.), Ocean Circulation and Climate. International Geophysics Series 77, Academic Press, San Diego, pp. 557-585.

Dubois, N., Kienast, M., 2011. Spatial reorganization in the equatorial divergence in the Eastern Tropical Pacific during the last 150 kyr. Geophysical Research Letters 38(16), L16606. doi:10.1029/2011GL048325.

Dubois, N., Kienast, M., Kienast, S., Normandeau, C., Calvert, S.E., Herbert, T.D., Mix, A., 2011. Millennial-scale variations in hydrography and biogeochemistry in the Eastern Equatorial Pacific over the last 100 kyr. Quaternary Science Reviews 30(1-2), 210-223. doi:10.1016/j.quascirev.2010.10.012.

Dueñas-Bohórquez, A., da Rocha, R.E., Kuroyanagi, A., Bijma, J., Reichart, G.-J., 2009. Effect of salinity and seawater calcite saturation state on Mg and Sr incorporation in cultured planktonic foraminifera. Marine Micropaleontology 73(3–4), 178-189. doi:10.1016/j.marmicro.2009.09.002.

Dueñas-Bohórquez, A., da Rocha, R.E., Kuroyanagi, A., de Nooijer, L.J., Bijma, J., Reichart, G.-J., 2011. Interindividual variability and ontogenetic effects on Mg and Sr incorporation in the planktonic foraminifer *Globigerinoides sacculifer*. Geochimica et Cosmochimica Acta 75(2), 520-532. doi:10.1016/j.gca.2010.10.006.

Dugdale, R.C., Wilkerson, F.P., 1998. Silicate regulation of new production in the equatorial Pacific upwelling. Nature 391, 270-273.

Dugdale, R.C., Wischmeyer, A.G., Wilkerson, F.P., Barber, R.T., Chai, F., Jiang, M.S., Peng, T.H., 2002. Meridional asymmetry of source nutrients to the equatorial Pacific upwelling ecosystem and its potential impact on ocean–atmosphere CO_2 flux; a data and modeling approach. Deep Sea Research Part II: Topical Studies in Oceanography 49, 2513-2531.

Dugdale, R.C., Lyle, M., Wilkerson, F.P., Chai, F., Barber, R.T., Peng, T.H., 2004. Influence of equatorial diatom processes on Si deposition and atmospheric CO_2 cycles at glacial/interglacial timescales. Paleoceanography 19(3), PA3011. doi:10.1029/2003PA000929.

Duplessy, J.-C., Shackleton, N.J., Matthews, R.K., Prell, W., Ruddiman, W.F., Caralp, M., Hendy, C.H., 1984. 13C Record of benthic foraminifera in the last interglacial ocean: Implications for the carbon cycle and the global deep water circulation. Quaternary Research 21, 225-243.

Duplessy, J.C., Shackleton, N.J., Fairbanks, R.G., Labeyrie, L., Oppo, D., Kallel, N., 1988. Deepwater source variations during the last climatic cycle and their impact on the global deepwater circulation. Paleoceanography 3, 343-360.

Elderfield, H., Ganssen, G., 2000. Past temperature and $\delta^{18}O$ of surface ocean waters inferred from foraminiferal Mg/Ca ratios. Nature 405, 442-445.

Elderfield, H., Vautravers, M., Cooper, M., 2002. The relationship between shell size and Mg/Ca, Sr/Ca, $\delta^{18}O$, and $\delta^{13}C$ of species of planktonic foraminifera. Geochemistry, Geophysics, Geosystems 3(8), 1-13. doi:10.1029/2001GC000194.

Elmore, A.C., McClymont, E.L., Elderfield, H., Kender, S., Cook, M.R., Leng, M.J., Greaves, M., Misra, S., 2015. Antarctic Intermediate Water properties since 400 ka recorded in infaunal (*Uvigerina peregrina*) and epifaunal (*Planulina wuellerstorfi*) benthic foraminifera. Earth and Planetary Science Letters 428, 193-203. doi:10.1016/j.epsl.2015.07.013.

Emiliani, C., 1955. Pleistocene temperatures. The Journal of Geology 63(6), 538-578.

Epstein, S., Buchsbaum, R., Lowenstam, H., Urey, H.C., 1951. Carbonate-water isotopic temperature scale. Geological Society of America Bulletin 62(4), 417-426.

Epstein, S., Buchsbaum, R., Lowenstam, H.A., Urey, H.C., 1953. Revised carbonate-water isotopic temperature scale. Geological Society of America Bulletin 64, 1315-1326.

Erez, J., Luz, B., 1983. Experimental paleotemperature equation for planktonic foraminifera. Geochimica et Cosmochimica Acta 47, 1025-1031.

Fairbanks, R.G., Wiebe, P.H., 1980. Foraminifera and chlorophyll maximum: vertical distribution, seasonal succession, and paleoceanographic significance. Science 209, 1524-1526.

Fairbanks, R.G., Sverdlove, M., Free, R., Wiebe, P.H., Be, A.W.H., 1982. Vertical distribution and isotopic fractionation of living planktonic foraminifera from the Panama Basin. Nature 298, 841-844.

Fairbanks, R.G., Mortlock, R.A., Chiu, T.-C., Cao, L., Kaplan, A., Guilderson, T.P., Fairbanks, T.W., Bloom, A.L., Grootes, P.M., Nadeau, M.-J., 2005. Radiocarbon calibration curve spanning 0 to 50,000 years BP based on paired $^{230}Th/^{234}U/^{238}U$ and ^{14}C dates on pristine corals. Quaternary Science Reviews 24(16-17), 1781-1796. doi:10.1016/j.quascirev. 2005.04.007.

Falkowski, P., Scholes, R.J., Boyle, E., Canadell, J., Canfield, D., Elser, J., Gruber, N., Hibbard, K., Högberg, P., Linder, S., Mackenzie, F.T., Moore III, B., Pedersen, T., Rosenthal, Y., Seitzinger, S., Smetacek, V., Steffen, W., 2000. The Global Carbon Cycle: A Test of Our Knowledge of Earth as a System. Science 290, 291-296.

Farmer, E.C., Kaplan, A., de Menocal, P.B., Lynch-Stieglitz, J., 2007. Corroborating ecological depth preferences of planktonic foraminifera in the tropical Atlantic with the stable oxygen isotope ratios of core top specimens. Paleoceanography 22(3), PA3205. doi:10.1029/ 2006PA001361.

Faul, K.L., Ravelo, A.C., Delaney, M.L., 2000. Reconstructions of upwelling, productivity, and photic zone depth in the eastern equatorial Pacific Ocean using planktonic foraminiferal stable isotopes and abundances. The Journal of Foraminiferal Research 30, 110-125. doi:10.2113/0300110.

Feely, R.A., Boutin, J., Cosca, C.E., Dandonneau, Y., Etcheto, J., Inoue, H.Y., Ishii, M., Quéré, C.L., Mackey, D.J., McPhaden, M., Metzl, N., Poisson, A., Wanninkhof, R., 2002. Seasonal and interannual variability of CO_2 in the equatorial Pacific. Deep Sea Research Part II: Topical Studies in Oceanography 49(13-14), 2443-2469. doi:10.1016/S0967-0645(02)00044-9.

Fiedler, P.C., Talley, L.D., 2006. Hydrography of the eastern tropical Pacific: A review. Progress in Oceanography 69(2–4), 143-180. doi:10.1016/j.pocean.2006.03.008.

Fine, R.A., Lukas, R., Bingham, F.M., Warner, M.J., Gammon, R.H., 1994. The western equatorial Pacific: A water mass crossroads. Journal of Geophysical Research: Oceans 99(C12), 25063-25080. doi:10.1029/94JC02277.

Firing, E., Wijffels, S.E., Hacker, P., 1998. Equatorial subthermocline currents across the Pacific. Journal of Geophysical Research: Oceans 103, 21413-21423. doi:10.1029/98JC01944.

Ford, H.L., Ravelo, A.C., Polissar, P.J., 2015. Reduced El Niño–Southern Oscillation during the Last Glacial Maximum. Science 347(6219), 255-258. doi:10.1126/science.1258437.

Friedrich, O., Schiebel, R., Wilson, P.A., Weldeab, S., Beer, C.J., Cooper, M.J., Fiebig, J., 2012. Influence of test size, water depth, and ecology on Mg/Ca, Sr/Ca, $\delta^{18}O$ and $\delta^{13}C$ in nine modern species of planktic foraminifers. Earth and Planetary Science Letters 319-320(0), 133-145. doi:10.1016/j.epsl.2011.12.002.

Galbraith, E.D., Jaccard, S.L., Pedersen, T.F., Sigman, D.M., Haug, G.H., Cook, M., Southon, J.R., Francois, R., 2007. Carbon dioxide release from the North Pacific abyss during the last deglaciation. Nature 449(7164), 890-893. doi:10.1038/nature06227.

Galbraith, E.D., Kienast, M., Jaccard, S.L., Pedersen, T.F., Brunelle, B.G., Sigman, D.M., Kiefer, T., 2008. Consistent relationship between global climate and surface nitrate utilization in the western subarctic Pacific throughout the last 500 ka. Paleoceanography 23(2), PA2212. doi:10.1029/2007PA001518.

Ganssen, G.M., Kroon, D., 2000. The isotopic signature of planktonic foraminifera from NE Atlantic surface sediments: implications for the reconstruction of past oceanic conditions. Journal of the Geological Society 157, 693-699.

Garcia, H.E., Locarnini, R.A., Boyer, T.P., Antonov, J.I., Zweng, M.M., Baranova, O.K., Johnson D.R., 2010. World Ocean Atlas 2009, Volume 4: Nutrients (phosphate, nitrate, silicate). In: Levitus, S. (Ed.), NOAA Atlas NESDIS, 71. U.S. Government Printing Office, Washington D.C., pp 398.

Gebbie, G., Peterson, C.D., Lisiecki, L.E., Spero, H.J., 2015. Global-mean marine $\delta^{13}C$ and its uncertainty in a glacial state estimate. Quaternary Science Reviews 125, 144-159. doi:10.1016/j.quascirev.2015.08.010.

Gebhardt, H., Sarnthein, M., Grootes, P.M., Kiefer, T., Kuehn, H., Schmieder, F., Röhl, U., 2008. Paleonutrient and productivity records from the subarctic North Pacific for Pleistocene glacial terminations I to V. Paleoceanography 23(4), PA4212. doi:10.1029/2007PA001513.

Gordon, R.M., Coale, K.H. Johnson K.S, 1997. Iron distributions in the equatorial Pacific: Implications for new production. Limnology and Oceanography 42(3), 419-431. doi:10.4319/lo.1997.42.3.0419.

Goodman, P.J., Hazeleger, W., de Vries, P., Cane, M., 2005. Pathways into the Pacific Equatorial Undercurrent: A Trajectory Analysis. Journal of Physical Oceanography 35(11), 2134-2151. doi:10.1175/JPO2825.1.

Grenier, M., Cravatte, S., Blanke, B., Menkes, C., Koch-Larrouy, A., Durand, F., Melet, A., Jeandel, C., 2011. From the western boundary currents to the Pacific Equatorial Undercurrent: Modeled pathways and water mass evolutions. Journal of Geophysical Research: Oceans 116(C12), C12044. doi:10.1029/2011JC007477.

Hamilton, C.P., Spero, H.J., Bijma, J., Lea, D.W., 2008. Geochemical investigation of gametogenic calcite addition in the planktonic foraminifera *Orbulina universa*. Marine Micropaleontology 68(3-4), 256-267. doi:10.1016/j.marmicro.2008.04.003.

Hathorne, E.C., Alard, O., James, R.H., Rogers, N.W., 2003. Determination of intratest variability of trace elements in foraminifera by laser ablation inductively coupled plasma-mass spectrometry. Geochemistry, Geophysics, Geosystems 4(12), 8408. doi:10.1029/2003 GC000539.

Hathorne, E.C., Gagnon, A., Felis, T., Adkins, J., Asami, R., Boer, W., Caillon, N., Case, D., Cobb, K.M., Douville, E., deMenocal, P., Eisenhauer, A., Garbe-Schönberg, D., Geibert, W., Goldstein, S., Hughen, K., Inoue, M., Kawahata, H., Kölling, M., Cornec, F.L., Linsley, B.K., McGregor, H.V., Montagna, P., Nurhati, I.S., Quinn, T.M., Raddatz, J., Rebaubier, H., Robinson, L., Sadekov, A., Sherrell, R., Sinclair, D., Tudhope, A.W., Wei, G., Wong, H., Wu, H.C., You, C.-F., 2013. Interlaboratory study for coral Sr/Ca and other element/Ca ratio

measurements. Geochemistry, Geophysics, Geosystems 14(9), 3730-3750. doi:10.1002/ggge.20230.

Haug, G.H., Sigman, D.M., Tiedemann, R., Pedersen T.F., Sarnthein, M., 1999. Onset of permanent stratification in the subarctic Pacific Ocean. Nature 401(6755), 779-782.

Hemleben, C., Bijma, J., 1994. Foraminiferal population dynamics and stable carbon isotopes. In: Zahn, R., Pedersen, T.F., Kaminski, M.A., Labeyrie, L. (Eds.), Carbon Cycling in the Glacial Ocean: Constraints on the Ocean's Role in Global Change: Quantitative Approaches in Paleoceanography. Springer, Berlin Heidelberg, pp. 145-166.

Hemleben, C., Spindler, M., Anderson, O.R., 1989. Modern Planktonic Foraminifera. Springer, New York, pp. 363.

Hendry, K.R., Brzezinski, M.A., 2014. Using silicon isotopes to understand the role of the Southern Ocean in modern and ancient biogeochemistry and climate. Quaternary Science Reviews 89(0), 13-26. doi:10.1016/j.quascirev.2014.01.019.

Hendy, I.L., Kennett, J.P., 2000. Stable isotope stratigraphy and paleoceanography of the last 170 ky: Site 1014, Tanner Basin, California. In: Lyle, M., Koizumi, I., Richter, C., Moore, T.C. (Eds.), Proceedings of the Ocean Drilling Program, Scientific Results, College Station, Texas, pp 1-12.

Herbland, A., Voituriez, B., 1979. Hydrological structure analysis for estimating the primary production in the tropical Atlantic Ocean. Journal of Marine Research 37, 87-101.

Herguera, J.C., Jansen, E., Berger, W.H., 1992. Evidence for a bathyal front at 2000-M depth in the glacial Pacific, based on a depth transect on Ontong Java Plateau. Paleoceanography 7, 273-288. doi:10.1029/92PA00869.

Herguera, J.C., Herbert, T., Kashgarian, M., Charles, C., 2010. Intermediate and deep water mass distribution in the Pacific during the Last Glacial Maximum inferred from oxygen and carbon stable isotopes. Quaternary Science Reviews 29(9-10), 1228-1245. doi:10.1016/j.quascirev.2010.02.009.

Hillbrecht, H., 1996. Extant Planktonic Foraminifera and the physical environment in the Atlantic and Indian Oceans. Mitteilungen aus dem Geologischen Institut der Eidgen. Technischen Hochschule und der Universität Zürich, http://www.ngdc.noaa.gov/mgg/geology/hh1996/aa_start.html.

Hoefs, J., 2009. Stable Isotope Geochemistry, 6 ed. Springer, Berlin Heidelberg, pp 285.

Honda, M.C., Imai, K., Nojiri, Y., Hoshi, F., Sugawara, T., Kusakabe, M., 2002. The biological pump in the northwestern North Pacific based on fluxes and major components of particulate matter obtained by sediment-trap experiments (1997-2000). Deep-Sea Research Part II-Topical Studies in Oceanography 49(24-25), 5595-5625. doi:10.1016/S0967-0645(02)00201-1.

Hönisch, B., Allen, K.A., Lea, D.W., Spero, H.J., Eggins, S.M., Arbuszewski, J., deMenocal, P., Rosenthal, Y., Russell, A.D., Elderfield, H., 2013. The influence of salinity on Mg/Ca in planktic foraminifers – Evidence from cultures, core-top sediments and complementary $\delta^{18}O$. Geochimica et Cosmochimica Acta 121(0), 196-213. doi:10.1016/j.gca.2013.07.028.

Horikawa, K., Asahara, Y., Yamamoto, K., Okazaki, Y., 2010. Intermediate water formation in the Bering Sea during glacial periods: Evidence from neodymium isotope ratios. Geology 38(5), 435-438. doi:10.1130/g30225.1.

Hu, R., Piotrowski, A.M., Bostock, H.C., Crowhurst, S., Rennie, V., 2016. Variability of neodymium isotopes associated with planktonic foraminifera in the Pacific Ocean during the Holocene and Last Glacial Maximum. Earth and Planetary Science Letters 447, 130-138. doi:10.1016/j.epsl.2016.05.011.

Huang, K.-F., Oppo, D.W., Curry, W.B., 2014. Decreased influence of Antarctic intermediate water in the tropical Atlantic during North Atlantic cold events. Earth and Planetary Science Letter 389(0), 200-208. doi:10.1016/j.epsl.2013.12.037.

Hut, G., 1987. Consultants Group Meeting on Stable Isotope Reference Samples for Geochemical and Hydrological Investigations. Report to the Director General, International Atomic Energy Agency, Vienna, pp 42.

Itou, M., Ono, T., Oba, T., Noriki, S., 2001. Isotopic composition and morphology of living *Globorotalia scitula*: a new proxy of sub-intermediate ocean carbonate chemistry? Marine Micropaleontology 42(3-4), 189-210. doi:10.1016/S0377-8398(01)00015-9.

Jaccard, S.L., Haug, G.H., Sigman, D.M., Pedersen, T.F., Thierstein, H.R., Röhl, U., 2005. Glacial/Interglacial Changes in Subarctic North Pacific Stratification. Science 308(5724), 1003-1006. doi:10.1126/science.1108696.

Jochum, K.P., Weis, U., Stoll, B., Kuzmin, D., Yang, Q., Raczek, I., Jacob, D.E., Stracke, A., Birbaum, K., Frick, D.A., Günther, D., Enzweiler, J., 2011. Determination of reference values for NIST SRM 610–617 glasses following ISO guidelines. Geostandards and Geoanalytical Research 35(4), 397-429. doi:10.1111/j.1751-908X.2011.00120.x.

Johnson, G.C., Moore, D.W., 1997. The Pacific Subsurface Countercurrents and an Inertial Model. Journal of Physical Oceanography 27, 2448-2459. doi:10.1175/1520-0485(1997)027< 2448:TPSCAA>2.0.CO;2.

Johnson, G.C., Sloyan, B.M., Kessler, W.S., McTaggart, K.E., 2002. Direct measurements of upper ocean currents and water properties across the tropical Pacific during the 1990s. Progress in Oceanography 52, 31-61. doi:10.1016/S0079-6611(02)00021-6.

Kawahata, H., Nishimura, A., Gagan, M.K., 2002. Seasonal change in foraminiferal production in the western equatorial Pacific warm pool: evidence from sediment trap experiments. Deep Sea Research Part II: Topical Studies in Oceanography 49(13-14), 2783-2800. doi:10.1016/S0967-0645(02)00058-9.

Keigwin, L.D., 1998. Glacial-age hydrography of the far northwest Pacific Ocean. Paleoceanography 13, 323-339.

Kemle-von Mücke, S., Oberhänsli, H., 1999. The distribution of living planktic foraminifera in relation to southeast Atlantic oceanography. In: Fischer, G., Wefer, G. (Eds.), Use of Proxies in Paleoceanography: Examples from the South Atlantic. Springer, Berlin Heidelberg, pp. 91-115.

Kennett, J.P., Ingram, B.L., 1995. A 20,000 Year Record of Ocean Circulation and Climate-Change from the Santa-Barbara Basin. Nature 377, 510-514.

Kessler, W.S., 2006. The circulation of the eastern tropical Pacific: A review. Progress in Oceanography 69(2-4), 181-217. doi:10.1016/j.pocean.2006.03.009.

Key, R.M., Kozyr, A., Sabine, C.L., Lee, K., Wanninkhof, R., Bullister, J.L., Feely, R.A., Millero, F.J., Mordy, C., Peng, T.-H., 2004. A global ocean carbon climatology: Results from Global Data Analysis Project (GLODAP). Global Biogeochemical Cycles 18, GB4031 doi:10.1029/2004GB002247.

Kiefer, T., McCave, I.N., Elderfield, H., 2006. Antarctic control on tropical Indian Ocean sea surface temperature and hydrography. Geophysical Research Letters 33(24), L24612. doi:10.1029/2006GL027097.

Kienast, S.S., Hendy, I.L., Crusius, J., Pedersen, T.F., Calvert, S.E., 2004. Export Production in the Subarctic North Pacific over the Last 800 kyrs: No Evidence for Iron Fertilization? Journal of Oceanography 60(1), 189-203. doi:10.1023/B:JOCE.0000038326.73943.aa.

Kienast, S.S., Kienast, M., Mix, A.C., Calvert, S.E., François, R., 2007. Thorium-230 normalized particle flux and sediment focusing in the Panama Basin region during the last 30,000 years. Paleoceanography 22(2), PA2213. doi:10.1029/2006PA001357.

Kim, S.-T., O'Neil, J.R., 1997. Equilibrium and nonequilibrium oxygen isotope effects in synthetic carbonates. Geochimica et Cosmochimica Acta 61, 3461-3475.

Kim, S., Khim, B.K., Uchida, M., Itaki, T., Tada, R., 2011. Millennial-scale paleoceanographic events and implication for the intermediate-water ventilation in the northern slope area of the Bering Sea during the last 71 kyrs. Global and Planetary Change 79(1-2), 89-98. doi:10.1016/j.gloplacha.2011.08.004.

King, A.L., Howard, W.R., 2003. Planktonic foraminiferal flux seasonality in Subantarctic sediment traps: A test for paleoclimate reconstructions. Paleoceanography 18(1), 1019. doi:10.1029/2002PA000839.

King, A.L., Howard, W.R., 2004. Planktonic foraminiferal $\delta^{13}C$ records from Southern Ocean sediment traps: New estimates of the oceanic Suess effect. Global Biogeochemical Cycles 18(2), GB2007. doi:10.1029/2003GB002162.

King, A.L., Howard, W.R., 2005. $\delta^{18}O$ seasonality of planktonic foraminifera from Southern Ocean sediment traps: Latitudinal gradients and implications for paleoclimate reconstructions. Marine Micropaleontology 56(1-2), 1-24. doi:10.1016/j.marmicro.2005.02.008.

Kisakürek, B., Eisenhauer, A., Böhm, F., Garbe-Schönberg, D., Erez, J., 2008. Controls on shell Mg/Ca and Sr/Ca in cultured planktonic foraminiferan, *Globigerinoides ruber* (white). Earth and Planetary Science Letters 273(3-4), 260-269. doi:10.1016/j.epsl.2008.06.026.

Knudson, K.P., Ravelo, A.C., 2015a. North Pacific Intermediate Water circulation enhanced by the closure of the Bering Strait. Paleoceanography 30(10), 1287-1304. doi:10.1002/2015PA002840.

Knudson, K.P., Ravelo, A.C., 2015b. Enhanced subarctic Pacific stratification and nutrient utilization during glacials over the last 1.2Myr. Geophysical Research Letters 42. doi:10.1002/2015GL066317.

Kozdon, R., Ushikubo, T., Kita, N.T., Spicuzza, M., Valley, J.W., 2009. Intratest oxygen isotope variability in the planktonic foraminifer *N. pachyderma*: Real vs. apparent vital effects by ion microprobe. Chemical Geology 258(3-4), 327-337. doi:10.1016/j.chemgeo.2008.10.032.

Kroon, D., Darling, K., 1995. Size and upwelling control of the stable isotope composition of *Neogloboquadrina dutertrei* (d'Orbigny), *Globigerinoides ruber* (d'Orbigny) and *Globingerina bulloides* (d'Orbigny): examples from the Panama Basin and Arabian Sea. Journal of Foraminiferal Research 25, 39-52.

Kroopnick, P.M., 1985. The distribution of ^{13}C of ΣCO_2 in the world oceans. Deep Sea Research Part A. Oceanographic Research Papers 32, 57-84.

Kucera, M., 2007. Chapter Six Planktonic Foraminifera as Tracers of Past Oceanic Environments. Developments in Marine Geology 1, 213-262.

Kuehn, H., Lembke-Jene, L., Gersonde, R., Esper, O., Lamy, F., Arz, H., Kuhn, G., Tiedemann, R., 2014. Laminated sediments in the Bering Sea reveal atmospheric teleconnections to Greenland climate on millennial to decadal timescales during the last deglaciation. Climate of the Past 10(6), 2215-2236. doi:10.5194/cp-10-2215-2014.

Kunioka, D., Shirai, K., Takahata, N., Sano, Y., Toyofuku, T., Ujiie, Y., 2006. Microdistribution of Mg/Ca, Sr/Ca, and Ba/Ca ratios in *Pulleniatina obliquiloculata* test by using a NanoSIMS: Implication for the vital effect mechanism. Geochemistry, Geophysics, Geosystems 7(12), 1525-2027. doi:10.1029/2006GC001280.

Kuroyanagi, A., Tsuchiya, M., Kawahata, H., Kitazato, H., 2008. The occurrence of two genotypes of the planktonic foraminifer *Globigerinoides ruber* (white) and paleo-environmental implications. Marine Micropaleontology 68(3-4), 236-243. doi:10.1016/j.marmicro.2008.04.004.

Le Borgne, R., Barber, R.T., Delcroix, T., Inoue, H.Y., Mackey, D.J., Rodier, M., 2002. Pacific warm pool and divergence: temporal and zonal variations on the equator and their effects on the biological pump. Deep Sea Research Part II: Topical Studies in Oceanography 49(13-14), 2471-2512. doi:10.1016/S0967-0645(02)00045-0.

Lea, D.W., Mashiotta, T.A., Spero, H.J., 1999. Controls on magnesium and strontium uptake in planktonic foraminifera determined by live culturing. Geochimica et Cosmochimica Acta 63, 2369-2379.

Lea, D.W., Pak, D.K., Spero, H.J., 2000. Climate impact of late Quaternary equatorial Pacific sea surface temperature variations. Science 289(5485), 1719-1724. doi:10.1126/science.289.5485.1719.

Leduc, G., Vidal, L., Tachikawa, K., Rostek, F., Sonzogni, C., Beaufort, L., Bard, E., 2007. Moisture transport across Central America as a positive feedback on abrupt climatic changes. Nature 445(7130), 908-911. doi:10.1038/nature05578.

Leduc, G., Vidal, L., Cartapanis, O., Bard, E., 2009. Modes of eastern equatorial Pacific thermocline variability: Implications for ENSO dynamics over the last glacial period. Paleoceanography 24(3), PA3202. doi:10.1029/2008PA001701.

Leduc, G., Vidal, L., Tachikawa, K., Bard, E., 2010. Changes in Eastern Pacific ocean ventilation at intermediate depth over the last 150 kyr BP. Earth and Planetary Science Letters 298(1-2), 217-228. doi:10.1016/j.epsl.2010.08.002.

Li, T., Zhao, J., Nan, Q., Sun, R., Yu, X., 2011. Palaeoproductivity evolution in the centre of the western Pacific warm pool during the last 250 ka. Journal of Quaternary Science 26(5), 478-484. doi:10.1002/jqs.1471.

Lin, H.-L., Wang, W.-C., Hung, G.-W., 2004. Seasonal variation of planktonic foraminiferal isotopic composition from sediment traps in the South China Sea. Marine Micropaleontology 53(3-4), 447-460. doi:10.1016/j.marmicro.2004.08.004.

Lisiecki, L.E., Raymo, M.E., 2005. A Pliocene-Pleistocene stack of 57 globally distributed benthic $\delta^{18}O$ records. Paleoceanography 20(1), PA1003. doi:10.1029/2004PA001071.

Lisiecki, L.E., 2010. A simple mixing explanation for late Pleistocene changes in the Pacific-South Atlantic benthic $\delta^{13}C$ gradient. Climate of the Past 6(3), 305-314. doi:10.5194/cp-6-305-2010.

Liu, Z., Yang, H., 2003. Extratropical control of tropical climate, the atmospheric bridge and oceanic tunnel. Geophysical Research Letters 30(5), 1230. doi:10.1029/2002GL016492.

Locarnini, R.A., Mishonov, A.V., Antonov, J.I., Boyer, T.P., Garcia, H.E., Baranova, O.K., Zweng, M.M., Johnson, D.R., 2010. World Ocean Atlas 2009, Volume 1: Temperature. In: Levitus, S. (Ed.), NOAA Atlas NESDIS, 68. U.S. Government Printing Office, Washington D.C., pp 184.

Locarnini, R.A., Mishonov, A.V., Antonov, J.I., Boyer, T.P., Garcia, H.E., Baranova, O.K., Zweng, M.M., Paver, C.R., Reagan, J.R., Johnson, D.R., Hamilton, M., Seidov, D., 2013. World Ocean Atlas 2013, Volume 1: Temperature. In: Levitus, S., Mishonov, A. (Eds.), NOAA Atlas NESDIS 73, MD, pp 40.

López-Otálvaro, G.-E., Flores, J.-A., Sierro, F.J., Cacho, I., 2008. Variations in coccolithophorid production in the Eastern Equatorial Pacific at ODP Site 1240 over the last seven glacial-interglacial cycles. Marine Micropaleontology 69(1), 52-69. doi:10.1016/j.marmicro.2007.11.009.

Loubere, P., 2001. Nutrient and oceanographic changes in the Eastern Equatorial Pacific from the last full Glacial to the Present. Global and Planetary Change 29(1-2), 77-98. doi:10.1016/S0921-8181(00)00085-0.

Loubere, P., Fariduddin, M., Murray, R.W., 2003. Patterns of export production in the eastern equatorial Pacific over the past 130,000 years. Paleoceanography 18(2), 1028. doi:10.1029/2001PA000658.

Loubere, P., Richaud, M., Mireles, S., 2007. Variability in tropical thermocline nutrient chemistry on the glacial/interglacial timescale. Deep Sea Research Part II: Topical Studies in Oceanography 54(5-7), 747-761. doi:10.1016/j.dsr2.2007.01.005.

Loubere, P., Fariduddin, M., Richaud, M., 2011. Glacial marine nutrient and carbon redistribution: Evidence from the tropical ocean. Geochemistry, Geophysics, Geosystems 12(8), Q08013. doi:10.1029/2011GC003546.

Lund, D.C., Mix, A.C., 1998. Millennial-scale deep water oscillations: Reflections of the North Atlantic in the deep Pacific from 10 to 60 ka. Paleoceanography 13(1), 10-19.

Luthi, D., Le Floch, M., Bereiter, B., Blunier, T., Barnola, J.-M., Siegenthaler, U., Raynaud, D., Jouzel, J., Fischer, H., Kawamura, K., Stocker, T.F., 2008. High-resolution carbon dioxide concentration record 650,000-800,000 years before present. Nature 453(7193), 379-382. doi:10.1038/nature06949.

Lutze, G., Thiel, H., 1989. Epibenthic foraminifera from elevated microhabitats: *Cibicidoides wuellerstorfi* and *Planulina ariminensis*. Journal of Foraminiferal Research 19, 153-158.

Lynch-Stieglitz, J., Fairbanks, R.G., Charles, C.D., 1994. Glacial-interglacial history of Antarctic Intermediate Water: Relative strengths of Antarctic versus Indian Ocean sources. Paleoceanography 9(1), 7-29. doi:10.1029/93PA02446.

Lynch-Stieglitz, J., Stocker, T.F., Broecker, W.S., Fairbanks, R.G., 1995. The influence of air-sea exchange on the isotopic composition of oceanic carbon: Observations and modeling. Global Biogeochemical Cycles 9(4), 653-665. doi:10.1029/95GB02574.

Lynch-Stieglitz, J., Polissar, P.J., Jacobel, A.W., Hovan, S.A., Pockalny, R.A., Lyle, M., Murray, R.W., Ravelo, A.C., Bova, S.C., Dunlea, A.G., Ford, H.L., Hertzberg, J.E., Wertman, C.A., Maloney, A.E., Shackford, J.K., Wejnert, K., Xie, R.C., 2015. Glacial-interglacial changes in central tropical Pacific surface seawater property gradients. Paleoceanography 30(5), 423-438. doi:10.1002/2014PA002746.

Mackensen, A., 2012. Strong thermodynamic imprint on recent bottom-water and epibenthic $\delta^{13}C$ in the Weddell Sea revealed: Implications for glacial Southern Ocean ventilation. Earth and Planetary Science Letters 317–318, 20-26. doi:10.1016/j.epsl.2011.11.030.

Mackensen, A., Hubberten, H.W., Bickert, T., Fischer, G., Fütterer, D.K., 1993. The $\delta^{13}C$ in benthic foraminiferal tests of *Fontbotia wuellerstorfi* (Schwager) relative to the $\delta^{13}C$ of dissolved inorganic carbon in Southern Ocean Deep Water: Implications for glacial ocean circulation models. Paleoceanography 8(5), 587-610. doi:10.1029/93PA01291.

Mackensen, A., Schumacher, S., Radke, J., Schmidt, D.N., 2000. Microhabitat preferences and stable carbon isotopes of endobenthic foraminifera: clue to quantitative reconstruction of oceanic new production? Marine Micropaleontology 40, 233-258.

Mackensen, A., Rudolph, M., Kuhn, G., 2001. Late Pleistocene deep-water circulation in the subantarctic eastern Atlantic. Global and Planetary Change 30(3-4), 197-229. doi:10.1016/S0921-8181(01)00102-3.

Mackey, D.J., Parslow, J., Higgins, H.W., Griffiths, F.B., O'Sullivan, J.E., 1995. Plankton productivity and biomass in the western equatorial Pacific: Biological and physical controls. Deep Sea Research Part II: Topical Studies in Oceanography 42(2), 499-533. doi:10.1016/0967-0645(95)00038-R.

Mackey, D.J., O'Sullivan, J.E., Watson, R.J., 2002. Iron in the western Pacific: a riverine or hydrothermal source for iron in the Equatorial Undercurrent? Deep Sea Research Part I: Oceanographic Research Papers 49(5), 877-893. doi:10.1016/S0967-0637(01)00075-9.

Marchant, M., Hebbeln, D., Wefer, G., 1998. Seasonal flux patterns of planktonic foraminifera in the Peru–Chile current. Deep Sea Research Part I: Oceanographic Research Papers 45(7), 1161-1185. doi:10.1016/S0967-0637(98)00009-0.

Marchitto, T.M., Lehman, S.J., Ortiz, J.D., Flückiger, J., van Geen, A., 2007. Marine radiocarbon evidence for the mechanism of deglacial atmospheric CO_2 rise. Science 316, 1456-1459. doi:10.1126/science.1138679.

Martin, J.H., Coale, K.H., Johnson, K.S., Fitzwater, S.E., Gordon, R.M., Tanner, S.J., Hunter, C.N., Elrod, V.A., Nowicki, J.L., Coley, T.L., Barber, R.T., Lindley, S., Watson, A.J., Van Scoy, K., Law, C.S., Liddicoat, M.I., Ling, R., Stanton, T., Stockel, J., Collins, C., Anderson, A., Bidigare, R., Ondrusek, M., Latasa, M., Millero, F.J., Lee, K., Yao, W., Zhang, J.Z., Friederich, G., Sakamoto, C., Chavez, F., Buck, K., Kolber, Z., Greene, R., Falkowski, P., Chisholm, S.W., Hoge, F., Swift, R., Yungel, J., Turner, S., Nightingale, P., Hatton, A., Liss, P., Tindale, N.W., 1994. Testing the iron hypothesis in ecosystems of the equatorial Pacific Ocean. Nature 371(6493), 123-129. doi:10.1038/371123a0.

Martínez-Botí, M.A., Marino, G., Foster, G.L., Ziveri, P., Henehan, M.J., Rae, J.W.B., Mortyn, P.G., Vance, D., 2015. Boron isotope evidence for oceanic carbon dioxide leakage during the last deglaciation. Nature 518(7538), 219-222. doi:10.1038/nature14155.

Matsumoto, K., Oba, T., Lynch-Stieglitz, J., Yamamoto, H., 2002a. Interior hydrography and circulation of the glacial Pacific Ocean. Quaternary Science Reviews 21(14-15), 1693-1704. doi:10.1016/S0277-3791(01)00142-1.

Matsumoto, K., Sarmiento, J.L., Brzezinski, M.A., 2002b. Silicic acid leakage from the Southern Ocean: A possible explanation for glacial atmospheric pCO_2. Global Biogeochemical Cycles 16, doi:10.1029/2001GB001442.

Matul, A.G., Abelmann, A., Gersonde, R., Nürnberg, D., Tiedemann, R., Kruglikova, S.B., 2015. Late quaternary distribution of the *Cycladophora davisiana* radiolarian species: Reflection of possible ventilation of the North Pacific intermediate water during the Last Glacial Maximum. Oceanology 55(1), 91-99. doi:10.1134/s0001437015010130.

Max, L., Riethdorf, J.-R., Tiedemann, R., Smirnova, M., Lembke-Jene, L., Fahl, K., Nürnberg, D., Matul, A., Mollenhauer, G., 2012. Sea surface temperature variability and sea-ice extent in the

subarctic northwest Pacific during the past 15,000 years. Paleoceanography 27, PA3213. doi:10.1029/2012PA002292.

Max, L., Lembke-Jene, L., Riethdorf, J.R., Tiedemann, R., Nürnberg, D., Kühn, H., Mackensen, A., 2014. Pulses of enhanced North Pacific Intermediate Water ventilation from the Okhotsk Sea and Bering Sea during the last deglaciation. Climate of the Past 10(2), 591-605. doi:10.5194/cp-10-591-2014.

Max, L., Rippert, N., Lembke-Jene, L., Tiedemann, R., Cacho, I., Mackensen, A., Nürnberg, D., Evidence for enhanced convection of North Pacific Intermediate Water to the low-latitude Pacific under glacial conditions. *Under review* at Paloceanography.

McCartney, M.S., 1977. Subantarctic mode water. In: Angel, M.V. (Ed.), A Voyage of Discovery: George Deacon 70th Anniversary Volume. Pergamon Press, Oxford, pp. 103-119.

McCave, I.N., Carter, L., Hall, I.R., 2008. Glacial–interglacial changes in water mass structure and flow in the SW Pacific Ocean. Quaternary Science Reviews 27(19-20), 1886-1908. doi:10.1016/j.quascirev.2008.07.010.

McCrea, 1950. On the isotopic chemistry of carbonates and a paleotemperature scale. The Journal of Chemical Physics 18, 849-857.

McCreary, J.P., Lu, P., 1994. Interaction between the Subtropical and Equatorial Ocean Circulations: The Subtropical Cell. Journal of Physical Oceanography 24(2), 466-497. doi:10.1175/1520-0485(1994)024<0466:IBTSAE>2.0.CO;2.

McGregor, S., Timmermann, A., Stuecker, M.F., England, M.H., Merrifield, M., Jin, F.-F., Chikamoto, Y., 2014. Recent Walker circulation strengthening and Pacific cooling amplified by Atlantic warming. Nature Climate Change 4(10), 888-892. doi:10.1038/nclimate2330.

Méheust, M., Stein, R. Fahl, K., Max, L., Riethdorf, J.R., 2016. High-resolution IP25-based reconstruction of sea-ice variability in the western North Pacific and Bering Sea during the past 18,000 years. Geo-Marine Letters 36(2), 1-11. doi:10.1007/s00367-015-0432-4.

Mewes, A., Langer, G., Thoms, S., Nehrke, G., Reichart, G.-J., de Nooijer, L.J., Bijma, J., 2015. Impact of seawater [Ca^{2+}] on the calcification and calcite Mg/Ca of *Amphistegina lessonii*. Biogeosciences 12(7), 2153-2162. doi:10.5194/bg-12-2153-2015.

Minas, H.J., Minas, M., Packard, T.T., 1986. Productivity in upwelling areas deduced from hydrographic and chemical fields. Limnology and Oceanography 31(6), 1182-1206. doi:10.4319/lo.1986.31.6.1182.

Mix, A.C., Pisias, N.G., Zahn, R., Rugh, W., Lopez, C., Nelson, K., 1991. Carbon 13 in Pacific deep and intermediate waters, 0-370 ka: Implications for ocean circulation and Pleistocene CO_2. Paleoceanography 6(2), 205-226. doi:10.1029/90PA02303.

Mix, A.C., Tiedemann, R., Blum, P., 2003. Shipboard Scientific Party. Leg 202 summary. Ocean Drilling Program, College Station, Texas, pp. 1-145.

Mohtadi, M., Steinke, S., Groeneveld, J., Fink, H.G., Rixen, T., Hebbeln, D., Donner, B., Herunadi, B., 2009. Low-latitude control on seasonal and interannual changes in planktonic foraminiferal flux and shell geochemistry off south Java: A sediment trap study. Paleoceanography 24(1), PA1201. doi:10.1029/2008PA001636.

Mook, W.G., Bommerso J.C., Staverma, W.H., 1974. Carbon isotope fractionation between dissolved bicarbonate and gaseous carbon-dioxide. Earth Planetary Science Letters 22, 169-176.

Morey, A.E., Mix, A.C., Pisias, N.G., 2005. Planktonic foraminiferal assemblages preserved in surface sediments correspond to multiple environment variables. Quaternary Science Reviews 24(7-9), 925-950. doi:10.1016/j.quascirev.2003.09.011.

Mulitza, S., Wolff, T., Pätzold, J., Hale, W., Wefer, G., 1998. Temperature sensitivity of planktonic foraminifera and its influence on the oxygen isotope record. Marine Micropaleontology 33(3-4), 223-240. doi:10.1016/S0377-8398(97)00040-6.

Mulitza, S., Donner, B., Fischer, G., Paul, A., Pätzold, J., Rühlemann, C., Segl, M., 2004. The South Atlantic oxygen isotope record of planktic foraminifera. In: Wefer, G., Mulitza, S., Ratmeyer, V. (Eds.), The South Atlantic in the Late Quaternary: Reconstruction of material budgets and current systems. Springer, Berlin, pp. 121-142.

Muratli, J.M., Chase, Z., Mix, A.C., McManus, J., 2010. Increased glacial-age ventilation of the Chilean margin by Antarctic Intermediate Water. Nature Geosciences 3(1), 23-26. doi:10.1038/ngeo715.

NASA Ocean Biology, 2015. Sea-viewing Wide Field-of-view Sensor (SeaWiFS) Ocean Color Data, 2014.0 Reprocessing. NASA OB.DAAC, Greenbelt, MD, USA. doi: 10.5067/ORBVIEW-2/SEAWIFS_OC.2014.0.

Nehrke, G., Keul, N., Langer, G., de Nooijer, L.J., Bijma, J., Meibom, A., 2013. A new model for biomineralization and trace-element signatures of Foraminifera tests. Biogeosciences 10(10), 6759-6767. doi:10.5194/bg-10-6759-2013.

Ni, Y., Foster, G.L., Bailey, T., Elliott, T., Schmidt, D.N., Pearson, P., Haley, B., Coath, C., 2007. A core top assessment of proxies for the ocean carbonate system in surface-dwelling foraminifers. Paleoceanography 22(3), PA3212. doi:10.1029/2006PA001337.

Niebler, H.S., Hubberten, H.W., Gersonde, R., 1999. Oxygen isotope values of planktic foraminifera: A tool for the reconstruction of surface water stratification. In: Fischer, G., Wefer, G. (Eds.), Use of Proxies in Paleoceanography. Springer, Berlin Heidelberg, pp. 165-189.

Ninkovich, D., Shackleton, N.J., 1975. Distribution, stratigraphic position and age of ash layer “L”, in the Panama Basin region. Earth and Planetary Science Letters 27, 20-34.

NOAA, 2015a. Oceanic Niño Index. http://www.cpc.ncep.noaa.gov/products/analysis_monitoring/ensostuff/ensoyears.shtml.

NOAA, 2015b. Equatorial Pacific Zonal Wind field. https://www.ncdc.noaa.gov/teleconnections/enso/indicators/uwind.php.

NOAA, 2016. Global impacts of El Niño and La Niña. https://www.climate.gov/news-features/featured-images/global-impacts-el-ni%C3%B1o-and-la-ni%C3%B1a.

Noble, T.L., Piotrowski, A.M., McCave, I.N., 2013. Neodymium isotopic composition of intermediate and deep waters in the glacial southwest Pacific. Earth and Planetary Science Letters 384, 27-36. doi:10.1016/j.epsl.2013.10.010.

Nürnberg, D., 1995. Magnesium in tests of *Neogloboquadrina pachyderma* sinistral from high northern and southern latitudes. Journal of Foraminiferal Research 25(4), 350-368. doi:10.2113/gsjfr.25.4.350.

Nürnberg, D., Bijma, J., Hemleben, C., 1996. Assessing the reliability of magnesium in foraminiferal calcite as a proxy for water mass temperatures. Geochimica et Cosmochimica Acta 60(5), 803-814. doi:10.1016/0016-7037(95)00446-7.

Nürnberg, D., Müller, A., Schneider, R.R., 2000. Paleo-sea surface temperature calculations in the equatorial east Atlantic from Mg/Ca ratios in planktic foraminifera: A comparison to sea surface temperature estimates from $U_{37}^{K'}$, oxygen isotopes, and foraminiferal transfer function. Paleoceanography 15(1), 124-134. doi:10.1029/1999PA000370.

Nürnberg, D., Dethleff, D., Tiedemann, R., Kaiser, A., Gorbarenko, S.A., 2011. Okhotsk Sea ice coverage and Kamchatka glaciation over the last 350 ka — Evidence from ice-rafted debris and planktonic $\delta^{18}O$. Palaeogeography, Palaeoclimatology, Palaeoecology 310(3-4), 191-205. doi:10.1016/j.palaeo.2011.07.011.

Nürnberg, D., Böschen, T., Doering, K., Mollier-Vogel, E., Raddatz, J., Schneider, R., 2015. Sea surface and subsurface circulation dynamics off equatorial Peru during the last ~17 kyr. Paleoceanography 30, PA002706. doi:10.1002/2014PA002706.

Okazaki, Y., Sagawa, T., Asahi, H., Horikawa, K., Onodera, J., 2012. Ventilation changes in the western North Pacific since the last glacial period. Climate of the Past 8(1), 17-24. doi:10.5194/cp-8-17-2012.

Oppo, D.W., Fairbanks, R.G., 1989. Carbon isotope composition of tropical surface water during the past 22,000 years. Paleoceanography 4(4), 333-351. doi:10.1029/PA004i004p00333.

Oppo, D.W., Fairbanks, R.G., 1990. Atlantic Ocean thermohaline circulation of the last 150,000 years: Relationship to climate and atmospheric CO_2. Paleoceanography 5(3), 277-288. doi:10.1029/PA005i003p00277.

Orsi, A.H., Johnson, G.C., Bullister, J.L., 1999. Circulation, mixing, and production of Antarctic Bottom Water. Progress in Oceanography 43(1), 55-109. doi:10.1016/S0079-6611(99)00004-X.

Ortiz, J.D., Mix, A.C., Rugh, W., Watkins, J.M., Collier, R.W., 1996. Deep-dwelling planktonic foraminifera of the northeastern Pacific Ocean reveal environmental control of oxygen and carbon isotopic disequilibria. Geochimica et Cosmochimica Acta 60(22), 4509-4523. doi:10.1016/S0016-7037(96)00256-6.

Pahnke, K., Zahn, R., 2005. Southern Hemisphere water mass conversion linked with North Atlantic climate variability. Science 307(5716), 1741-1746. doi:10.1126/science.1102163.

Pahnke, K., Sachs, J.P., Keigwin, L., Timmermann, A., Xie, S.-P., 2007. Eastern tropical Pacific hydrologic changes during the past 27,000 years from D/H ratios in alkenones. Paleoceanography 22(4), PA4214. doi:10.1029/2007PA001468.

Pahnke, K., Goldstein, S.L., Hemming, S.R., 2008. Abrupt changes in Antarctic Intermediate Water circulation over the past 25,000 years. Nature Geoscience 1(12), 870-874. doi:10.1038/ngeo360.

Paillard, D., Labeyrie, L., Yiou, P., 1996. Macintosh program performs time-series analysis, Eos, Transactions American Geophysical Union 77(39), 379-379. doi:10.1029/96EO00259.

Pena, L.D., Cacho, I., Ferretti, P., Hall, M.A., 2008. El Niño-Southern Oscillation-like variability during glacial terminations and interlatitudinal teleconnections. Paleoceanography 23(3), PA3101. doi:10.1029/2008PA001620.

Pena, L.D., Goldstein, S.L., Hemming, S.R., Jones, K.M., Calvo, E., Pelejero, C., Cacho, I., 2013. Rapid changes in meridional advection of Southern Ocean intermediate waters to the tropical Pacific during the last 30kyr. Earth and Planetary Science Letters 368(0), 20-32. doi:10.1016/j.epsl.2013.02.028.

Peterson, C.D., Lisiecki, L.E., Stern, J.V., 2014. Deglacial whole-ocean $\delta^{13}C$ change estimated from 480 benthic foraminiferal records. Paleoceanography 29(6), 549-563. doi:10.1002/2013PA002552.

Petit, J.R., Jouzel, J., Raynaud, D., Barkov, N.I., Barnola, J.M., Basile, I., Bender, M., Chappellaz, J., Davis, M., Delaygue, G., Delmotte, M., Kotlyakov, V.M., Legrand, M., Lipenkov, V.Y., Lorius, C., Pepin, L., Ritz, C., Saltzman, E., Stievenard, M., 1999. Climate and atmospheric history of the past 420,000 years from the Vostok ice core, Antarctica. Nature 399(6735), 429-436. doi:10.1038/20859.

Pichevin, L.E., Reynolds, B.C., Ganeshram, R.S., Cacho, I., Pena, L., Keefe, K., Ellam, R.M., 2009. Enhanced carbon pump inferred from relaxation of nutrient limitation in the glacial ocean. Nature 459(7250), 1114-1117. doi:10.1038/nature08101.

Qu, T., Lindstrom, E.J., 2004. Northward intrusion of Antarctic Intermediate Water in the western Pacific. Journal of Physical Oceanography 34(9), 2104-2118. doi:10.1175/1520-0485(2004)034<2104:NIOAIW>2.0.CO;2.

Qu, T., Gao, S., Fukumori, I., Fine, R.A., Lindstrom, E.J., 2009. Origin and pathway of equatorial 13°C Water in the Pacific identified by a simulated passive tracer and its adjoint. Journal of Physical Oceanography 39(8), 1836-1853. doi:10.1175/2009JPO4045.1.

Radenac, M.-H., Rodier, M., 1996. Nitrate and chlorophyll distributions in relation to thermohaline and current structures in the western tropical Pacific during 1985-1989. Deep Sea Research Part II: Topical Studies in Oceanography 43(4-6), 725-752. doi:10.1016/0967-0645(96)00025-2.

Raddatz, J., Nürnberg, D., Tiedemann, R., Rippert, N., Southeastern marginal West Pacific Warm Pool seasurface and thermocline dynamics during the Pleistocene (2.5–0.5 Ma). *Submitted to* Palaeogeography, Palaeoclimatology, Palaeoecology.

Rafter, P.A., Sigman, D.M., 2015. Spatial distribution and temporal variation of nitrate nitrogen and oxygen isotopes in the upper equatorial Pacific Ocean. Limnology and Oceanography 61, 14-31. doi:10.1002/lno.10152.

Parker, F.L., 1962. Planktonic foraminiferal species in Pacific sediments. Micropaleontology 8, 219-254.

Ravelo, A.C., Fairbanks, R.G., 1992. Oxygen isotopic composition of multiple species of planktonic foraminifera: Recorders of the modern photic zone temperature gradient. Paleoceanography 7(6), 815-831. doi:10.1029/92PA02092.

Ravelo, A.C., Fairbanks, R.G., 1995. Carbon isotopic fractionation in multiple species of planktonic foraminifera from core-tops in the tropical Atlantic. The Journal of Foraminiferal Research 25(1), 53-74. doi:10.2113/gsjfr.25.1.53.

Ravelo, A.C., Fairbanks, R.G., Philander, S.G.H., 1990. Reconstructing tropical Atlantic hydrography using planktontic foraminifera and an ocean model. Paleoceanography 5(3), 409-431. doi:10.1029/PA005i003p00409.

Regenberg, M., Steph, S., Nürnberg, D., Tiedemann, R., Garbe-Schönberg, D., 2009. Calibrating Mg/Ca ratios of multiple planktonic foraminiferal species with δ^{18}O-calcification temperatures: Paleothermometry for the upper water column. Earth and Planetary Science Letters 278(3-4), 324-336. doi:10.1016/j.epsl.2008.12.019.

Reichart, G.-J., Jorissen, F., Anschutz, P., Mason, P.R.D., 2003. Single foraminiferal test chemistry records the marine environment. Geology 31(4), 355-358. doi:10.1130/0091-7613(2003)031<0355:sftcrt>2.0.co;2.

Reid, J.L., 1965. Intermediate water of the Pacific Ocean. Johns Hopkins Oceanographic Studies No 2, John Hopkins Press, Baltimore, Maryland, pp 85.

Rella, S.F., Tada, R., Nagashima, K., Ikehara, M., Itaki, T., Ohkushi, K.i., Sakamoto, T., Harada, N., Uchida, M., 2012. Abrupt changes of intermediate water properties on the northeastern slope of the Bering Sea during the last glacial and deglacial period. Paleoceanography 27(3), PA3203. doi:10.1029/2011PA002205.

Reverdin, G., Morliere, A., Gerard, E., 1991. Compagne Oceanographique Trans-Pacifique (janvier–mars 1991). Receuil de données. Rapport interne LODYC 91/13, University of Paris, pp 341.

Rickaby, R.E.M., Elderfield, H., 2005. Evidence from the high-latitude North Atlantic for variations in Antarctic Intermediate water flow during the last deglaciation. Geochemistry, Geophysics, Geosystems 6(5), Q05001. doi:10.1029/2004GC000858.

Riethdorf, J.-R., Nürnberg, D., Max, L., Tiedemann, R., Gorbarenko, S.A., Malakhov, M.I., 2013. Millennial-scale variability of marine productivity and terrigenous matter supply in the western Bering Sea over the past 180 kyr. Climate of the Past 9(3), 1345-1373. doi:10.5194/cp-9-1345-2013.

Riethdorf, J.-R., Thibodeau, B., Ikehara, M., Nürnberg, D., Max, L., Tiedemann, R., Yokoyama, Y., 2016. Surface nitrate utilization in the Bering Sea since 180 ka BP: Insight from sedimentary nitrogen isotopes. Deep Sea Research Part II: Topical Studies in Oceanography, 125–126, 163-176. doi:10.1016/j.dsr2.2015.03.007.

Rincón-Martínez, D., Steph, S., Lamy, F., Mix, A., Tiedemann, R., 2011. Tracking the equatorial front in the eastern equatorial Pacific Ocean by the isotopic and faunal composition of planktonic foraminifera. Marine Micropaleontology 79(1-2), 24-40. doi:10.1016/j.marmicro. 2011.01.001.

Rippert, N., Baumann, K.-H., Pätzold, J., 2015. Thermocline fluctuations in the western tropical Indian Ocean during the past 35 ka. Journal of Quaternary Science 30(3), 201-210. doi:10.1002/jqs.2767.

Rippert, N., Nürnberg, D., Raddatz, J., Maier, E., Hathorne, E., Bijma, J., Tiedemann, R., 2016. Constraining foraminiferal calcification depths in the western Pacific warm pool. Marine Micropaleontology 128, 14-27. doi:10.1016/j.marmicro.2016.08.004.

Robinson, R.S., Sigman, D.M., DiFiore, P.J., Rohde, M.M., Mashiotta, T.A., Lea, D.W., 2005. Diatom-bound N-15/N-14: New support for enhanced nutrient consumption in the ice age subantarctic. Paleoceanography 20, PA3003. doi:10.1029/2004PA001114.

Robinson, R.S., Martinez, P., Pena, L.D., Cacho, I., 2009. Nitrogen isotopic evidence for deglacial changes in nutrient supply in the eastern equatorial Pacific. Paleoceanography 24(4), PA4213. doi:10.1029/2008PA001702.

Robinson, R.S., Brzezinski, M.A., Beucher, C.P., Horn, M.G.S., Bedsole, P., 2014. The changing roles of iron and vertical mixing in regulating nitrogen and silicon cycling in the Southern Ocean over the last glacial cycle. Paleoceanography 29(12), 1179–1195. doi:10.1002/ 2014PA002686.

Rohling, E.J., Cook, S., 1999. Stable oxygen and carbon isotope ratios in foraminiferal carbonate. In: Sen Gupta, B.K. (Ed.), Modern Foraminifera. Kluwer Academic Dordrecht, pp. 239-258.

Ronge, T.A., Steph, S., Tiedemann, R., Prange, M., Merkel, U., Nürnberg, D., Kuhn, G., 2015. Pushing the boundaries: Glacial/interglacial variability of intermediate and deep waters in the southwest Pacific over the last 350,000 years. Paleoceanography 30(2), 23-38. doi:10.1002/2014PA002727.

Ronge, T.A., Tiedemann, R., Lamy, F., Kohler, P., Alloway, B.V., De Pol-Holz, R., Pahnke, K., Southon, J., Wacker, L., 2016. Radiocarbon constraints on the extent and evolution of the South Pacific glacial carbon pool. Nature Communications 7. doi:10.1038/ncomms11487.

Rosenthal, Y., Boyle, E.A., Slowey, N., 1997. Temperature control on the incorporation of magnesium, strontium, fluorine, and cadmium into benthic foraminiferal shells from Little Bahama Bank: Prospects for thermocline paleoceanography. Geochimica et Cosmochimica Acta 61(17), 3633-3643. doi:10.1016/S0016-7037(97)00181-6.

Rosenthal, Y., Linsley, B.K., Oppo, D.W., 2013. Pacific Ocean Heat Content During the Past 10,000 Years. Science 342(6158), 617-621. doi:10.1126/science.1240837.

Rousseau, J., Ellwood, M.J., Bostock, H., Neil, H., 2016. Estimates of late Quaternary mode and intermediate water silicic acid concentration in the Pacific Southern Ocean. Earth and Planetary Science Letters 439, 101-108. doi:10.1016/j.epsl.2016.01.023.

Rowe, G.D., Firing, E., Johnson, G.C., 2000. Pacific Equatorial Subsurface Countercurrent Velocity, Transport, and Potential Vorticity. Journal of Physical Oceanography 30(6), 1172-1187. doi:10.1175/1520-0485(2000)030<1172:PESCVT>2.0.CO;2.

Russell, A.D., Hönisch, B., Spero, H.J., Lea, D.W., 2004. Effects of seawater carbonate ion concentration and temperature on shell U, Mg, and Sr in cultured planktonic foraminifera. Geochimica et Cosmochimica Acta 68(21), 4347-4361. doi:10.1016/j.gca.2004.03.013.

Russon, T., Elliot, M., Sadekov, A., Cabioch, G., Corrège, T., De Deckker, P., 2010. Inter-hemispheric asymmetry in the early Pleistocene Pacific warm pool. Geophysical Research Letters 37(11), L11601. doi:10.1029/2010GL043191.

Ryan, J.P., Ueki, I., Chao, Y., Zhang, H., Polito, P.S., Chavez, F.P., 2006. Western Pacific modulation of large phytoplankton blooms in the central and eastern equatorial Pacific. Journal of Geophysical Research: Biogeosciences 111(G2), G02013. doi:10.1029/2005JG000084.

Sadekov, A.Y., Ganeshram, R., Pichevin, L., Berdin, R., McClymont, E., Elderfield, H., Tudhope, A.W., 2013. Palaeoclimate reconstructions reveal a strong link between El Nino-Southern Oscillation and Tropical Pacific mean state. Nature Communications 4, 2692. doi:10.1038/ncomms3692.

Sagawa, T., Yokoyama, Y., Ikehara, M., Kuwae, M., 2012. Shoaling of the western equatorial Pacific thermocline during the last glacial maximum inferred from multispecies temperature reconstruction of planktonic foraminifera. Palaeogeography, Palaeoclimatology, Palaeoecology 346-347(0), 120-129. doi:10.1016/j.palaeo.2012.06.002.

Sallée, J.-B., Speer, K., Rintoul, S., Wijffels, S., 2010. Southern Ocean thermocline ventilation. Journal of Physical Oceanography 40(3), 509-529. doi:10.1175/2009JPO4291.1.

Sanyal, A., Bijma, J., 1999. A comparative study of the northwest Africa and eastern equatorial Pacific upwelling zones as sources of CO_2 during glacial periods based on boron isotope paleo-pH estimation. Paleoceanography 14(6), 753-759. doi:10.1029/1999PA900036.

Sarmiento, J.L., Toggweiler, J.R., 1984. A new model for the role of the oceans in determining atmospheric pCO_2. Nature 308(5960), 621-624. doi:10.1038/308621a0.

Sarmiento, J.L., Gruber, N., Brzezinski, M.A., Dunne, J.P., 2004. High-latitude controls of thermocline nutrients and low latitude biological productivity. Nature 427(6969), 56-60. doi:10.1038/nature02127.

Sarnthein, M., Winn, K., Jung, S.J.A., Duplessy, J.-C., Labeyrie, L., Erlenkeuser, H., Ganssen, G., 1994. Changes in East Atlantic deepwater circulation over the last 30,000 years: Eight time slice reconstructions. Paleoceanography 9(2), 209-267. doi:10.1029/93PA03301.

Schiebel, R., 2002. Planktic foraminiferal sedimentation and the marine calcite budget. Global Biogeochemical Cycles 16(4), 1065. doi:10.1029/2001GB001459.

Schiebel, R., Hemleben, C., 2005. Modern planktic foraminifera. Paläontologische Zeitschrift, Schweizerbart'sche Verlagsbuchhandlung, Stuttgart, pp. 135-148.

Schiebel, R., Waniek, J., Bork, M., Hemleben, C., 2001. Planktic foraminiferal production stimulated by chlorophyll redistribution and entrainment of nutrients. Deep Sea Research Part I: Oceanographic Research Papers 48(3), 721-740. doi:10.1016/S0967-0637(00)00065-0.

Schiraldi, B., Sikes, E.L., Elmore, A.C., Cook, M.S., Rose, K.A., 2014. The Southwest Pacific subtropics responds to the last deglacial warming with changes in shallow water sources. Paleoceanography 29, 595-611. doi:10.1002/2013PA002584.

Schlitzer, R., 2015. Ocean Data View, http://odv.awi.de.

Schlung, S.A., Ravelo, C.A., Aiello, I.W., Andreasen, D.H., Cook, M.S., Drake, M., Dyez, K.A., Guilderson, T.P., LaRiviere, J.P., Stroynowski, Z., Takahashi, K., 2013. Millennial-scale climate change and intermediate water circulation in the Bering Sea from 90 ka: A high-resolution record from IODP Site U1340. Paleoceanography 28(1), 54-67. doi:10.1029/2012 PA002365.

Schmidt, G.A., Bigg, G.R., Rohling, E.J., 1999. Global Seawater Oxygen-18 Database- v1.21. http://data.giss.nasa.gov/o18data/.

Schmittner, A., Gruber, N., Mix, A.C., Key, R.M., Tagliabue, A., Westberry, T.K., 2013. Biology and air-sea gas exchange controls on the distribution of carbon isotope ratios ($\delta^{13}C$) in the ocean. Biogeosciences 10(9), 5793-5816. doi:10.5194/bg-10-5793-2013.

Schmuker, B., Schiebel, R., 2002. Planktonic foraminifers and hydrography of the eastern and northern Caribbean Sea. Marine Micropaleontology 46(3-4), 387-403. doi:10.1016/S0377-8398(02)00082-8.

Schweizer, M., Pawlowski, J., Kouwenhoven, T., van der Zwaan, B., 2009. Molecular phylogeny of common *Cibicidids* and related *Rotaliida* (Foraminifera) based on small subunit rDNA sequences. Journal of Foraminiferal Research 39(4), 300-315. doi:10.2113/gsjfr.39.4.300.

Shaari, H.b., Yamamoto, M., Irino, T., 2013. Enhanced upwelling in the eastern equatorial Pacific at the last five glacial terminations. Palaeogeography, Palaeoclimatology, Palaeoecology 386, 8-15. doi:10.1016/j.palaeo.2013.03.022.

Shackleton, N.J., 1967. Oxygen isotope analyses and Pleistocene temperatures re-assessed. Nature 215(5096), 15-17.

Shackleton, N.J., 1974. Attainment of isotopic equilibrium between ocean water and the benthic foraminifera genua *Uvigerina*: isotopic changes in the ocean during the last glacial. Centre Natl. Rech. Sci. Coll. Inter 219, 203-209.

Shcherbina, A.Y., Talley, L.D., Rudnick, D.L., 2003. Direct observations of North Pacific ventilation: brine rejection in the Okhotsk Sea. Science 302(5652), 1952-1955. doi:10.1126/science.1088692.

Siegenthaler, U., 1979. Stable Hydrogen and Oxygen Isotopes in the Water Cycle. In: Jäger, E., Hunziker, J.C., (Eds.), Lectures in Isotope Geology. Springer, Berlin Heidelberg, pp. 264-273.

Siegenthaler, U., Wenk, T., 1984. Rapid atmospheric CO_2 variations and ocean circulation. Nature 308(5960), 624-626. doi:10.1038/308624a0.

Sigman, D.M., Boyle, E.A., 2000. Glacial/interglacial variations in atmospheric carbon dioxide. Nature 407(6806), 859-869. doi:10.1038/35038000.

Sigman, D.M., Hain, M.P., Haug, G.H., 2010. The polar ocean and glacial cycles in atmospheric CO_2 concentration. Nature 466(7302), 47-55. doi:10.1038/nature09149.

Skinner, L.C., Fallon, S., Waelbroeck, C., Michel, E., Barker, S., 2010. Ventilation of the Deep Southern Ocean and Deglacial CO_2 Rise. Science 328(5982), 1147-1151. doi:10.1126/ science.1183627.

Skinner, L., McCave, I.N., Carter, L., Fallon, S., Scrivner, A.E., Primeau, F., 2015. Reduced ventilation and enhanced magnitude of the deep Pacific carbon pool during the last glacial period. Earth and Planetary Science Letters 411, 45-52. doi:10.1016/j.epsl.2014.11.024.

Sloyan, B.M., Rintoul, S.R., 2001. Circulation, renewal, and modification of Antarctic Mode and Intermediate Water. Journal of Physical Oceanography 31(4), 1005-1030. doi:10.1175/1520-0485(2001)031<1005:CRAMOA>2.0.CO;2.

Spero, H.J., 1992. Do planktic foraminifera accurately record shifts in the carbon isotopic composition of seawater ΣCO_2? Marine Micropaleontology 19(4), 275-285. doi:10.1016/0377-8398(92)90033-G.

Spero, H.J., Lea, D.W., 1993. Intraspecific stable isotope variability in the planktic foraminifera *Globigerinoides sacculifer*: Results from laboratory experiments. Marine Micropaleontology 22(3), 221-234. doi:10.1016/0377-8398(93)90045-Y.

Spero, H.J., Lea, D.W., 2002. The cause of carbon isotope minimum events on glacial terminations. Science 296(5567), 522-525. doi:10.1126/science.1069401.

Spero, H.J., Parker, S.L., 1985. Photosynthesis in the symbiotic planktonic foraminifer *Orbulina universa*, and its potential contribution to oceanic primary productivity. Journal of Foraminiferal Research 15(4), 273-281. doi:10.2113/gsjfr.15.4.273.

Spero, H.J., Lerche, I., Williams, D.F., 1991. Opening the carbon isotope "vital effect" black box, 2, Quantitative model for interpreting foraminiferal carbon isotope data. Paleoceanography 6(6), 639-655. doi:10.1029/91PA02022.

Spero, H.J., Bijma, J., Lea, D.W., Bemis, B.E., 1997. Effect of seawater carbonate concentration on foraminiferal carbon and oxygen isotopes. Nature 390(6659), 497-500. doi:10.1038/37333.

Spero, H.J., Mielke, K.M., Kalve, E.M., Lea, D.W., Pak, D.K., 2003. Multispecies approach to reconstructing eastern equatorial Pacific thermocline hydrography during the past 360 kyr. Paleoceanography 18(1), 1022. doi:10.1029/2002PA000814.

Spero, H.J., Eggins, S.M., Russell, A.D., Vetter, L., Kilburn, M.R., Hönisch, B., 2015. Timing and mechanism for intratest Mg/Ca variability in a living planktic foraminifer. Earth and Planetary Science Letters 409(0), 32-42. doi:10.1016/j.epsl.2014.10.030.

Staines-Urías, F., González-Yajimovich, O., Beaufort, L., 2015. Reconstruction of past climate variability and ENSO-like fluctuations in the southern Gulf of California (Alfonso Basin) since the last glacial maximum. Quaternary Research 83(3), 488-501. doi:10.1016/j.yqres.2015.03.007.

Steinke, S., Chiu, H.-Y., Yu, P.-S., Shen, C.-C., Löwemark, L., Mii, H.-S., Chen, M.-T., 2005. Mg/Ca ratios of two *Globigerinoides ruber* (white) morphotypes: Implications for reconstructing past tropical/subtropical surface water conditions. Geochemistry, Geophysics, Geosystems 6(11), Q11005. doi:10.1029/2005GC000926.

Steinke, S., Prange, M., Feist, C., Groeneveld, J., Mohtadi, M., 2014. Upwelling variability off southern Indonesia over the past two millennia. Geophysical Research Letters 41(21), 7684-7693. doi:10.1002/2014GL061450.

Steph, S., Regenberg, M., Tiedemann, R., Mulitza, S., Nürnberg, D., 2009. Stable isotopes of planktonic foraminifera from tropical Atlantic/Caribbean core-tops: Implications for reconstructing upper ocean stratification. Marine Micropaleontology 71(1-2), 1-19. doi:10.1016/j.marmicro.2008.12.004.

Stott, L.D., Neumann, M., Hammond, D., 2000. Intermediate water ventilation on the Northeastern Pacific Margin during the Late Pleistocene inferred from benthic foraminiferal $\delta^{13}C$. Paleoceanography 15(2), 161-169. doi:10.1029/1999PA000375.

Stott, L., Poulsen, C., Lund, S., Thunell, R., 2002. Super ENSO and Global Climate Oscillations at Millennial Time Scales. Science 297(5579), 222-226. doi:10.1126/science.1071627.

Stott, L., Southon, J., Timmermann, A., Koutavas, A., 2009. Radiocarbon age anomaly at intermediate water depth in the Pacific Ocean during the last deglaciation. Paleoceanography 24, PA2223, doi:10.1029/2008PA001690.

Svensson, A., Andersen, K.K., Bigler, M., Clausen, H.B., Dahl-Jensen, D., Davies, S.M., Johnsen, S.J., Muscheler, R., Parrenin, F., Rasmussen, S.O., Röthlisberger, R., Seierstad, I., Steffensen, J.P., Vinther, B.M., 2008. A 60 000 year Greenland stratigraphic ice core chronology. Climate of the Past 4(1), 47-57. doi:10.5194/cp-4-47-2008.

Takahashi, T., Sutherland, S.C., Sweeney, C., Poisson, A., Metzl, N., Tilbrook, B., Bates, N., Wanninkhof, R., Feely, R.A., Sabine, C., Olafsson, J., Nojiri, Y., 2002. Global sea-air CO_2 flux based on climatological surface ocean pCO_2, and seasonal biological and temperature effects. Deep-Sea Research Part II-Topical Studies in Oceanography 49(9-10), 1601-1622. doi:10.1016/S0967-0645(02)00003-6.

Takahashi, T., Sutherland, S.C., Wanninkhof, R., Sweeney, C., Feely, R.A., Chipman, D.W., Hales, B., Friederich, G., Chavez, F., Sabine, C., Watson, A., Bakker, D.C.E., Schuster, U., Metzl, N., Yoshikawa-Inoue, H., Ishii, M., Midorikawa, T., Nojiri, Y., Körtzinger, A., Steinhoff, T., Hoppema, M., Olafsson, J., Arnarson, T.S., Tilbrook, B., Johannessen, T., Olsen, A., Bellerby, R., Wong, C.S., Delille, B., Bates, N.R., de Baar, H.J.W., 2009. Climatological mean and decadal change in surface ocean pCO_2, and net sea–air CO_2 flux over the global oceans. Deep Sea Research Part II: Topical Studies in Oceanography 56(8-10), 554-577. doi:10.1016/j.dsr2.2008.12.009.

Talley, L.D., 1991. An Okhotsk Sea water anomaly: implications for ventilation in the North Pacific. Deep Sea Research Part A: Oceanographic Research Papers 38, S171-S190. doi:10.1016/S0198-0149(12)80009-4.

Talley, L.D., 1993. Distribution and formation of North Pacific Intermediate Water. Journal of Physical Oceanography 23(3), 517-537. doi:10.1175/1520-0485(1993)023<0517:DAFONP>2.0.CO;2.

Talley, L.D., 2008. Freshwater transport estimates and the global overturning circulation: Shallow, deep and throughflow components. Progress in Oceanography 78(4), 257-303. doi:10.1016/j.pocean.2008.05.001.

Talley, L.D., 2013. Closure of the global overturning circulation through the Indian, Pacific, and Southern Oceans: Schematics and transports. Oceanography 26(1), 80–97. doi:10.5670/oceanog.2013.07.

Tanaka, S., Takahashi, K., 2005. Late Quaternary paleoceanographic changes in the Bering Sea and the western subarctic Pacific based on radiolarian assemblages. Deep Sea Research Part II: Topical Studies in Oceanography 52(16-18), 2131-2149. doi:10.1016/j.dsr2.2005.07.002.

Tapia, R., Nürnberg, D., Ronge, T., Tiedemann, R., 2015. Disparities in glacial advection of Southern Ocean Intermediate Water to the South Pacific Gyre. Earth and Planetary Science Letters 410, 152-164. doi:10.1016/j.epsl.2014.11.031.

Tapia, R., 2016. Paleo-Water Column Structure in the South Pacific: Evidence from Foraminiferal $\delta^{13}C$ and Mg/Ca. Dissertation, University of Kiel.

Tchernia, P., 1980. Descriptive Regional Oceanography. Pergamon Press, Oxford, pp 253.

Thunell, R.C., Honjo, S., 1981. Planktonic foraminiferal flux to the deep ocean: Sediment trap results from the tropical Atlantic and the central Pacific. Marine Geology 40(3-4), 237-253. doi:10.1016/0025-3227(81)90142-0.

Thunell, R.C., Curry, W.B., Honjo, S., 1983. Seasonal variation in the flux of planktonic foraminifera: time series sediment trap results from the Panama Basin. Earth and Planetary Science Letters 64(1), 44-55. doi:10.1016/0012-821X(83)90051-1.

Toggweiler, J.R., Russell, J.L., Carson, S.R., 2006. Midlatitude westerlies, atmospheric CO_2, and climate change during the ice ages. Paleoceanography 21(2), PA2005. doi:10.1029/2005PA001154.

Tomczak, M., Godfrey, J.S., 1994. Regional Oceanography: An Introduction. Pergamon, Oxford, pp. 422.

Tomczak, M., Godfrey, J.S., 2005. Regional Oceanography: an Introduction. Pergamon, Oxford, pp 390. pdf Version 1.1, http://suche.suub.uni-bremen.de/remote_access.php?http%3A%2F%2Fgaea.es.flinders.edu.au%2F~mattom%2Fregoc%2Fpdfversion.html.

Tsuchiya, M., 1972. A subsurface north equatorial countercurrent in the eastern Pacific ocean. Journal of Geophysical Research 77(30), 5981-5986. doi:10.1029/JC077i030p05981.

Urey, H.C., 1947. The thermodynamic properties of isotopic substances. Journal of the Chemical Society (Resumed), 562-581. doi:10.1039/JR9470000562.

Urey, H.C., Lowenstam, H.A., Epstein, S., McKinney, C.R., 1951. Measurement of paleotemperatures and temperatures of the Upper Cretaceous of England, Denmark, and the southeastern United States. Geological Society of America Bulletin 62(4), 399-416. doi:10.1130/0016-7606(1951)62[399:mopato]2.0.co;2.

Wang, L., 2000. Isotopic signals in two morphotypes of *Globigerinoides ruber* (white) from the South China Sea: implications for monsoon climate change during the last glacial cycle.

Palaeogeography, Palaeoclimatology, Palaeoecology 161(3-4), 381-394. doi:10.1016/S0031-0182(00)00094-8.

Wara, M.W., Ravelo, A.C., Delaney, M.L., 2005. Permanent El Niño-Like conditions during the Pliocene Warm Period. Science 309(5735), 758-761. doi:10.1126/science.1112596.

Watkins, J.M., Mix, A.C., Wilson, J., 1996. Living planktic foraminifera: tracers of circulation and productivity regimes in the central equatorial Pacific. Deep Sea Research Part II: Topical Studies in Oceanography 43(4-6), 1257-1282. doi:10.1016/0967-0645(96)00008-2.

Watkins, J.M., Mix, A.C., Wilson, J., 1998. Living planktonic foraminifera in the central tropical Pacific Ocean: articulating the equatorial 'cold tongue' during La Niña, 1992. Marine Micropaleontology 33(3-4), 157-174. doi:10.1016/S0377-8398(97)00036-4.

Wefer, G., 1985. Die Verteilung stabiler Isotope in Kalkschalen mariner Organismen. Geologisches Jahrbuch, Bundesanstalt für Geowissenschaften und Rohstoffe, Reihe A, Heft 82, pp. 114.

Wefer, G., Berger, W.H., 1991. Isotope paleontology: growth and composition of extant calcareous species. Marine Geology 100(1-4), 207-248. doi:10.1016/0025-3227(91)90234-U.

Wejnert, K.E., Thunell, R.C., Astor, Y., 2013. Comparison of species-specific oxygen isotope paleotemperature equations: Sensitivity analysis using planktonic foraminifera from the Cariaco Basin, Venezuela. Marine Micropaleontology 101, 76-88. doi:10.1016/j.marmicro. 2013.03.001.

Werner, R., Nürnberg, D., Hauff, F., Party, S.S.S., 2013. RV SONNE Fahrtbericht/Cruise Report SO225, Manihiki II Leg 2, The Manihiki Plateau - Origin, structure and effects of oceanic plateaus and Pleistocene dynamic of the West Pacific warm water pool; 19.11.2012 - 06.01.2013, Suva/Fiji - Auckland/New Zealand, GEOMAR Report. GEOMAR Helmholtz-Zentrum für Ozeanforschung, Kiel, Germany, pp 176.

Wilke, I., Meggers, H., Bickert, T., 2009. Depth habitats and seasonal distributions of recent planktonic foraminifers in the Canary Islands region (29°N) based on oxygen isotopes. Deep Sea Research Part I: Oceanographic Research Papers 56(1), 89-106. doi:10.1016/j.dsr. 2008.08.001.

Winckler, G., Anderson, R.F., Fleisher, M.Q., McGee, D., Mahowald, N., 2008. Covariant glacial-interglacial dust fluxes in the equatorial Pacific and Antarctica. Science 320(5872), 93-96. doi:10.1126/science.1150595.

Wyrtki, K., Kilonsky, B., 1984. Mean water and current structure during the Hawaii-to-Tahiti shuttle experiment. Journal of Physical Oceanography 14(2), 242-254. doi:10.1175/1520-0485(1984)014<0242:MWACSD>2.0.CO;2.

Xiong, Z., Li, T., Crosta, X., Algeo, T., Chang, F., Zhai, B., 2013. Potential role of giant marine diatoms in sequestration of atmospheric CO_2 during the Last Glacial Maximum: $\delta^{13}C$ evidence from laminated *Ethmodiscus rex* mats in tropical West Pacific. Global and Planetary Change 108, 1-14. doi:10.1016/j.gloplacha.2013.06.003.

Yamanaka, Y., Tajika, E., 1996. The role of the vertical fluxes of particulate organic matter and calcite in the oceanic carbon cycle: Studies using an ocean biogeochemical general circulation model. Global Biogeochemical Cycles 10(2), 361-382. doi:10.1029/96GB00634.

Yamasaki, M., Sasaki, A., Oda, M., Domitsu, H., 2008. Western equatorial Pacific planktic foraminiferal fluxes and assemblages during a La Niña year (1999). Marine Micropaleontology 66(3-4), 304-319. doi:10.1016/j.marmicro.2007.10.006.

Yan, X.H., Ho, C.R., Zheng, Q., Klemas, V., 1992. Temperature and size variabilities of the Western pacific warm pool. Science 258(5088), 1643-1645. doi:10.1126/science.258. 5088.1643.

Yu, J., Elderfield, H., 2008. Mg/Ca in the benthic foraminifera *Cibicidoides wuellerstorfi* and *Cibicidoides mundulus*: Temperature versus carbonate ion saturation. Earth and Planetary Science Letters 276(1-2), 129-139. doi:10.1016/j.epsl.2008.09.015.

Yu, P.-S., Kienast, M., Chen, M.-T., Cacho, I., Flores, J.A., Mohtadi, M., Mix, A.C., 2012. Influences of extratropical water masses on equatorial Pacific cold tongue variability during the past 160 ka as revealed by faunal evidence of planktic foraminifers. Journal of Quaternary Science 27(9), 921-931. doi:10.1002/jqs.2582.

Zahn, R., Winn, K., Sarnthein, M., 1986. Benthic foraminiferal $\delta^{13}C$ and accumulation rates of organic carbon: *Uvigerina peregrina* group and *Cibicidoides wuellerstorfi*. Paleoceanography 1(1), 27-42. doi:10.1029/PA001i001p00027.

Zahn, R., Pedersen, T.F., Bornhold, B.D., Mix, A.C., 1991. Water mass conversion in the glacial subarctic Pacific (54°N, 148°W): Physical constraints and the benthic-planktonic stable isotope record. Paleoceanography 6(5), 543-560. doi:10.1029/91PA01327.

Žarić, S., Donner, B., Fischer, G., Mulitza, S., Wefer, G., 2005. Sensitivity of planktonic foraminifera to sea surface temperature and export production as derived from sediment trap data. Marine Micropaleontology 55(1-2), 75-105. doi:10.1016/j.marmicro.2005.01.002.

Zeebe, R.E., Wolf-Gladrow, D., 2001. CO_2 in seawater: equilibrium, kinetics, isotopes. Elsevier Oceanography Book Series, Amsterdam, pp 346.

Zweng, M.M., Reagan, J.R., Antonov, J.I., Locarnini, R.A., Mishonov, A.V., Boyer, T.P., Garcia, H.E., Baranova, O.K., Johnson, D.R., Seidov, D., Biddle, M.M., 2013. World Ocean Atlas 2013, Volume 2: Salinity. In: Levitus, S., Mishonov, A. (Eds.), NOAA Atlas NESDIS. MD, pp 39.

Appendix

A.I. Co-authored ISI peer-reviewed publication

Southeastern marginal West Pacific Warm Pool sea-surface and thermocline dynamics during the Pleistocene (2.5-0.5 Ma)

Jacek Raddatz, Dirk Nürnberg, Ralf Tiedemann and Nadine Rippert

A.II. First author ISI peer-reviewed publication

Thermocline fluctuations in the western tropical Indian Ocean during the past 35 ka

Nadine Rippert, Karl-Heinz Baumann and Jürgen Pätzold

A.III. List of Abbreviations

A.I. Co-authored ISI peer-reviewed publication

Southeastern marginal West Pacific Warm Pool sea-surface and thermocline dynamics during the Pleistocene (2.5 – 0.5 Ma)

Jacek Raddatz[1,2,*] Dirk Nürnberg[1], Ralf Tiedemann[3] and Nadine Rippert[3]

[1]GEOMAR Helmholtz Centre for Ocean Research Kiel, Wischhofstr. 1-3, 24148 Kiel, Germany
[2]Goethe University Frankfurt, Institute of Geosciences, Altenhöferallee 1, 60438 Frankfurt am Main, Germany
[3]Alfred-Wegner-Institute Helmholtz Centre for Polar and Marine Research, 27570 Bremerhaven, Germany
*corresponding author: Jacek Raddatz, raddatz@em.uni-frankfurt.de

submitted to Paleogeography, Paleoclimatology, Paleoecology

Abstract

The internal development of the tropical West Pacific Warm Pool and its interaction with other ocean regions on geological timescales is only poorly constrained. Based on two newly recovered sediment cores from the southeastern margin of the West Pacific Warm Pool (northern and southern Manihiki Plateau), we provide new aspects on the dynamically interacting ocean circulation at surface, subsurface, thermocline, and deep thermocline levels during the Pleistocene (~2.5 – 0.5 Ma). Notably, the variability of thermocline and deep thermocline (~150– 400 m water depth) foraminiferal Mg/Ca-based temperatures with up to ~6°C amplitude variations exceeds those at shallower depths (down to ~120 m) with only ~2 – 3°C temperature variations. A major gradual reorganization of the West Pacific Warm Pool oceanography occurred during the transitional time period of ~1.7 – 1.35 Ma. Prior to ~1.7 Ma, pronounced meridional and latitudinal gradients in sea-surface to subsurface ocean properties point to the sustained eastward displacement of the West Pacific Warm Pool, with the South Pacific Convergence Zone being shifted further northeastward across Manihiki Plateau. Simultaneously, the low amplitude variations of thermocline and deep thermocline temperatures refer to an overall deep and stable thermocline. Our data further suggest that pronounced upper ocean temperature gradients between the Eastern and western equatorial Pacific were established by several hundred thousand years earlier than previously suspected, contradicting notions on permanent El Niño-like conditions until

~1.7 Ma. The meridional and zonal gradients in sea-surface and subsurface ocean properties diminished within the West Pacific Warm Pool, pointing to close-to-present-day temperature conditions particularly between ~1.7 – 1.35 Ma and ~0.9 – 0.75 Ma, and the more southward position of the warm South Pacific Convergence Zone at ~1.35 – 0.9 Ma and ~0.75 – 0.5 Ma. Synchronous to the changes in the upper ocean, the deeper water masses experienced high amplitude variations in temperature, most prominently since ~1.5 Ma. This and the dynamically changing thermocline conditions most likely occurred in response to the impact of southern-sourced mode waters, which developed coincidently with the emergence of the East Pacific Cold Tongue and high latitude sea-surface cooling.

A.II. First author ISI peer-reviewed publication

Thermocline fluctuations in the western tropical Indian Ocean during the past 35 ka

Nadine Rippert[1*], Karl-Heinz Baumann[2], and Jürgen Pätzold[3]

[1]Alfred-Wegener-Institut Helmholtz Zentrum für Polar- und Meeresforschung, Postfach 12 01 61, 27515 Bremerhaven, Germany

[2]Faculty of Geosciences, University of Bremen, Bremen, Germany
[3]MARUM – Center for Marine Environmental Sciences and Faculty of Geosciences, University of Bremen, Bremen, Germany
*corresponding email: Nadine.Rippert@awi.de

Journal of Quaternary Science 30(3), 201-210.
doi:10.1002/jqs.2767

Abstract

To reconstruct the still poorly understood thermocline fluctuations in the western tropical Indian Ocean, a sediment core located off Tanzania (GeoB12610-2; 04°49.00'S, 39°25.42'E, 399 m water depth) covering the last 35 ka was analysed. Mg/Ca-derived temperatures from the planktonic foraminifera *Globigerinoides ruber* (white) and *Neogloboquadrina dutertrei* indicate that the last glacial was ~2.5°C colder in the surface waters and ~3.5°C colder in the thermocline compared with the present day. The depth of the thermocline and thus the stratification of the water column were shallower during glacial periods and deepened during the deglaciation and Holocene. The increased inflow of Southern Ocean Intermediate Waters via 'ocean tunnels' appears to cool the thermocline from below, leading to a similarity between the thermocline record of GeoB12610-2 with the Antarctic EDML temperature curve during the glacial. With rising sea level and the corresponding greater inflow of Red Sea Waters and Indonesian Intermediate Waters, the proportion of Southern Ocean Intermediate Water within the South Equatorial Current is reduced and, by Holocene time, the correlation to Antarctica is barely traceable. Comparison with the eastern Indian Ocean reveals that the thermocline depth reverses from the last glacial to present.

A.III. List of Abbreviations

Areal, climate, current and water mass abbreviations:

AABW	Antarctic Bottom Water
AAIW	Antarctic Intermediate Water
CC	California Current
CDW	Circumpolar Deep Water
EEP	Eastern Equatorial Pacific
ENSO	El Niño Southern Oscillation
EqPIW	Equatorial Pacific Intermediate Water
ETNP	Eastern Tropical North Pacific
EUC	Equatorial Undercurrent
GNPIW	Glacial North Pacific Intermediate Water
HNLC	high-nutrient low-chlorophyll
ITCZ	Intertropical Convergence Zone
KC	Kuroshio Current
LGM	Last Glacial Maximum
MIS	Marine Isotope Stage
NADW	North Atlantic Deep Water
NEC	North Equatorial Current
NECC	North Equatorial Countercurrent
NGCUC	New Guinea Coastal Undercurrent
NPIW	North Pacific Intermediate Water
NSCC	Northern Subsurface Countercurrent
OSIW	Okhotsk Sea Intermediate Water
PDW	Pacific Deep Water
PEqD	Pacific Equatorial Divergence
SAMW	Subantarctic Mode Water
SAZ	Subantarctic Zone
SEC	South Equatorial Current
SSCC	Southern Subsurface Countercurrent
SOIW	Southern Ocean Intermediate Water
UCDW	Upper Circumpolar Deep Water

WPWP	Western Pacific Warm Pool

Proxy, chemical and analytical definitions:

ACD	Apparent Calcification Depth
bem	paleotemperature equation of *Bemis et al*. [1998]
$CaCO_3$	calcium carbonate
CO_2	carbon dioxide
C_{org}	organic carbon
CTD	Conductivity-Temperature-Depth
$\delta^{13}C$	stable carbon isotope of foraminiferal calcite
$\delta^{13}C_{DIC}$	stable carbon isotope of total dissolved inorganic carbon
$\delta^{15}N$	stable nitrogen isotope
$\delta^{18}O$	stable oxygen isotope
$\delta^{18}O_{calcite}$	stable oxygen isotope of foraminiferal calcite
$\delta^{18}O_{equilibrium}$	the predicted theoretical stable oxygen isotope values of inorganic calcite
$\delta^{18}O_{water}$	stable oxygen isotope of water
$\delta^{18}O_{seawater}$	stable oxygen isotope of seawater
$\delta^{30}Si_{Diatom}$	silicon isotope of diatoms
$\Delta^{14}C$	radiocarbon activity of a sample relative to the absolute international standard (year 1950)
DIC	total dissolved inorganic carbon
ε_{Nd}	neodymium isotope record
$HgCl_2$	mercury chloride
kim	paleotemperature equation of *Kim and O'Neil* [1997]
(LA)-ICP-MS	(Laser-Ablation) Inductively Coupled Plasma-Mass Spectrometer
mul	paleotemperature equation of *Mulitza et al*. [2004]
NaClO	sodium hypochlorite
NO_3^-	nitrate
Mg/Ca	Magnesium/Calcium
PO_4	phosphate
psu	practical salinity unit
sha	paleotemperature equation of *Shackleton* [1974]
$Si(OH)_4$	silicic acid
VPDB	Vienna PeeDee Belemnite

VSMOW	Vienna standard mean ocean water
XRF	X-ray fluorescence

Facility, institute and cruise names:

AWI	Alfred-Wegener-Institut, Helmholtz Zentrum für Polar- und Meeresforschung
BMBF	Bundesministerium für Bildung und Forschung
GEOMAR	GEOMAR, Helmholtz Centre for Ocean Research Kiel
GLODAP	Global Ocean Data Analysis Project
MD06	RV Marion Dufresne cruises MD106 (year 1997)
NOAA	National Oceanic and Atmospheric Administration
ODP	Ocean Drilling Project
ONI	Oceanic Niño Index
SO136/201/225	RV Sonne cruises 136, 201 and 225 (year 1998, 2009 and 2012/2013)
U1342	Sediment core obtained during Integrated Ocean Drilling Program 323 (year 2009)

Other:

DCM	deep chlorophyll maximum
LR04	global benthic $\delta^{18}O$ stack 2004 [*Lisiecki and Raymo*, 2005]
MRA	mean relative abundance
MSD	maximum shell diameter
OM	oxygen minimum
s.s.	*Globiderinoides ruber* morphoytpe sensu strictu
s.l.	*Globiderinoides ruber* morphoytpe sensu lato
SALH	Silicic acid leakage hypothesis
SML	surface mixed layer
SST	sea-surface temperature
SSS	sea-surface salinity
WOA09/13	World Ocean Atlas of 2009 and 2013